

**INTEGRATED GEOPHYSICAL METHODS FOR
CHARACTERIZATION OF SUBSURFACE CONDITIONS
AROUND ILOKUN, ADO-EKITI, SOUTHWESTERN, NIGERIA**

BY

FASHINA TIMILEHIN GBENGA

Matriculation Number: GPY/11/0295

**A THESIS REPORT SUBMITTED TO THE DEPARTMENT OF GEOPHYSICS,
FEDERAL UNIVERSITY OYE-EKITI, EKITI STATE NIGERIA.**

**IN PARTIAL FULFILLMENT OF THE AWARD OF BACHELOR OF SCIENCE
(B.Sc.) DEGREE IN GEOPHYSICS.**

OCTOBER, 2015.

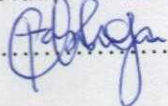
CERTIFICATION

By Student

I certify that this work has not been presented elsewhere for the award of a degree, or any other purpose.

Candidate's Name: Fashina Timilehin Gbenga

Matriculation Number: GPY/11/0295

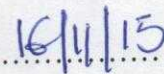
Signature:.....

By Supervisor

I certify that this research work was carried out by Fashina Timilehin Gbenga (GPY/11/0295) in the department of Geophysics, Federal University Oye-Ekiti.

Supervisor's Name: Mr. A.O Fajana

Signature:.....

Date.....

DEDICATION

This project work is dedicated to my family, my best friend and God Almighty for his assistance throughout the program.

ACKNOWLEDGEMENT

This dissertation would not have been possible without the guidance and help of several individuals who in one way or another contributed and extended their valuable assistance in the preparation and completion of this study.

My utmost gratitude to Mr. A.O Fajana, my project supervisor, whose encouragement I will never forget. He has been my inspiration in completing this research work

Mr. O.E Bamidele, my level adviser, who had kind concern and consideration towards this research work.

I so much appreciate the advices and supports of every lecturer and staff of the department to making this research a success.

My colleagues in the department are also acknowledged for their supports during the data acquisition of all the geophysical data used during the course of this work.

I would not forget to acknowledge my friends; **Adomayi Favour, Fasanmi Temitope, Olajide Olawale, Sliyuk Rebecca and Adaramola Elizabeth, Nnawhuihe Chibuchi** who put in so much efforts to ensure that I have successful research work.

Finally, my family and the one above all of us, the omnipresent God, for giving me the strength to plod on despite my constitution wanting to give up and throw in the trowel, thank you so much Dear Lord.

ABSTRACT

Refuse disposal is a major environmental problem in most Nigeria cities and towns. The leachates from such sites may infiltrate or seep into the subsurface layers and pollute groundwater. Therefore, integrated geophysical methods such as electromagnetic, magnetics and electrical resistivity methods were applied to characterize the subsurface and assess the impact of the leachate on the groundwater quality around Ilokun dumpsite, Ado-Ekiti Southwestern Nigeria. Two wells were selected for analysis and water samples collected for detailed physicochemical analysis. A total of eight traverses were established, trending in the NW-SE and W-E direction. Both the VLF-EM and the magnetics data were acquired along the traverses established at station intervals of 5m. Of these eight traverses, five traverses were investigated using dipole -dipole technique for data acquisition with an electrode spacing of 5m with the expansion factor (N) ranging from 1-5.

Seventeen (17) VES stations were occupied within the study area using the Schlumberger electrode array with maximum spread length (AB) ranging from 100m to 130m. The VES data were processed and interpreted by the method of partial curve matching and computer iteration technique to generate the subsurface model.

The VLF-EM results showed series of conductive zones varying from highly conductive zones to moderately conductive zones. The geoelectric section generally revealed a maximum of four geoelectric layers which could be classified into three major geologic layers: the topsoil; the weathered layer and the Fresh basement. Thin layers of laterite were found in the subsurface beneath some traverses. The top soil resistivity varies from 30 ohm-m to 210 ohm-m and thickness ranging from 0.5m to 1.6m. The weathered layer resistivity varies from 6 ohm-m to 52 ohm-m and thickness ranging from 1.5m to 16.5m. The resistivity values of the basement varies from 1500 ohm-m to 13500 ohm-m. The results of the dipole-dipole 2-D resistivity structure correlated with that of electromagnetic profiles, magnetics and geoelectric sections revealed that the subsurface in the dump area is polluted by the infiltrated leachates. The elevation map of the entire area corroborates the downward flow of leachates emanating from the dumpsite as shown in the iso-resistivity maps. The results of the physico-chemical analysis showed that the electrical conductivity, temperature, chloride, COD, DO, TDS, TSS, pH fall within WHO and FEPA's standard for portable water.

It was therefore concluded that the leachate from the dumpsite is gradually migrating towards the western part of the study area; thereby polluting the near surface and underground water within the area while areas along the control points and the second well are free from pollution.

TABLE OF CONTENT

• Title Page.	
• Certification page	ii
• Dedication page	iii
• Acknowledgement	iv
• Abstract	v
• Table of Content	vi
• List of Figures	vii
• List of Tables	viii

CHAPTER ONE- INTRODUCTION

1.1	Preamble	1
1.2	Aim and Objectives of the Study	8
1.3	Justification	8
1.4	Previous works	9
1.5	Location and Description of Study Area	11
	1.5.1 Location and Accessibility	11
	1.5.2 Geomorphology	14
1.6	Expected Contribution to Knowledge	15

CHAPTER TWO- GEOLOGIC SETTINGS

2.1	Regional Geological Setting of South-Western Nigeria	16
	2.1.1 Regional Geology of Nigeria	16
	2.1.1.1 Regional Geology of Southwestern Nigeria	16
	2.1.1.2 Geochronology of the basement rocks of southwestern Nigeria	22
	2.1.1.3 Geological setting of southwestern Nigeria Basement complex	23
	2.1.2 Local Geology	26
	2.1.3 Hydrogeology	28
2.2	Basic Principles and Theory of Geophysical Method used	29

2.2.1	Electromagnetic method	30
2.2.1.1	Electromagnetic Theory	30
2.2.1.2	Biot-Savart Law	32
2.2.1.3	The Field of a Vertical Wire	34
2.2.1.4	Principle of VLF-EM Method	37
2.2.1.5	Depth of Penetration of Electromagnetic Field	39
2.2.1.6	Application of VLF-EM Method	40
2.2.1.7	Limitations of VLF-EM Method	40
2.2.2	Magnetic Prospecting Method	40
2.2.2.1	Fundamental Definition and the Physical Concept of Magnetics	42
2.2.2.2	Magnetic Intensity	44
2.2.2.3	The Magnetic Elements and Their Characteristics	46
2.2.2.4	Magnetic Properties	48
2.2.2.5	The Geomagnetic Field	49
2.2.2.6	Limitation of Magnetic Survey	51
2.2.3	Electrical Prospecting Method	52
2.2.3.1	Basic Principles and Theory of Electrical Resistivity Method	52
2.2.3.2	Generalized Apparent Resistivity Equation	57
2.2.3.3	Electrode Configurations	58
2.2.3.4	Field Procedure	64
2.2.3.5	Field Operational Problems	65

CHAPTER THREE- MATERIALS AND METHOD OF STUDY

3.1	Materials	66
3.2	Methodology	70
3.2.1	Very-low Frequency Electromagnetics method	70
3.2.1.1	Data Acquisition	70
3.2.1.2	Data Processing	71

3.2.1.3 Data Interpretation	72
3.2.2 Magnetic Prospecting Method	72
3.2.2.1 Data Acquisition	73
3.2.2.2 Data Processing	74
3.2.2.3 Data Interpretation	75
3.2.3 Electrical Resistivity Method	79
3.2.3.1 Data Acquisition	79
3.2.3.2 Data Processing	80
3.2.3.3 Data Interpretation	81
3.2.4 Physico-chemical Analysis	82

CHAPTER FOUR- RESULTS AND DISCUSSION

4.1 Presentation of Results	89
4.2 Discussion of results	89
4.2.1 Very-Low Frequency Electromagnetics Method (VLF-EM) Profiles	89
4.2.2 Magnetic profiles	105
4.2.3 Dipole-dipole pseudo sections	114
4.2.4 Vertical Electrical Sounding Curves	121
4.2.4.1 Geo-electric sections	121
4.2.5 Correlation of VLF-EM 2-D Models, 2-D Resistivity structures, Geomagnetic sections and Geoelectric sections	129
4.2.6 Geoelectric maps	137

CHAPTER FIVE- CONCLUSION AND RECOMMENDATION

5.1 Conclusion	147
5.2 Recommendation	148
References	149
Appendix	154

LIST OF FIGURES

	Page
Figure 1.1	Pictures of showing the general overview of the Ilokun dumpsite 12
Figure 1.2	Base Map of Ilokun dumpsite showing the Traverses, VES points and the Control point. 13
Figure 2.1	Geological map of Nigeria showing the Basement Complex of the Southwestern Nigeria (modified from Oyinloye, 2011). 18
Figure 2.2	Geological Map of the Area around Ado-Ekiti, Showing the Study Area (Adapted from Akure Sheet 56 Geological Map). 27
Figure 2.3	Illustration of Biot – Savart Law 33
Figure 2.4	Field of a Current Flowing in a Short Straight Element of a Conductor. 35
Figure 2.5	Typical Tx-Rx Electromagnetic Layout. 38
Figure 2.6	Line of Force around a Bar Magnet. 43
Figure 2.7	Intensity at a Point Due to A bar Magnet 45
Figure 2.8	Element of the Earth Magnetic Field 47
Figure 2.9	Histogram showing mean values and ranges in susceptibility of common rock types. (After Dobrin & Savit 1988) 51
Figure 2.10	Schematic Diagram of the Flow of Current through a Cylindrical Model (Conductor). 54
Figure 2.11	Current Source on a Spherical Surface 57
Figure 2.12	Current Source at the Hemispherical Surface 57
Figure 2.13	A Simple Current Source 59
Figure 2.14	Array Configuration for Generalized Apparent Resistivity Equation 60
Figure 2.15	Typical Wenner Configuration 60
Figure 2.16	Typical Schlumberger Configuration 62
Figure 2.17	Dipole-Dipole Configuration 62
Figure 3.1	Image showing an electrical resistivity meter 65

Figure 3.2	Image showing a pH meter	65
Figure 3.3	ABEM-WADI VLF-EM Equipment	66
Figure 3.4	Input and output unit of a proton precision	71
Figure 3.5	Schematic Diagram Showing Half Slope Method of Estimating Depth	77
Figure 4.1a	VLF profile along Traverse 1	90
Figure 4.1b	Karous Hjelt Pseudo section along Traverse 1	91
Figure 4.2a	VLF profile along Traverse 2	92
Figure 4.2b	Karous Hjelt Pseudo section along Traverse 2	93
Figure 4.3a	VLF profile along Traverse 3	94
Figure 4.3b	Karous Hjelt Pseudo section along Traverse 3	95
Figure 4.4a	VLF profile along Traverse 4	96
Figure 4.4b	Karous Hjelt Pseudo section along Traverse 4	97
Figure 4.5a	VLF profile along Traverse 5	98
Figure 4.5b	Karous Hjelt Pseudo section along Traverse 5	99
Figure 4.6a	VLF profile along Traverse 6	100
Figure 4.6b	Karous Hjelt Pseudo section along Traverse 6	101
Figure 4.7a	VLF profile along Traverse 7	102
Figure 4.7b	Karous Hjelt Pseudo section along Traverse 7	103
Figure 4.8	Euler profile and geomagnetic section of Traverse 1	106
Figure 4.9	Euler profile and geomagnetic section of Traverse 2	107
Figure 4.10	Euler profile and geomagnetic section of Traverse 3	108
Figure 4.11	Euler profile and geomagnetic section of Traverse 4	109
Figure 4.12	Euler profile and geomagnetic section of Traverse 5	110
Figure 4.13	Euler profile and geomagnetic section of Traverse 6	111
Figure 4.14	Euler profile and geomagnetic section of Traverse 7	112
Figure 4.15	2-D Resistivity Structure of Traverse 2	115
Figure 4.16	2-D Resistivity Structure of Traverse 3	116
Figure 4.17	2-D Resistivity Structure of Traverse 4	117

Figure 4.18	2-D Resistivity Structure of Traverse 5(In the village)	118
Figure 4.19	2-D Resistivity Structure along the Control point	119
Figure 4.20	Lithological characterization of the subsurface along Traverse 1	123
Figure 4.21	Lithological characterization of the subsurface along Traverse 2	123
Figure 4.22	Lithological characterization of the subsurface along Traverse 3	124
Figure 4.23	Lithological characterization of the subsurface along Traverse 4	124
Figure 4.24	Lithological characterization of the subsurface along Traverse 5	125
Figure 4.25	Lithological characterization of the well in the village.	126
Figure 4.26	Lithological characterization of the subsurface along the Control Point	127
Figure 4.27a-c	2-D Resistivity Structure, KH Model and Geoelectric and Geomagnetic section of Traverse 1	130
Figure 4.28a-c	2-D Resistivity Structure, KH Model and Geoelectric section of Traverse 2	131
Figure 4.29a-c	2-D Resistivity Structure, KH Model and Geoelectric section of Traverse 3	132
Figure 4.30a-c	2-D Resistivity Structure, KH Model and Geoelectric section of Traverse 4	133
Figure 4.31a-c	KH Model, 2-D Resistivity structure and Geoelectric section of Travers 6	134
Figure 4.32a-b	2-D Resistivity Structure and Geoelectric section of Control point	135
Figure 4.33	Isoresistivity map of Topsoil	138
Figure 4.34	Isopach map of Topsoil	139
Figure 4.35	Isoresistivity map of Weathered Layer	140
Figure 4.36	Isopach map of Weathered Layer	141
Figure 4.37	Isoresistivity map of Fresh basement	142
Figure 4.38	Elevation map of the study area	143

LIST OF TABLES

Table 1.1	Sources of some waste materials and their composition	3
Table 3.1	Typical changes in leachate concentrations with age of refuse	85
Table 4.1	Summary of the Vertical electrical sounding curves	122
Table 4.2	Physico-chemical analysis of the water sample collected at the Control point	145
Tables 4.3	Physico-chemical analysis of water sample collected from the village	146

CHAPTER ONE

INTRODUCTION

1.1 PREAMBLE

Landfill sites are geotechnically classified as inert sites, urban and low-strength industrial sites, or high strength industrial or hazardous/co-disposal sites, depending on the type of fill content. Although there will be no single model that can adequately characterize all types of landfills, we will adopt a generalized approach in this paper. To understand how the attendant processes in landfill environments can influence our geo-electrical measurements, it is instructive to examine the consistent features of models derived from geological, geotechnical, biological and biogeochemical observations on landfills plus other contaminated lands and rock weathering that can be adopted as the basic building blocks for any geo-electrical model for landfill sites. Three main features complex geometry of landfill sites, heterogeneous material composition, and complex biogeomorphic processes in harsh environmental conditions are recognized and adapted into a simplified geoelectric model in this section.

Geometry of landfill sites

Landfill sites come in various shapes, sizes and depths, and as previously mentioned, they may be located in purpose-built facilities, disused softrock/hardrock quarries, opencast coal mines or other convenient holes in the ground. They may be situated above, below or astride the regional water table. In some old/abandoned waste disposal sites, a lining of relatively impermeable material may be present, or the refuse may be in direct contact with granular or crystalline geological materials dubbed the geomatrix in geotechnical parlance. In landfill capping, a soil cover layer is required when returning the site to agricultural or amenity use and steep sided cover systems are often incorporated in the cover design see Fig. 1 to maximize the landfill capacity Hall and Gilchrist, 1995. The cover system could be multi-layered in sophisticated waste storage facilities or single-layered in some old uncontrolled landfills. The

side slopes of cover systems commonly vary from about 38 up to a maximum of 408. In the UK, for example, the Fig. 1. Common cover types at old landfill sites. A Steeply sloping side, and b domed cap side slopes of the lining system are often required to be in excess of 208 and “doming” of capping systems Fig. 1 is common Hall and Gilchrist, 1995 . There may be basal floor slopes to promote leachate drainage to sumps but it can be expected that many pre-regulation landfill sites may have inadequate basal containment and leachate collection systems; there will also be cases where the landfill bottom is neither graded nor lined. Landfills generally range in thickness from about 3 to 20 m but deeper sites ca. 30 m are known to exist.

Nature and characteristics of anthropogenic deposits

Landfill deposits are characterized by complex material composition, non-uniform compaction within each layer, non-uniform decomposition process, non-uniform settlement and varying pore fluid composition Fang, 1995a. The deposits may be intermixtures of domestic and industrial wastes, soils and exhumed geological materials see Table 1 but are geotechnically grouped into four classes: inert wastes, urban sanitary or compostable wastes, low strength industrial non-hazardous wastes, and high strength industrial hazardous wastes. The composition of urban waste will vary from community to community, from country to country,

and from season to season Fang, 1995a as partly illustrated in Table 1. The wastes in old landfill sites may not be as well compacted as in modern regulated landfill practice and will thus have substantial internal permeability. They will, in general, consist of degradable and non-degradable materials food and garden wastes, ashes, paper, textiles, plastics, metals, building

Table 1.1: Sources of some waste materials and their

Sources	Type of wastes	Approximate composition
Food and food products		
Additives	Trimmings	Organics and acids
Grain mills	Residues	
Meat/fish	Sludges	
Paper and paper products	Sludges, pulping sludges	Sulphates, organics, soaps, mercaptans
Soaps, detergents	Sludges	Surfactants, polyphosphates, aluminium-copper-oxides
Textile products: silk, cotton, wool, synthetics	Sludges	Acids, alkalis, metallic salts, solvents
Leather products	Sludges	Chrome salts, oils, dyes
Wood and wood products	Sludges, residues / mill tailings	Solvents, preservatives
Paints, varnishes	Sludges	Metallic salts, toxic liquids
Energy and petroleum coal, nuclear and petroleum refining	Sludges, residues, cindered coking, fly ash	Hydrocarbons, acids, metallic salts, radioactive materials
Metals, fabricated / scrap metals	Sludges, slag, slime, tailings scrap heap	Sulphur, chlorides, phenols, PCBs, oils, grease, chrome, alkalis, acids, metallic salts
Mining/mineral processing	Sludges, mine tailings	Acids, cyanide, metallic salts
Chemicals, fertilizer	Sludges	Sulphuric acids, organo-phosphates, copper sulphate, mercury arsenates

Waste, mill tailings, organic liquids etc. but it is their chemical composition Table 2 that is important when assessing their potential for groundwater pollution. For example, the chemical composition of the unprocessed waste from Zagreb in Croatia listed in Table 1 is 75.8% mineral content and 24.2% organic matter Kovacic et al., 1995, and its influence on groundwater will be dominated by the amount of heavy metals and trace elements or the organic acid derivable from the solid waste. Many potentially hazardous materials find wide application in industry. For example, polychlorinated biphenyls PCBs have wide industrial usage due to their high dielectric constant, fire resistance and thermal stability; they come under various trade names — for example “askarel oil” found in some old transformers. Some of the common industrial wastes are listed in Table 2. Many of these wastes ultimately find their resting places in landfill sites. Methylene chloride, trichloroethylene TCE, toluene and m-xylene are among the hazardous organic compounds most commonly found in landfill sites. Since landfills are a complex mixture of anthropogenic deposits, their physical properties would show a wide range of variation. For example, the density of urban refuse varies from 275 kg/m to 6400 kg/m depending on the amount of metal and construction debris it contains e.g. Knight, 1990; Sharma et al., 1990; Fang, 1995a; Sanchez-Alciturri et al., 1995b but in general, old landfills normally have low density and seismic velocity Whiteley and Jewell, 1992 . The published resistivity of solid waste and contaminated substrate range from 1.5 to ca. 20 Vm e.g. Knight et al., 1978; Laine et al., 1982; Everett et al., 1984; Carpenter et al., 1991 with the associated leachate being highly conductive Whiteley and Jewell, 1992. The seismic P-wave velocity of urban refuse may range from 180 to over 700 m/s e.g. Knight et al., 1978; Calkin, 1989; Sharma et al., 1990 depending on the degree of compaction and state of saturation with the cover material having higher velocities than the underlying fill e.g. Calkin obtained a cover velocity of 320 m/s and refuse velocity of 180 m/s over a municipal landfill near Chicago. Fortunately, these physical

properties are often markedly different from those of the host geological materials so that geophysical methods can be used for determining the volumetric distribution of fill.

Leachate formation and dispersal

Degradable refuse will decompose with time into organic and/or inorganic soils plus other byproducts depending on its chemical composition. Plausible biogeomorphic processes are summarized here and draws from observations and concepts in other geoscientific disciplines e.g. Schoell, 1980; Levinson, 1980; Perec, 1981; Robinson et al., 1982; Crawford and Smith, 1984; Jones, 1985; Bennet and Siegel, 1987; Palacky, 1987; Farquhar, 1989; Robinson, 1989; Yong et al., 1992; Bell and Jermy, 1995; Fang, 1995a,b.

Mechanical decomposition

Urban waste deposit undergoes an initial short-term process of mechanical alteration due to loading and its bulk density and other physical properties may change in response to this preliminary settlement process Fang, 1995a. Other transient mechanical loads such as snow, rainwater and surcharge loads will also contribute to the settlement process. Owing to the heterogeneous nature of the usually organic-rich urban waste, the distribution of settlement will be non-uniform Fang, 1995a and often leads to severe fracturing of the top seal of the landfill cover. The top seal is then highly vulnerable to erosion and infiltration of rainwater and snowmelts. Poor management of solid wastes materials leads to potentially disastrous environmental and health hazards. Among health hazards that have resulted from the lack of an effective disposal system are periodic epidemics and communicable diseases. Decomposition of organic matter by microorganisms in landfills generates leachate, whose volume is influenced by excess rainwater percolating through the waste layers (Kjeldsen, 1993). In landfills without liners there might be migration of different organic and inorganic chemical compounds to the unsaturated zone of the soil which may reach the saturated zone (Mondelli, 2004). Some of the major effects of poorly managed dumpsite are leachate

formation, disease spread, attraction of Vermin, mosquito breeding, strong odor spread in the entire area, gas formation e.g. methane, increase in soil acidity and alkalinity and destruction of the ecosystem (Hussain et, al.1989).

Ground water pollution in and around a waste disposer site occurs due solely to the contaminants potential of leachate from the wastes. These leachates are solution or suspensions of stabilize, essentially organic or inorganic complexes of biodegradation of components of solid wastes flowing out from the refuse dumps, saturated with rainwater flowing through them. (De Rooy, C.1986).

Solid waste can be classified into different types depending on their source;

- i. Household waste is generally classified as municipal waste.
- ii. Industrial or hazardous waste.
- iii. Municipal solid waste consists of household construction and demolition debris, sanitation residue, and waste from residential and commercial complexes.
- iv. Biomedical waste or hospital waste as infections waste.

Landfills can have a strong impact on the surrounding environment, mainly in relation to the possible leakage of contaminated fluids into the subsoil and groundwater. Landfill leachate is generally very saline, rich in organic matter, and electrically conductive. Therefore it is no surprise that geophysical, and particularly electrical, techniques have long been used as diagnostic tools for the visualization of landfill impacts in the shallow subsurface. Geophysics has the competitive advantage of being minimally-invasive, inexpensive and fast while still providing good resolution at the field scale. Note that the alternative use of direct methods, such as drilling and sampling, implies the considerable risk of damaging the landfill liners and creating new pathways for contaminant migration. Moreover, the application of electrical resistivity methods to the characterization of municipal waste landfills has become popular also

because the electrical resistivity of waste varies considerably with time due to waste decomposition and leachate formation. (Lorenzo De Carlo, Maria Teresa Perri and Rita Deiana. 2013).

Geophysical methods increasingly are being used to investigate the nature of abandoned solid waste landfills. These indirect techniques are efficient and eliminate potential hazards associated with direct investigation methods such as trenching and drilling. Geophysical methods can furnish useful data for locating the boundaries of a landfill site and fill thickness. Physical property distribution in the subsurface, which may have geotechnical significance, can be derived from the geophysical data (Meju, 2000). Additionally, since some geophysical methods respond to changes in the physico-chemical conditions in the subsurface, useful chemical information may be gleaned from continuous geophysical site monitoring investigations (Meju, 2000).

In Ado -Ekiti, Nigeria, groundwater serves as a major source of potable water for the population at large. Since the quality of groundwater is more important than its quantity, there is need to study the possible effect(s) of the leachate emanating from the Ilokun dumpsite on the surrounding aquifer unit(s).

In this present work, very low frequency (VLF) electromagnetic ,magnetics and electrical resistivity methods were employed to study the groundwater contamination due to a solid waste disposal facility at the Ilokun Dumpsite Ado-Ekiti, Southwestern Nigeria. This dumpsite has been in operation for more than fifteen (15) years over which some portions have risen to a height of more than 15 meters above ground level with compressed wastes. Conductivity geophysical techniques can be used to map out areas where conductive materials are concentrated; the magnetic geophysical techniques can be used to delineate geologic fissures (such as faults, fractures, dykes, shear zones, etc.) present in the subsurface while the

resistivity geophysical technique have the potential of not only mapping the dumpsites but can also reveal potential pollution plumes and their direction of migration and therefore provide a basis for remediation if the environment is under threat.

1.2 AIM AND OBJECTIVES OF THE STUDY

The aim of this study is to assess the impact of the dumpsite leachate on the qualities of surface water and subsurface water around Ilokun, Ado- Ekiti, Southwestern Nigeria.

In order for this to be accomplished, the following are to be done:

- i. determination of the overburden thickness/depth to bedrock
- ii. delineation of subsurface contaminated zone, if any
- iii. establishment of structural control/direction within subsurface profile
- iv. revealing potential pollution plumes and their direction of migration.

1.3 JUSTIFICATION

Solid wastes are produced on daily basis as a result of direct consequence of inevitable human activities. The intensity of man's activities has led to increasing volume of solid waste worldwide despite the current level of global technological advancement and industrialization. These solid wastes could pose a serious threat to human and its immediate environments, so it is important for us to investigate the impact of the leachate from waste materials which could percolate into the aquifer units in the subsurface. Of the non-invasive geophysical methods used during this research work, the vertical electrical sounding of the electrical resistivity method would delineate the subsurface layers to the aquifer layers, showing if the aquifer units are well protected or are already contaminated by the leachate.

1.4 PREVIOUS WORKS

Various research works related to the study of the effect of leachate on the groundwater system in different parts of Nigeria. Some of these works are;

Ganiyu S.A et.al (2015) carried out a study delineating leachate plume migration using Electrical Resistivity Imaging on Lapite Dumpsite in Ibadan, Southwestern Nigeria with the aim of mapping the conductive leachate plume and extent of migration of leachate plumes in the subsurface for possible groundwater contamination. The 2 D resistivity survey was carried out Campus Tigre model resistivity meter with Wenner array configuration of electrode spacing distance ranging from 5-25m. A total of nine (9) 2D resistivity profiles with length ranging between 80 and 120m were conducted within the dumpsite. A control profile of 2D resistivity survey was also carried out at about 300m away from the dumpsite. Result showed that there is possible contamination of shallow groundwater systems in the western part of the dumpsite in years to come due to migration depth of the leachate plume. The heterogeneous nature of the dumpsite and the complexity of its subsurface condition require that an effective remediation measures be put in place to reduce environmental hazards from the dumpsite.

T.A Lateef et.al (2015) geo-electrically assessed the impact of the Ilokun dumpsite, Ado-Ekiti Southwestern Nigeria on the Surrounding Groundwater Aquifers with the aim of establishing the possible impact the contaminant plumes emanating from the dumpsite have on the subsurface aquifers. The Vertical Electrical Sounding (VES) field technique of the electrical resistivity method was adopted for the study, and the half-electrode spacing $AB/2$ varied from 1 to 65 m. A total of eight VES stations were occupied and a control VES point was located on the refuse dump. It was concluded in this research work that the anomalously low resistivity characteristics of the weathered layer beneath the Control VES point have been attributed to the presence of conductive contaminant plume. The anomalously low resistivity (16 – 47

ohm-m) within the fractured basement beneath VES 4, 5, 6 and 7 are evidences of pollution from the contaminant. The fractured basement beneath VES 2 and 3 which possess the characteristics of a good aquifer unit is under a threat of being contaminated due to its interconnection with the polluted fractured zones.

Opeyemi A. (2013) carried out an investigation on the effect of the dumpsite situated along Ilesha-Ife express road, 1.5 km from Iwara junction, Ilesha with the aim of determining the possible extent of latent subsurface structures as conduit for leachate and contaminant potential of pollution plumes. The geophysical prospecting methods employed during the course of this research work are the Very-Low Electromagnetic method and the Electrical Resistivity method involving the Schlumberger and the Wenner array technique. A total of fifty-five (55) Vertical Electrical Sounding points along ten (10) profiles within the vicinity of the site and one (1) profile (control) outside the area at about 300m from the dumpsite, four 2-D Wenner Electrical resistivity and four (4) profiles of Very-Low frequency EM method. It is also confirmed after the whole exercise that there are presence of high conductivity zones/fractures and joints under and within the vicinity of the Ilesha waste dumpsite.

Ugwu, S.A.; Nwosu .J.I (2009) employed both the electrical resistivity method and laboratory water sample analysis in assessing the effect of waste dumps on groundwater in Choba. An ABEM SAS 1000 terrameter was used to acquire the resistivity data. Two Vertical Electrical Soundings were traversed at Choba, one at the Eastern end of the Total Filling Station along the East-West road i.e. the position of the dumpsite and the other at the University Demonstration Secondary field. The second station was free from dump and served as the Control. It was observed that the aquifer units delineated at both sounding points were overlain with a layer suspected to be dry clay thereby protecting the aquifer units. It was recommended in this paper work that drilling of bore hole for portable drinking water should exceed 50m in the environment of the study area.

1.5 LOCATION AND DESCRIPTION OF STUDY AREA

1.5.1 Location and Accessibility

The Ilokun dumpsite is located in Ado-Ekiti which lies between latitude 850100 to 850600 and longitude 748600 to 749900 in Universal Traverse Mercator (UTM). It lies south of Kwara and Kogi State, East of Osun State and bounded by Ondo State in the East and in the south. The dumpsite is situated in an Ebira community along Ado-Iworoko road and it has good accessibility which is by a minor road (Figure 1.2). This dumpsite has being in existence for more fifteen (15) years and still in use till date. It is owned and maintained by the Ekiti State Waste Management Authority (ESWMA). The Ilokun dumpsite is one of the designated open waste disposals in Ekiti state managed by ESWMA. The general overview of the dumpsite is shown in Figure 1.1



Figure 1.1: Pictures of showing the general overview of the Ilokun dumpsite.

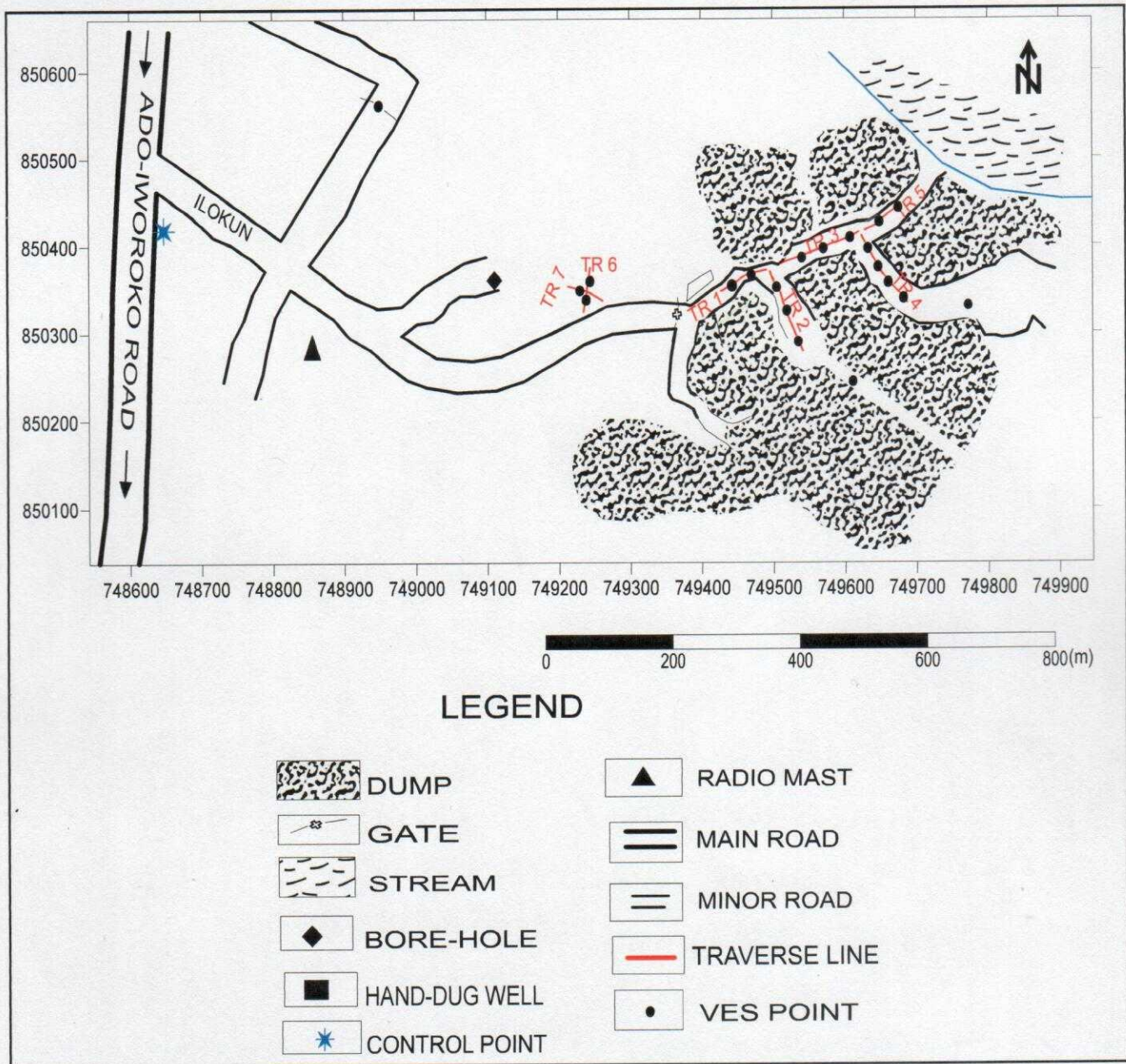


Figure 1.2: Base Map of Ilokun dumpsite showing the Traverses, VES points and the Control point.

1.5.2 Geomorphology

The Study area enjoys a tropical climate with two distinct seasons. These are the rainy season (April – October) and the dry season (November – March). Temperature ranges between 21°C and 28°C with high humidity. The south – westerly winds and the North East Trade winds blow in the raining and dry (Harmattan) seasons respectively. Tropical Forest exists in the south, while guinea savanna predominates in the northern peripheries (ekitistate.gov.ng). The relief of the study area is low with isolated hills and Isenberg that are dome-shaped. The major river draining the area is the Ireje river which flows south-east, it is associated with simple form of tributaries. The river is seasonal with reduction in volume of its water or total dry up in case of extreme drought. (Ebisemiyu, 1989).

1.6 EXPECTED CONTRIBUTION TO KNOWLEDGE

This research work is expected to make the under listed contribution to knowledge;

- The findings will enhance our knowledge of the subsurface geology, the structural setting and the hydrogeological characteristics of the study area.
- It will enable an assessment of the flow direction of the leachates and the area of highest concentration of the plume within the study area
- The information gathered will serve as reference material for further researchers.

CHAPTER TWO

LITERATURE REVIEW

2.1 GEOLOGIC SETTINGS

2.1.1 Regional Geology of Nigeria

Nigeria lies approximately between latitudes 4°N and 15°N and Longitudes 3°E and 14°E, within the Pan African mobile belt in between the West African and Congo cratons. The Geology of Nigeria is dominated by crystalline and sedimentary rocks both occurring approximately in equal proportions (Woakes et. al 1987). The crystalline rocks are made up of Precambrian basement complex and the Phanerozoic rocks which occur in the eastern region of the country and in the north central part of Nigeria. The Precambrian basement rocks in Nigeria consist of the migmatite gneissic –quartzite complex dated Archean to Early Proterozoic (2700-2000 Ma). Other units include the NE-SW trending schist belts mostly developed in the western half of the country and the granitoid plutons of the older granite suite dated Late Proterozoic to Early Phanerozoic (750-450Ma).

2.1.1.1 Regional Geology of Southwestern Nigeria

The area covered by the southwestern Nigeria basement complex lies between latitudes 7°N and 10°N and longitude 3°E and 6°E right in the equatorial rain forest region of Africa (Figure 2.0). The study area belongs to the Precambrian Basement complex of southwestern Nigeria which lies to the west of the West African Craton in the region of late Precambrian to early Paleozoic orogenesis. The Nigeria basement complex extends westward and is continuous with the dahomeyan of the Dahomey – Togo - Ghana region to east and the south Mesozoic recent sediments of Dahomey and Niger coastal basins over the basement complex. The west African Craton and the Pan African event, which presents the framework of West Africa in the entire igneous or metamorphic Structural framework of Africa consist of Precambrian rocks that have been subjected to major supracrustal plutonic events, such as;

_ Liberian (3,000 ± 200my)

_ Eburnean (1,850 ± 250my)

_ Kibarian (1,150 ± 100my)

_ Pan-African (600my)

The Crystalline rocks which forms the basement complex rocks of Nigeria are exposed in about half the surface area of the country. The remaining half is covered by sedimentary rocks of Sokoto, Chad or Bornu basin, Niger valley, Benue trough and Anambra basin. The Basement rocks are also exposed in the North central, southwestern and eastern part of the country and the basement complex are separated by sedimentary rocks except in the north central where they are interwoven for descriptive purposes.

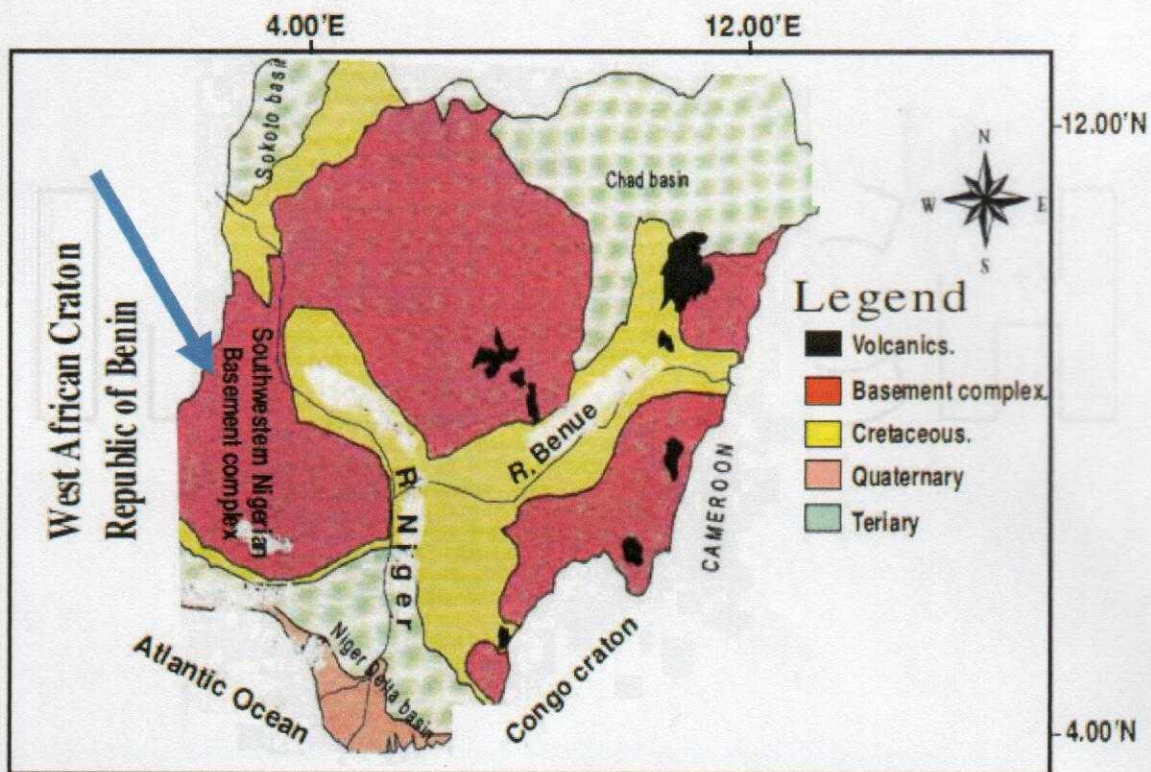


Figure 2.1: Geological map of Nigeria showing the Basement Complex of the Southwestern Nigeria (modified from Oyinloye, 2011).

The main lithologies include the amphibolites, migmatite gneisses, granites and pegmatites. Other important rock units are the schists, made up of biotite schist, quartzite schist, tremolite schist, and the muscovite schists. The crystalline rocks intruded into these schistose rocks. For the purpose of this chapter, discussion is limited to the crystalline basement rocks of southwestern Nigeria.

The Amphibolite and the hornblende gneiss

The amphibolite and the hornblende gneiss are the mafic and intermediate rocks in southwestern Nigeria. The amphibolites are made up of the massive melanocratic and foliated amphibolites. In Ilesha and Ife areas these amphibolites occur as low lying outcrops and most are seen in riverbeds. The massive melanocratic amphibolite is darkish green and fine grained. Commonly hornblende gneiss outcrops share common boundaries with the melanocratic amphibolite. This rock (hornblende gneiss) crops out at Igangan, Aiyetoro and Ifewara, along Ile-Ife road as low lying hills in southwestern Nigeria. The hornblende gneiss is highly foliated, folded and faulted in places.

The Magmatite -gneissic complex

This geotectonic complex which constitutes over 75% of the surface area of the south-western Nigerian basement complex is said to have evolved through 3 major geotectonic events:

- Initiation of crust forming process during the Early Proterozoic (2000Ma) typified by the Ibadan (Southwestern Nigeria) grey gneisses considered by Woakes et al; (1987) as to have been derived directly from the mantle.
- Emplacement of granites in Early Proterozoic (2000Ma) and
- The Pan African events (450Ma-750Ma). Rahaman and Ocan (1978) on the basis of geological field mapping reported over ten evolutionary events within the basement complex with the emplacement of dolerite dykes as the youngest.

Metamorphism in the southwestern Nigeria basement rocks

On the basis of petrology a medium pressure Barrovian and Low-medium pressure types of metamorphism had been suggested for the Precambrian basement rocks in south western Nigeria (Rahaman 1988). These metamorphic types are based on the occurrence of index minerals like chlorite, biotite and sillimanite in the basement rocks of southwestern Nigeria. Rahaman (1988) therefore concluded that metamorphism in all Nigerian Precambrian complex rocks especially that of Ife-Ilesha (Southwestern Nigeria) ranges from green schist to lower amphibolite metamorphic facies. However, Oyinloye (1992) on the basis of petrology, field mapping and structural analyses reported that the prominent gneissic foliations observed on some of the gneisses suggest that metamorphism actually reached an upper amphibolite facies in the rocks of the basement complex in Southwestern Nigeria. Egbuniwe (1982) suggested 3 phases of metamorphism (M1, M2 and M3) associated with 3 phases of deformation (D1, D2, D3) within the crystalline rocks of the basement complex in northern Nigeria. According to this author M1 represents a period of progressive metamorphism to lower amphibolite facies. M2 is described as retrogressive and reached only green schist grade as did M3. In the southwest Boesse and Ocan (1988) recognized 3 phases of metamorphism but only 2 phases of deformation. M1 is considered to be a syntectonic progressive phase of metamorphism to amphibolite facies with isoclinal folding, mineralogical banding and development of staurolite, sillimanite and garnet. M2 is described as syntectonic and associated with shear deformation and M3 being static retrogressing the earlier formed garnet and biotite to chlorite. Oyinloye (1992) however suggested that M1 is syntectonic and perhaps synchronous with the formation of the large scale major fault zone indicated by formation of mylonite outcrops at Iwaraja, Southwestern Nigeria. M2 is also syntectonic and contemporaneous with D2 as indicated by the development of micro faulting folding, fracturing, shearing, formation of phyllonite and

mylonite with distorted garnet crystals surrounded by sillimanite crystals and mylonitised granite gneisses.

Geology of Nigeria is made up of three major geological components:

- i. Basement complex: Pan African and older (Precambrian) greater than 600 million years.
- ii. Younger granites: (Jurassic 200-145) million years
- iii. Sedimentary Basins: Cretaceous to recent less than 145 million years (Obaje 2009).

The Nigerian Basement complex lies within the Pan African mobile belt to the east of West Africa craton and Northwest of the Congo craton. The Nigerian Basement complex can be divided into two provinces:

1. The western province approximately west of latitude 8°E is characterized by narrow, sediment dominated N-S trending low grade Schist belts in a predominantly Migmatite-gneiss "Older" Basement and the whole was intruded by Pan African Granitic Plutons.
2. The eastern province comprises mainly Migmatite-gneiss complex intruded by larger volumes of Pan African Granites and the Mesozoic ring complexes of central Nigeria (Ajibade, Woakes, and Rahaman).

Evidence from the eastern and northern margins of West Africa craton indicates that the Pan African belt evolve by plate tectonic processes which involved the collision between the passive continental margin of the West Africa craton and the active continental margin (Pharusian belt of the Tuareg shield about 600 mya (Burke and Dewey, 1978; Leblanc, 1976, 1981; Black et al., 1976; Caby et.al., 1981). The collision at the plate margin is believed to have led to the reactivation of the internal region of the belt. The Nigeria Basement complex lies in the reactivated part of the belt. Radiometric ages indicate that the Nigerian Basement complex is polycyclic and includes rocks of Liberian (2700 ± 200 ma), Eburnian (2000 ± 200 ma), Pan Africa (600 ± 150 ma), and questionably Kibaran (1100 ± 200 ma) ages .The most

obvious effects of the Pan African orogeny in Nigeria is the emplacement of large volumes of Granitoids and the resetting of mineral ages in virtually all rock types in the basement. However, little is known about the nature of the Pan African event in Nigeria or indeed about any of the earlier events.

2.1.1.2 Geochronology of the basement rocks of southwestern Nigeria

It has been established that the Precambrian basement complex of Nigeria including Southwestern Nigeria is polycyclic in nature, (Ajibade and Fitches 1988). The southwestern Nigeria basement complex had undergone 4 major orogenesis in:-

- i. Liberian (Archaean) 2500Ma-2750± 25Ma
- ii. The Eburnean orogeny (Early Proterozoic), 2000Ma-2500Ma
- iii. The Kibaran orogeny (Mid Proterozoic), 1100Ma - 2000Ma
- iv. The Pan African Orogeny, 450Ma-750Ma.

Of all the above, the Eburnean and the Pan-African are major events which modified the Precambrian Geology of Nigeria including the Southwestern Nigerian basement complex. The Eburnean event is marked by the emplacement of the Ibadan granite gneiss in Southwestern Nigeria which has been dated 2500±200Ma (Rahaman 1988) and a pink granite gneiss at Ile-Ife Southwestern Nigeria dated 1875Ma using U-Pb on Zircon. Thus Archaean to Pan African ages had been suggested for the basement rocks of the Southwestern Nigeria. Few studies have been carried out on the basement complex due to its assumed monotonous petrology and mineralogy and the erroneous belief that it contains no mineralization. This current chapter will therefore contribute immensely to the debate on geology of the basement complex of Southwestern Nigeria.

2.1.1.3 Geological setting of southwestern Nigeria basement complex

The basement rocks which occur in southwestern Nigeria are all duplicated in the Ilesha area of southwestern Nigeria and samples of rocks here were analyzed and used as a case study of the basement rocks in Southwestern Nigeria to avoid repetition. These rocks are amphibolite, the hornblende gneiss and the granite gneisses. These rocks are described in that order.

The massive melanocratic amphibolite

Amphibolite occurs widely in southwestern Nigeria in Ile-Ife area, Ibodi, Itaganmodi in Ilesha area. Most outcrops of the massive melanocratic amphibolites are exposed in streams and river channels in these areas. The overburden soil here is strikingly red due to the presence of hematite and magnetite liberated during the weathering of the amphibolites to form the overburden soil. Two major textural varieties of amphibolites occur in this region. These are the leucocratic amphibolites and (not discussed in this study) the massive melanocratic amphibolites. The massive melanocratic amphibolite is darkish green and fine grained without any obvious folds or foliations. In places thin colourless quartz veins occur on the outcrops. This amphibolite variety is composed of hornblende, actinolite and tremolite. In thin section the mineral composition includes (apart from the above) magnetite, sphene calcite and minor monazite and zircon. The skeletal olivine contains small, opaque inclusions which are probably magnetite.

The hornblende gneiss

The hornblende gneiss shares a common boundary with the massive melanocratic amphibolite in Ilesha area, southwestern Nigeria. This rock crops out as low lying hills in Ife-Ilesha area Southwestern Nigeria. It is composed predominantly of porphy- roblastic plagioclase and hornblende phenocrysts almost in equal proportion. This rock is highly foliated folded and faulted in places and varies from medium to coarse in texture. These outcrops trend in a NE-SW direction and dip to the east at an average angle of between 50-70°. The apparent character

varies from intermediate to acid. Micro bands of foliation rich in plagioclase and some K-feldspars alternate with bands rich in amphiboles. In thin section this foliated hornblende gneiss consists largely of hornblende and plagioclase porphyroblasts in a ground mass of ilmenite fine grained recrystallized quartz and pyroxene fragments. Brown colored epidote (with dark cracks) apatite, sphene, zircon and monazite constitute major accessory minerals in this rock. Foliations defined by parallel arrangement of feldspars alternating with amphiboles are conspicuous in thin sections. Fine grained quartz and orthoclase feldspars are observed in the felsic micro band, garnet, monazite, calcite and microcline containing well-formed zircon crystals (as inclusions) occur in this rock as observed in thin sections.

The biotite granite gneiss complex

This rock group occurs widely in every part of the southwestern Nigerian basement complex. Again description is restricted to Ilesha area to avoid repetition. Biotite granite gneiss complex occurs in the southern part of Ilesha schist belt. Outcrops of this rock group consist of high and low lying hills with myriads of flat boulders on top in places and roundish boulders on tops of hills elsewhere. This rock complex is foliated and folded with prominent synclinal and anticlinal axes. Foliations are defined by mafic (biotite rich) and felsic (quartz and feldspars) mineral bands. Drilled core samples from the biotite granite gneiss revealed that microfolds, pinkish garnet rich mylonite, greenish friable schistose phyllonite, occur in this rock. In thin section the mylonite contains fine grains of biotite and sillimanite surrounding large crystals of garnet which show some evidence of distortion. The mylonite contains little quartz and the biotite flakes form thin foliation bands which are closely packed around garnet crystals. These later events may be due to movements along the major Ifewara-Zungeru fault system.

The biotite granite gneiss are surrounded by muscovite-quartzite schists and in places the later are in-folded into the gneisses where they occur as remnants. At outcrop scale, the biotite granite gneiss is composed of biotite, Kfeldspar, quartz and garnet. In thin section the biotite flakes are

pencil-like as a result of metamorphic deformation and are aligned in parallel to sub parallel manner. The K-feldspar is mostly microcline and is porphyroblastic in texture. Well-formed zircon crystals occur in association with some of the microcline grains. Apartite, monazite, magnetite, ilmenite and sphene are other accessory minerals. In places distorted and fractured garnet grains due to metamorphic deformation are observed. Continuous well defined foliation bands of micas and felsic minerals are also common features of this gneiss. These gneissic fabrics probably indicate that metamorphism here was perhaps higher than the green schist-lower amphibolite facie regarded as the metamorphic grade for rocks in the basement complex in southwestern Nigeria. The presence of mylonite, mylonitised granite and gneissic banding are probable indications of a localized dynamic metamorphism possibly reaching an upper amphibolite facie.

The pink granite gneisses

This variety of gneiss occurs widely in the southwestern Nigeria basement complex at Ile Ife, Ibadan, Iseyin, Eruwa and Iwaraja and in Ilesha area. The granite gneiss is pinkish with large pherocrysts of K-feldspar and porphyroblasts of hornblende. The texture of the pink granite gneiss varies from medium grained to very coarse almost becoming pegmatitic in places. According to Boesse and Ocan (1988) this major fault (marked by the mylonite outcrops) marks a break between the granite gneissic complex and the metasediments in this region.

The grey granite gneiss

The grey granite gneiss occurs prominently at Ibadan, Oyan, and in Ilesha areas of southwestern Nigeria basement complex. Usually outcrops consist of high and low hills and at Erinmo in Ilesha area occur very close to the pink granite gneiss and only separated by a narrow strip of muscovite quartzite schist. The overall color is greyish. The texture of this variety of gneiss is fine to medium grained with well-developed foliation defined by preferred orientation of biotite. This rock is mostly composed of quartz, biotite, plagioclase, K-feldspar and

hornblende. In thin section recrystallized fine grained quartz covers the surface of microcline phenocrysts as overgrowths. This is a common phenomenon in all the granite gneisses investigated in this study. Mosaic textures formed by fragments of plagioclase, biotite and recrystallized quartz are also observed. Intergrowths of orthoclase and microcline forming a perthitic texture occur in places. Quartz crystals consist of fractured and recrystallized fine varieties. Well-formed rod-like and fragmented zircon crystals, apatite, monazite plus minor garnet form important accessory minerals.

2.1.2 Local Geology

The study area is underlain by Pre-Cambrian Basement Complex rocks which include coarse grained Charnokite, medium grained Granite and Porphyrite Biotite Hornblende (Figure 2.1). The local geological mapping of the study area show that the area is characterized by mainly by Migmatite-gneiss (Figure 2.2).

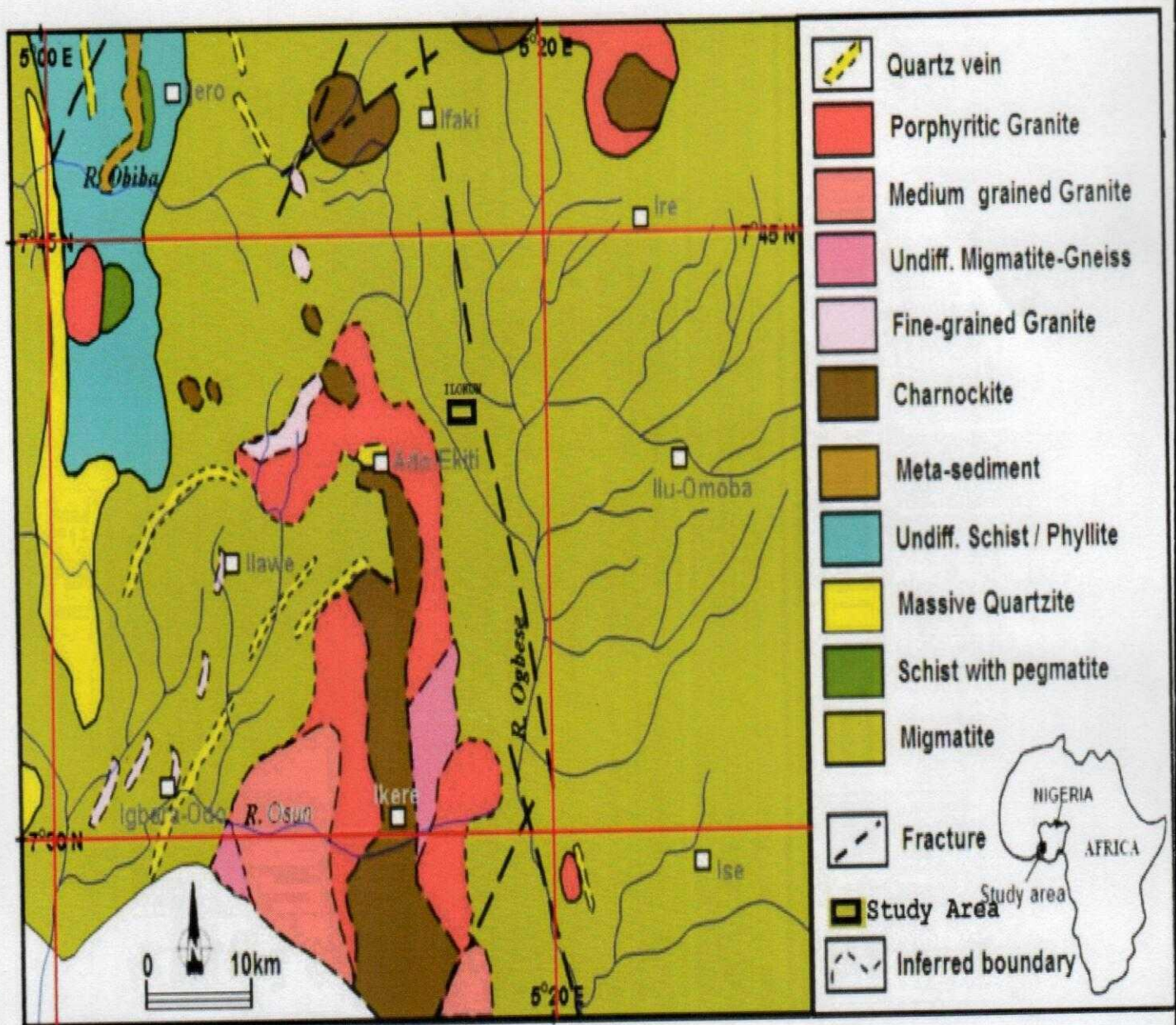


Figure 2.2: Geological Map of the Area around Ado-Ekiti, Showing the Study Area
(Adapted from Akure Sheet 56 Geological Map)

2.1.3 Hydrogeology

The hydrogeology of an area is controlled by some factors such as geology, structures and climate of the area (Raghynath, 2002). This is because the geologic formations underlying the area and the structures determine the types of aquifer to be encountered and the means of recharging them while the climate determines the amount and rate of recharge of the aquifer (Shemang, 1990). Groundwater in general originate as surface water, but their occurrence and distribution are controlled by geologic factors such as lithology, texture of the rock and climatic factors such as rainfall. Sources of surface water supply to the study area is River Ireje and its major tributaries, and it is the only perennial river around the area.

Generally in the crystalline basement terrain, aquifers often occur at shallow depths, thus making them vulnerable to environmental risks. An effective groundwater protection is often provided by impermeable geologic materials with sufficient thickness and low hydraulic conductivity. This is because the earth medium acts as a natural filter to percolating fluids containing contaminants. Its ability to retard contaminated fluid is a measure of its protective capacity. However, in the disturbed environment constituting the waste dump, the overburden consists of a thin soil cover and the leachate saturated refuse. The development of secondary porosity and permeability resulting from these weathering and fracturing processes has led the crystalline igneous and metamorphic rocks to experience water ingress and storage thus creating aquiferous zones that are capable of yielding sufficient quantities of water. The highest groundwater yield in basement terrains is found in areas where thick overburden overlies fractured zones (Olorunfemi and Olorunniwo, 1987). The basement complex rocks in southwestern Nigeria has undergone various degrees of weathering leading to various depths and thickness of the overburden material or regolith thus producing reservoirs which are of restricted vertical and lateral extent. These have sufficient hydraulic

conductivity and storage to yield groundwater to wells and boreholes (Acworth, 1987). However, pockets of weathered and fractured rocks may form isolated groundwater below the reservoirs. The variation in porosity and permeability of these isolated reservoirs thus result in varying yields. Although, weathering and fracturing enhances groundwater potentials, however, the groundwater availability also depends on the rock material or type and composition as well as the thickness of the weathered or fractured zone. For instance, more stable minerals like quartz will disintegrate into porous and permeable water bearing gravely or sandy medium (Offodile, 1983), while the less stable minerals like the ferromagnesian types will disintegrate into clayey, sometimes micaceous impermeable non water bearing rock formation. The storage of water in the study area depends mainly on the thickness of the weathered or fractured zone. On the basis of variation of the thickness and hydraulic properties of the altered fresh crystalline rocks recognized in the weathered profile, the zone has been divided into three or four hydrogeological units. These are the residual topsoil, the weathered layer, the fractured layer and the fresh bedrock.

2.2 BASIC PRINCIPLES AND THEORY OF GEOPHYSICAL METHOD USED

In the geophysical survey of Ilokun dumpsite, Ado-Ekiti three (3) geophysical methods were used

- i. Electromagnetic method
- ii. Magnetic method
- iii. Electrical Resistivity method

2.2.1 ELECTROMAGNETIC METHOD

Electromagnetic methods in general may be either natural or artificial. In principle, the VLF-EM method is a type of artificial electromagnetic method which makes use of the field of a vertical wire.

2.2.1.1 Electromagnetic Theory

The determination of both magnetic and electric fields generated in any region requires the use of some field vectors stated below

E = Electric field intensity (V/M)

B = Magnetic flux density (Webers/m²)

H = Magnetic field intensity (Ampere turns/m)

D = Electric displacement (Coulombs/m)

J = Current density (Ampere/m²)

A = Vector magnetic potential

Maxwell's electromagnetic equation in equation 2.1 relates these vector fields

$$\nabla \times E = \frac{\partial B}{\partial t} \quad 2.1$$

$$\nabla \times H = J + \frac{\partial D}{\partial t} \quad 2.2$$

$$\text{But } B = \mu H \quad 2.3$$

Where μ = magnetic permeability

$$\nabla \times E = -\mu \frac{\partial H}{\partial t} \quad 2.4$$

These equations and the Maxwell's law of induction are the basis on which electromagnetic theory is pivoted.

The use of a potential to obtain field vectors is allowed in potential theory. Therefore, on differentiation, both electric and magnetic field vectors are obtainable from this magnetic induction B below:

$$\nabla \times E = B \quad 2.5$$

Combining equation 2.1, 2.2 and 2.5, then:

$$E = \frac{-\partial A}{\partial t} \quad 2.6$$

Taking the divergence of equation 2.1 and 2.2 using the vector identity

$$\nabla \cdot \nabla \times A = 0 \quad 2.7$$

Time varying fields given below are obtained

$$\nabla \cdot \nabla \times E = -\nabla \cdot \frac{\partial B}{\partial t} = -\frac{\partial}{\partial t} [\nabla \cdot B] \quad 2.8$$

Similarly,

$$\nabla \cdot J + \nabla \cdot \frac{\partial D}{\partial t} = \nabla \cdot J + \frac{\partial}{\partial t} [\nabla \cdot D] = 0 \quad 2.9$$

Hence

$$\nabla \cdot B = \nabla \cdot E = 0 \quad 2.10$$

The following vectors identified below are useful when taking the curl of a vector.

$$\nabla \times \nabla \times A = \nabla(\nabla \cdot A) - \nabla^2 A = -\nabla^2 A \quad 2.11$$

Since $\nabla \cdot A = 0$ from equation (2.10) then taking the curl of equation (2.5) and using the identity in equation (2.11) results into:

$$\nabla \times \nabla \times A = -\nabla^2 A = \nabla \times B \quad 2.12$$

On substituting $B = \mu H$ into equation (2.12)

$$-\nabla^2 A = \nabla \times \mu H = -\mu(\nabla \times H) \quad 2.13$$

Since, $\nabla \times H = J + \frac{\partial D}{\partial t}$ from equation (2.2)

$$D = \epsilon E \quad 2.14$$

Where, ϵ = Electric permeability

Then equation (2.13) becomes

$$\nabla^2 A = -\mu \left[J + \frac{\epsilon \partial E}{\partial t} \right] \quad 2.15$$

When ϵ is very small, $\epsilon \partial E$ becomes negligible such that equation (2.15) becomes

$$\nabla^2 A = -\mu J \quad 2.16$$

This relation stated in equation (2.16) resembles Poisson's equation in gravity and magnetic with the solution

$$A = \frac{\mu}{4\pi} \int \frac{J \partial v}{r} \quad 2.17$$

$$\text{Where } r = (x^2 + r^2 + z^2)^{1/2}$$

Equation (2.17) is of great importance when determining various magnetic fields for different configurations of electromagnetic transmitters.

2.2.1.2 Biot-Savart Law

This law relates the magnetic field at a point in a space to a current flowing in a short straight element of a conductor some distance away (Figure. 2.3). This law can be derived using vector potential expression established in equation (2.17),

$$A = \frac{\mu}{4\pi} \int \frac{J \partial v}{r} \quad 2.17$$

Equation (2.17) can be expressed in terms of a line integral as:

$$A = \frac{\mu}{4\pi} \oint \frac{I \partial s}{r} \quad 2.18$$

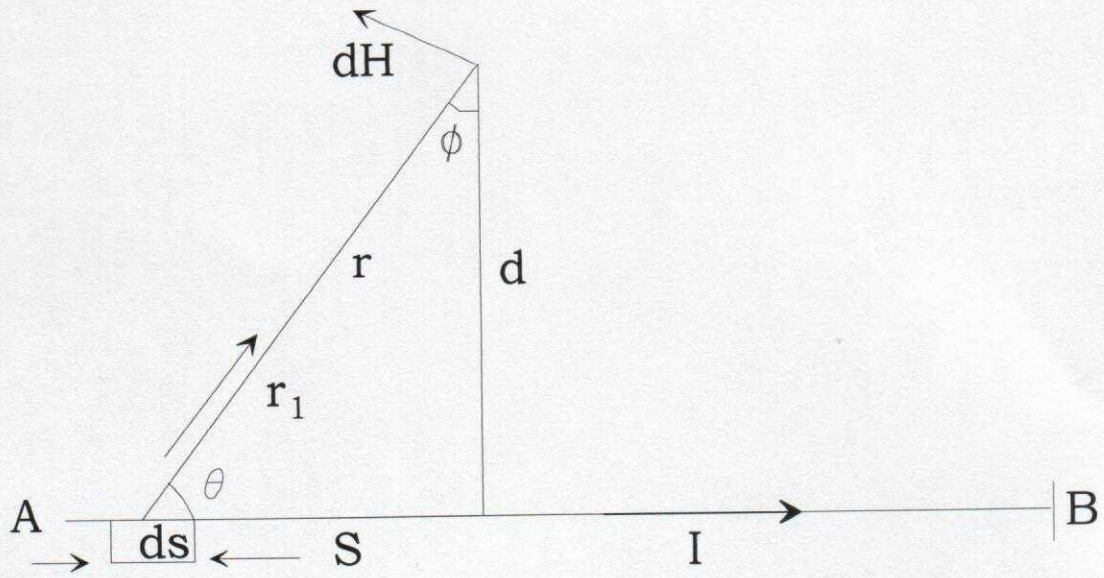


Figure 2.3: Illustration of Biot – Savart Law.

Using equation 2.3, 2.5 in equation 2.18 and carrying out the line integral over a closed path surrounding the wire element, gives:

$$dH = \frac{\partial B}{\mu} = \frac{\nabla \times \partial A}{\mu} \quad 2.19a$$

$$dH = \nabla \times \frac{\partial \left[\frac{\mu}{4\pi} \oint \frac{I \partial s}{r} \right]}{\mu} \quad 2.19b$$

$$dH = \frac{I \partial s}{4\pi} \left[\hat{r} \times \nabla \left[\frac{1}{r} \right] \right] \quad 2.19c$$

$$dH = \frac{I \partial s \times \hat{r}}{4\pi r} \quad 2.19d$$

This on further simplification yields

$$dH = \frac{I \partial \sin \theta}{4\pi r} \quad 2.20$$

Equation (2.20) is referred to as the Biot-Savart equation. It describes the magnetic field dH at a point P a distance r away to current I flowing through an element ds of a wire.

2.2.1.3 The Field of a Vertical Wire

It is applicable in VLF-EM method. In theory, there are two electric field components E_θ and E_r and one magnetic field component H_θ (Figure. 2.4),

$$H_\theta = \frac{I \partial l}{4\pi} e^{j\omega \left[t - \frac{r}{c} \right]} \left[\frac{j\omega}{rc} + \frac{1}{r^2} \right] \sin \theta \quad 2.21$$

$$E_\theta = \frac{I \partial l}{4\pi} e^{j\omega \left[t - \frac{r}{c} \right]} \left[\frac{j\omega}{rc^2 \epsilon} + \frac{1}{r^2 c \epsilon} - \frac{j}{r^3 \omega \epsilon} \right] \sin \theta \quad 2.22$$

$$E_r = \frac{I \partial l}{2\pi} e^{j\omega \left[t - \frac{r}{c} \right]} \left[\frac{1}{r^2 c \epsilon} - \frac{j}{r^3 \omega \epsilon} \right] \cos \theta \quad 2.23$$

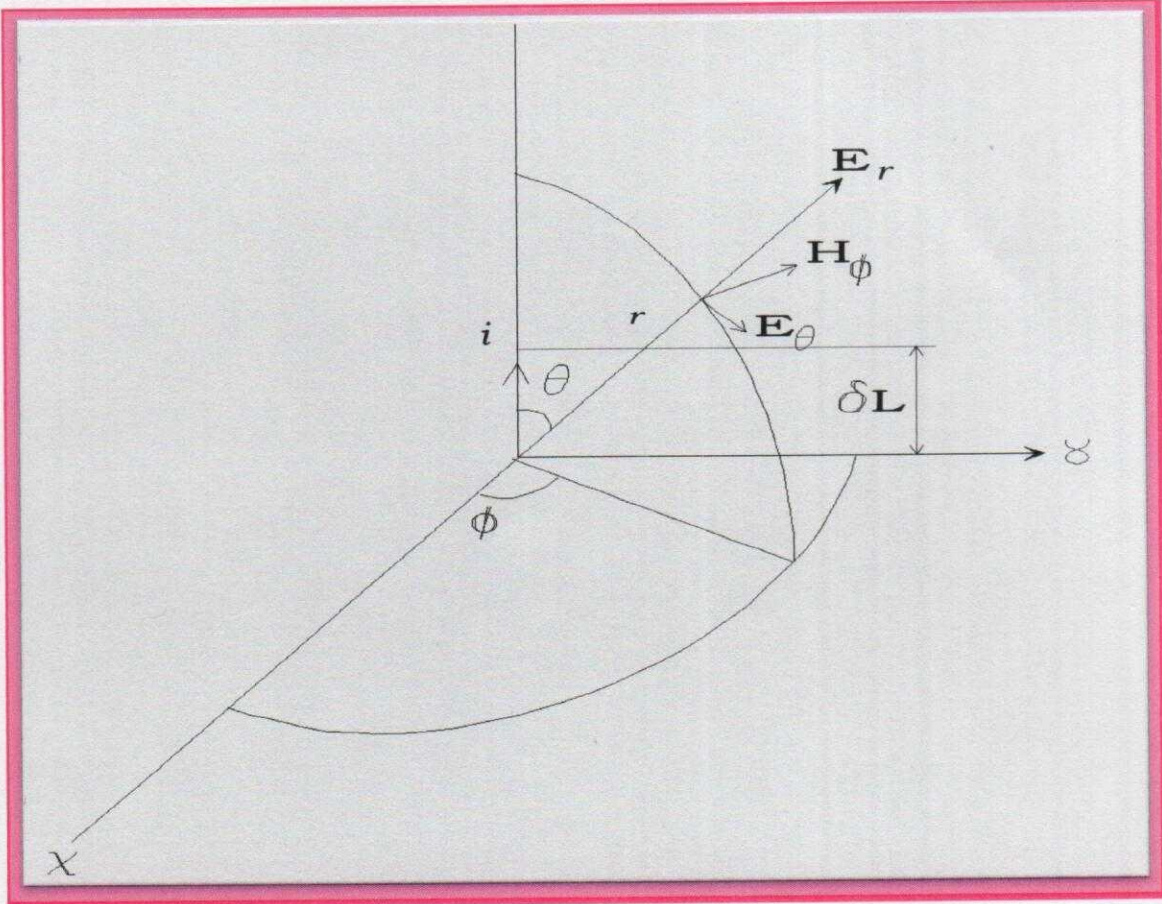


Figure 2.4: Field of a Current Flowing in a Short Straight Element of a Conductor.

Where,

$$C = \frac{1}{\sqrt{\mu\epsilon}}$$

$$\omega = 2\pi f$$

At a large distance from the source (transmitter) $\frac{1}{r^2}$ and $\frac{1}{r^3}$ becomes negligible. Thus equation

2.21, 2.22 and 2.23 becomes;

$$H_{\theta} = \frac{j\omega I \delta l}{4\pi cr} e^{j\omega\left[t - \frac{r}{c}\right]} \sin\theta \quad 2.24$$

$$E_{\theta} = \frac{j\omega I \delta l}{4\pi c^2 \epsilon r} e^{j\omega\left[t - \frac{r}{c}\right]} \sin\theta \quad 2.25$$

$$E_r \approx 0 \quad 2.26$$

Where,

C = Speed of light in free space

j = Current Density

ω = Angular Velocity

r = Radius

I = Current

l = Length of the vertical wire

t = Time

ℓ = Electric Resistivity

E = Electric Field Intensity (volt/m)

ϵ = Permittivity of a medium

H = Magnetic Field Intensity (Teslas)

2.2.1.4 Principle of VLF-EM Method

An alternating current usually with a frequency of between 15 to 30 kilohertz is passed through a transmitting vertical coil into the ground which generates an electromagnetic field around the coil. When the field emitted by the transmitter strikes an anomaly having low electrical resistivity, it generates secondary current or eddy current, which in turn creates a magnetic (secondary) field that opposes the original field that is emitted from the transmitter (Figure. 2.5). The magnetic field received and measured by the receiver at the surface is the resultant of the secondary field created by this induced current and that of the primary field due to the transmitter. Usually, there is difference in direction and phase between the primary and the secondary field, and the current induced in resultant field and its magnitude. The signal from the receiver is usually divided into two components; one that is in-phase with the signal generated in the receiving coil by the transmitter in the presence of a secondary field and the other is out of phase (or quadrature part) by a difference of 90° with it. The in-phase represents the real part of the signal while the quadrature part represents the imaginary part. A body must have a minimum size and sufficient low resistivity for any secondary field to be created. More so, the strike length of the body must exceed about 5 m, and the depth extent must exceed about 10 m for induction to occur. The thickness of the body in any case needs only to be about 0.5 – 1 m. Nevertheless, the field from the VLF transmitter must pass perpendicularly through the body, i.e. the direction to the transmitter is in the strike direction of the body.

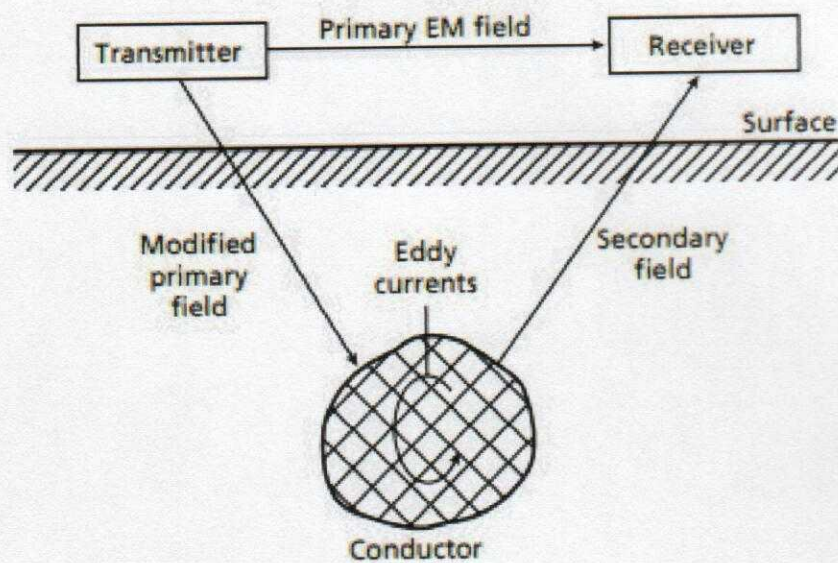


Figure 2.5: Typical Tx-Rx Electromagnetic Layout.

2.2.1.5 Depth of Penetration of Electromagnetic Field

The depth of penetration of an electromagnetic field depends on its frequency and electrical conductivity of the medium through which it is propagated. The passage of electromagnetic field through the ground causes their attenuation and thus results in the decrease in their amplitude exponentially with depth. The depth of penetration of electromagnetic wave 'd' is defined as the depth at which the amplitude of the field A_d is decreased by a factor e^{-1} compared with its surface amplitude A_0 .

Therefore,

$$A_d = A_0 e^{-1} \quad 2.27$$

Thus,

$$D = 503.8 (\sigma f)^{-1/2} \quad 2.28$$

Where D (skin depth) is in meters, the conductivity of the ground (σ) is in Sm^{-1} and the frequency (f) of the field is in Hertz. The depth of penetration is therefore inversely proportional to both the frequency of the electromagnetic field and the conductivity of the ground.

Equation (2.28) above only analyses a theoretical path of penetration, hence Z_c is used and this represents the maximum depth at which a conductor may be and still produces a recognizable electromagnetic anomaly.

Thus,

$$Z_c = 100(\sigma f)^{-1/2} \quad 2.29$$

Equation (2.29) is approximate because the penetration of electromagnetic waves depends upon such factors as the nature and magnitude of the effects of near surface variations in conductivity, the geometry of the subsurface conductor and instrumental noise.

2.2.1.6 Applications of VLF-EM Method

- (i) to delineate fracture zones for groundwater development.
- (ii) to locate buried pipes, electrical cables and tanks.
- (iii) to map metallic ores particularly sulphides.
- (iv) to delineate steeply dipping structures such as faults and fractures.

2.2.1.7 Limitation of VLF-EM Method

The limitation of VLF-EM method is that the depth of penetration is somewhat less than that attainable by tilt-angle method using a local transmitter. More so, for a particular survey area, there may be no suitable transmitter providing a magnetic vector across the geological strike.

2.2.2 MAGNETIC PROSPECTING METHOD

The aim of magnetic survey is to investigate subsurface geology on the basis of anomalies in the earth's magnetic field resulting from magnetic properties of the underlying rock forming minerals are non-magnetic but certain rock types contain sufficient magnetic anomalies. Also man made ferrous object generate magnetic anomalies. The study of the earth's magnetic is the oldest method of geological investigation exploration works used to explore for oil, minerals and locating features and faults zones. This method in applied geophysics depends on measuring accurately the anomalies of local magnetic field produced by the variations in the intensity of magnetization in rock formation. The magnetization of rock is partly due to the induction of magnetizing forces associated with the earth fields and partly by their permanent (remanent) magnetization.

The induced intensity depends primarily on the magnetic susceptibility as well as magnetizing force and the permanent (remanent), intensity depends on the geological history of the rock.

The method is the measurement of direction of gradient or intensity of the earth's magnetic field and interpretation of variation in quantities over the area of investigation. The magnetic

method is of great relevance in areas of contrasting magnetic contents bringing out variations due to change in magnetic properties of subsurface rock. The anomaly caused by these changes in physical properties is termed the magnetic anomalies which are often diagnostic of minerals. Structures as well as regional structures: The horizontal and the vertical variations in magnetic susceptibilities of under lying rock units causing these departure are the origin of the magnetic anomaly. The conventional unit of magnetic intensity is the oersted through most geological literature and works often use the numerically equivalent gamma. This is due to the fact that, the practical use is prospecting. The gamma defined as 10^{-5} Oe is more convenient and has become most common unit of field intensity for geophysical works. The most significant magnetic property of rocks is their susceptibility K which is defined as a measure of the magnetic mineral content in a rock (Folami, 1980). It is the fundamental parameter in magnetic prospecting. Another property of rocks is natural magnetization.

For a vacuum and for entirely non-magnetic substances, K is equal to zero ($K=0$). Magnetic mineral having positive susceptibility are known as para-magnetic grains of such material tends to line up with their long dimension in the direction of the external field. A Para-magnetic material of very high susceptibility may be referred as ferromagnetism. These are few cases of negative as rock salt and anhydrites. These are designated as diamagnetic. Grains of such material tend to line up with their long dimension across the external field. In case of homogenous external field H, for a field normal to the surface of a material, capable of being magnetized, the induced pole strength per unit area is:

$$J = KH \quad 2.30$$

$$J = KH \cos \theta \quad 2.31$$

Where, J = Magnetization

K = Susceptibility (proportional constant)

H = External Magnetic field

For low magnetic concentration, there is an approximately linear relationship between the percentage of magnetic and susceptibility, K , which is expressed as $K = 0.3P$, where P is the percentage (by volume) of magnetic dissemination (Owoeye, 2000). Generally, the darker basic rocks are more magnetic than the light colored acidic rocks.

2.2.2.1 Fundamental Definition and the Physical Concepts of Magnetism

2.2.2.1.1 Magnetic Force

A magnetic force is the mechanical force which a magnet experiences in the area of an electric current and the converse; mechanical force exerts on the current (Parasmic, 1975). This may be attractive or repulsive depending on the nature of its poles. Magnetic poles are region where lines of force leaves and enter a magnetic body following a curve path from one end of the magnetic body designated as the North pole to a corresponding South pole near the other end (Figure 2.16).

The Magnetic force for the poles of strength M_1 and M_2 at a distance r apart is thus

$$F(r) = \frac{M_1 M_2}{r^2} \quad 2.32$$

This is obtained from the Coulomb's law for magnetic poles. This force is one of repulsion between like pole and attraction between unlike poles for dipole interpretation, if M , is a limit pole straight at the point P , the force per unit pole strength $H(r)$ is given by

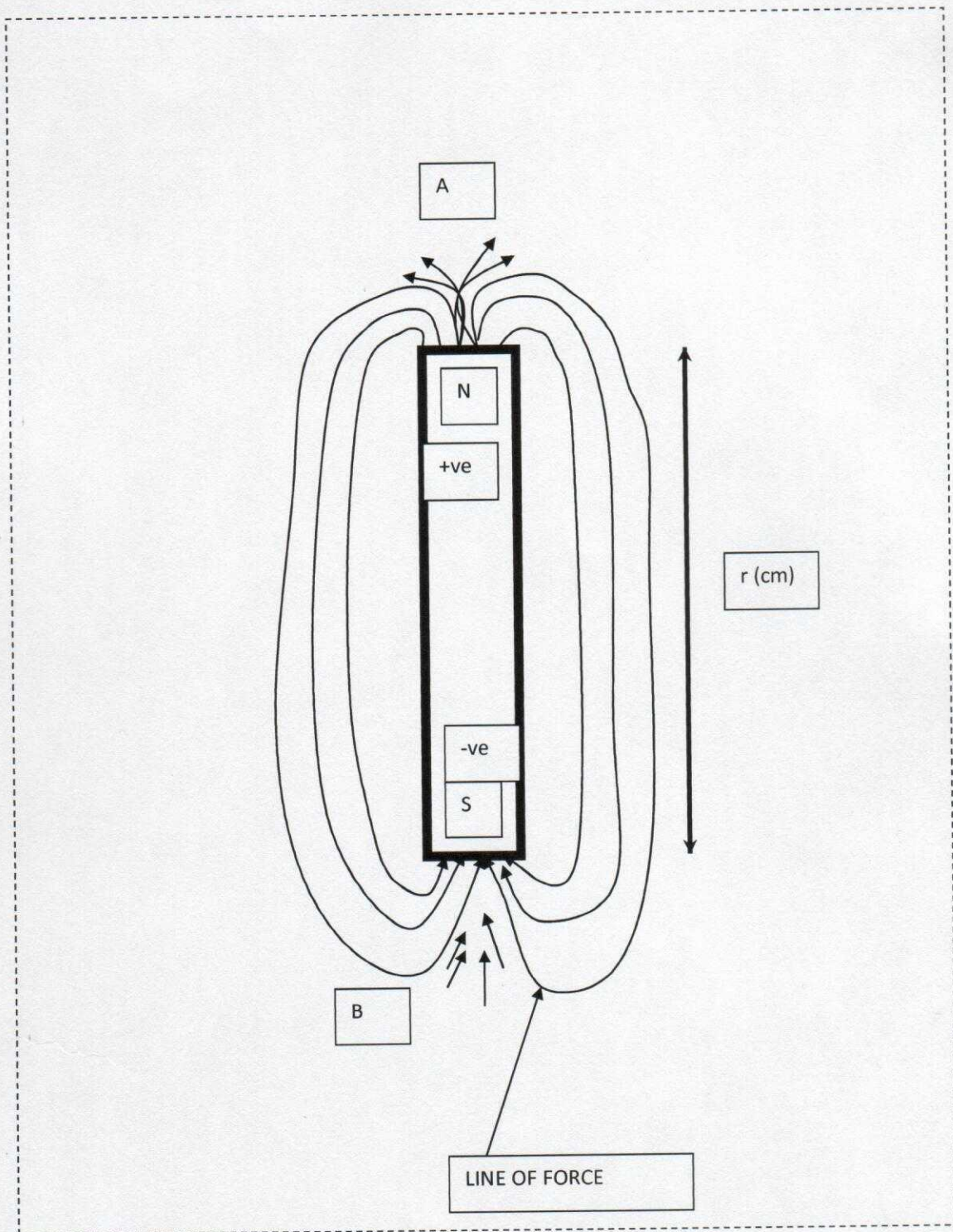


Figure 2.6: Line of Force around a Bar Magnet.

$$\vec{H}(r) = \frac{F(r)}{m_1} \frac{m_2}{r^2} \quad 2.33$$

The field is conservative and is therefore desirable for a scalar potential $A(r)$, such that

$$\vec{H}(r) = \frac{F(r)}{m_1} = A(r) \quad 2.34$$

Where,

$$A(r) = \frac{m_2 \cos \theta}{r^2} \quad 2.35$$

Where,

θ is the angle measured from m to r

r and θ are unit vectors

$H(r)$ is the force per unit pole strength of magnetic field intensity at P .

Putting equation (2.34) into (2.35) and expressing it in the form of equation (2.36), we obtain

$$T = M/r^3 \quad 2.36$$

M is the magnetic moment and r is the distance to the pole. Where, $H(r)$ is equivalent to T , the total magnetic intensity along the axis $\theta = 0^\circ$,

$T = 2m$ end along the line of right angle to the dipole where

$\theta = 90^\circ$,

2.2.2.2 Magnetic Intensity

The intensity of the field is a function of the magnetic flux density which is proportional to the strength of the field and its direction in the direction of the external field (Figure 2.17).

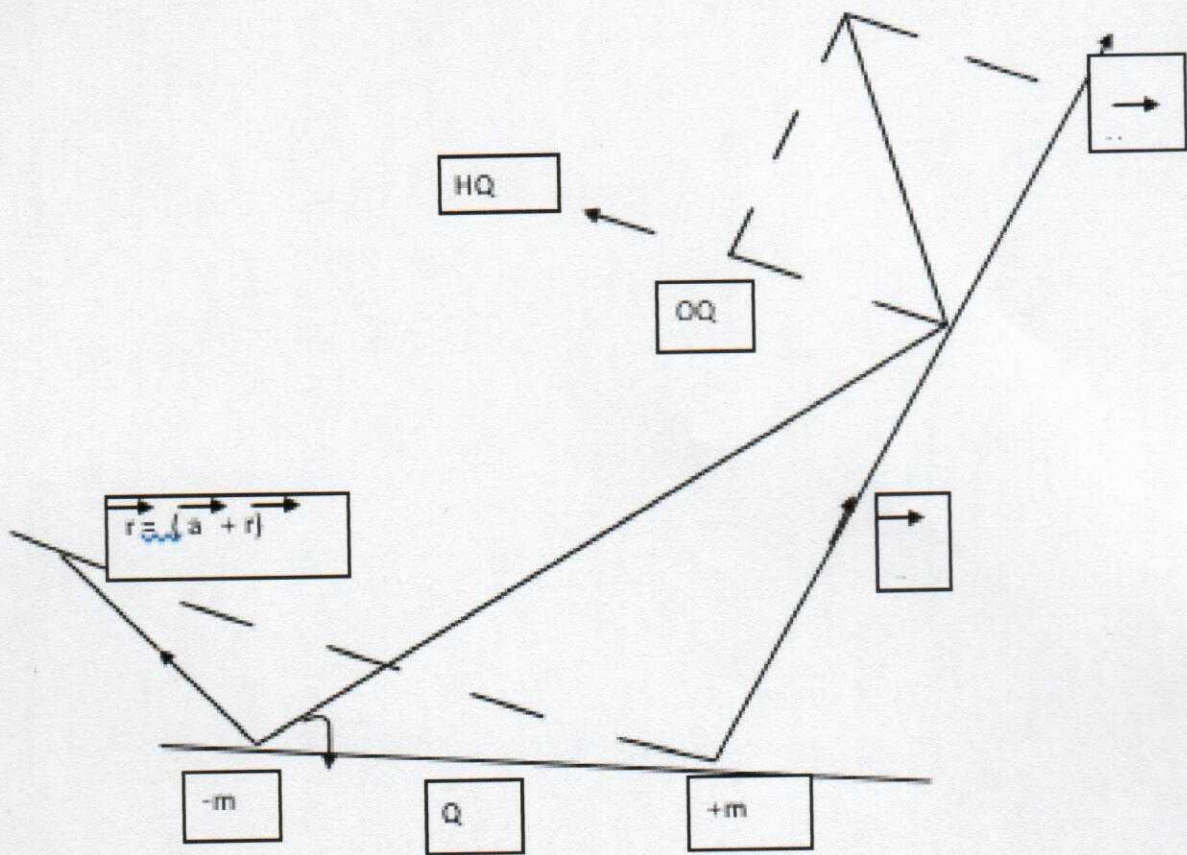


Figure 2.7: Intensity at a Point Due to A bar Magnet

$$T = \frac{M}{V}$$

2.37

Where, T = magnetic intensity

M = magnetic moment

V = volume

The SI unit of magnetic intensity is gamma. The body is said to be uniformly magnetized if "T" is constant and its direction is the same all through. A gamma is defined as 10^{-5} oersted and oersted being the magnetic intensity at a point that will exert a force of 1 dyne on a unit magnetic pole.

The intensity of the magnetic field on or above the earth surface is dependent upon the location of the observation point in the primary magnetic material. The intensity of the earth's undisturbed magnetic field ranges from a minimum of about 2500 gamma at the magnetic equator to more than 69,000 gammas near the pole.

2.2.2.3 The Magnetic Elements and Their Characteristics

A magnetic needle, at any point along the earth's surface is free to orient itself in any direction around a point at its center which will assume a position in space determined by the direction of the earth's magnetic field T at that point. This direction will be at an angle with the vertical and its horizontal projection will make an angle with the North-South direction. The measuring instrument in the magnetic observations responds only to resolve the total field T unto its horizontal component H (separated into X and Y projection and its vertical component as shown in Figure 2.8).

The angle which T makes with its horizontal component H is the inclination I and the angle between H and X (which by convention points North) is the declination D. The quantities X, Y, Z, D, I, H and T, known as magnetic elements are related as follows:

$$H = \cos I$$

2.38

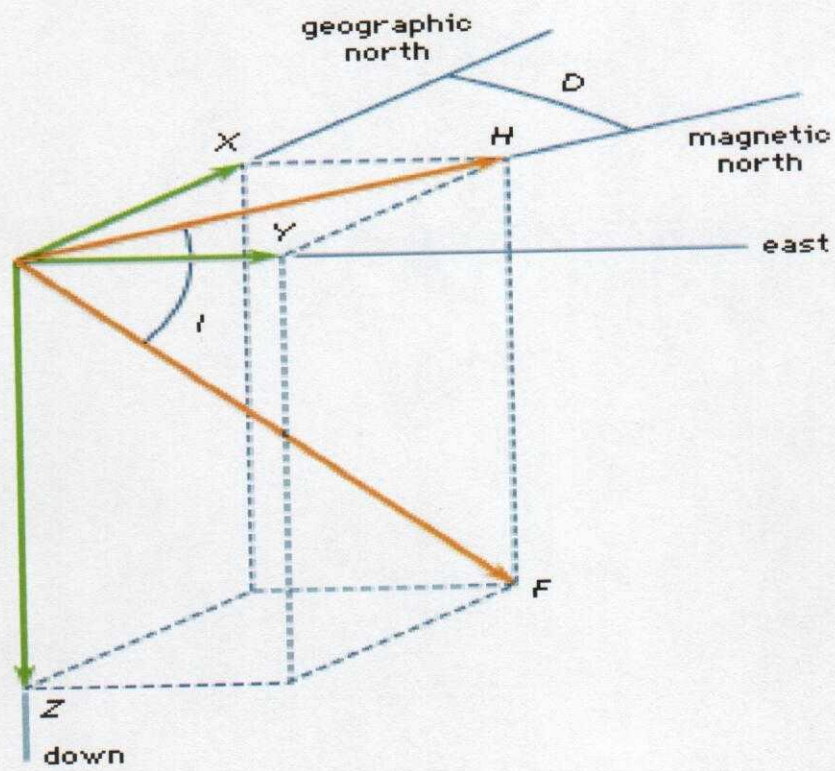


Figure 2.8: Element of the Earth Magnetic Field

$Z = T \sin i$ or $H \sin I$	2.39
$X = H \cos D$	2.40
$Y = H \sin D$	2.41
$H^2 = X^2 + Y^2$	2.42
$T^2 = H^2 + Z^2$	2.43
$T^2 = H^2 + Y^2 + Z^2$	2.44

The two points (in principle) on the earth's surface where the dip is equal to 90° are known as the dipoles. However, because of local anomalies there may be several points in the general polar region where the dip is vertical ($+90^\circ$). The earth's magnetic field resembles the field of a large bar magnet near its center. But unlike the field of a bar magnet, it does not vary in intensity with distance from the poles on the surface of the earth according to the inverse square law.

2.2.2.4 Magnetic Properties

Magnetic mineral content in a rock are of varying properties such as the magnetic susceptibility and remanent magnetization. The magnetic susceptibility is the measure of magnetic mineral content in a rock (Folami, 1980) given by:

$$K = \frac{J}{N \times 10^{-5}} \quad 2.45$$

Where,

J = Induced magnetization

N = Field strength

K = Susceptibility (Constant of proportionality depending on the material of the body).

This is called magnetic susceptibility per unit volume.

For an anisotropy crystal, the susceptibility along the three principal magnetic axis are different and the measurement on their power samples given the average of the three values. However, for isotropic crystals, the susceptibility is the same in all direction. Magnetic anomalies are by induced and remanent (permanent) magnetization. The induced magnetization refers to the

action of the field on the materials where in the ambient field is enhanced while the remanent magnetization is preserved in the rock and is dependent on the direction and the intensity on the earth's field at the time the rock last cooled. Though, the curie temperature of the magnetic mineral present in the rock, the remanent magnetization is of great importance in mapping and interpretation which often dominates the induced ore and should not be omitted so as to avoid errors in calculating the dip, breadth, and volume. In practice, residual magnetism often contributes to the total magnetization in rocks both in amplitude and direction. The effect is quite complicated because of dependence on magnetic history of the rocks.

2.2.2.5 The Geomagnetic Field

The earth magnetic field is a vector quantity with variable magnitude and direction defined over an almost spherical polarized sphere. Physically, the origin of the field seems to be a system of electric currents within the earth (Parasnis, 1979). The earth's field is not constant at any point on its surface but undergoes variation of different periods.

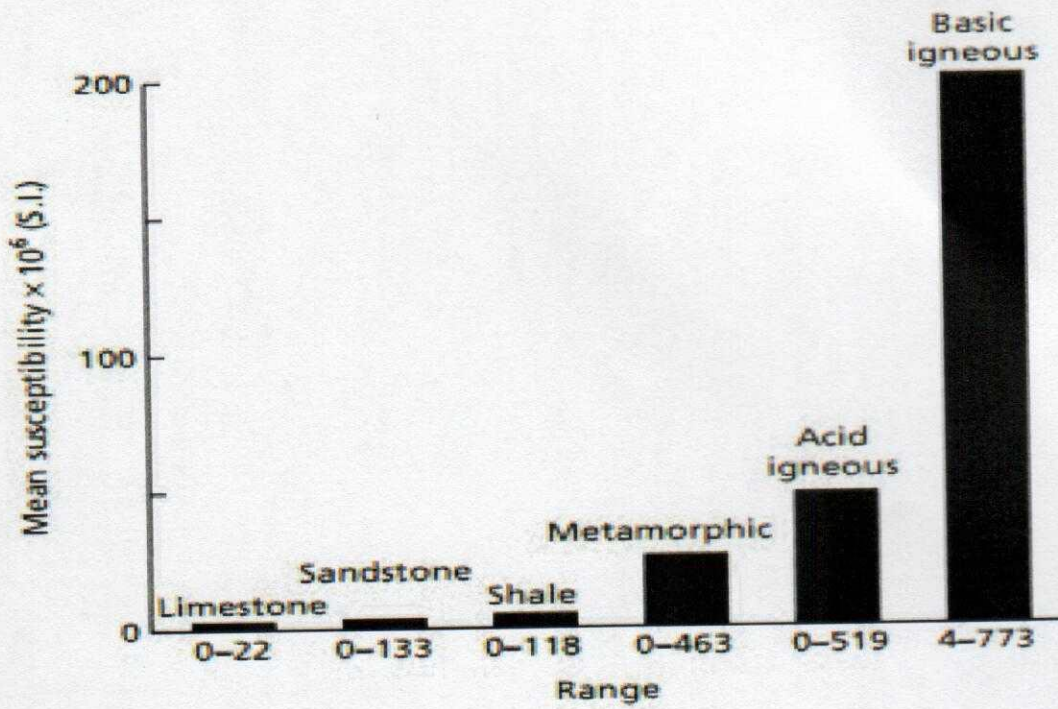


Figure 2.9: Histogram showing mean values and ranges in susceptibility of common rock types. (After Dobrin & Savit 1988)

It is established that the geomagnetic field is composed of two parts:

The Main Field: This is the field of internal origin not constant in time. It varies relatively slowly.

The External Field: This is a small fraction of the main field which varies rather rapidly, partly cyclically, partly randomly and originates outside the earth.

2.2.2.6 Limitation of Magnetic Survey

- **Secular Variation:** Changes in the earth magnetic field which occur over many years are called secular variation. From continuous observation at many stations one can conclude that secular are not regular and varies depending on the position and epoch. The cause may be attributed mostly to the internal phenomenon of the earth.
- **Diurnal Variation:** In addition to secular variation magnetic element changes within a period of 24hrs. The variations are not all that regular for each day but depend on the position of the observation and the day of observation. This effect is also called Solar Diurnal Variation. The Diurnal variation is usually corrected for from the observed magnetic values.
- **Magnetic Storm:** Sudden and violent variation in geomagnetic field which affect the magnetic reading. There is no satisfactory method of correcting it. The safest method is to discontinue the field and resume when the storm is over.

2.2.3 ELECTRICAL PROSPECTING METHOD

2.2.3.1 Basic Principles and Theory of Electrical Resistivity Method

Electrical resistivity prospecting method involves the passage of electric current (usually direct current or low frequency alternating current) into the subsurface, through two electrodes (the current electrodes). The potential difference is measured between another pair of electrodes, which may or may not be within the current electrodes depending on the electrode array in use.

Consider a current flowing in a cylindrical conductor of length, L , with cross-sectional area A , and current I , flowing through it (Figure 2.20).

The resistance R is expressed as:

$$R \propto \frac{L}{A} \quad 2.46$$

$$R = \rho \frac{L}{A} \quad 2.47$$

Where ρ is the constant of proportionality called resistivity.

However, from ohms law:

$$R = \frac{\Delta V}{I} \quad 2.48$$

By substituting for 'R' in equation (2.48)

$$\frac{\Delta V}{I} = \rho \frac{L}{A}$$

$$\frac{\Delta VA}{I} = \rho L$$

$$\therefore \rho = \frac{\Delta VA}{IL} \quad 2.49$$

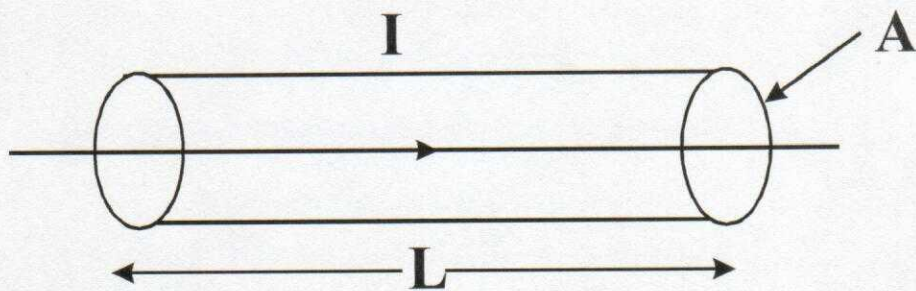


Figure 2.10: Schematic Diagram of the Flow of Current through a Cylindrical Model (Conductor).

Where; ΔV = Potential difference between any two points measured in volts. Equation (2.49) can be used to determine the resistivity of a homogeneous and isotropic medium provided the geometry is simple e.g. cylinder, cuboid, parallelepiped.

$$\rho = \frac{\lim_{L \rightarrow 0} \frac{\Delta V}{L}}{\lim_{A \rightarrow 0} \frac{I}{A}} = \frac{E}{J} \quad 2.50$$

Where, E is the electric field and J is the current density.

From Equation (2.50);

$$E = J\rho \quad 2.51$$

Imagine that the current source is located at the center of a spherical body (earth) of radius 'r' (Figure 2.20), then the current density at the spherical surface is:

$$J = \frac{I}{A} \quad 2.52$$

Where A = area of the spherical surface,

Given; $A = 4\pi r^2$;

$$J = \frac{I}{A} = \frac{I}{4\pi r^2} \quad 2.53$$

Substitute equation (2.51) into (2.53);

$$E = \frac{I\rho}{4\pi r^2} \quad 2.54$$

Since, E is the gradient of scalar potential;

$$E = -\Delta V = \frac{-\delta V}{\delta r} \quad 2.55$$

Equating equations (2.54) and (2.55);

$$\delta V = \frac{-I\rho\delta r}{4\pi r^2} \quad 2.56$$

Taking the integral of both sides:

$$V = \frac{I\rho}{4\pi r} \quad 2.57$$

In practice the earth surface structure is taken as an approximate hemisphere (Figure 2.22). The current density (J) is defined as:

$$J = \frac{I}{A} \quad 2.58$$

The area of a hemisphere is $2\pi r^2$, thus

$$J = \frac{I}{2\pi r^2} \quad 2.59$$

$$E = \frac{I\rho}{2\pi r^2} \quad 2.60$$

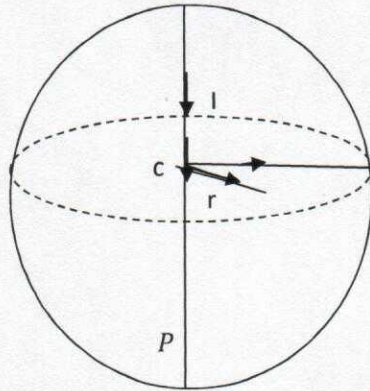


Figure 2.11: Current Source on a Spherical Surface

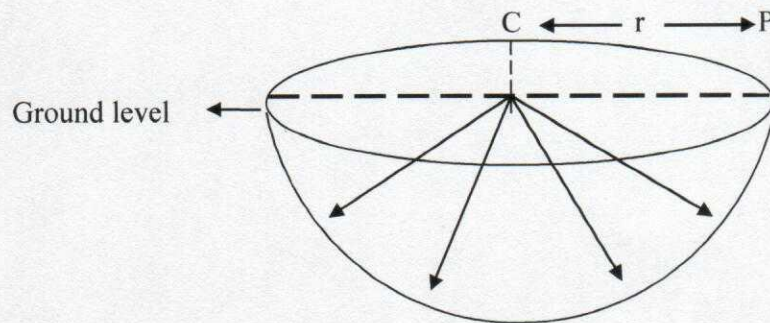


Figure 2.12: Current Source at the Hemispherical Surface

2.2.3.2 Generalized Apparent Resistivity Equation

Consider the diagram in Figure 2.21; it illustrates a simple current source at the surface of the earth. The potential 'V' is at a distance 'r' from the current source.

The potential at point P₁ due to current at point C₁ at the earth's surface is given as:

$$V_{11} = \frac{\rho I}{2\pi r_1} \quad 2.60$$

The potential at P₁ due to current at C₂ is given at

$$V_{12} = \frac{-\rho I}{2\pi r_2}$$

The potential (V_{11, 12}) at an interval electrode P₁ is the sum of the potential contribution V₁₁ and V₁₂ from the current source C₁ and the source C₂, that is

$$V_{11, 12} = V_{11} + V_{12}$$

$$V_{11, 12} = \frac{\rho I}{2\pi r_1} + \frac{-\rho I}{2\pi r_2}$$

$$V_{11, 12} = \frac{I\rho}{2\pi} \left[\frac{1}{r_1} - \frac{1}{r_2} \right]$$

But in practice, four electrodes are usually used in resistivity survey as shown in Figure 2.24.

2.2.3.3 Electrode Configurations

There are several types of electrode configurations used in electrical resistivity method.

Generally four electrodes are used in resistivity survey and the common electrode arrays are:

- i. Wenner Array
- ii. Schlumberger Array
- iii. Dipole-dipole Array
- iv. Pole-dipole Array
- v. Pole-pole Array.
- vi. Square Array.
- vii. Gradient Array.
- viii. Lee Partition Array

Wenner Electrode Array

Wenner array utilizes four electrodes system that are collinearly arranged with uniform spacing between them as shown in Figure 2.15. The potential electrodes are fixed in between

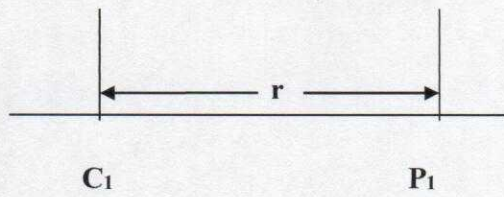


Figure 2.13: A Simple Current Source

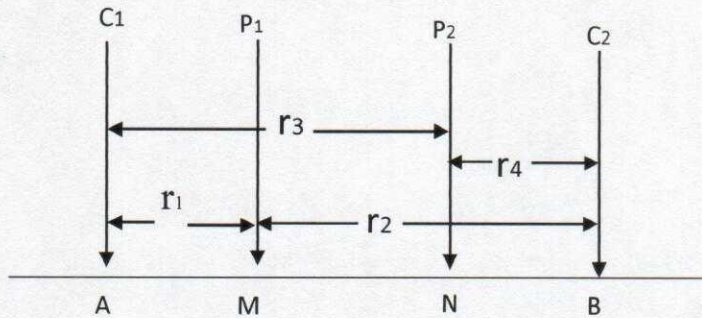
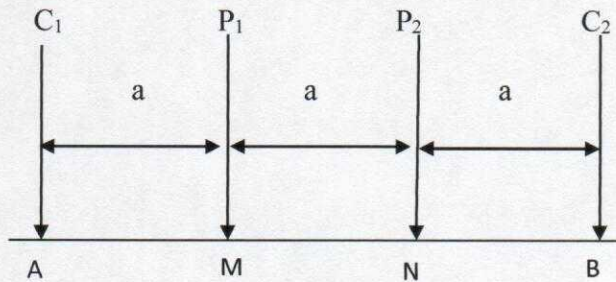


Figure 2.14: Array Configuration for Generalized Apparent Resistivity Equation.



Where AB = Current Electrode Distance
 MN = Potential Electrode Distance
 AB = MN = a

Figure 2.15: Typical Wenner Configuration

the current electrode, that is, the current electrodes are at both ends. The apparent resistivity equation for wenner array is derived as:

$$\rho_a = 2\pi R \left[\frac{1}{AM} - \frac{1}{MB} - \frac{1}{AN} + \frac{1}{NB} \right]^{-1}$$

If $AM = a$, $MB = 2a$, $AN = 2a$ and $NB = a$:

Hence, substituting them into Equation (2.41)

$$\rho_a = 2\pi R \left[\frac{1}{a} - \frac{1}{2a} - \frac{1}{2a} + \frac{1}{a} \right]^{-1}$$

$$\rho_a = 2\pi R \left[\frac{2 - 1 - 1 + 2}{2a} \right]^{-1}$$

Schlumberger Electrode Array

Schlumberger electrode array also utilizes four electrodes system like Wenner array but they are arranged linearly with different inter-electrode spacing as shown in Figure 2.15. The electrodes are arranged such that the distance AB between the current electrodes is greater or equal to five times the distance MN, between the potential electrodes. The potential electrodes are fixed about the data station in which the current electrodes are spread until the required maximum separation is attained.

The apparent resistivity equation for Schlumberger array is derived as:

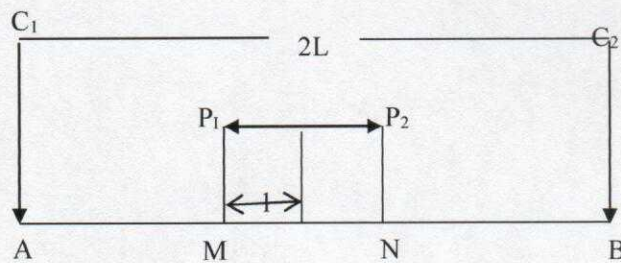
$$\rho_a = 2\pi R \left[\frac{1}{AM} - \frac{1}{MB} - \frac{1}{AN} + \frac{1}{NB} \right]^{-1}$$

$$\text{If } AM = L - 1$$

$$MB = L + 1$$

$$AN = L + 1$$

$$NB = L - 1$$



Where: AB = Current Electrode Distance

MN = Potential Electrode Distance

AB = $2L$

MN = $2l$

$AB \geq 5MN$

Figure 2.16: Typical Schlumberger Configuration.

Dipole-Dipole Electrode Array

Dipole-Dipole Electrode Array also makes use of four electrodes with two potential electrodes outside the current electrodes (Figure 2.17). The potential electrodes would move "n" times before the current electrode were moved. The potential difference of the current passed into the earth sub-surface is measured from the response of the two potential electrodes

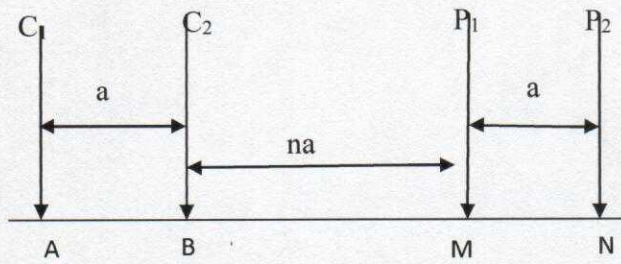


Figure 2.17: Dipole-Dipole Configuration

2.2.3.4 Field Procedure

There are three main field techniques used in electrical resistivity survey. These are;

- i. Horizontal Resistivity Profiling (HRP),
 - ii. Vertical Electrical Sounding (VES),
 - iii. Combined Horizontal Profiling and Vertical Electrical Sounding (VES).
- i. **Horizontal Resistivity Profiling (HRP):** This involves the use of fixed electrode spacing/between the four electrodes which is moved across area of interest to determine the resistivity of each station. It is mostly used to determine lateral variation in resistivity with respect to a fixed depth. Array type usually used is Wenner Array and results are presented as profiles. It is used to map 2D bodies.
 - ii. **Vertical Electrical Sounding (VES):** it is used to map vertical variation in electrical properties beneath the earth surface with respect to a fixed center of the array. The survey is carried out by gradually increasing the electrode spacing about a central position whose vertical resistivity variation is sought. Resistance measurements are made at each expansion and multiplied by the respective geometric factor (K) to give the resistivity. The depth of investigation is dependent on the electrode spacing (expansion). It can be used to map the depth to bedrock and delineate aquifers. Array types used include: Wenner, Schlumberger and Dipole-dipole array. Results are presented as depth sounding curves.
 - iii. **Combined Horizontal Profiling and Vertical Electrical Sounding (VES):** Measurement is done in two dimension but in a vertical sense or section. Electrode spacing are increased on the field in such a way that measurements are taken both laterally and vertically. The data can be inverted (modeled). Array types usually used include: Dipole-Dipole and Pole-Dipole. Results are presented as presented as pseudosections.

2.2.3.5 Field Operational Problems

- i. **Lateral In-homogeneity:** This usually degrades the quality of resistivity data. The problem could be reduced by using multiple electrodes or mechanical smoothing.
- ii. **Poor Electrical Contact:** This could lead to acquisition of erroneous data especially if the poor contact is at current electrodes position. It may be due to a very dry ground surface. The problem could be solved by creating saline water medium around the electrodes or watering the electrode positions.
- iii. **Dip Effect:** In a situation where the interface is dipping, the quality of data is seriously affected likewise the interpretation. However, if the dip angle is less than 45° the effect is negligible.
- iv. Cable Leakages.
- v. Cultural and Geological Noise such as fences, topography, etc.

CHAPTER THREE

MATERIALS AND METHODS OF STUDY

3.1 MATERIALS

During this research work, both geophysical methods and physico-chemical studies of some water samples were employed. The equipment used in carrying out the geophysical investigations involving the Very Low Frequency Electromagnetics Method (VLF-EM); Magnetic Prospecting Method and Electrical Resistivity Method were the ABEM WADI Terrameter, Proton Precision Magnetometer and Campus Resistivity meter respectively. Other materials used during this work were;

- Hammer
- Connecting Cable
- Stop watch
- Crocodile Clip
- Global Position System
- Compass Clinometer
- Note pad
- Electrodes
- Tape-rule
- Tag-line
- Safety kits
- Cutlass
- Digital Camera
- Calculator
- Car battery
- pH meter



Figure 3.1: Image showing an electrical resistivity meter



Figure 3.2: Image showing a pH meter



Figure 3.3: ABEM-WADI VLF-EM Equipment

HAMMER: This was used in driving down the electrodes into the ground at the respective electrode positions during investigations.

TAPE RULE: This was used to measure horizontal distance between stations or traverses and distance between electrode separations.

CONNECTING CABLES: In the electrical resistivity data acquisition, four connecting cables were used to pass electric current from the Campus resistivity meter into the subsurface. The connecting cables are attached to crocodile clips which are then attached to the electrodes mounted into the ground. Two connecting cables are connected to the potential electrode while the remaining two are attached to the current electrode.

ELECTRODES: These are steel metal rods which are about half a meter in length so that it can be driven into the ground firmly for good electrical contact. Four were employed in the survey; two electrodes were used for sounding the current into the ground and the other two for potential difference.

GLOBAL POSITIONING SYSTEM (GPS): It was used to measure the longitude and latitude (Eastings and Northings, UTM), elevation (above sea level), data points and important features in the study area.

COMPASS CLINOMETER: This instrument was used in determining the traverse direction/azimuth in the study area.

STOP WATCH: The stop watch was majorly used during the magnetic survey in the dumpsite. It was used to measure and know the time at which readings were collecting at each stations of the seven traverses outlined.

CROCODILE CLIPS: This is a metallic clip with a crocodile mouth. They were used to connect the connecting cables to the electrodes mounted into the ground.

CUTLASS: This was used to clear path ways for traverse lines in the study area.

NOTE PAD: This was very much needed as it was used in the take down the readings of the data acquired on the field.

DIGITAL CAMERA: It was to take the pictures of important features in the study area like stream, dumps. It was also used in taking the pictures of the electrode configuration layouts.

CALCULATOR: It was used majorly in the resistivity data acquisition for multiplying the resistivity values of each station with the geometric factor to give the apparent resistivity.

BATTERY: Different kind of batteries were used during this research work. A car battery was used to power the electrical resistivity meter. The ABEM WADI terrameter has a battery that is attached the ABEM kit. The GPS also make use of a battery to operate.

pH METER: This equipment was used to test the power of hydrogen of the water samples. It enabled us to know the level of acidity and alkalinity of the water samples.

3.2 METHODOLOGY

Some geophysical methods of survey and physico-chemical analysis of some water samples were employed during this research work.

The geophysical methods employed were;

- Very-Low Frequency Electromagnetics method (VLF-EM)
- Magnetism Prospecting method and the
- Electrical prospecting method

3.2.1 VERY-LOW FREQUENCY ELECTROMAGNETICS METHOD

3.2.1.1 Data Acquisition

The VLF-EM measurements conducted in the dumpsite were made with an ABEM WADI terrameter with an operating frequency ranging from 25.2 to 25.5 KHz. This method majorly served as a reconnaissance tool for detecting conductive zones and subsurface structures in the study area. Seven traverses were established during the course of this study with a station interval of 5 meters for the VLF-EM data acquisition. Five of these traverses were established

within the perimeter of the dumpsite while the other two were established along a hand-dug well in the village (Ebira Village) outside the dumpsite. Traverses 1, 3, 5 and 7 were established perpendicular to the general strike of the target while traverses 2, 4 and 6 were established in the NW-SE direction. The lengths of the traverses were 105m at maximum and 50m at minimum. A total of 104 station positions were occupied for the VLF profiling. The WADI VLF-EM equipment detects the ratio (in percentage) between the vertical and horizontal components of the EM signal. The primary field is horizontal; the normal reading on the WADI will be zero even when horizontal lying conductors are present. The VLF method is very sensitive to small changes in ground conductivity.

3.2.1.2 Data Processing

The VLF data obtained were filtered using a Karous-Hjelt filter. Also by plotting of the filtered real and filtered imaginary components against distance using Microsoft Excel package while the corresponding Karous-Hjelt (K-H) pseudo sections of the profiles are shown in Figures 4.1b to 4.7b respectively. The Karous-Hjelt filter computes the approximate subsurface current density giving rise to a given profile of data, and the values are relative across the profile. The output of the Karous-Hjelt filter is relative current density versus surface position at a chosen depth. Lower values of relative current density correspond to higher values of resistivity. Interpretations were done normally by considering the high amplitude signal, which is diagnostic of weathered or fractured zones. The double plots of the filtered real and filtered imaginary enable qualitative identification of linear features.

The VLF data, i.e. (real and imaginary components) of the EM fields measured was subjected to Fraser (1969) filtering to increase the signal to noise ratio of the data set and enhance the anomaly signature. The Fraser Filter (Q) was computed using a filter operator as shown in the following relation:

$$Q = (Q_4 + Q_3) - (Q_2 + Q_1)$$

Where Q is EM data and the subscript are station positions.

This was applied to the real component VLF data to transform the data set to the filtered real VLF data (Karous and Hjelt, 1983). The filtered real transform every genuine crossover or inflection points of the real anomaly to positive peaks while reverse cross over become negative peaks.

3.2.1.3 Data Interpretation

Interpretation is done by considering the high amplitude signals, which is diagnostic of weathered or fracture zones. The double plots of the filtered real and filtered imaginary components enable qualitative identification of the top of linear features i.e. points of coincident of crossovers and positive peaks of the real and filtered anomaly. From these plots Figures 4.1b to 4.7b, minor linear features suspected to be faults/fractured zones (plumes) were identified which were used to pick points for VES survey. These suspected geological interfaces delineated from the profiles were shown occurring at varying distances on the profiles. These positive peaks mapped on the filtered real are zones of interest in groundwater contamination which show the contaminant plume as a resistivity low surrounded on both sides by materials of higher resistivity. The asymmetry of these conductive anomalies suggests that the conductive structures are dipping. Also, the anomaly patterns exhibit varying amplitudes, which are controlled by depth of the body to the surface, its geometry, and attitude.

3.2.2 MAGNETIC PROSPECTING METHOD

The magnetic method was also used during the course of this research work to determine contact zones, faults, fractures, shear zones and also to delineate the depth to bedrock. This geophysical method was employed to complement the Very-Low Frequency electromagnetic results. It is important to note the following precautions before and while taking the readings;

- Steel and other ferrous metals in the vicinity of a magnetometer can distort the data. Large belt buckles, etc., must be removed when operating the unit.

- A compass should be more than 3 m away from the magnetometer when measuring the field.
- A final test is to immobilize the magnetometer and take readings while the operator moves around the sensor. If the readings do not change by more than 1 or 2 nT, the operator is "magnetically clean." Zippers, watches, eyeglass frames, boot grommets, room keys, and mechanical pencils can all contain steel or iron. On very precise surveys, the operator effect must be held under 1 nT.
- To obtain a representative reading, the sensor should be operated well above the ground. This procedure is done because of the probability of collections of soil magnetite disturbing the reading near the ground.

3.2.2.1 Data Acquisition

A precision magnetometer type Geometric model G.856 was used for the survey. A base station was located on point 1 of the study area in order to have a base station reading for which other reading in the study area will be referenced to, usually the survey exercise started very late in the day and efforts were made to minimize man made noise but taking profile perpendicular to such interference.



Figure 3.4: Input and output unit of a proton precision

The seven traverse lines established for the magnetic data acquisition were the same seven traverse lines established for the Very-Low Frequency electromagnetic method. Five of these traverses were also established within the perimeter of the dumpsite while the other two were also established along a hand-dug well in the village (Ebira Village) outside the dumpsite. Traverses 1, 3, 5 and 7 were also established perpendicular to the general strike of the target while traverses 2, 4 and 6 were also established in the NW-SE direction. The lengths of the traverses were 105m at maximum and 50m at minimum. A total of 104 station positions were occupied for the magnetic profiling. At the beginning of the survey, a base station away from the station position was known. At each station, the time, as well as any relevant topographic or geological information observed was recorded. At the end of the magnetic survey, a final reading was made at the base station.

3.2.2.2 Data Processing

A magnetic survey involved data reduction technique because of instrumental drift amongst others. Softwares such as Euler Deconvolution and Sulpher 10 were employed for the processing. The automated Euler deconvolution was used to estimate the depth to bedrock. Therefore, the data obtained in the study area were subjected to drift correction after which a three point moving average filter was used to smoothen the data. The relative magnetic values obtained are the difference in the filtered corrected magnetic reading and the base station reading. The drift can be calculated as follows.

Calculation of Drift

Drift Correction = (Final BS Reading – Initial BS Reading) / Time Taken (s)

Instrumental Drift: Drift is the difference in base reading per changes in its time (in seconds) multiplied by the time interval between the successive station reading and the initial base reading. The unit is gamma.

Drift Corrected Magnetic Reading: The difference between the average observed reading and drift. The unit is gamma.

Filter Drift Corrected: This is the three point moving average. The unit is gamma.

Relative Magnetic Intensity: The difference between the initial base station reading and the filter drift corrected.

3.2.2.3 Data Interpretation

The interpretation of magnetic anomalies utilizes the natural potential field based on the inverse square laws of attraction. There are several differences which increase the complexity of magnetic interpretation.

The magnetic anomaly of a finite body invariably contains positive and negative elements arising from the dipolar nature of magnetism. The intensity of magnetisation is a vector and the direction of magnetisation in a body closely controls the shape of the anomaly. Thus bodies of similar shape can give rise to very different anomalies. The intensity of magnetisation of a body depends on the amount, size, shape and distribution of its contained ferromagnetic minerals and this represents only a small portion of its constituents. It can vary by a factor of 10^6 between different rock types.

Magnetic anomalies are independent of the distant units employed, for instance, the same magnitude anomalies is produced by, say, a 3m cube [on a meter scale] as a 3km cube [on a km scale] with the same magnetic properties. One of the major ambiguities in the interpretation of magnetic data is the inverse problem.

The magnetic anomaly profile or contour obtained and displayed at this stage is rightly assumed to be due ONLY to the response from the magnetic properties displayed by subsurface rocks. Whatever deductions that are made or calculated are then the interpretation of the presence or absence of magnetic rocks.

Qualitative Interpretation

For most purposes, the magnetic anomaly profiles are generally interpreted in the form of noting and describing areas of high/positive and low/negative magnetic anomalies and also the amplitude of these anomalies and their extent along measurement profile line.

In the case of the magnetic anomaly contour presentation (Figure 4.7 to 4.13) it is necessary to:

- ✓ Note the areas of high magnetic gradient (closely packed contour lines) and areas of low magnetic gradient (sparse distribution of contour lines]
- ✓ Identify the trend (attitude/pattern) of the contour and their closures (if any).
- ✓ Describe the trend noted and figure whether this trend so identified agrees with known geology or suspected feature.

Quantitative Interpretation

Magnetic anomaly data presented in a profile form can directly be interpreted, although total field data is usually complex to interpret as this may include both the desired induced magnetization and the undesired remnant magnetization. This is one of the reasons we use a drift corrected relative magnetic reading for profile presentation and quantitative interpretation.

In the case of magnetic anomaly contours, a section or sections are usually chosen across the contour in a direction usually intended to cross an identified feature perpendicularly (if possible). When the chosen section is plotted, a profile anomaly is obtained and interpreted.

In the absence of other information, the interpretation of a magnetic anomaly is a process of developing graphical models of a hypothetical subsurface structure of assumed magnetic properties, calculating the magnetic anomaly that would be produced. The model is then adjusted until it fits the measured magnetic data as closely as possible

Inverse problem

Although it is relatively easy to calculate the magnetic anomaly caused by a structure of known shape and magnetic character, there is no unique solution to the reverse problem of calculating the shape and magnetic properties of a subsurface structure from the anomaly if no other information about it is available. This ambiguity represents the inverse problem of potential field interpretation, which states that although the anomaly of a given body may be calculated uniquely; there are an infinite number of bodies that could give rise to any specified anomaly. If magnetic measurements can be combined with another geophysical technique, then interpretation may become more precise.

Approximate Interpretation

As stated above, the calculation of the depth and dimension of a causative body directly from a magnetic anomaly is only feasible if a given geometrical shape is assumed as the causative body. If a sphere is assumed to be the causative body of a given magnetic anomaly, the Half-width method can be used to estimate the depth of burial to the centre of source (Z_c).

$$\begin{aligned} X_{1/2} &= 0.75 Z_c \\ Z_c &= 1.33 X_{1/2} \end{aligned} \quad (3.1)$$

Peter's slope can also be utilised for these estimates of depth:

$$Z_c = 0.63S \quad (3.2)$$

S = Peter's slope which is the horizontal distance between the positive and negative peaks of the anomaly.

Equations 3.1 and 3.2 are valid only for the vertical components of the field (H_z).

For Horizontal components (H_h) equation 3.1 and 3.2 become

$$Z_c = X_{1/3}$$

$X_{1/3}$ is half-width of the anomaly at the point of one third value of the anomaly maximum.

$$Z_c = 0.67S$$

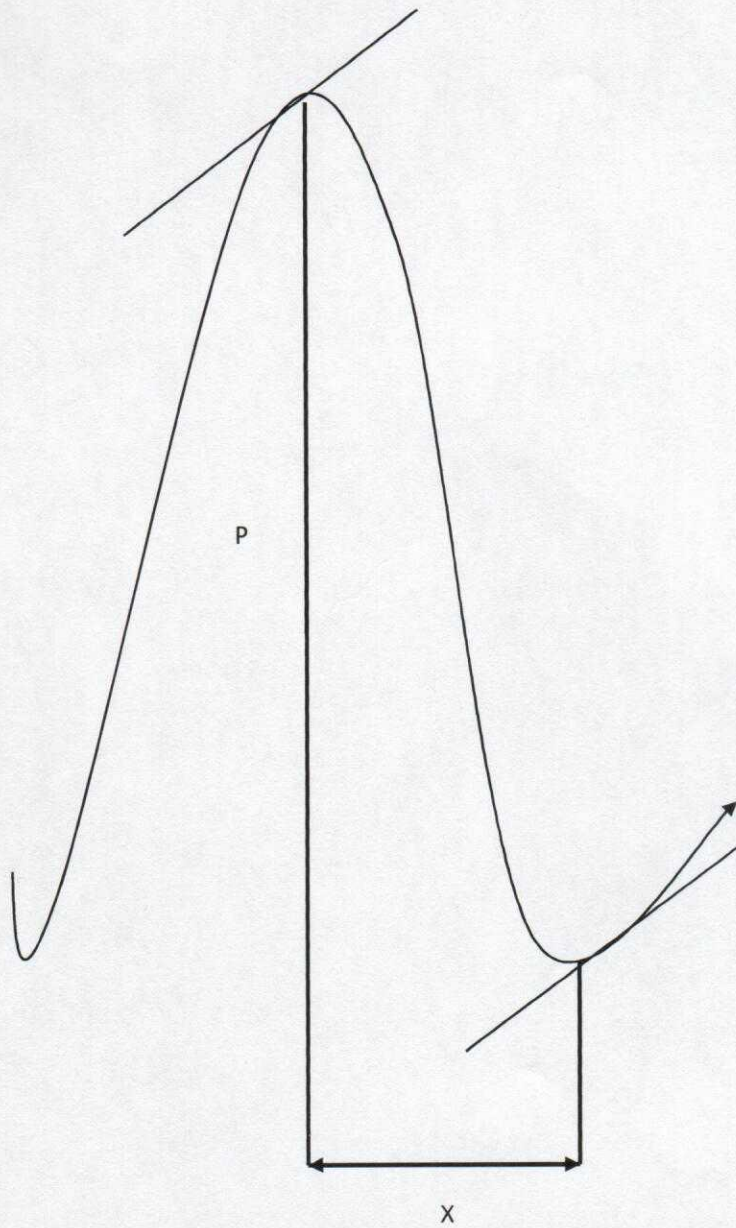


Figure 3.5: Schematic Diagram Showing Half Slope Method of Estimating Depth

$$P = X * K$$

Where P is the depth and K is a constant with a value of 0.63 for half slope method

3.2.3 ELECTRICAL RESISTIVITY METHOD

The electrical resistivity method investigates subsurface conditions by passing an electric current (I) into the ground through a pair of electrodes called current electrodes while the resulting potential difference (Δv) arising from the current flow is measured through a pair of electrode called potential electrodes which may or may not be located within the current electrode pair. The ground resistivity value is obtained from parameter I, Δv and the geometric factors of the electrode array used.

In this study, Dipole-dipole and vertical electrical sounding (VES) using Schlumberger array were adopted in order to investigate the changes of electrical resistivity laterally and vertically.

The equipment employed for the resistivity field data measurements was the CAMPUS RESISTIVITY METER.

3.2.3.1 Data Acquisition

Dipole-dipole geophysical technique was implemented along some of the traverses established for both electromagnetics and magnetic survey in order to measure the ground apparent resistivity both laterally and vertically. Of the seven traverses established for VLF-EM and Magnetics, only five traverses were established for the dipole-dipole configuration with the following spread length: Traverse 2 at 95m Traverse 3 at 95m; Traverse 4 at 105m; Traverse 6 at 65m and the control point at 65m. These traverses were designed with a station interval of 5m. The two current electrodes were hammered first then the two potential electrodes, the distance between the inner current electrode and inner potential electrode varied while other electrode were equidistance. The potential electrodes were moved 5 times that is $n=5$ before the current electrodes were moved. Moreover, current were passed into the subsurface through

electrode and cables. The resultant resistances read off from the resistivity metre were multiplied with the geometric factor G for dipole-dipole configuration to give the apparent resistivity.

The vertical variation in ground apparent resistivity values are measured with respect to a fixed centre of array. The survey is carried out by gradual increase in the electrode spacing with respect to the centre of the electrode array. The Schlumberger array is commonly used. Seventeen schlumberger vertical electrical sounding (VES) measurements were conducted with a maximum spread length of 105m of AB. Fifteen vertical electrical sounding were carried out in the dumpsite. Two parametric soundings were also carried, one in the village while the other was carried out at the control point situated at about 1 km away from the dumpsite.

Half schlumberger configuration was carried out on eight ves points due to insufficient space to accommodate a full schlumberger configuration.

3.2.3.2 Data Processing

The data acquired through the dipole-dipole technique was processed through the use of a computer software known as Dippro. The data are then presented as pseudo section. The resistivity value are plotted at the point of intercession and then contoured to give a pseudo section. The result is in the form of 2-Dimension. The pseudo section measures the resistivity of the subsurface with respect to both the lateral inhomogeneity and depth of the interface. The Dipole-Dipole profile gives the Field Data Pseudo-sections, Theoretical data pseudo-sections and the 2-D Resistivity structure. The computer program is used to determine the resistivity of the blocks so that the calculated apparent resistivity values agree with the measured values from the field survey. The computer program automatically subdivides the subsurface into a number of blocks and uses a least-squares inversion scheme to determine the appropriate resistivity value for each block. The location of the electrodes and apparent resistivity values value was entered into a text file which can be read by the DIPPRO program.

A pseudosection contour is obtained. Here, the horizontal location of the point is placed at the midpoint of the electrodes used to make that measurement. The vertical location of the plotting point is placed at a distance which is proportional to the separation between the electrodes.

For vertical electrical soundings data, plotting the apparent resistivity values against half the current electrode separation ($AB/2$ or half the spread length) at each station on a bi logarithmic (log-log) graph sheet yielded the Depth Sounding Curves. Partial curve matching of field curves with relevant Schlumberger developed master and auxiliary curves were carried out to obtain the layer resistivity values and corresponding thicknesses. Before the availability of personal computers, the curve-matching process was done graphically by plotting the field data plotted on transparent log-log graph. The use of standard curves requires an identification of the curve type followed by a comparison with standard curves of that type to obtain the best match. Geo-electric parameters from this manual interpretation were improved upon through the use of computer iteration technique using the computer algorithm. Two layers and three layers curve can be used for complete interpretation of VES curves of more layers by the Auxiliary Point Method, which requires the use of a small set of auxiliary curves and some construction. In the iterative forward modeling application, the manually obtained curves were used as starting model.

The sounding curves are classified into different types on the basis of layered resistivity combinations. We have four primary curve types which are; H, K, Q and A.

3.2.3.3 Data Interpretation

The major interpretation of dipole-dipole processed data was done using the 2-D Resistivity structure. The various color shown by the image profile depicts the conductivity and resistivity nature of the subsurface. Generally, the blue color indicates conductive zones, while the Red and yellow colors indicate resistive zones. The more the blue color, the more conductive (weak or fractured) the area is, and vice versa. I.e. the scale is from conductive to more resistive areas.

The observed VES curves (H, HA, HK, and KH) were interpreted quantitatively by partial curve matching and computer assisted 2-D forward modeling using Win Resist 1.0 software.

3.2.4 PHYSICO-CHEMICAL ANALYSIS

The decomposition of landfilled wastes by long-term physico-chemical, chemical notably hydrolysis, hydration, carbonation, oxidation and solution and biological degradation mostly microbial processes cause the dissolution or deterioration of landfill materials, gas generation and production of leachate. Landfill sites provide ideal environments for bacterial colonies to grow since nutrients availability, and substrate composition and temperature requirements are met and most bacteria flourish in the aerobic condition above the groundwater table e.g. Fang, 1995b. Initially, the microbial degradation of landfill materials occurs under aerobic conditions. As the oxygen becomes depleted by the microbial activity, anaerobic conditions rapidly set in and the biodegradation of organic materials becomes anaerobic. Methane gas is generated bacterially from the abundant organic materials under the prevailing anaerobic conditions. Although it is now widely required in land filling that refuse be dynamically compacted to minimize volume and then covered by a thin layer of soil or clayey seal to minimize wind dispersion at the end of each operative day, rainwater ingress commonly takes place in wet seasons during landfilling and for capped sites, through cracks in the cover and along contact points between fill and host material. Infiltrating rainwater, groundwater, or other liquids disposed of within the wastes will dissolve some soluble mineral constituents of the landfill once the absorbent or field capacity of the fill is exceeded and free drainage of water can occur.

This leaching process may remove the common mineral elements such as calcium, magnesium, potassium, nitrogen and phosphorous or remove the bonding materials e.g. clay resulting in changes in matrix cement or the ion concentration within the landfill-pore water system and consequently causing significant physical property changes. The ion exchange reaction,

speeded up by bacterial activity, also causes changes to the structure and composition of the landfill-pore water system. For example, hydrogen sulphide may be converted to sulphuric acid, methane gas may become converted to carbon dioxide and water by microbial metabolism while the carbon dioxide by-product may combine with water to form carbonic acid. The resulting liquid termed leachate is rich in fungi, bacteria, inorganic salts and organic matter; but the compositional trend may be water and dissolved inorganic salts, water and dissolved organic wastes and organic fluids, or simply organic acids depending on the availability of solvent and solute types in the leached mass.

In terms of availability of solute types, the bottom ash residues from urban solid waste incinerators contain considerable amounts of leachable heavy metals lead, zinc, cadmium, copper, and chromium and salts Bahout et al., 1995, and this will be reflected in the composition of leachate derived from such deposits. If pyrite is available in wastes containing mine tailings, it may be oxidized to sulphuric acid while the decomposition of vegetation may produce organic acids. PCBs have low solubility in water, and if present in the landfilled wastes, we can expect low concentrations of PCBs in the leachate dissolved phase, but they are more likely to occur in solid organic matter or in the oil fraction. Since higher volumes of water would have passed through poorly compacted waste materials in old landfill sites compared to modern compacted landfills, there should be relatively lower concentrations of chemical constituents in leachates derived from old landfills with efficient migration processes Radnoff et al., 1992. Note that for poorly consolidated or uncompacted wastes at shallow burial depths, and with inadequate capping, the absorbent or field capacity may be achieved within only a few years following initial waste emplacement, thus allowing early generation of leachate. For well compacted and deeply buried wastes with low permeability capping, the field capacity may not be achieved until after several years, but the waste compression process may facilitate early formation and expulsion of leachate from the lower layers of waste into the substrate

Lewin et al., 1997. Note also that the decomposition of organic and inorganic solids will be associated with a fill volume change causing shrinkage or swelling.

In general, the pore fluids produced from landfill are mostly acidic, but will vary in composition from country to country, community to community and with season. Bacteriogenic methane is formed by fermentation of organic material in conditions of depleted oxygen supply, and for a given leachate, a number of chemical changes occur as it evolves from the aerobic acetogenic stage to the anaerobic methanogenic stage Robinson, 1989; the total organic content TOC, total free fatty acids content or acetone content and TDS are high during acetogenesis and low during methanogenesis. That is, the composition of the leachate will change as the refuse in the landfill ages Farquhar, 1989. In general, the leachate from a young landfill may be characterized by high levels of organic acids, ammonia and TDS, but as much of the biodegradable mass is broken down with time, the concentrations of these parameters will decrease in the leachate produced from the ageing landfill see Table 4. The leachate may contain toxic or hazardous substances in solid or gaseous forms and might show up as high concentrations of chloride, iron and zinc ions. Those elements with high ionic mobility generally have the highest concentration whilst those having low mobility usually have the lowest concentration in leachates Bagchi, 1987. The pH tends to increase with time i.e., from an initial acidic state to a neutral state while the biological and chemical oxygen demands BOD/COD decrease with age see Table 4. The concentration of organic carbon often exceeds 8000 mg/l in the leachates

Table 3.1

Typical changes in leachate concentrations with age of refuse (after Farquhar, 1989; Birks and Eyles, 1997). All quantities are in mg/l except pH (in standard units)

Parameter	Age of refuse			
	0-5 years	5-10 years	10-20 years	> 20 years
TDS	10 000-25 000	5000-10 000	2000-5000	< 1000
pH	5-6	6-7	7-7.5	7.5
BOD	10 000-25 000	1000-4000	50-100	< 50
COD	15 000-40 000	10 000-20 000	1000-5000	< 1000
Ammoniacal N	500-1500	300-500	50-200	< 30
Total P	100-300	10-100		< 10
Chloride	1000-3000	500-2000	100-500	< 100
Sulphate	500-2000	200-1000	50-200	< 50
Calcium	2000-4000	500-2000	300-500	< 500
Sodium + potassium	2000-4000	500-1500	100-500	< 100
Magnesium + iron	500-1500	500-1000	100-500	< 100
Zinc + aluminium	100-200	50-100	10-50	< 10
Alkalinity	10 000-15 000	1000-6000	500-2000	< 500

from young landfills and 465 mg/l in leachates from old landfills Dearlove, 1995.

The composition of the leachate will depend on the type and age of fill, water infiltration rate and pH Farquhar, 1989 but the rate and quantity of leachate and landfill gas production will be affected by the depth of burial of fill, regional climatic conditions, variations in water table, the landfill capping practice and fluid inflow and outflow controls at the site. It can be expected that surface layers of refuse i.e., shallow burial depth may experience rapid aerobic decomposition whilst the bulk of the waste at depth may have only been partially decomposed under anaerobic conditions thus leading to different physical properties. Also, landfill degradation will be quicker in humid tropical regions than in cold regions and for identical fill composition and water influx-efflux conditions, the leachate from the warmer climate will

have a higher concentration of dissolved materials relative to the background groundwater composition in analogy to variation in saprolite composition in chemically weathered rock. If precipitation is the main source of water for leachate generation in the fill, then it can be expected that storms will have a role in leachate discharge.

The transport of leachate through the landfill is slow, unsteady, non-uniform and sometimes discontinuous Fang, 1995a depending on the degree of compaction of the fill and seasonal changes in water supply to the system. Within the landfill, this liquid may collect in various areas e.g. perched saturated zones or mound at the bottom of the landfill. This leachate starts seeping as soon as enough hydrostatic head is developed. Biochemically controlled exothermic reactions are known to cause higher groundwater temperatures in leachate MacFarlane et al., 1983 and because of the ingress of leachate from the upper leached zones, the temperature in the lower portion of the landfill is often significantly higher than elsewhere in the leached section Fang, 1995a. Consequently, there are higher bacterial activities and higher ion exchange reactions in the lower parts of the landfill as time progresses. These microbial chemical decomposition reactions may cause significant changes to the existing pore fluids and to the substrate if the fill is in direct contact with geological materials.

On passing through the base of the landfill, the metal ions in solution may be removed from the aqueous phase by ion exchange, sorption or precipitation onto the substrate especially if clayey. However, organic carbon in colloidal form in the leachate often has higher cation exchange capacity than clay and can sorb high concentrations of metal ions from solution as can some inorganic colloids which form under certain chemical conditions. The metal ions sorbed preferentially onto the surface of colloidal particles may thus by-pass the natural attenuation processes as the leachate seeps into the substrate Dearlove, 1995. Within the substrate, it mixes with groundwater forming a leachate plume. Initially, on entering the anaerobic groundwater system, the organic material in the leachate is slowly biodegraded

forming more acids which may react with aquifer materials cf. Bennett and Siegel, 1987 with attendant changes in the fluid chemistry near the water table. In this deoxygenated environment, inorganic materials in the leachate e.g. iron, manganese may be dissolved in the groundwater. The dispersing leachate extends laterally and vertically as it sinks towards the bottom of the substrate forming a 3-D contaminant plume that may be steeply dipping see Fig. 2. The amount of groundwater contamination resulting from this invasion will depend on the hydrogeology of the area and the attenuation capacity of the substrate. It may be effectively diluted and dispersed by groundwater in highly permeable geological formations with high flow rates. Given enough time in less permeable formations, or with slowly moving groundwater, the plume laden with inorganic salts may enhance mineralization of groundwater. Since it is a moving and continuously evolving 3-D feature, it will in time be dispersed over a sizeable area, possibly with distinct compositional zonations.

The water samples collected from the study area were stored separately in an acid-cleaned plastic bottle which were rinsed with the sampled water twice before the water samples were collected. After collection, the water container was securely corked with a plastic lid wand then taken to the laboratory for analysis on electrical conductivity, total dissolved solid, Total solid, turbidity total hardness, pH, temperature, anions, cations and trace elements (heavy metals).

3.2.4.1 Electrical Conductivity

A conductivity meter and cell were used for the analysis. The conductivity cell was filled with the standard reference solution of known conductivity, EC₂₅. The conductivity meter was adjusted to read the standard conductivity. The cell was later rinsed with the solution to be measured. Sufficient portion of the filtrate was transferred to the conductivity cell and its conductivity reading was taken. The cell was rinsed with distilled water for subsequent measurements.

3.2.4.2 The Cations

Standard solutions (1000mg/l) of Na, K, Ca, Mg, Zn, Pb, Cu, Mn, Cd, Fe and Co were prepared. From the stock solution (1000mg/l) 100mg/l was prepared by diluting 10ml stock solution to 100mg/l. 2, 4, 8 and 10ml of 100mg/l were pipetted into 100ml standard flask and diluted to 100ml mark. These solutions gave 2, 4, 8 and 10mg/l working standards.

Determination of K and Na in Water

The working standards were aspirated into the flame photometer. The emissions of the standards were recorded against concentration and graph of emission against concentration of K and Na were plotted.

Determination of Ca, Mg, Zn, Pb, Mn, Cu, Fe and Co in Water.

The working standards were aspirated to AAS Buck 210 Model. The Absorbances of the standards for each element were recorded against concentration and graphs were plotted.

3.2.4.3 The Anions

The water analysis for the anions (chloride, nitrate, phosphate etc.) was carried out using the conventional volumetric method of titration. Reagents used for the analysis are Potassium chromate indicator (K_2CrO_4), $AgNO_3$ and NaCl or KCl.

CHAPTER FOUR

RESULTS AND DISCUSSION

4.1 PRESENTATION OF RESULTS

The results of the data obtained from the field are presented in form of Tables, Profiles (VLF-EM and Magnetics), Pseudosections and Depth Sounding Curves and Geoelectric sections. Typical example of these are shown in the tables and figures presented in this chapter. The remaining tables and figures of the results are presented in the appendix.

4.2 DISCUSSION OF RESULTS

4.2.1 Very-Low Frequency Electromagnetics Method (VLF-EM) Profiles

EM PROFILE 1 was about 65m in length and measurements were taken in the W-E direction. Both the profiles (Figure 4.1a) and the Karous Hjelt Pseudo section (Figure 4.1b) indicated two regions of conductivity at about 25m and a very high conductive zone extending from about 50m to 65m. This conductive zones were bisected by a resistive section of about 15m. The region of very high conductivity could be indicative of leachate seeping into the subsurface layers.

EM PROFILE 2 had 20 station points with a total spread length of 100m along which measurement were taken in the NW-SE direction. Both the VLF profiles (Figure 4.2a) and the Karous Hjelt Pseudo section (Figure 4.2b) showed conductive zones which were picked for vertical electrical sounding at about 10m, 50m and 85m. Beside the very high conductive zone at about 50m is the presence of a very resistive zone. The high conductive zone at 50m could indicate a pocket of contaminant present in the subsurface.

EM PROFILE 3 had a spread length of 105m with 21 station points along which measurements were taken in the W-E direction. Both the VLF profiles (Figure 4.3a) and the Karous Hjelt Pseudo section (Figure 4.3b) showed conductive zones which were eventually

picked for vertical electrical sounding at about 35m, 65m and 100m. The subsurface layer around 100m showed to be a bit resistive.

EM PROFILE 4 was about 100m and was taken in the NW-SE direction. Both the VLF profile and the Karous Hjelt showed the entire subsurface of this profile to be moderately conductive; this could be due to the presence of contaminant in the subsurface. Although, three zones were picked for vertical electrical sounding and these are at about 20m, 50m and 60m.

EM PROFILE 5 was situated at the North-eastern part of the study area and has a total spread length of 50m. Along this profile, there are presence of both resistive and conductive zones as observed in the VLF profile (Figure 5a) and Karous Hjelt Pseudo section (Figure 5b). The resistive zones along this profile extend from about 7m to 15m and about 27m to 46m while the conductive zone extend from about 20m and 25m; at this zone was a vertical electrical sounding carried out.

EM PROFILE 6 was situated in the Ebira village along a hand dug well. This profile had a total spread length of 50m and was orientated in the NW-SE. Majorly all areas along this profile showed to be conductive except for a resistive zone present at 22 to 33m of the profile. There was also a presence of a very high conductive layer at about 3m to the end of the profile; this could be as a presence of a clayey layer in the subsurface.

EM PROFILE 7 was situated in the perpendicular direction to profile 6. This profile also had a total spread length of 50m with measurements taken in the N-S direction. Both the VLF-EM graph and the Karous Hjelt pseudo section showed a high peak conductive zone at about 30m of the entire profile; at that particular point was a vertical electrical sounding made.

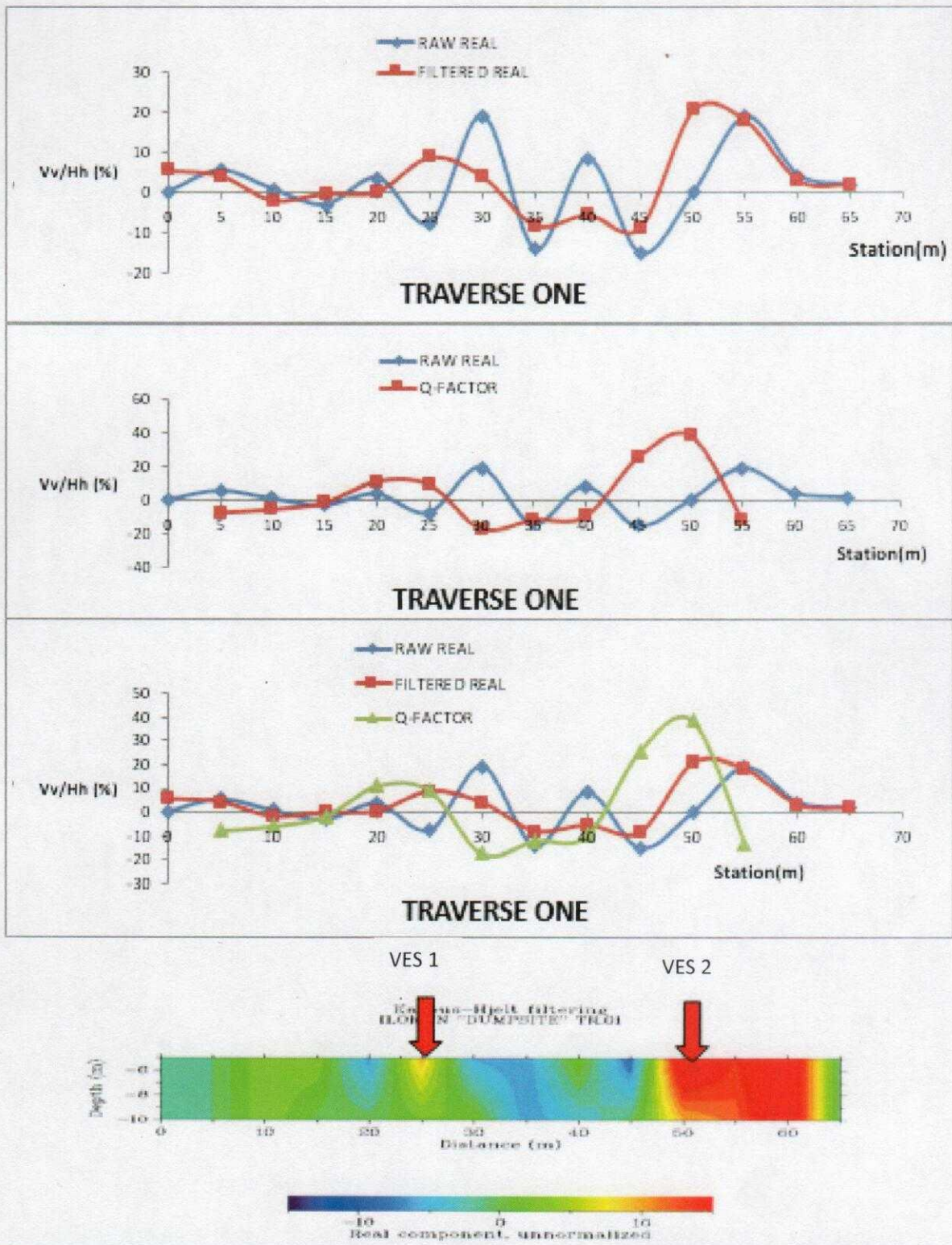


Figure 4.1a: VLF profile along Traverse 1

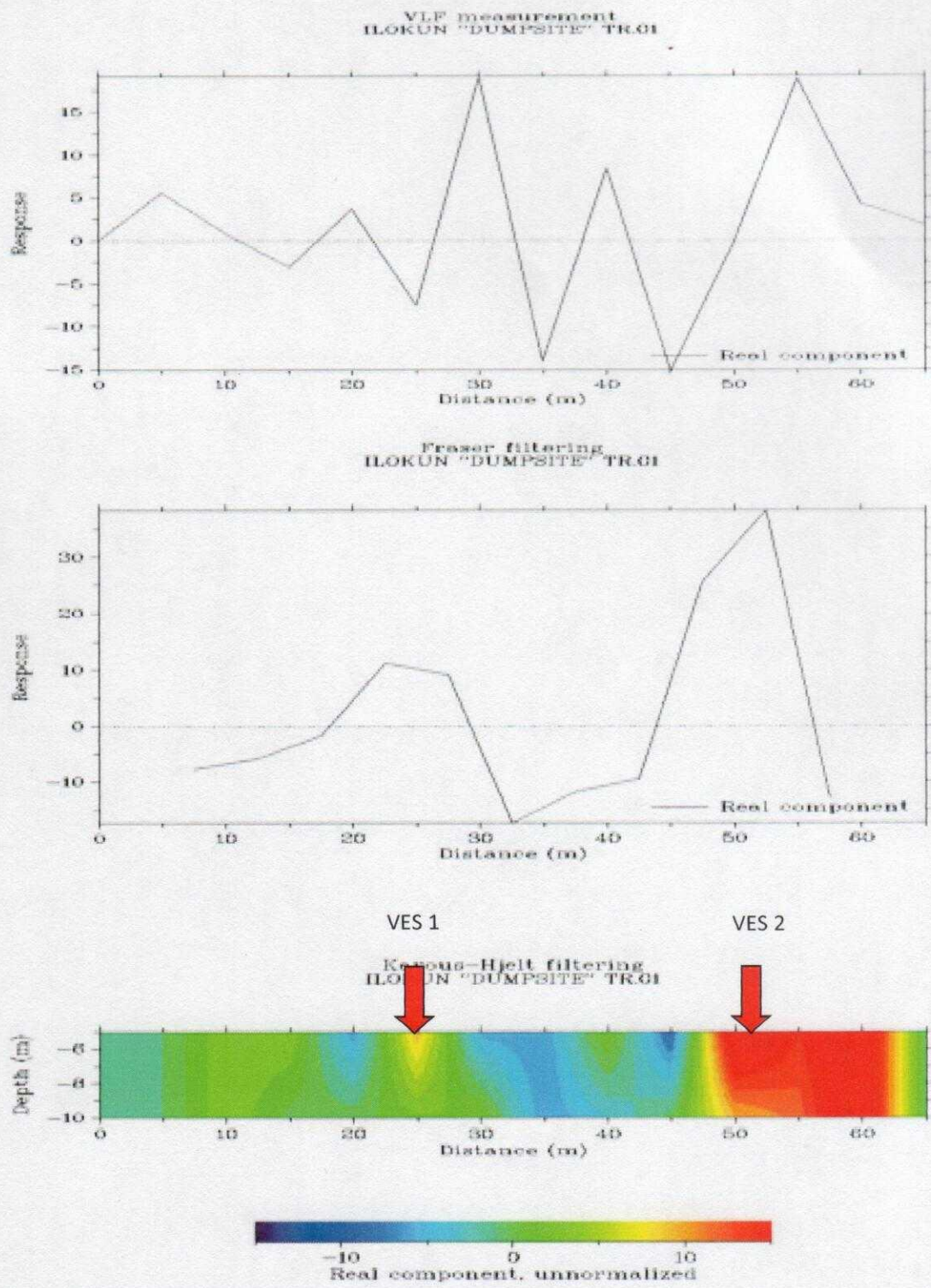


Figure 4.1b: Kerous Hjelt Pseudo section along Traverse 1

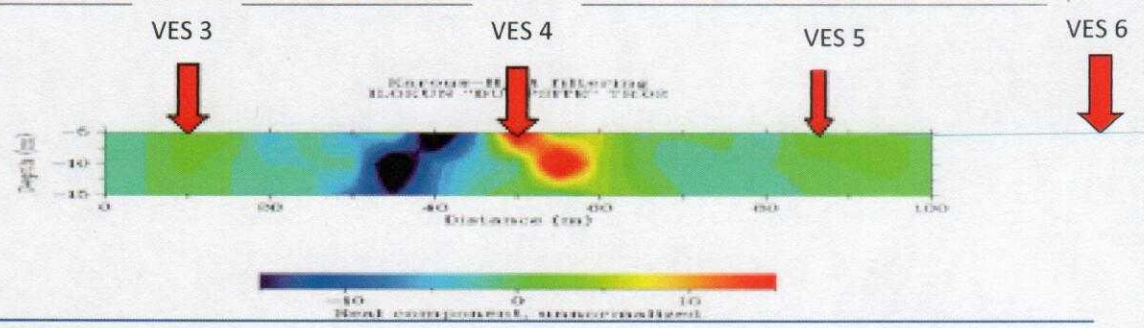
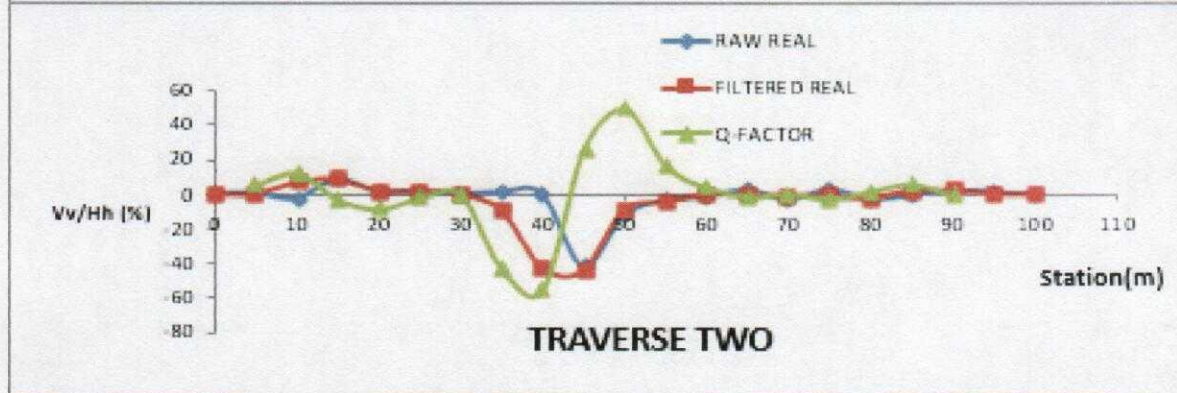
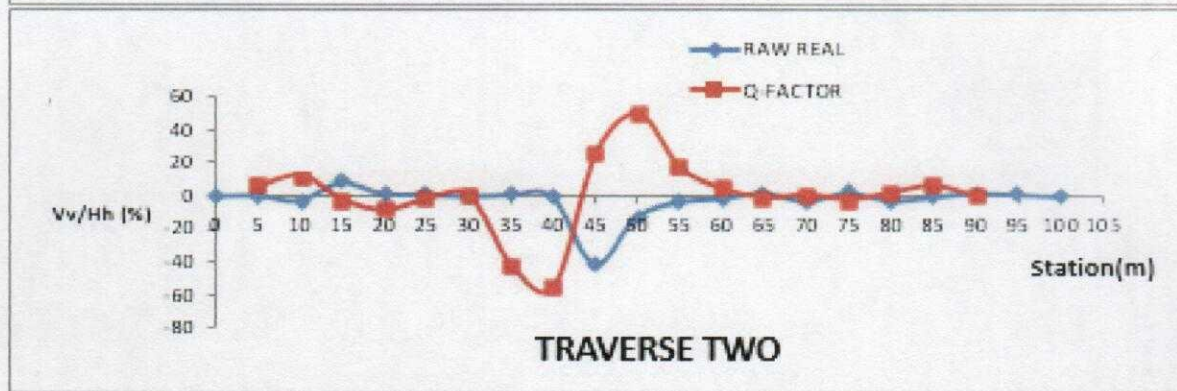
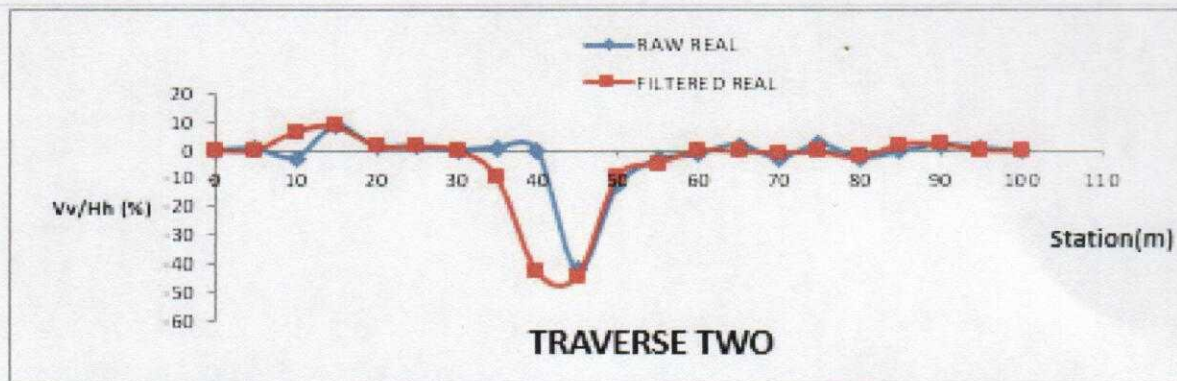


Figure 4.2a: VLF profile along Traverse 2

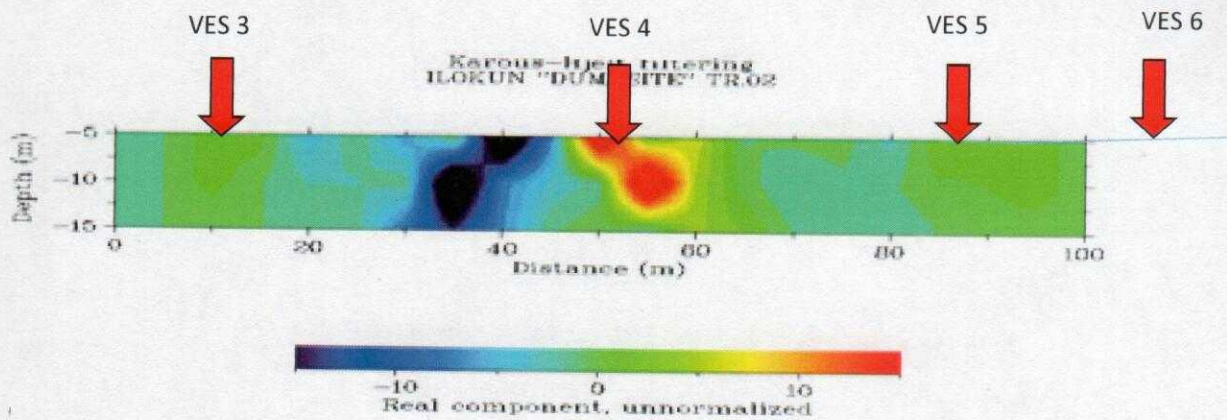
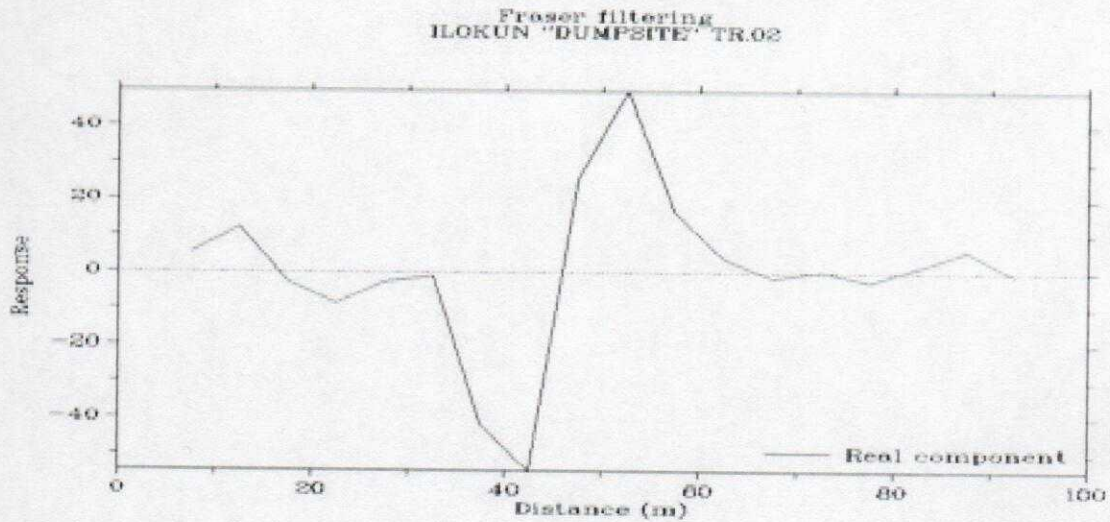
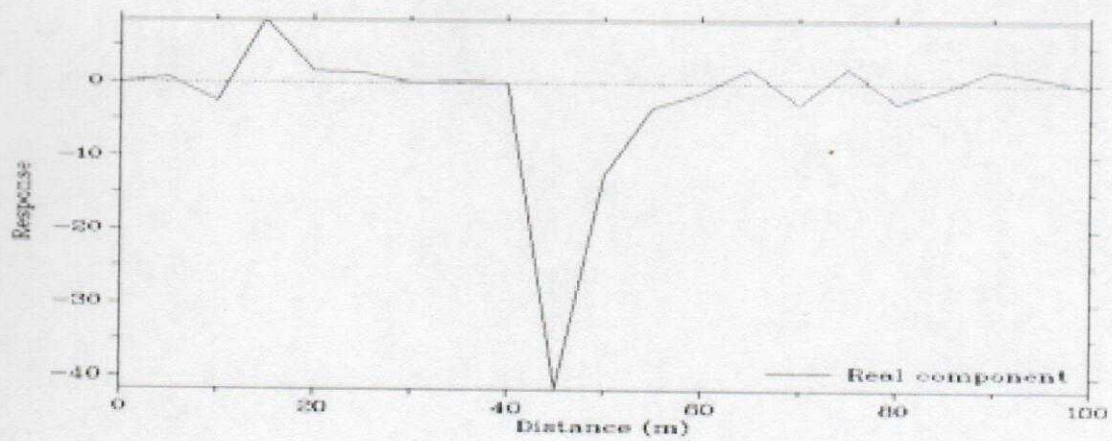


Figure 4.2b: Karous Hjelt Pseudo section along Traverse 2

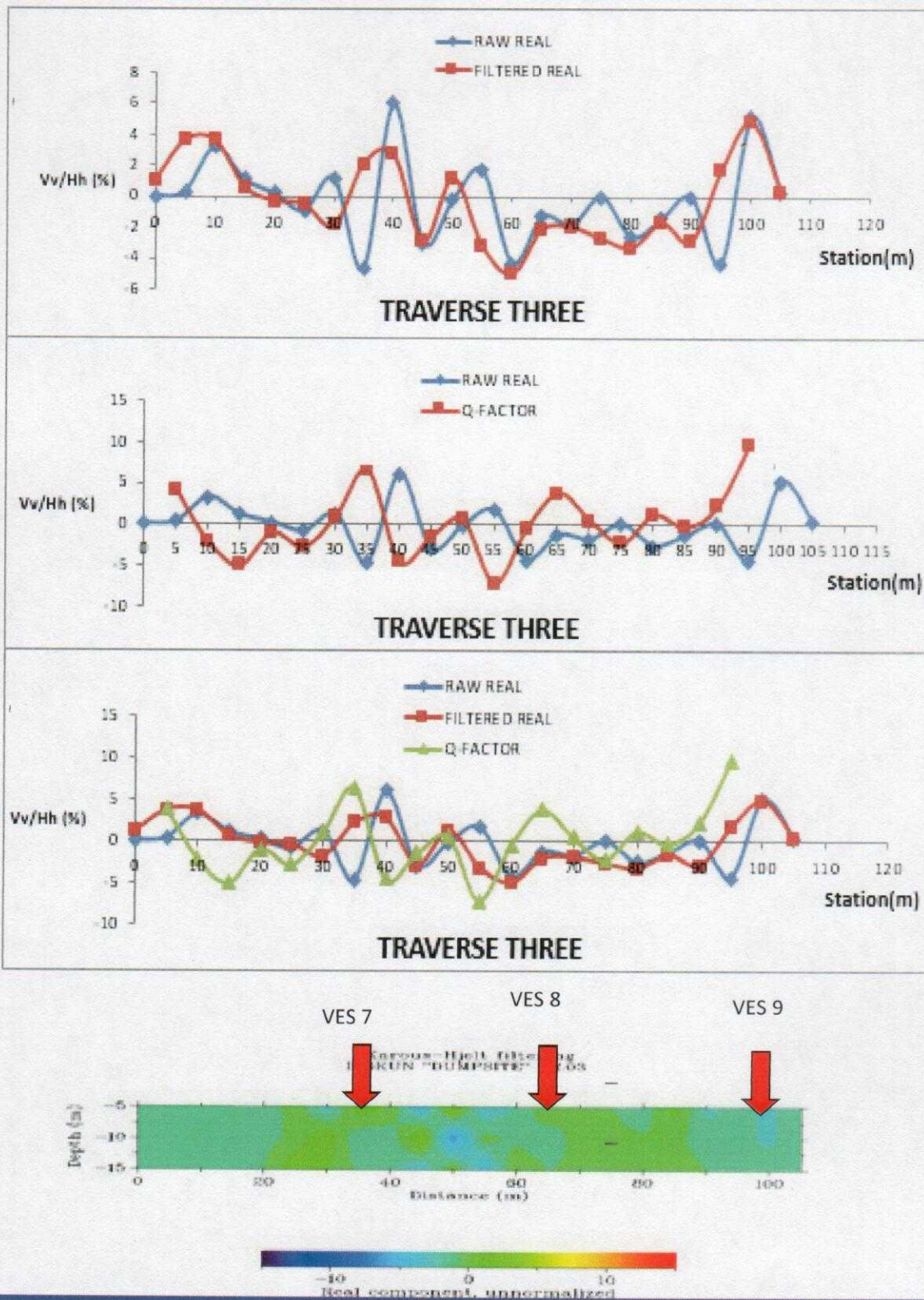


Figure 4.3a: VLF profile along Traverse 3

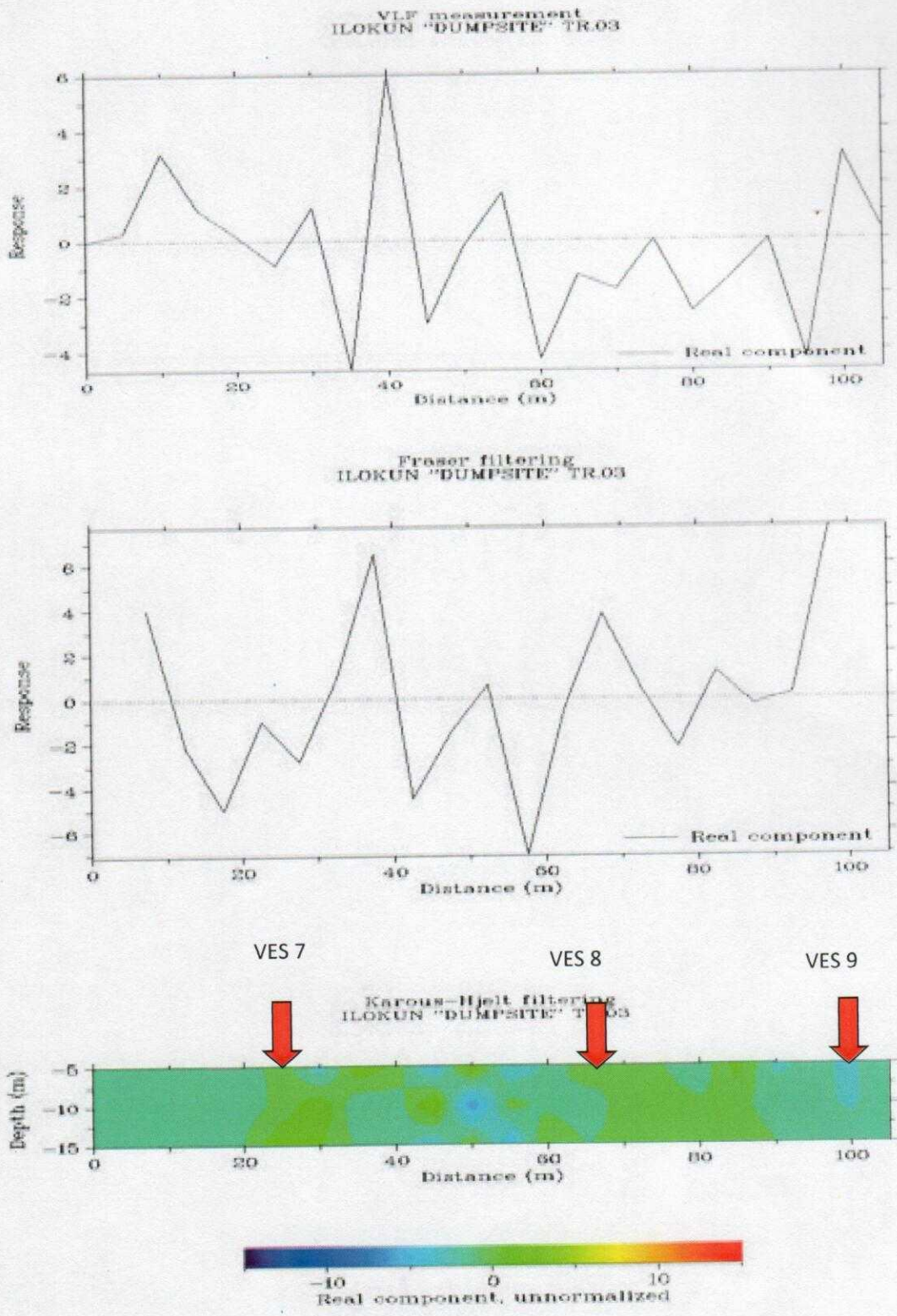


Figure 4.3b: Karous Hjelt Pseudo section along Traverse 3

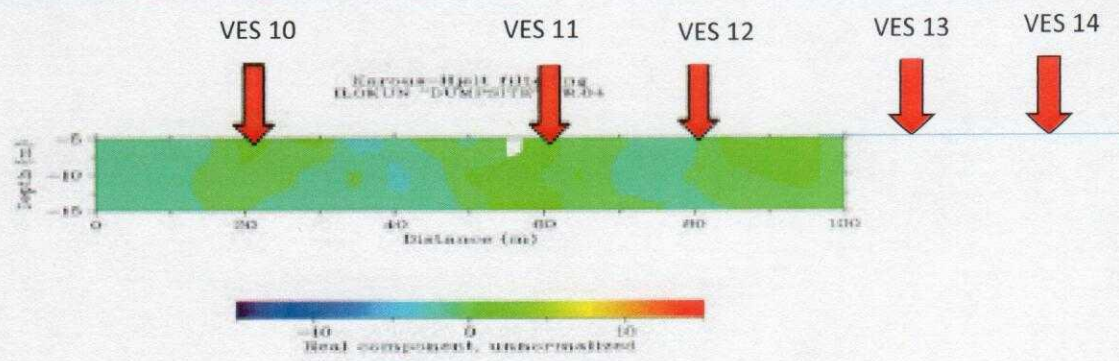
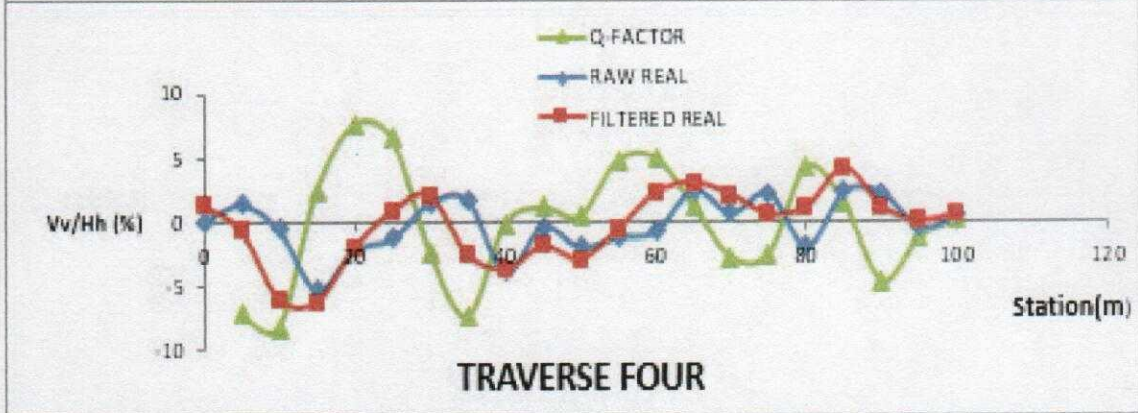
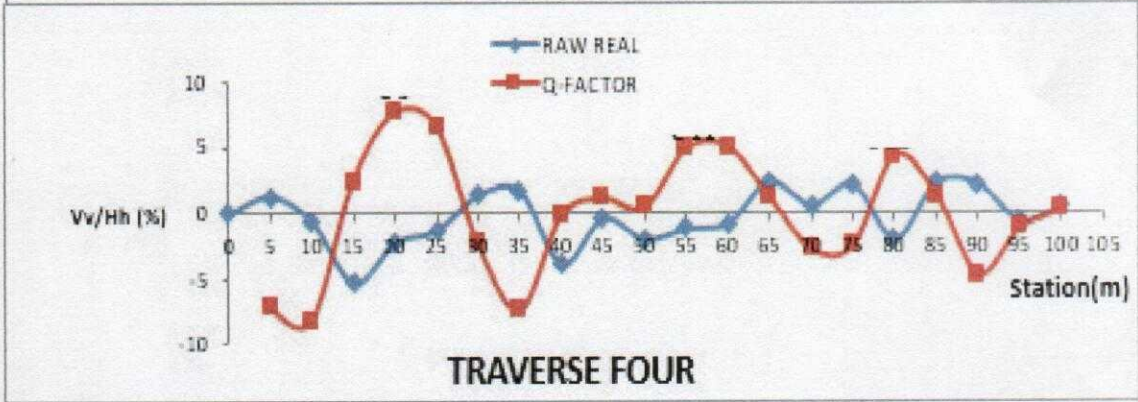
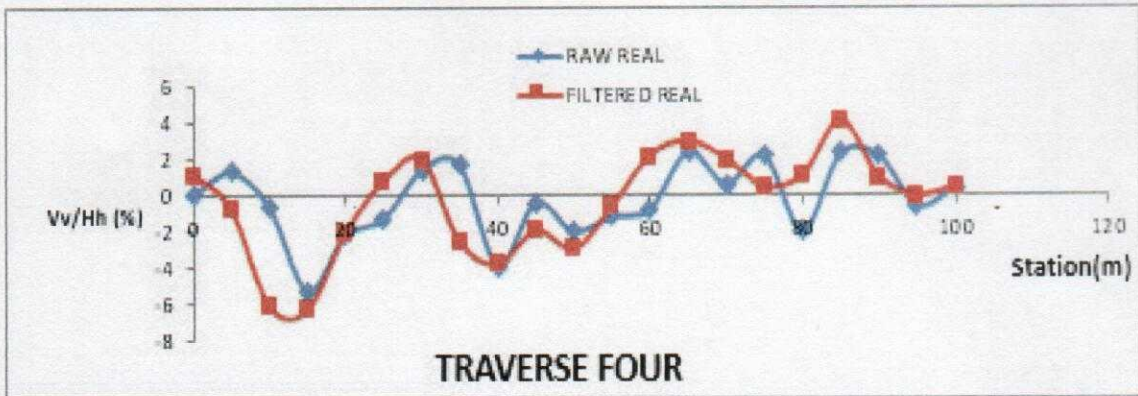


Figure 4.4a: VLF profile along Traverse 4

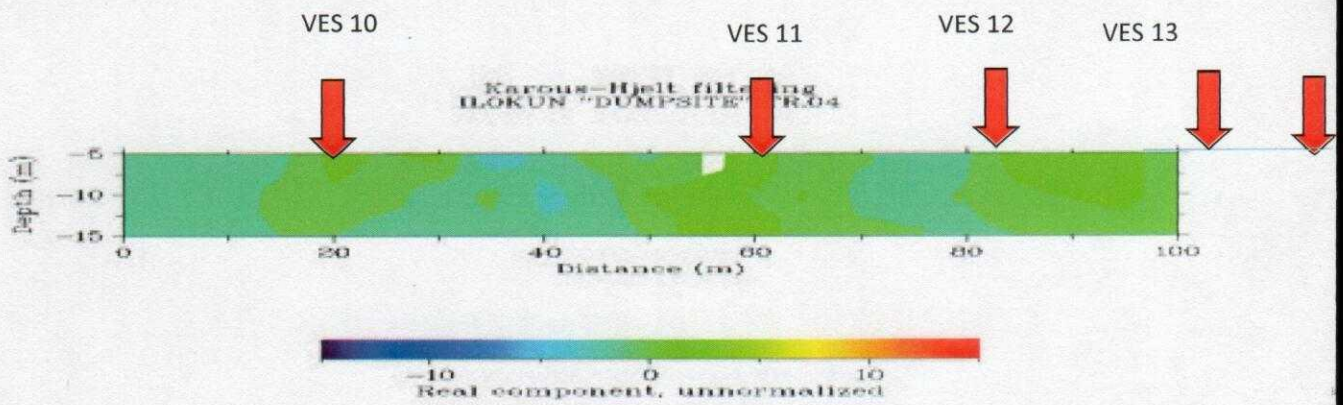
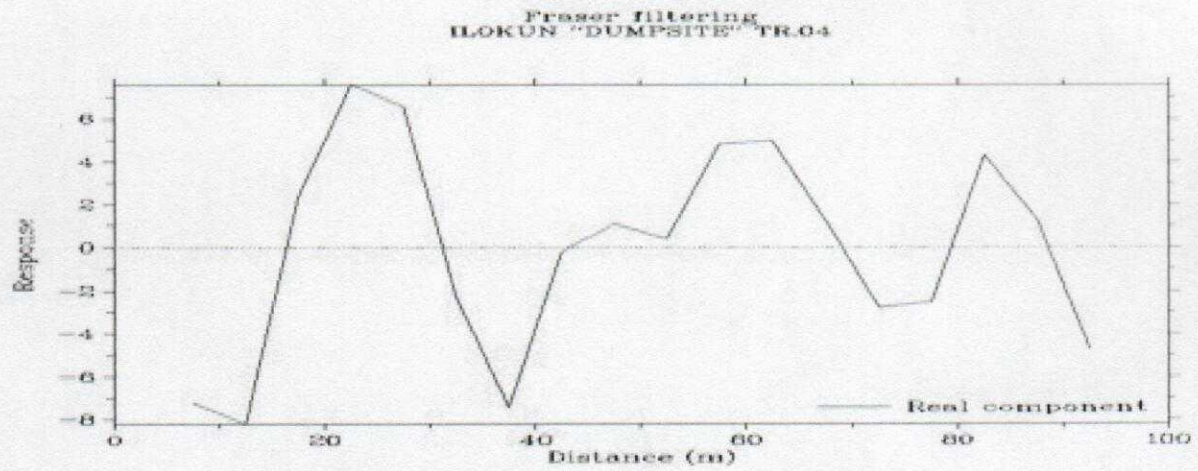
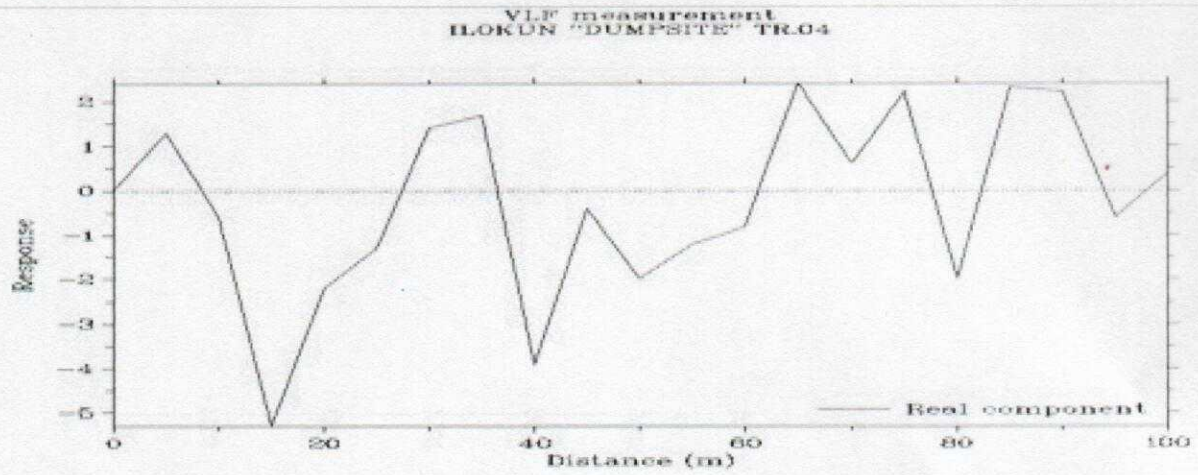


Figure 4.4b: Karous Hjelt Pseudo section along Traverse 4

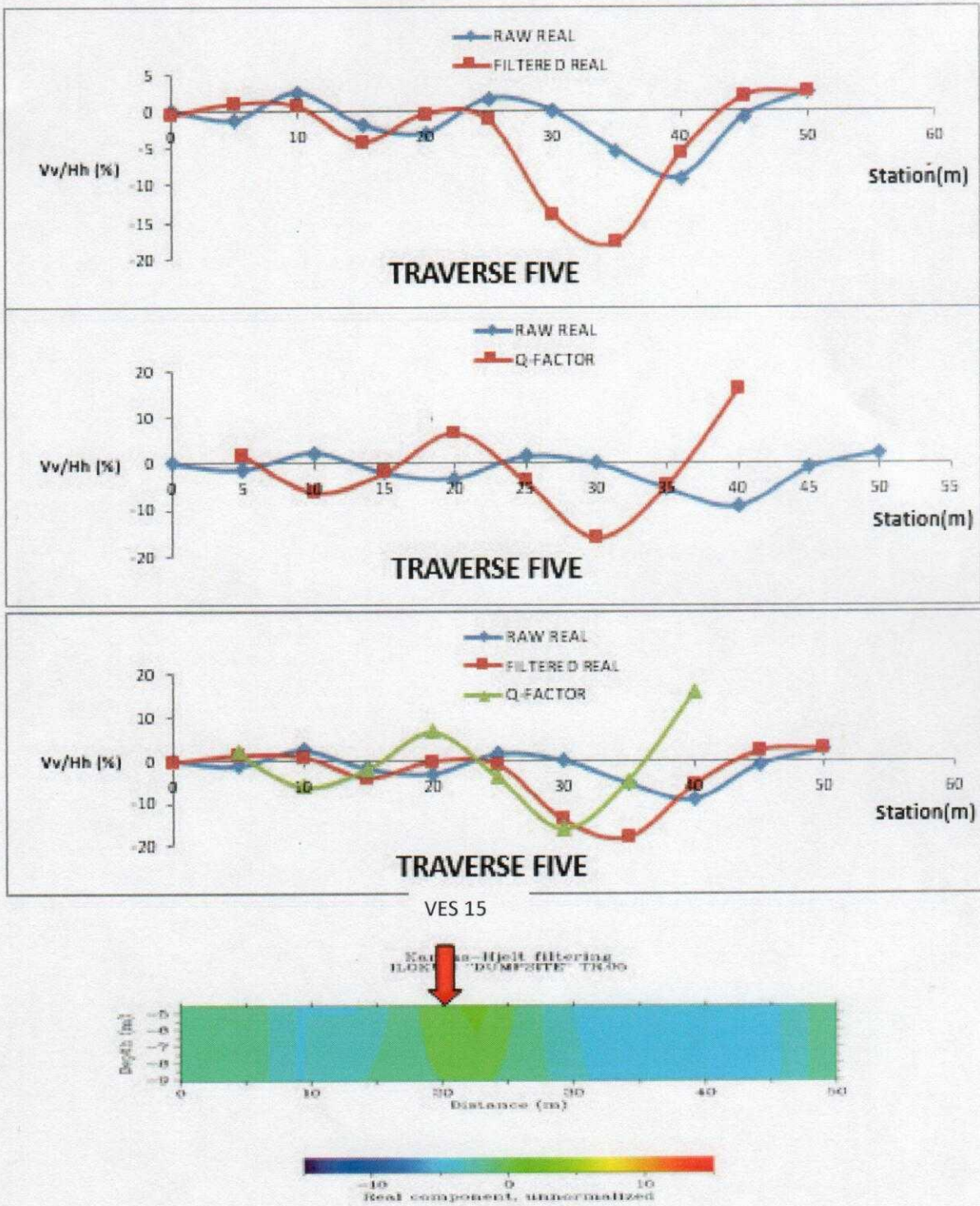


Figure 4.5a: VLF profile along Traverse 5

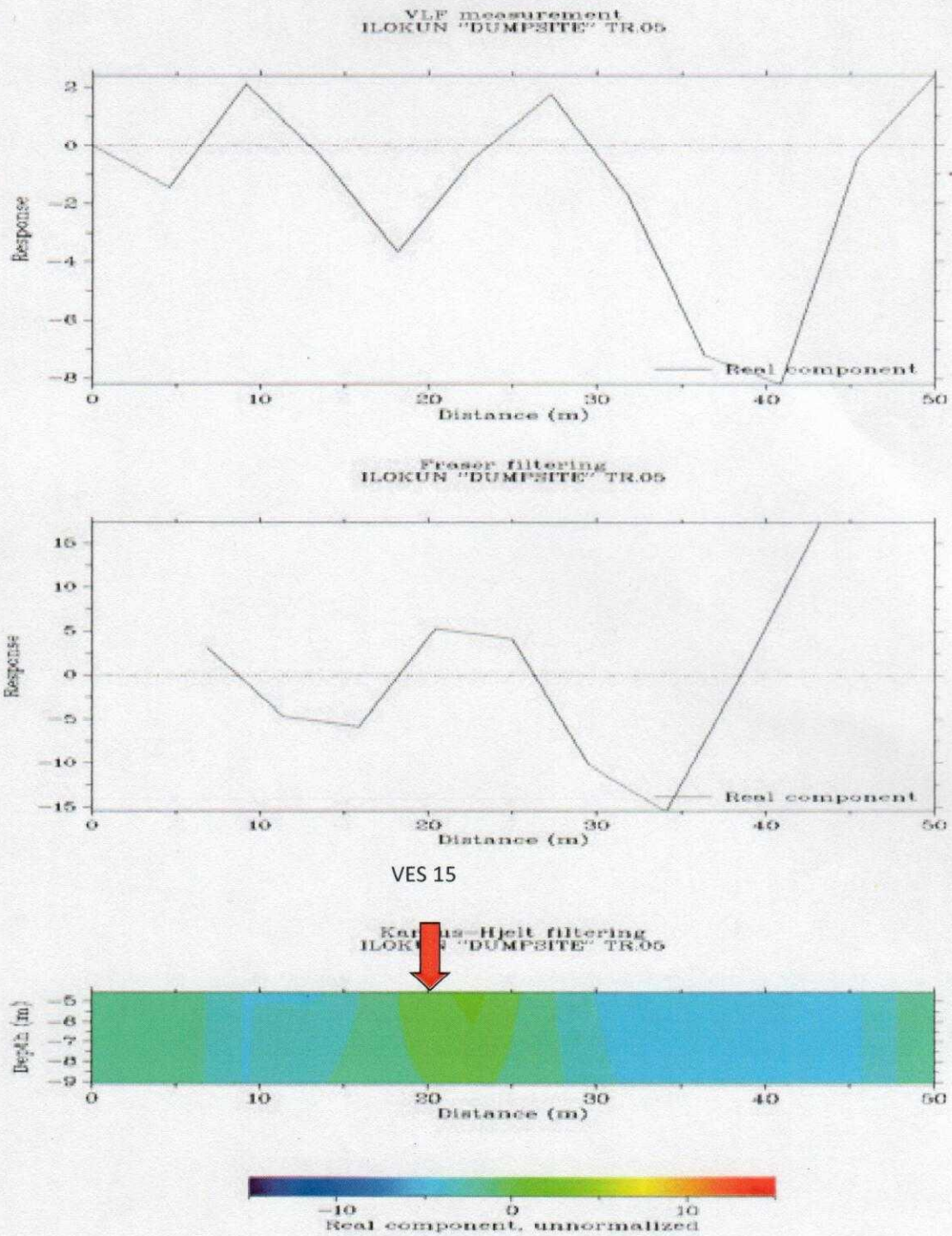


Figure 4.5b: Karous Hjelt Pseudo section along Traverse 5

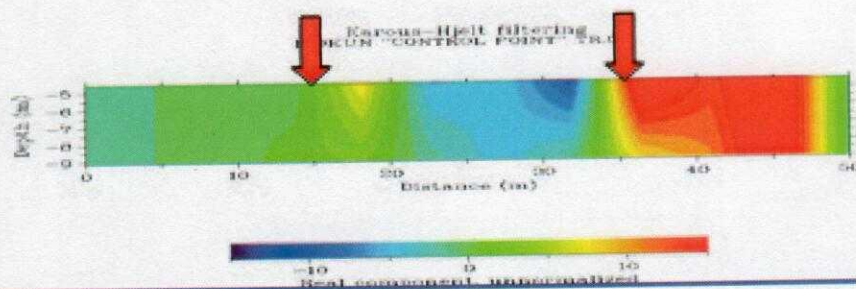
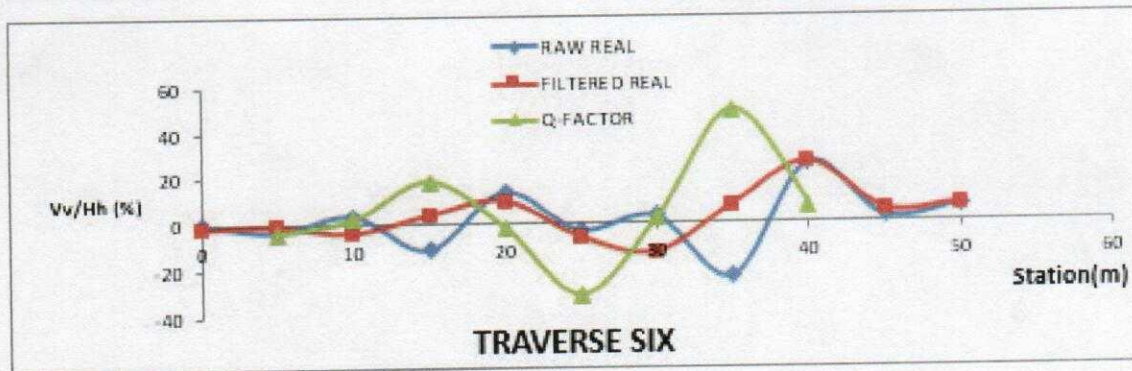
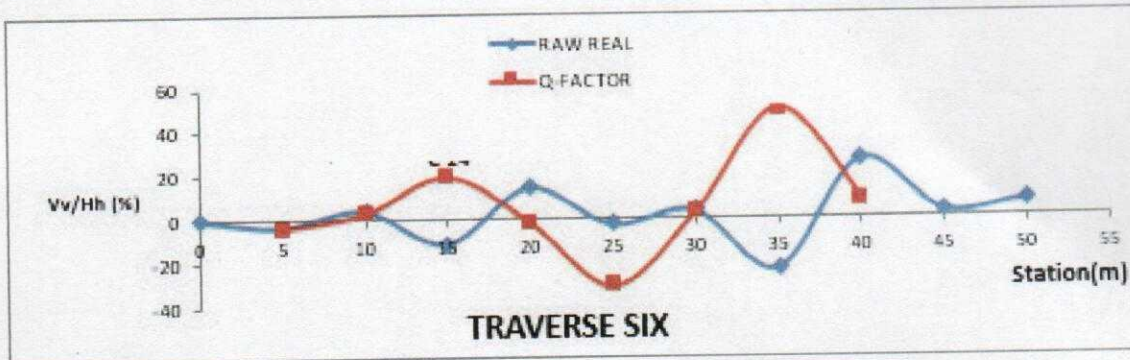
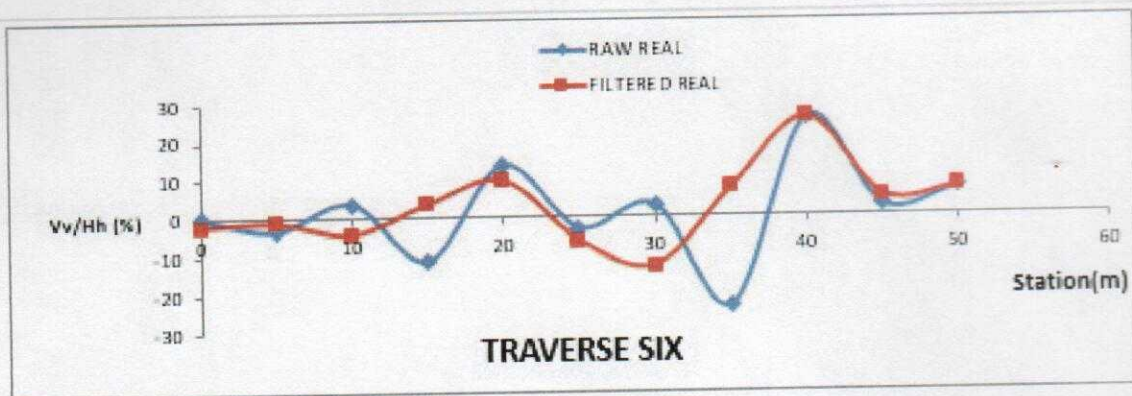


Figure 4.6a: VLF profile along Traverse 6

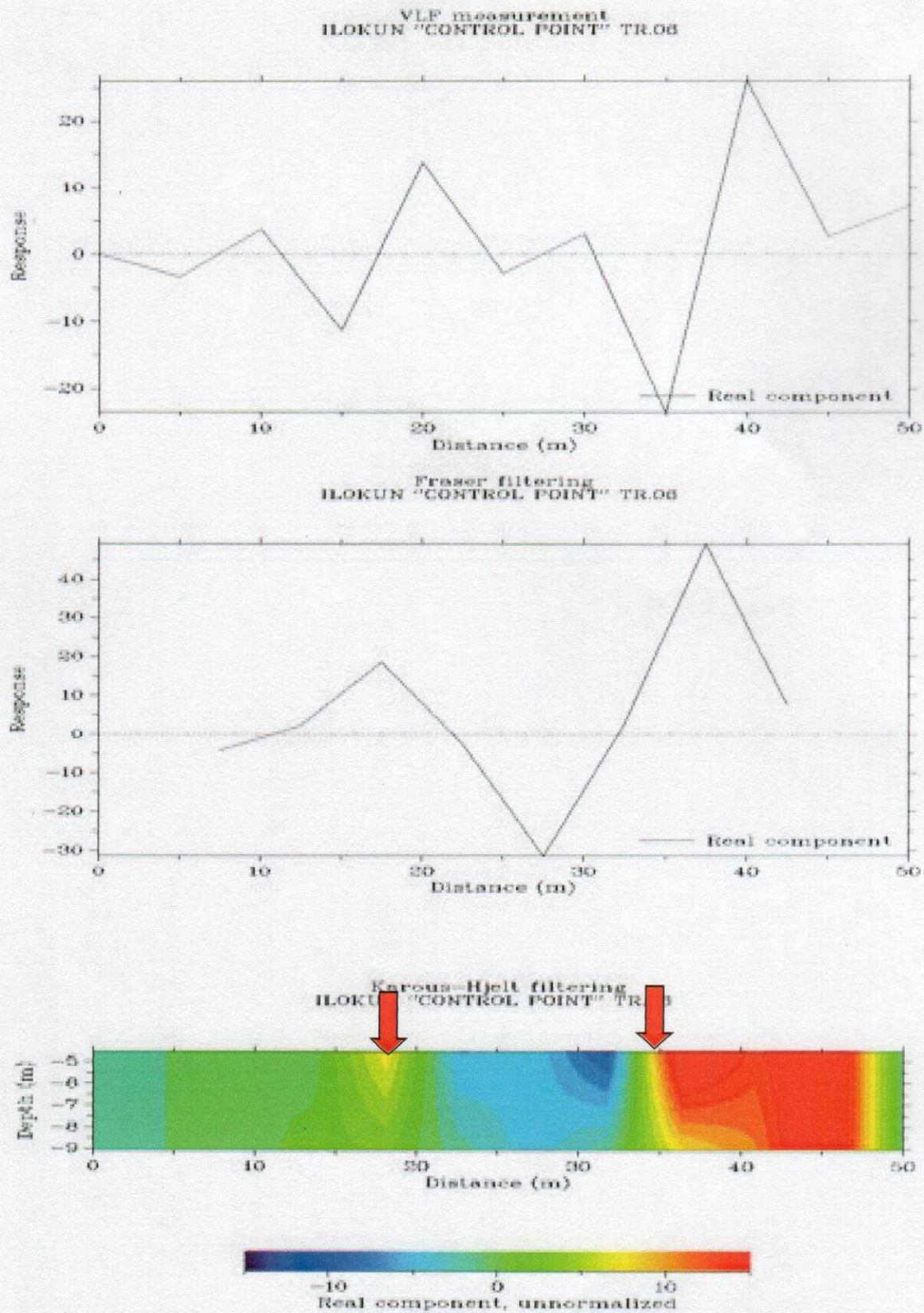
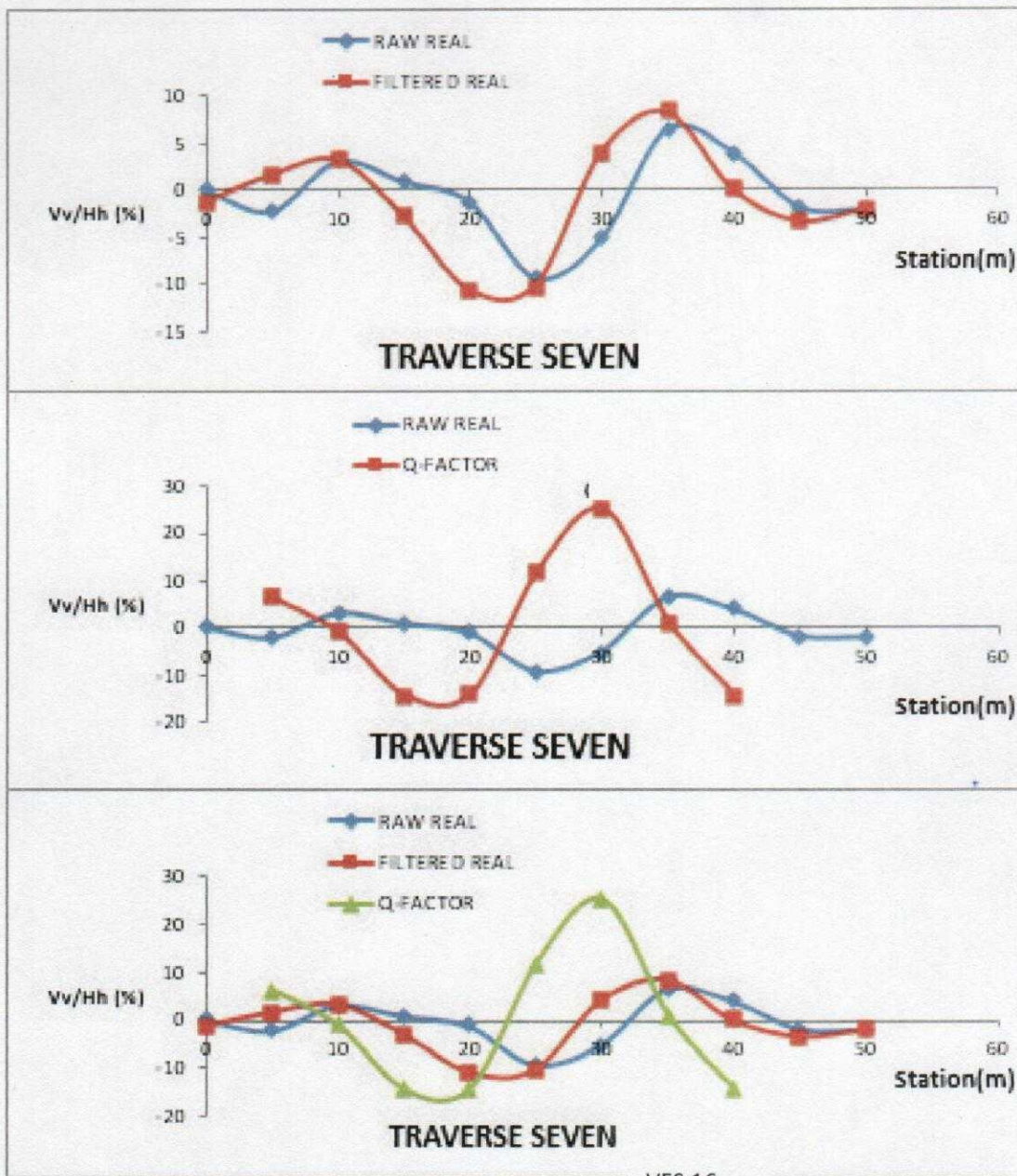


Figure 4.6b: Karous Hjelt Pseudo section along Traverse 6



VES 16

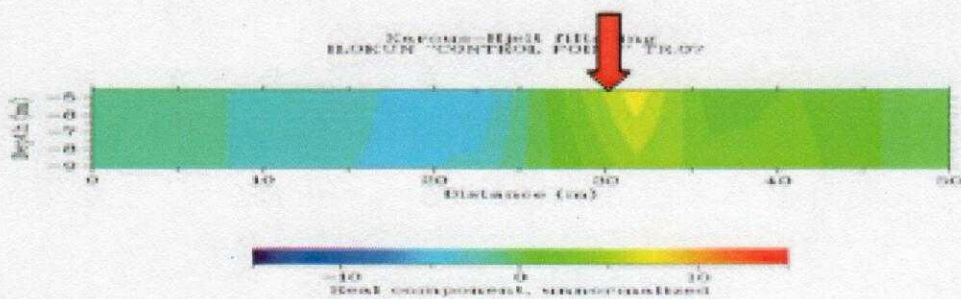
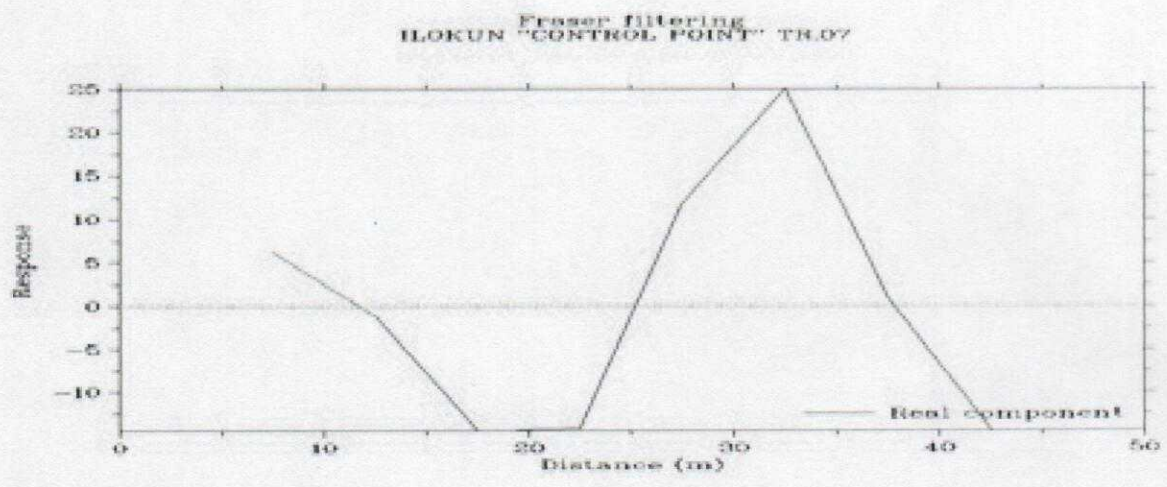
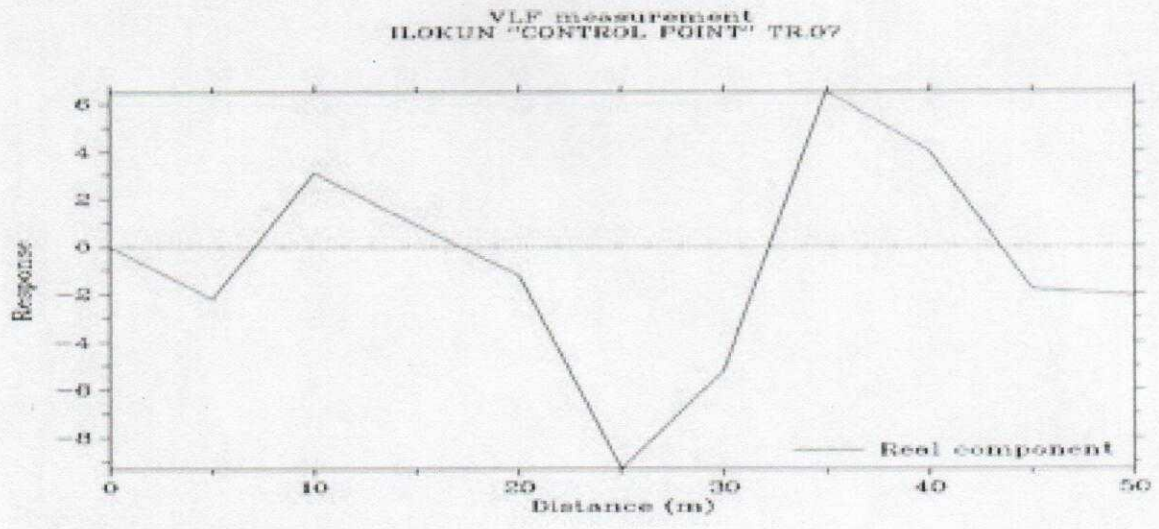


Figure 4.7a: VLF profile along Traverse 7



VES 16

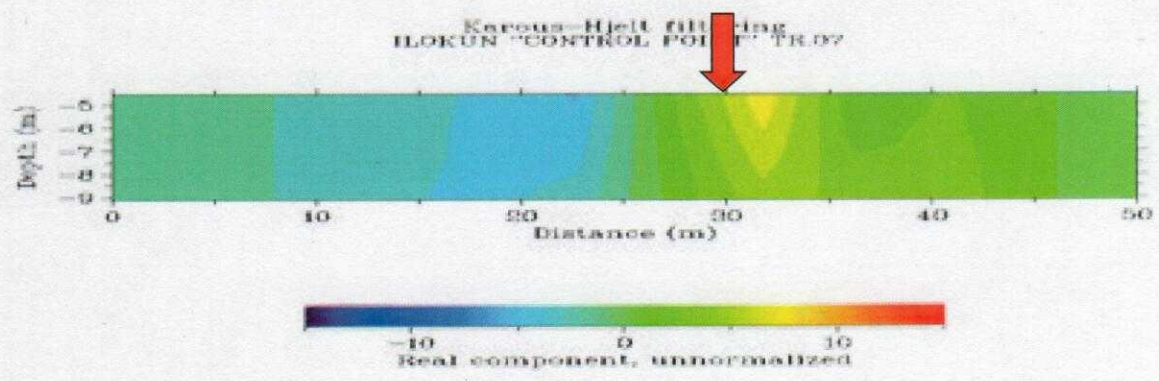


Figure 4.7b: Karous Hjelt Pseudo section along Traverse 7

4.2.2 MAGNETIC PROFILES

TRAVERSE 1 covered a total length of 65m and trend west to east direction. The relative magnetic intensity observed ranges from -1000nT to 990nT. Areas of magnetic lows were observed between 12m and 17m along the profile and this could indicate the presence of subsurface structure such as fault and fracture. The overburden thickness along this profile show to be uniform throughout the entire profile. Figure 4.8

TRAVERSE 2 covered a total spread length of 100m with 20 station points. Measurements along this traverse were taken along north-west to south-eastern direction. The relative magnetic intensity ranges from 0 to 200nT. In the geomagnetic section as shown in Figure (Figure 4.9), there seem to be series of fracturing/faulted zones between 25m to 74m.

TRAVERSE 3 covered a total spread length of 105m with 21 station points. Measurements along this traverse were taken in the west to east direction. The relative magnetic intensity ranges from -75nT to 83nT. Areas of low magnetic lows were observed between 40m to 90m along the profile and this could indicate the presence of subsurface fissures such as fault, fracture and shear zone. Figure 4.10

TRAVERSE 4 covered a total length of 100m and trends north-west to south-eastern direction. The relative magnetic intensity observed from the Euler profile (see figure 4.11) ranges from -60nT to 500nT. From the geomagnetic sectional view of this traverse, it could be seen that the subsurface look to be fractured at about 60m along the traverse. The geomagnetic section show a clear uniformity in the overburden thickness of the subsurface geology.

TRAVERSE 5 had a total spread length of 50m with 10 station points which trends west to east direction. Areas of low magnetic intensity were observed at about 30m and 44m along the traverse. The areas of possessing low relative magnetic intensities could be an indication of the presence of a pronounced dyke, fault of fracture. Figure 4.12

TRAVERSE 6 was situated in the Ebira village which exist along the road that leads to the dumpsite. This traverse had 10 station points with the total spread length of 50m which trends from North-west to South-eastern direction. Areas of low relative magnetic intensity were observed at about 20m and 40m. The areas are suspected to areas with fractures or fault. Figure 4.13

TRAVERSE 7 was established in a perpendicular direction to traverse 6. This traverse also had 10 station points with a total traverse length of 50m. The geomagnetic section of this traverse showed the subsurface to be fractured at 30m along the traverse. With respect to the low relative magnetic intensity of the fractured layer, the weathered layer beneath the subsurface could serve as a good aquifer. Figure 4.14.

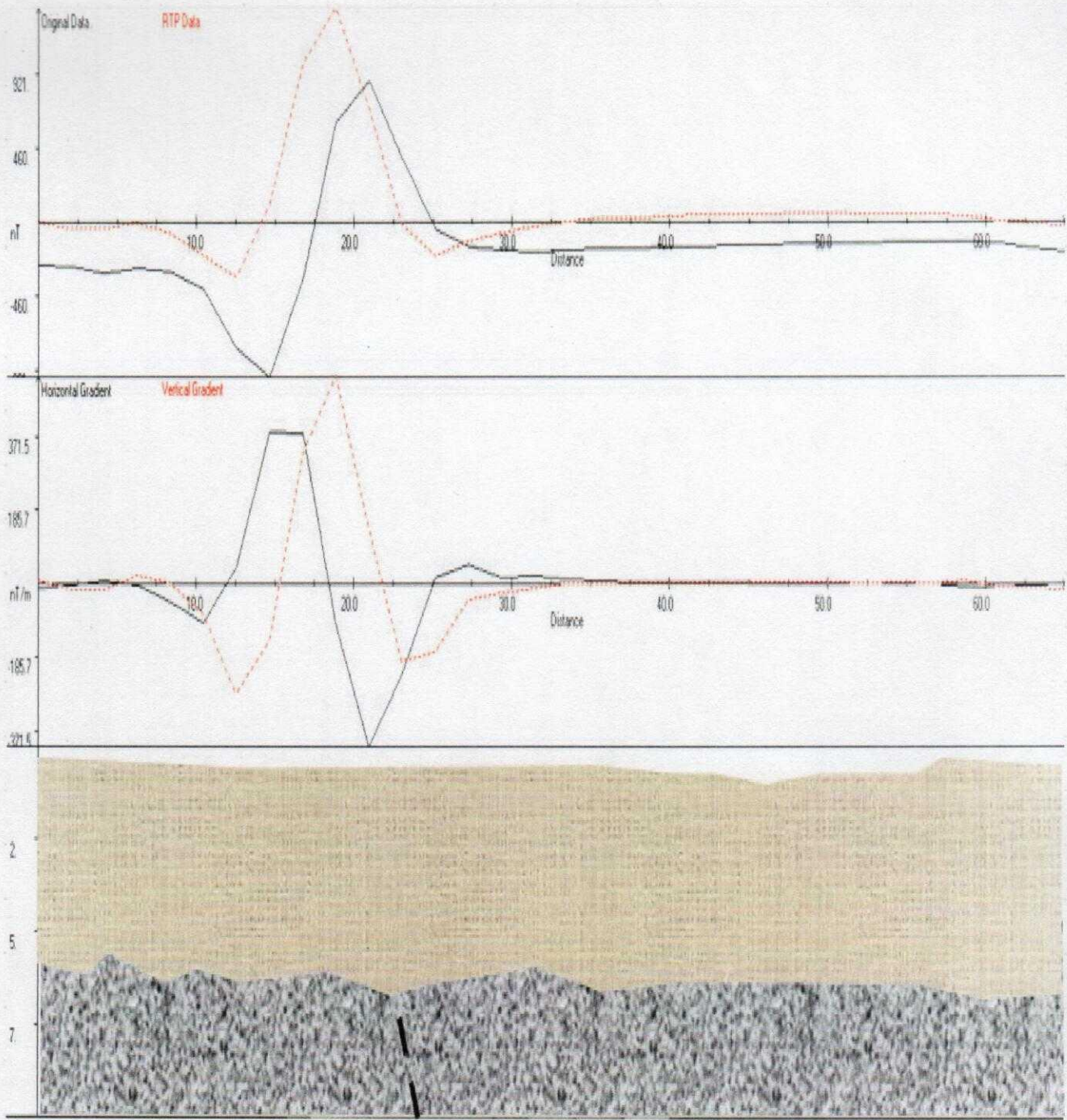
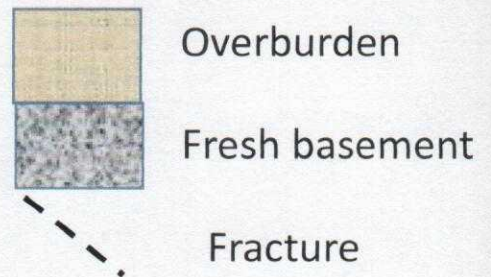


Figure 4.8: Euler profile and geomagnetic section of Traverse 1



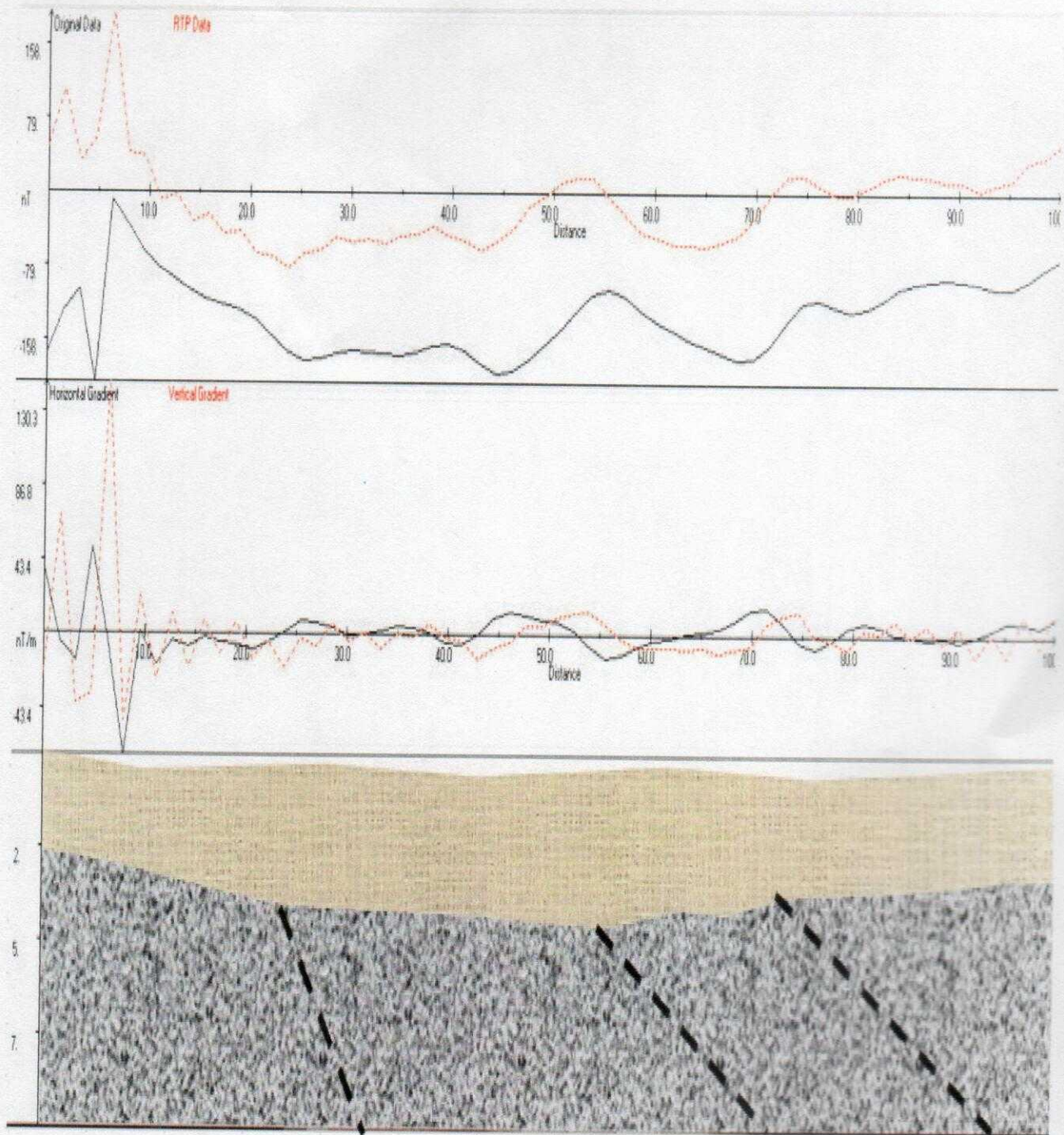
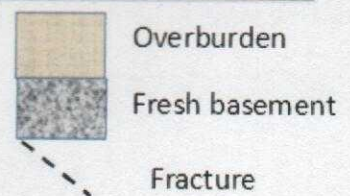


Figure 4.9: Euler profile and geomagnetic section of Traverse 2



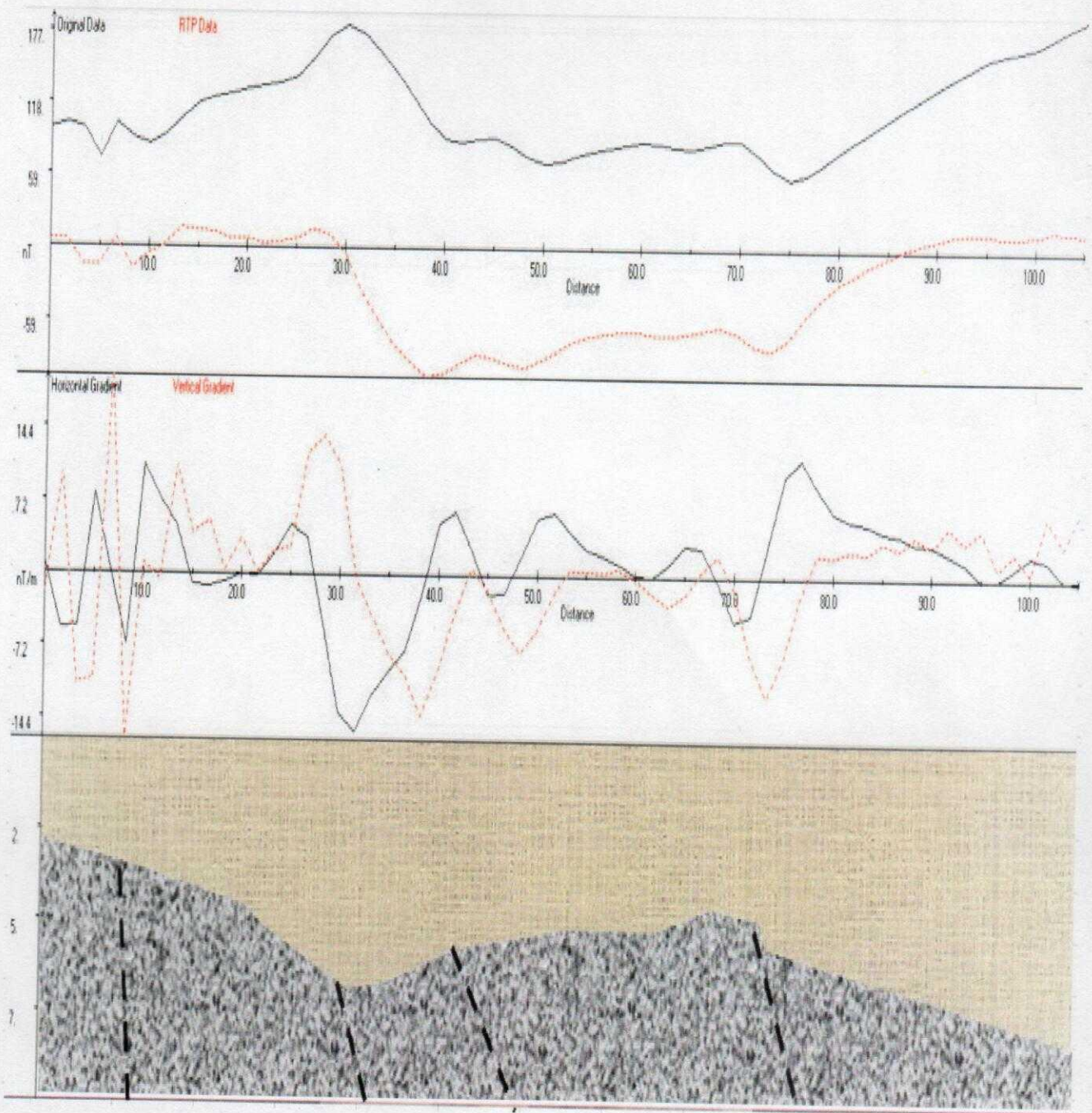
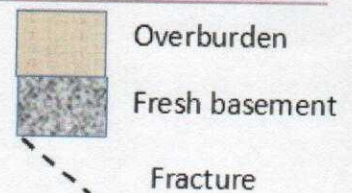


Figure 4.10: Euler profile and geomagnetic section of Traverse 3



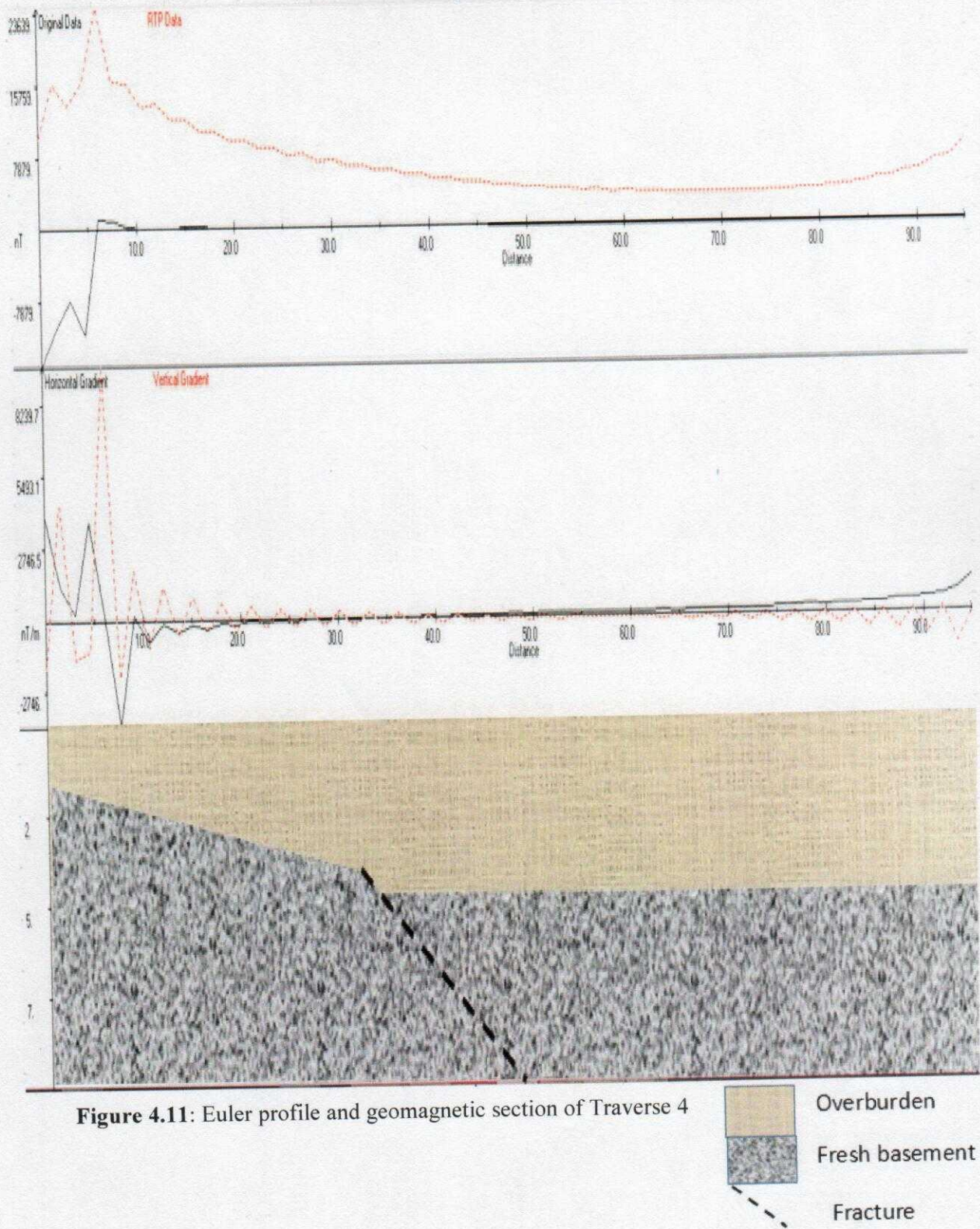


Figure 4.11: Euler profile and geomagnetic section of Traverse 4

- Overburden
- Fresh basement
- Fracture

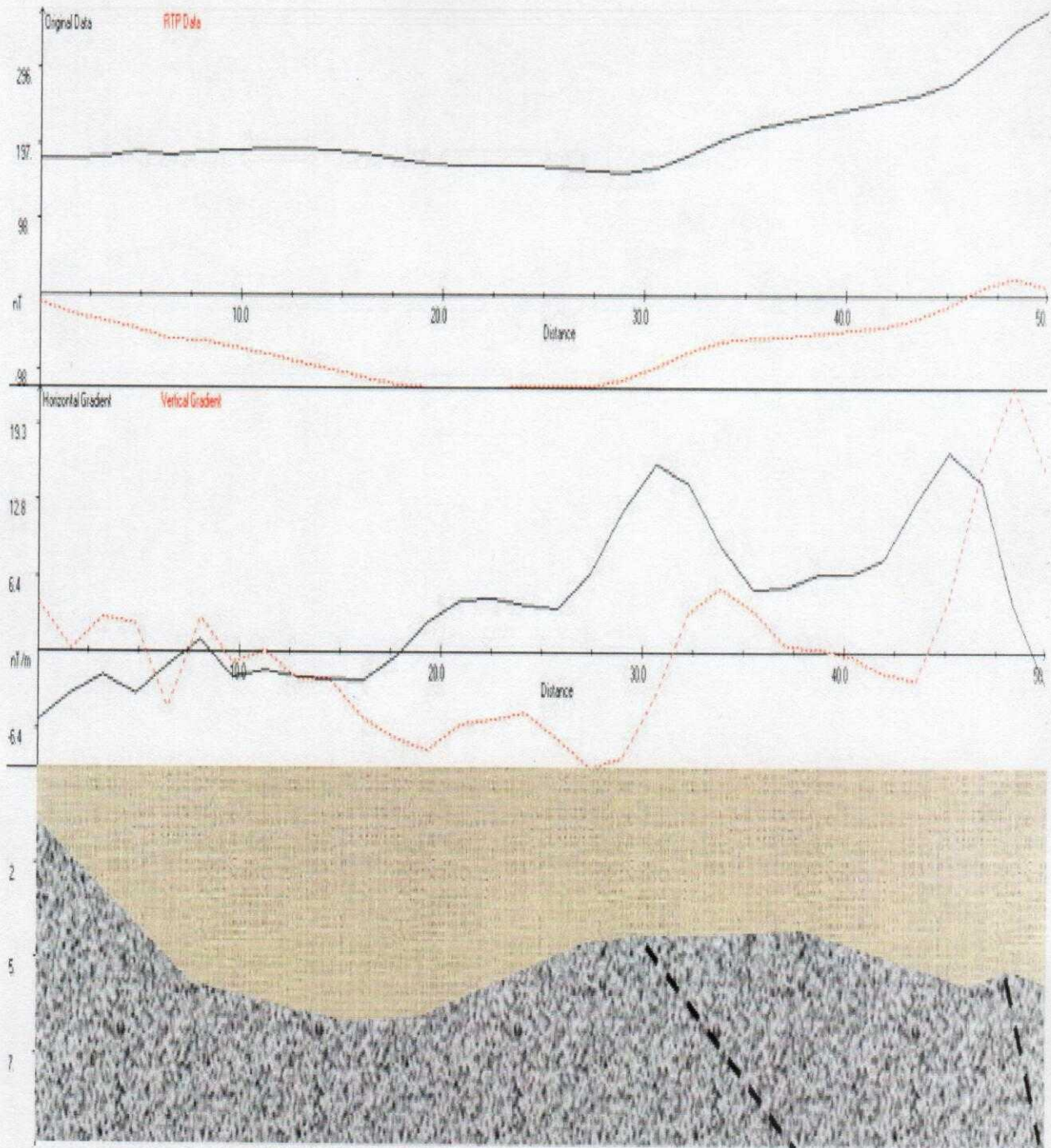
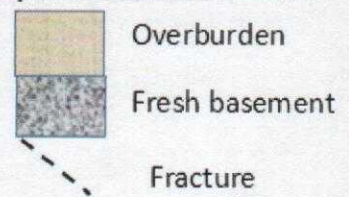


Figure 4.12: Euler profile and geomagnetic section of Traverse 5



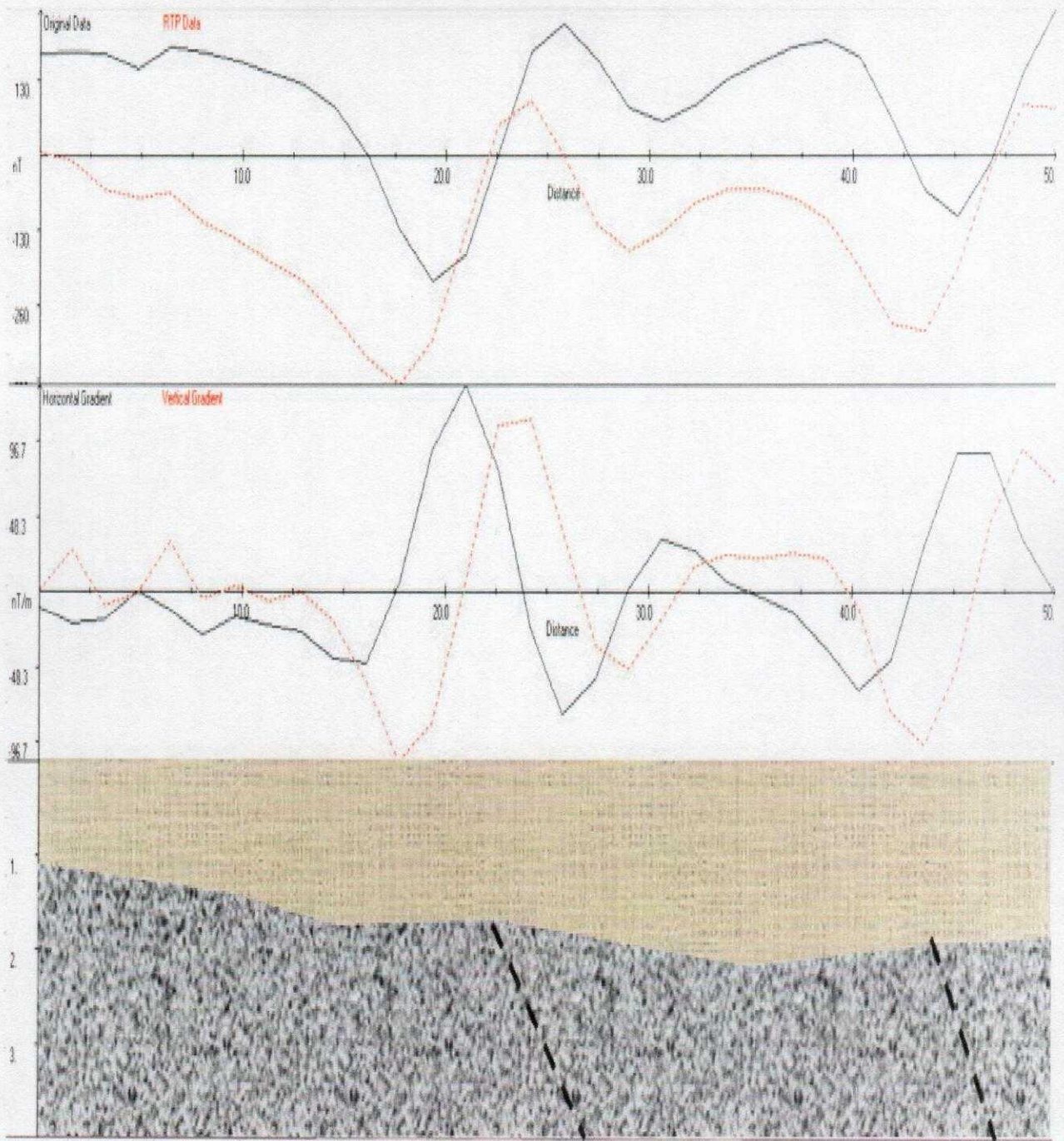
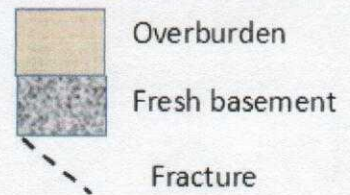


Figure 4.13: Euler profile and geomagnetic section of Traverse 6



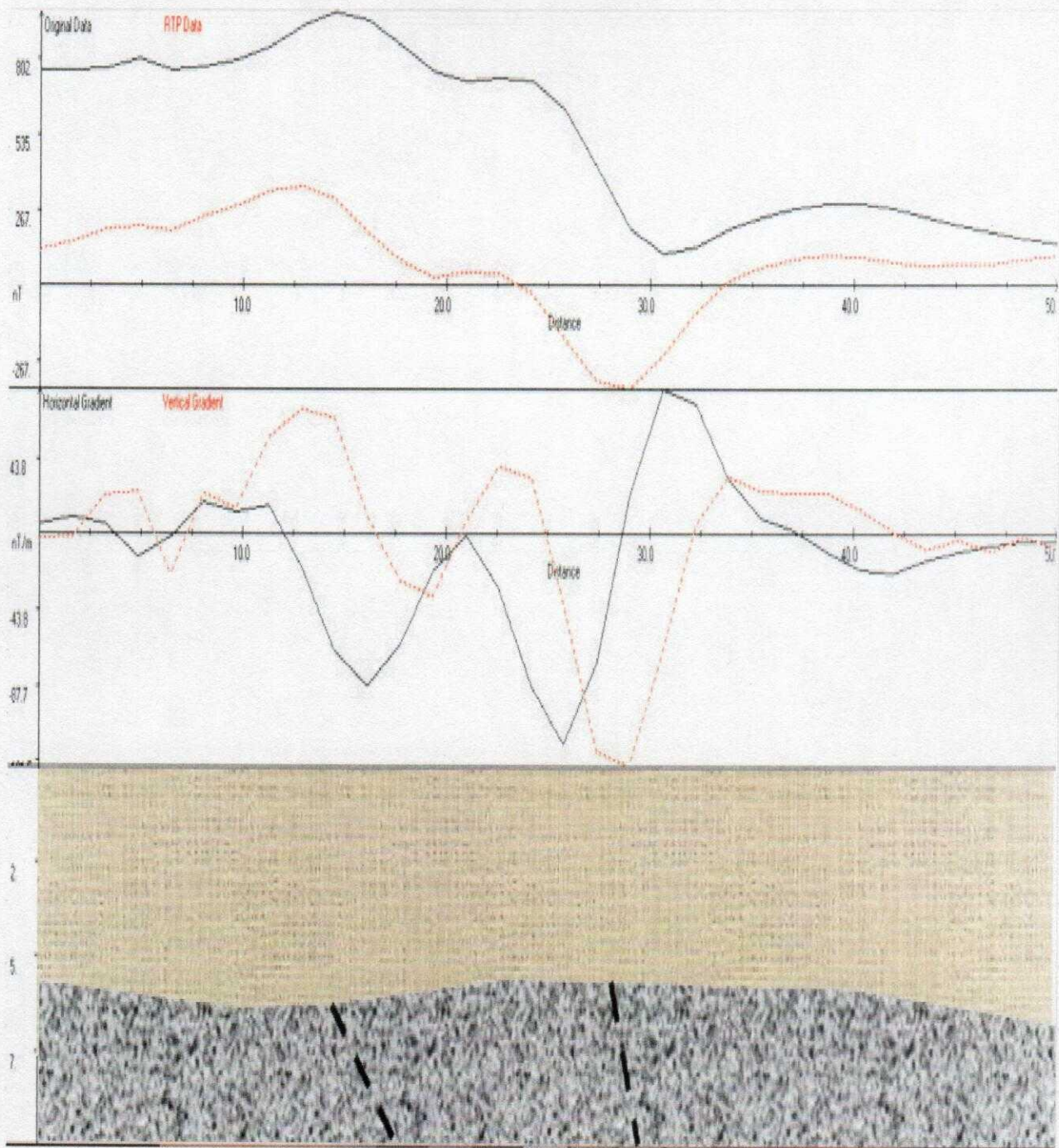
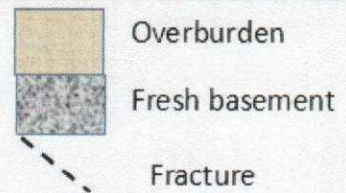


Figure 4.14: Euler profile and geomagnetic section of Traverse 7



4.2.3 DIPOLE-DIPOLE PSEUDOSECTIONS

The dipole-dipole pseudosections and the 2-D resistivity structures shown in Figures 4.15 to 4.19 were obtained within the study area. The 2-D resistivity structures showed the subsurface images inverted from the field data and its calculated theoretical data pseudo section revealing both lateral and horizontal variations in ground apparent resistivity values of the subsurface. The 2-D resistivity structures delineated three major subsurface layers; the top soil (blue to bluish green color band), the weathered layer (blue to green color band) and the basement bedrock (in yellow/reddish/purple color band). The topsoil generally transit into the weathered and the weathered layer into the fractured basement because of their close resistivity values.

The 2-D resistivity structure beneath traverse 2 (Figure 4.15) shows a very thin layer of the topsoil of about 0.2m with low resistivity values of less than 150 ohm-m. In the weathered layer at about 4 to 5m, there were pockets of very low resistive materials which could be indicative of leachate seeping from the top surface. These contaminants were clearly seen between stations (13 to 14), stations (15 to 16) and stations (18 to 19). The low resistivity values at stations (2 to 6) observed beneath depth 0.1m to above 15m of the subsurface showed an extension of the weathered layer towards the fresh basement which existed between stations (6 to 18) at depth of about 5m to 15m below the subsurface.

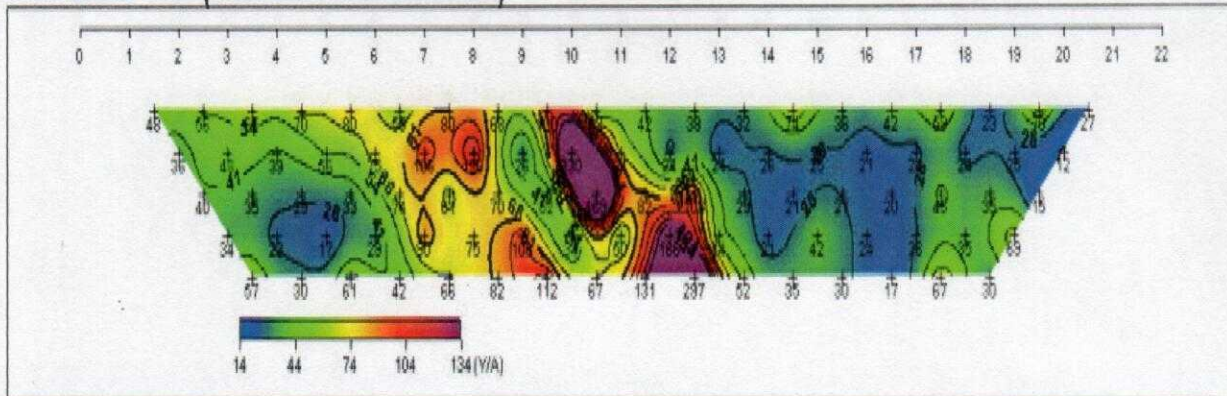
The 2-D resistivity structure beneath traverse 3 (Figure 4.16) shows the whole subsurface to be weathered. Below 5m of the subsurface, the 2-D resistivity structure showed series of fractures or suppressions between distances 15 to 30m; 35 to 45m; 50 to 65m and 70 to 85m. The most pronounced fracture or suppression occurred at the distance between 15 to 30m. No real form of fracturing or suppression of the basement between distances 60 to 95m. The entire subsurface in this traverse seemed to be highly weathered due to the presence of contaminant which could have passed through the fractures.

The 2-D resistivity structure beneath traverse 4 (Figure 4.17) shows the entire subsurface along this profile to be strongly affected by leachate infiltration. The resistivity value of the entire area along this profile ranges from 0.58 to 21120 ohm-m. A very high overburden with thickness of more than 15m is observed between distances 0 to 35m. A basement suppression could be seen between distances 60 to 80m.

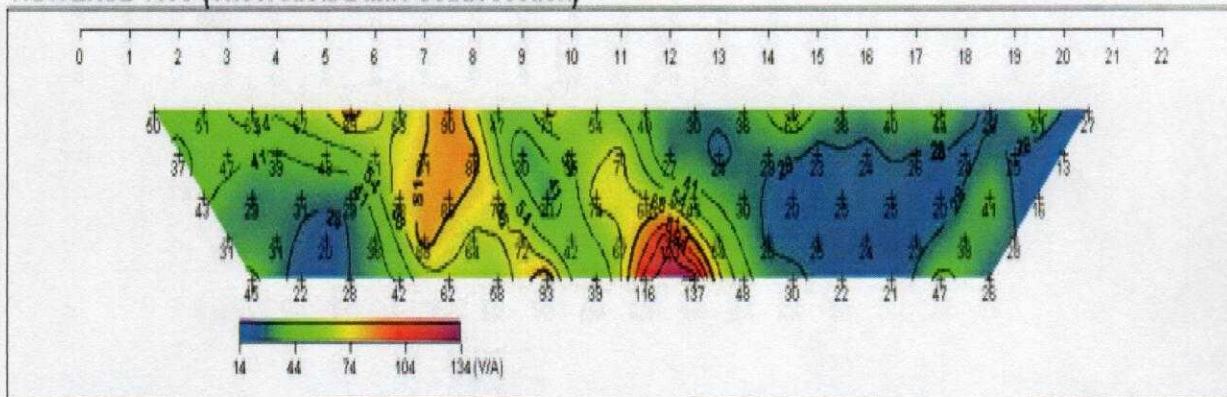
Traverse five was established beside a hand dug well in the village. The 2-D resistivity structure beneath traverse 5 (Figure 4.18) shows a thick top soil with resistivity value ranging from 90 to 160 ohm-m; this layer is suspected to be composed of sand while the second layer (weathered layer) is suspected to be composed of sandy-clay. The weathered layer beneath the topsoil have a low resistivity ranging from 21 to 93.5 ohm-m. Between 20 to 25m and 40 to 50m along the traverse, very low resistive materials were revealed and this could indicate the presence of contaminants. Due to the impermeable nature of clay present below the subsurface along this traverse, the contaminants would not be able to pollute the groundwater in this environment. Between 25 to 45m at depth 7m below the surface, there is the presence of the fresh basement.

The 2-D resistivity structure beneath the traverse established at the control point (Figure 4.19) reveals that the topsoil has high resistivity value ranging from 149 to 527m and thickness of about 10m. This layer is suspected to be a lateritic layer. This lateritic layer extended from about 15m of the profile to about the end of the profile but there is a different layer of probably sand formation between 55m and 60m. The weathered layer has a low resistivity value ranging from 51.9m to 79.9m. The last layer which is the fractured basement has a very low resistivity of less than 43.3 ohm-m indicating the presence of groundwater.

TRAVERSE TWO (Field Data Pseudosection)



TRAVERSE TWO (Theoretical Data Pseudosection)



VES 3

VES 4

VES 5

VES 6

TRAVERSE TWO (2-D Resistivity Structure)

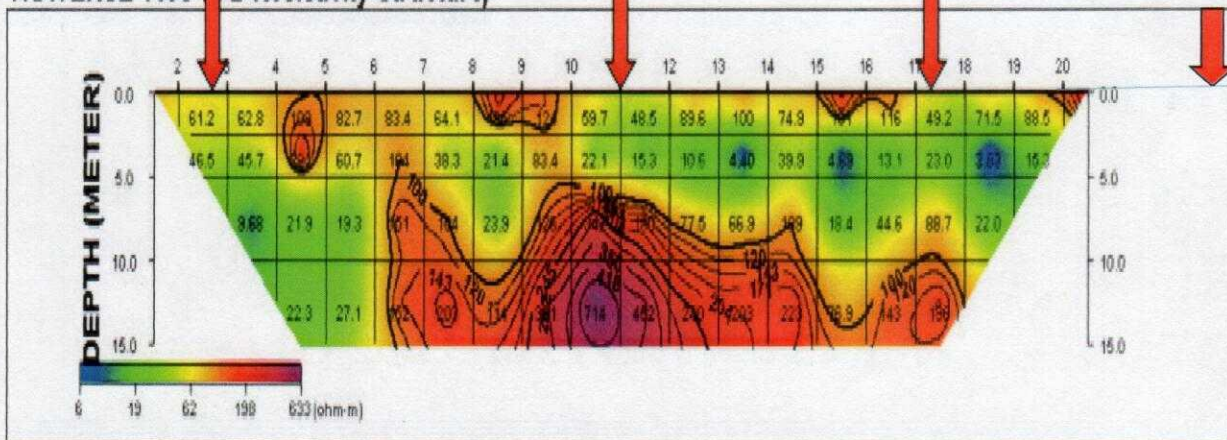
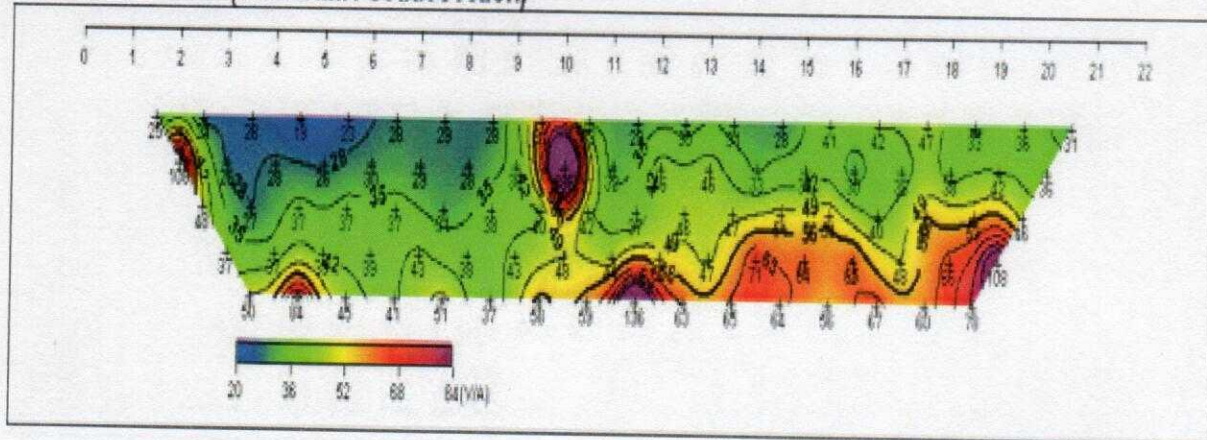
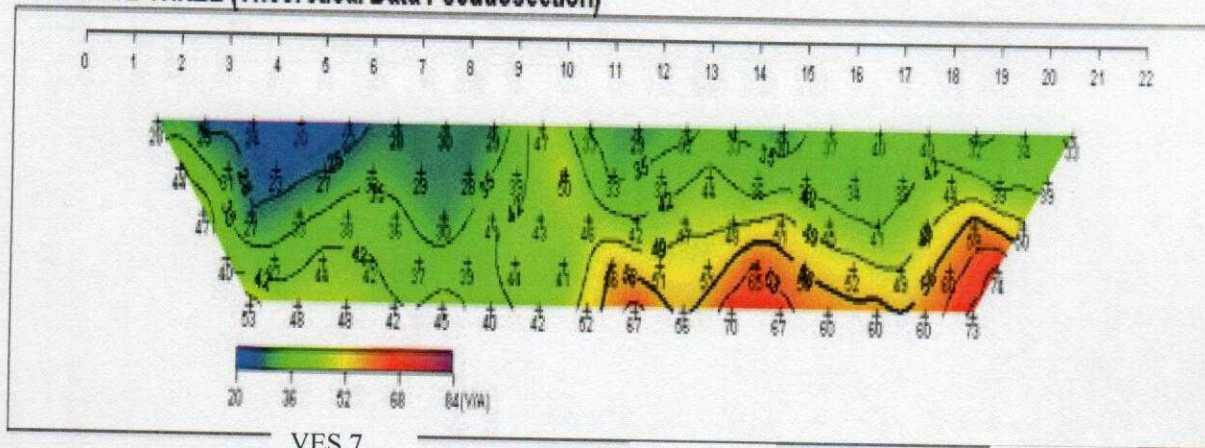


Figure 4.15: 2-D Resistivity Structure of Traverse 2

TRAVERSE THREE (Field Data Pseudosection)



TRAVERSE THREE (Theoretical Data Pseudosection)



VES 7

VES 8

VES 9

TRAVERSE THREE (2-D Resistivity Structure)

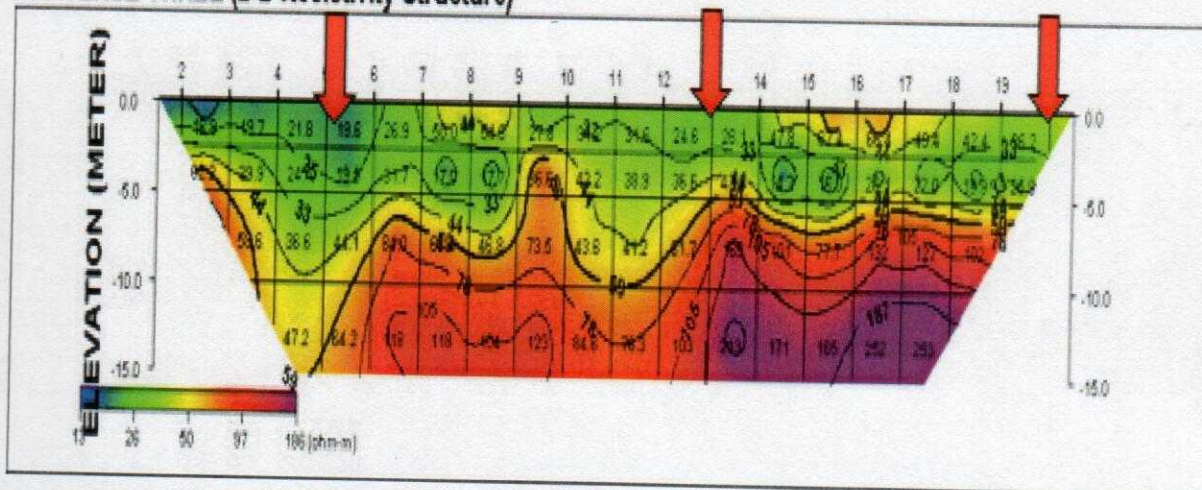
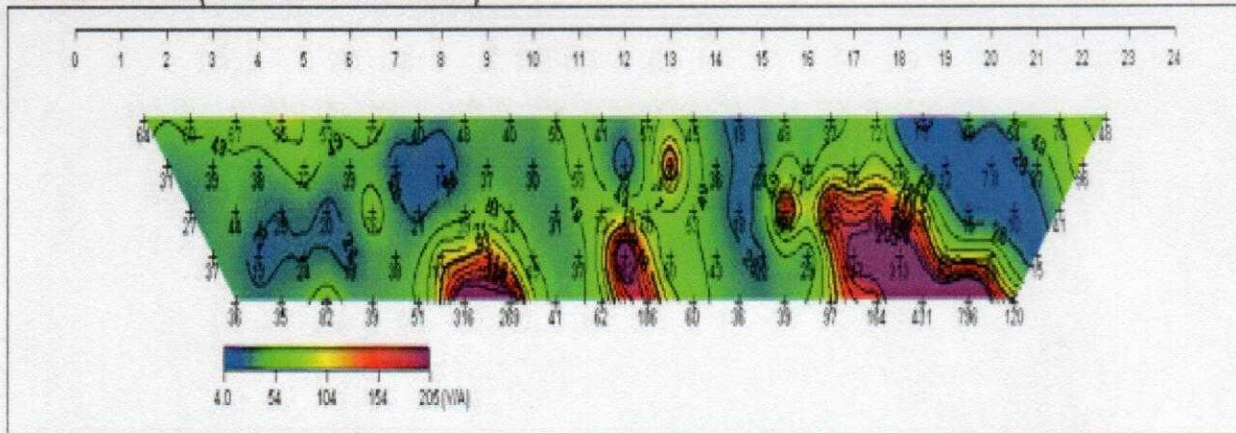
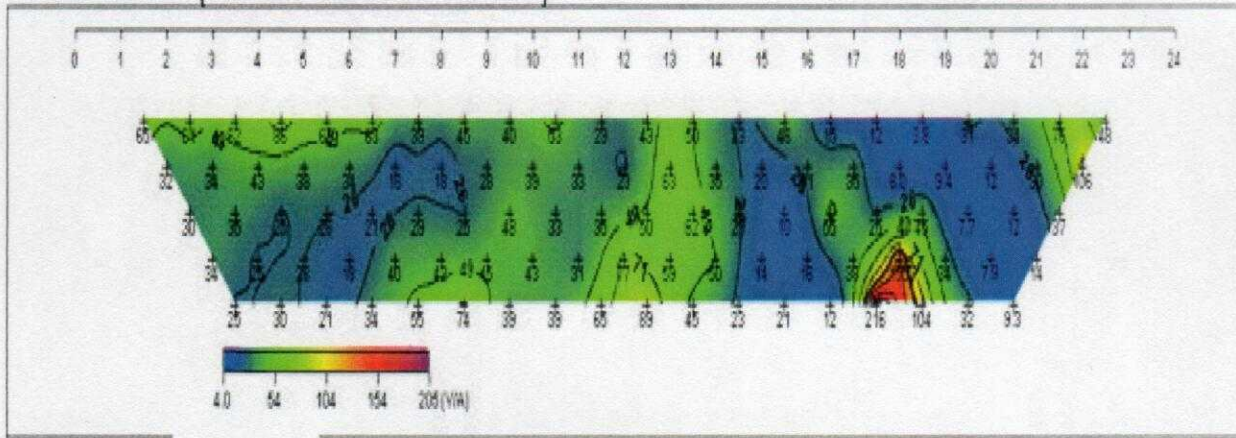


Figure 4.16: 2-D Resistivity Structure of Traverse 3

TRAVERSE FOUR (Field Data Pseudosection)



TRAVERSE FOUR (Theoretical Data Pseudosection)



VES 10

VES 11

VES 12

VES 13

VES 14

TRAVERSE FOUR (2-D Resistivity Structure)

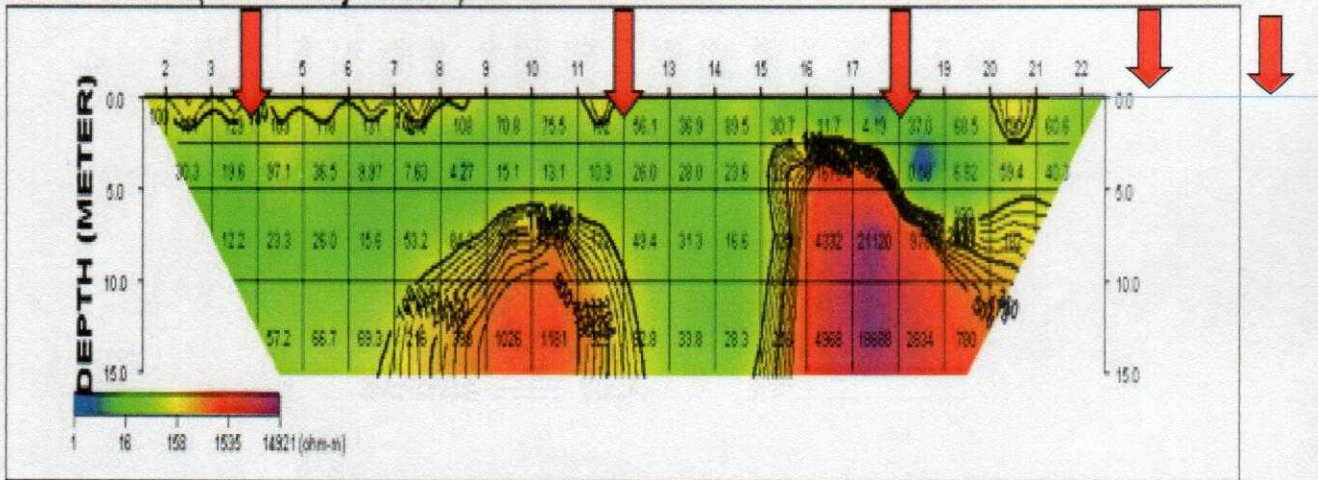
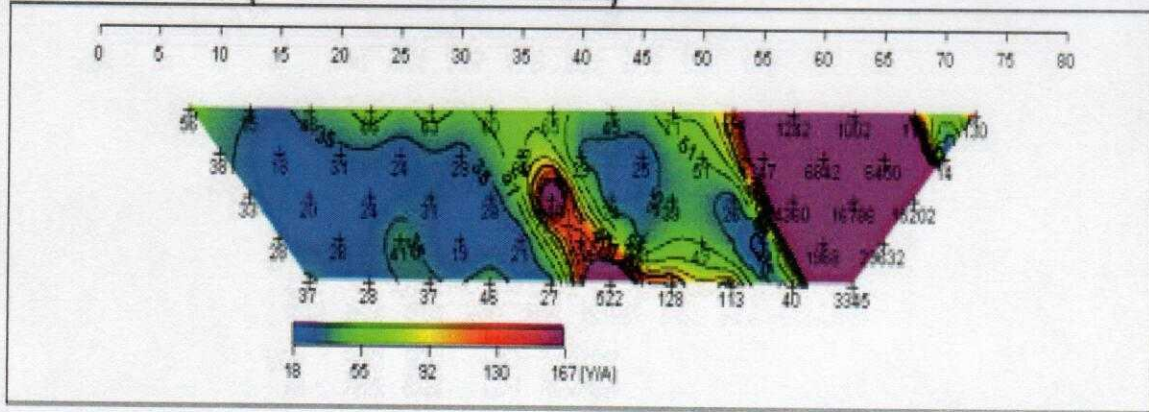
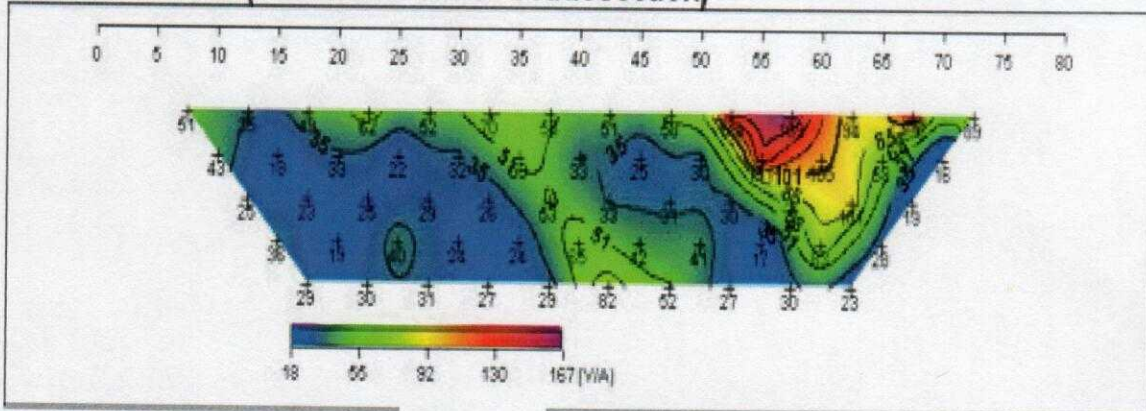


Figure 4.17: 2-D Resistivity Structure of Traverse 4

TRAVERSE FIVE (Field Data Pseudosection)



TRAVERSE FIVE (Theoretical Data Pseudosection)



VES 16

TRAVERSE FIVE (2-D Resistivity Structure)

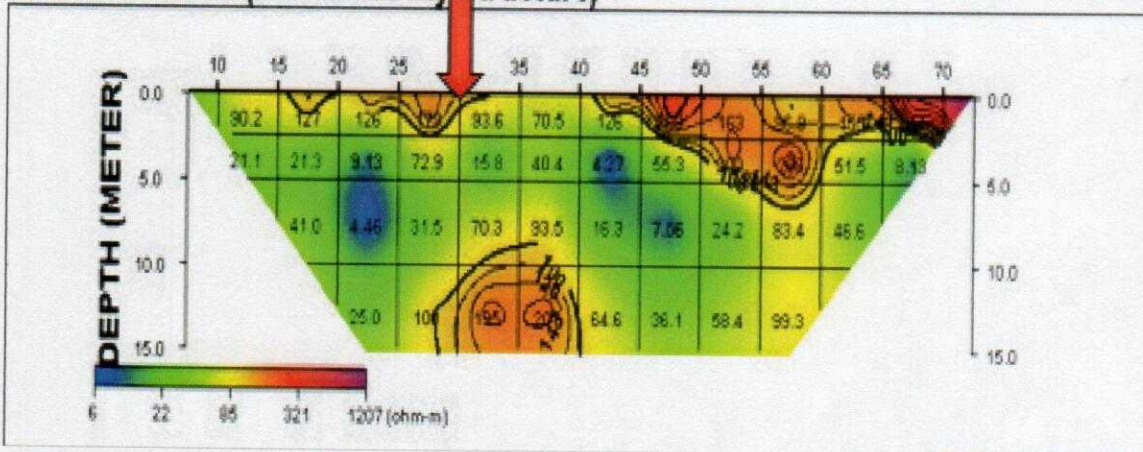
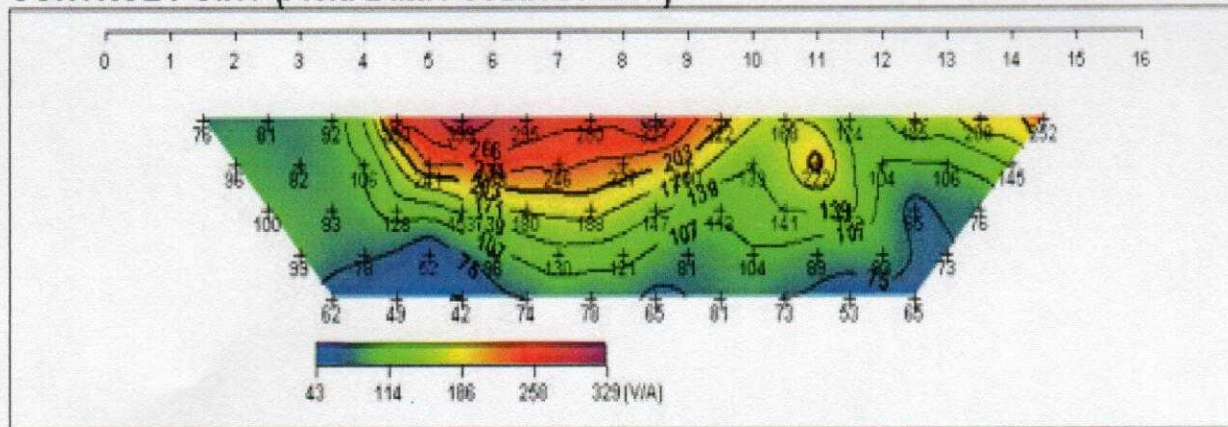
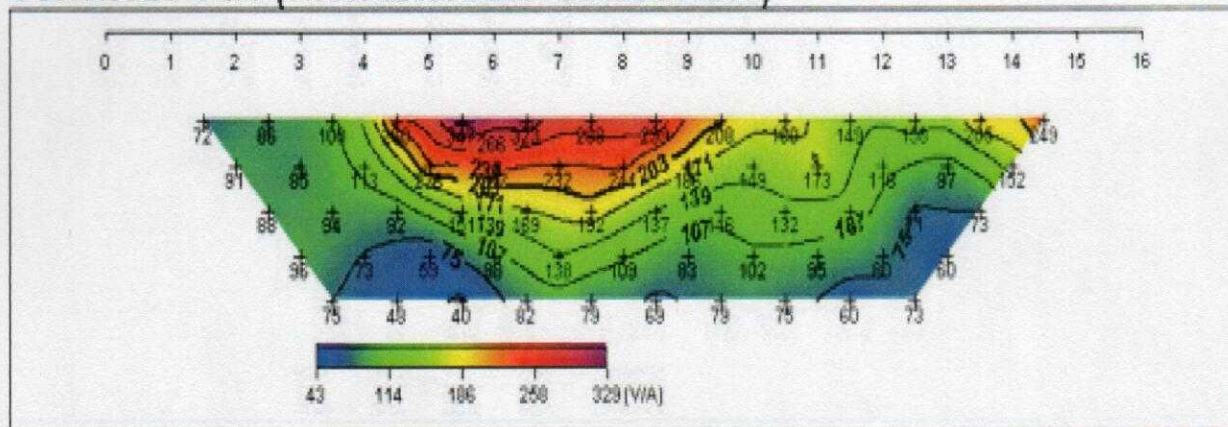


Figure 4.18: 2-D Resistivity Structure of Traverse 5(In the Village)

CONTROL POINT (Field Data Pseudosection)



CONTROL POINT (Theoretical Data Pseudosection)



CONTROL POINT (2-D Resistivity Structure)

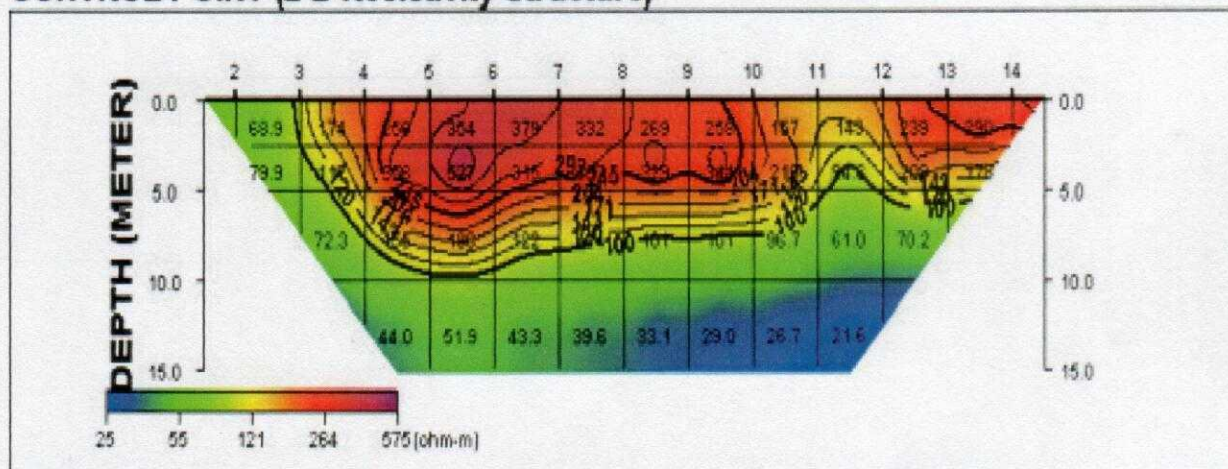


Figure 4.19: 2-D Resistivity Structure along the Control point

4.2.4 VERTICAL ELECTRICAL SOUNDING CURVES

The VES data were presented as depth sounding curves. The resistivity sounding curves of the 17 vertical electrical sounding stations obtained from the surveyed areas vary from 3-layer (H) to 4-layer (KH, HA and HK) as shown in the table 4.1. Typical curve types found within the study area are shown in the appendix.

4.2.4.1 GEO-ELECTRIC SECTIONS

The curves were characterized according to their signatures, which mirror the layering of the subsurface

Figure 4.20-4.26 shows the lithological characterization of the seventeen vertical electrical soundings carried out along the seven traverses established. The sections generally reveals maximum of four geoelectric layers within the study area which could be classified into three major geologic layers: the top soil, the weathered layer and the fresh basement rock.

The topsoil resistivity varies from 30 to 210 ohm-m with thickness range of between 0.5 to 1.5m. It is composed of sand, clay, sandy-clay and clayey-sand. The weathered layer's resistivity varies from 6 to 52 ohm-m with thickness range of between 1.5 to 16.5m. This layer is composed of majorly sand. There were also presence of lateritic materials of thickness of 3.3m at VES 9 and thickness of 0.9m at VES 2. The real formation of the weathered have being highly distorted through the infiltration of contaminants.

From the geoelectric sections of each traverse, it is observed that the leachate from the waste materials have polluted the groundwater in the environment. The wells in the village and at the control point seemed not to have being polluted due to the presence of a clay formation in the subsurface.

Table 4.1: Summary of the Vertical electrical sounding curves

STATION POSITION	LAYER NO	RESISTIVITY OHM-M	DEPTH (m)	LITHOLOGY	CURVE TYPE
TR1(VES1)	1	42	0.8	Topsoil	KH
	2	99	2.2	Topsoil	
	3	14	7.0	Weathered layer	
	4	1664	----	Fresh basement	
TR1(VES2)	1	70	0.5	Topsoil	KH
	2	442	1.4	Lateritic layer	
	3	22	8.2	Weathered layer	
	4	923	-----	Fresh basement	
TR2(VES3)	1	24	0.6	Topsoil	KH
	2	130	1.6	Topsoil	
	3	33	14.5	Weathered basement	
	4	10022	-----	Fresh basement	
TR2(VES4)	1	106	1.4	Topsoil	H
	2	10	3.7	Weathered layer	
	3	13583	----	Fresh basement	
TR2(VES5)	1	109	1.3	Topsoil	H
	2	26	8.6	Weathered layer	
	3	11963	----	Fresh basement	
TR2(VES6)	1	177	1.6	Topsoil	HA
	2	14	3.7	Weathered layer	
	3	58	8.8	Weathered layer	
	4	3262	-----	Fresh basement	
TR3(VES7)	1	56	0.8	Topsoil	H
	2	42	11.8	Weathered basement	
	3	1813	-----	Fresh basement	
TR3(VES8)	1	44	0.7	Topsoil	KH
	2	94	1.9	Clay	
	3	26	8.3	Weathered layer	
	4	1430	-----	Fresh basement	

TR3 (VES9)	1	78	0.8	Topsoil	KH
	2	1155	4.1	Lateritic layer	
	3	53	16.5	Weathered layer	
	4	872	-----	Fresh basement	
TR4 (VES 10)	1	33	1.1	Topsoil	KH
	2	25	7.6	Topsoil	
	3	196	11.1	Weathered layer	
	4	10765	-----	Fresh basement	
TR4 (VES11)	1	33	0.5	Top soil	KH
	2	120	1.2	Topsoil	
	3	10	3.0	Weathered layer	
	4	432	-----	Fresh basement	
TR4 (VES12)	1	53	1.1	Topsoil	HA
	2	15	3.7	Topsoil	
	3	166	11.4	Weathered basement	
	4	3575	-----	Fresh basement	
TR4 (VES 13)	1	27	0.5	Topsoil	KH
	2	333	0.7	Lateritic layer	
	3	37	6.3	Weathered layer	
	4	2216	-----	Fresh basement	
TR4 (VES 14)	1	203	1.1	Topsoil	H
	2	16	2.4	Weathered layer	
	3	220	-----	Fresh basement	
TR5 (VES 15)	1	75	0.7	Topsoil	H
	2	6	2.2	Weathered layer	
	3	1529	-----	Fresh basement	
VES 16	1	155	1.6	Topsoil	H
	2	12	11.6	Weathered layer	
	3	1404	-----	Fresh basement	
CONTROL	1	39	1.5	Topsoil	HK
	2	16	1.8	Topsoil(clay)	
	3	148	3.0	Fractured basement	
	4	48	-----	Weathered layer	

GEOELECTRIC SECTIONS

TRAVERSE ONE

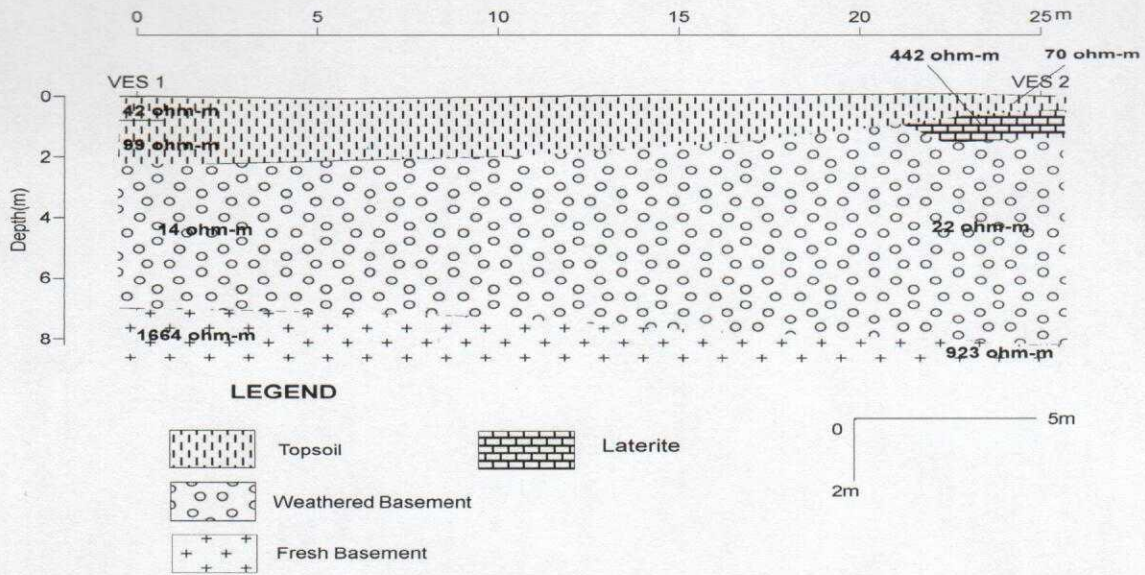


Figure 4.20: Lithological characterization of the subsurface along Traverse 1

TRAVERSE TWO

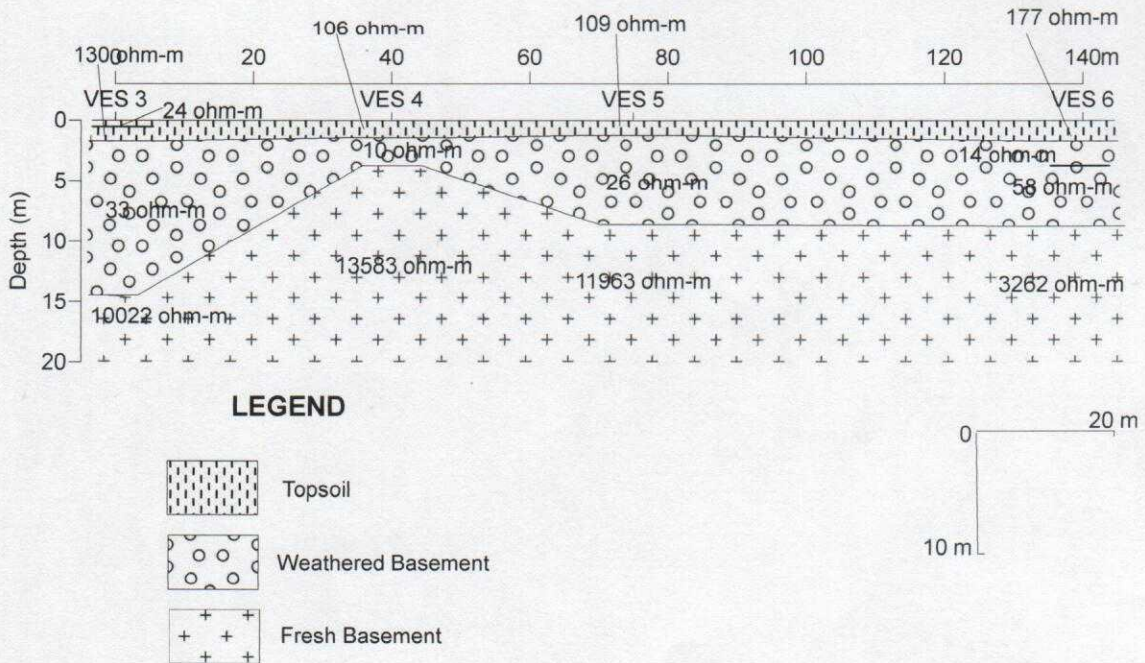


Figure 4.21: Lithological characterization of the subsurface along Traverse 2

TRAVERSE FIVE



LEGEND

-  Topsoil
-  Weathered Basement
-  Fresh Basement

Figure 4.24: Lithological characterization of the subsurface along Traverse 5

COLUMNAL SECTION OF A PARAMETRIC SOUNDING OF THE WELL IN THE VILLAGE

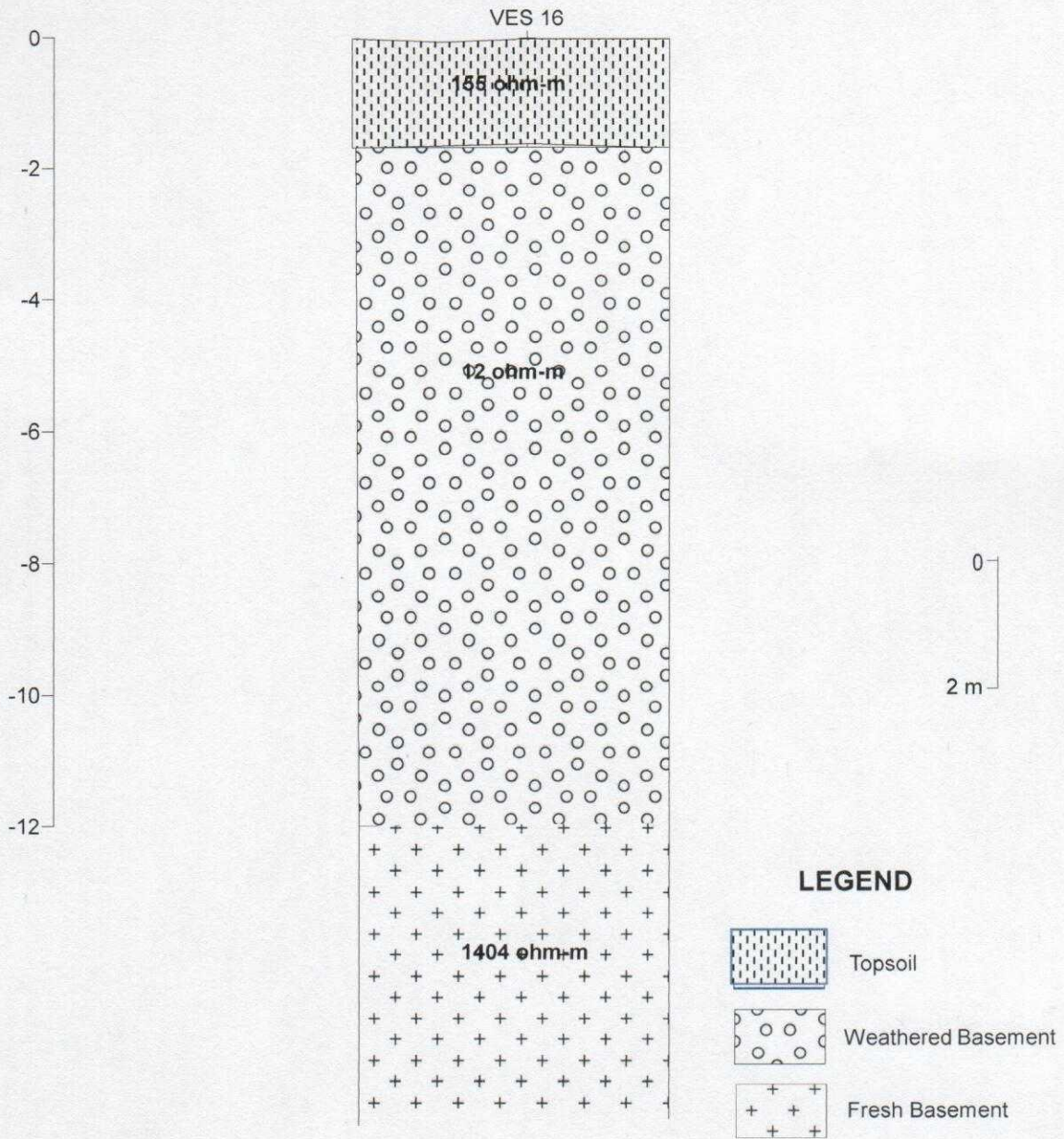


Figure 4.25: Lithological characterization of the well in the village.

CONTROL POINT

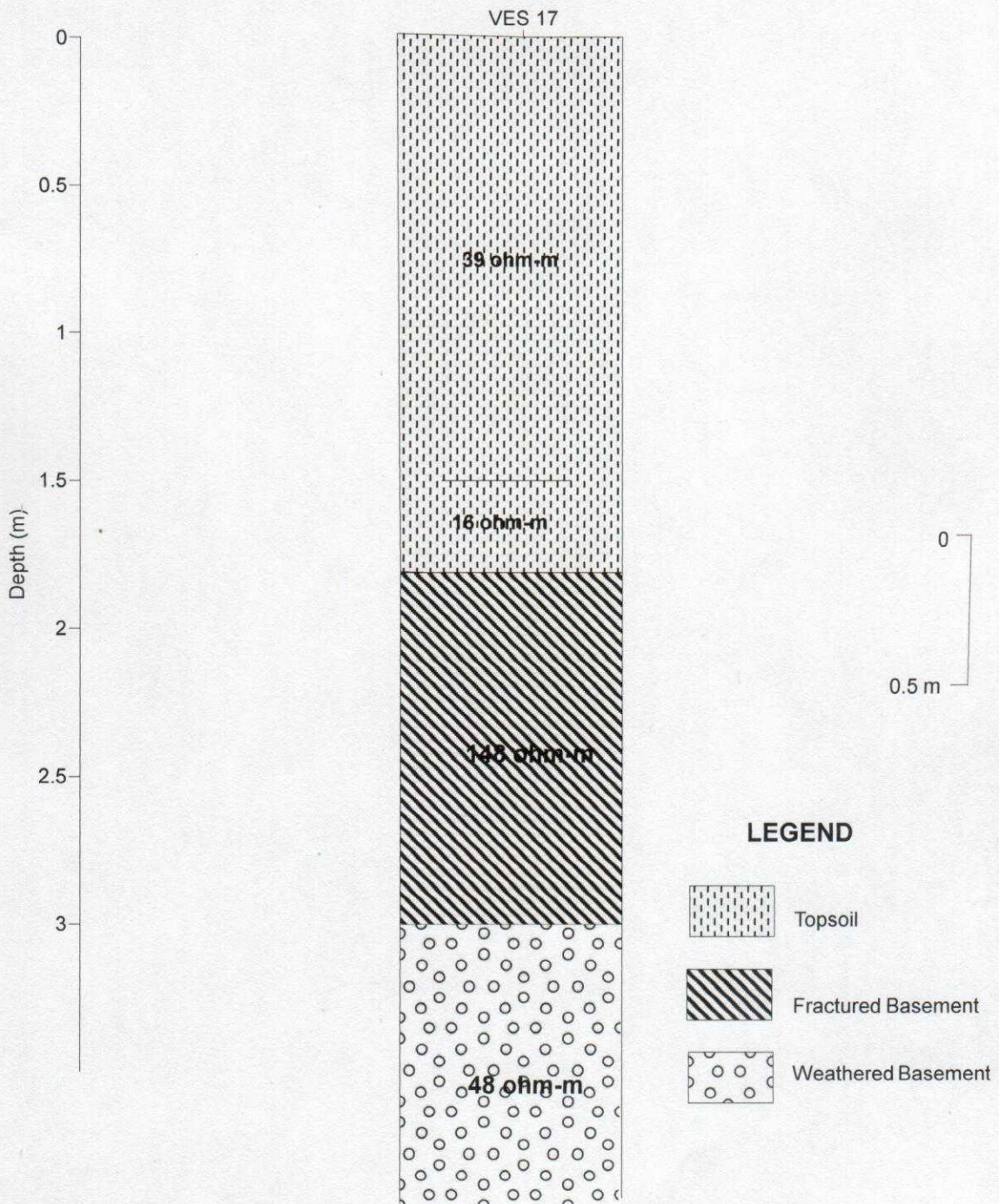


Figure 4.26: Lithological characterization of the subsurface along the Control Point

4.2.5 CORRELATION OF 2-D MODELS (VLF-EM); 2-D RESISTIVITY STRUCTURES; GEOMAGNETIC SECTIONS AND GEOELECTRIC SECTIONS.

Figure 4.27 to 4.32 shows the combined correlation of all the geophysical results obtained within the study area.

The VLF-EM 2-D model obtained on traverse 1 Figure (4.27a) showed the presence of a conductive zone at 25m along the traverse which could indicate the presence of a fault or fracture. This geologic fissure was also seen in the geomagnetic section generated for this traverse (Figure 4.27b). The geomagnetic section revealed the presence of a high overburden thickness. Due to the presence of a geologic fissure (fracture or fault) in the overburden; there is a high possibility of infiltration of leachate from the waste dump into the groundwater system below this traverse. The high overburden thickness observed in the geomagnetic section was also seen in the geoelectric section designed for this traverse. Figure 4.27a-c

The VLF-EM Karous Hjelt pseudosection obtained along traverse 2 (Figure 4.28a) revealed a low conductive body at distance between 20-43m suspected to be a sandy layer, the same layer was also revealed through the 2-D resistivity structure. Both the KH pseudo section and the 2-D resistivity structure reveals the presence of a conductive zone of 55m long. A shallow overburden of about 5m was revealed at distance between 30 to 80m on the traverse by both the geo-electric section and the 2-D resistivity structure. Figure 4.28a-c.

The VLF 2-D Model and the 2-D resistivity structure obtained along traverse 3 show an overburden of high conductivity. The high degree of conductivity in this area could be due to the infiltration of leachate emanating from the waste materials. The 2-D resistivity structure show a basement suppression beneath VES 7; a similar observation was very much noted in the geoelectric section designed of this traverse. Figure 4.29a-c

The dipole 2-D resistivity structure obtained along traverse 4 (Figure 4.30b) show that the subsurface is high polluted by leachates. The suppressed basement observed at distance between 60-75m on the 2-D resistivity structure correlate with the very the geoelectric section of the area showing that the basement is at the depth 12m below the top surface.

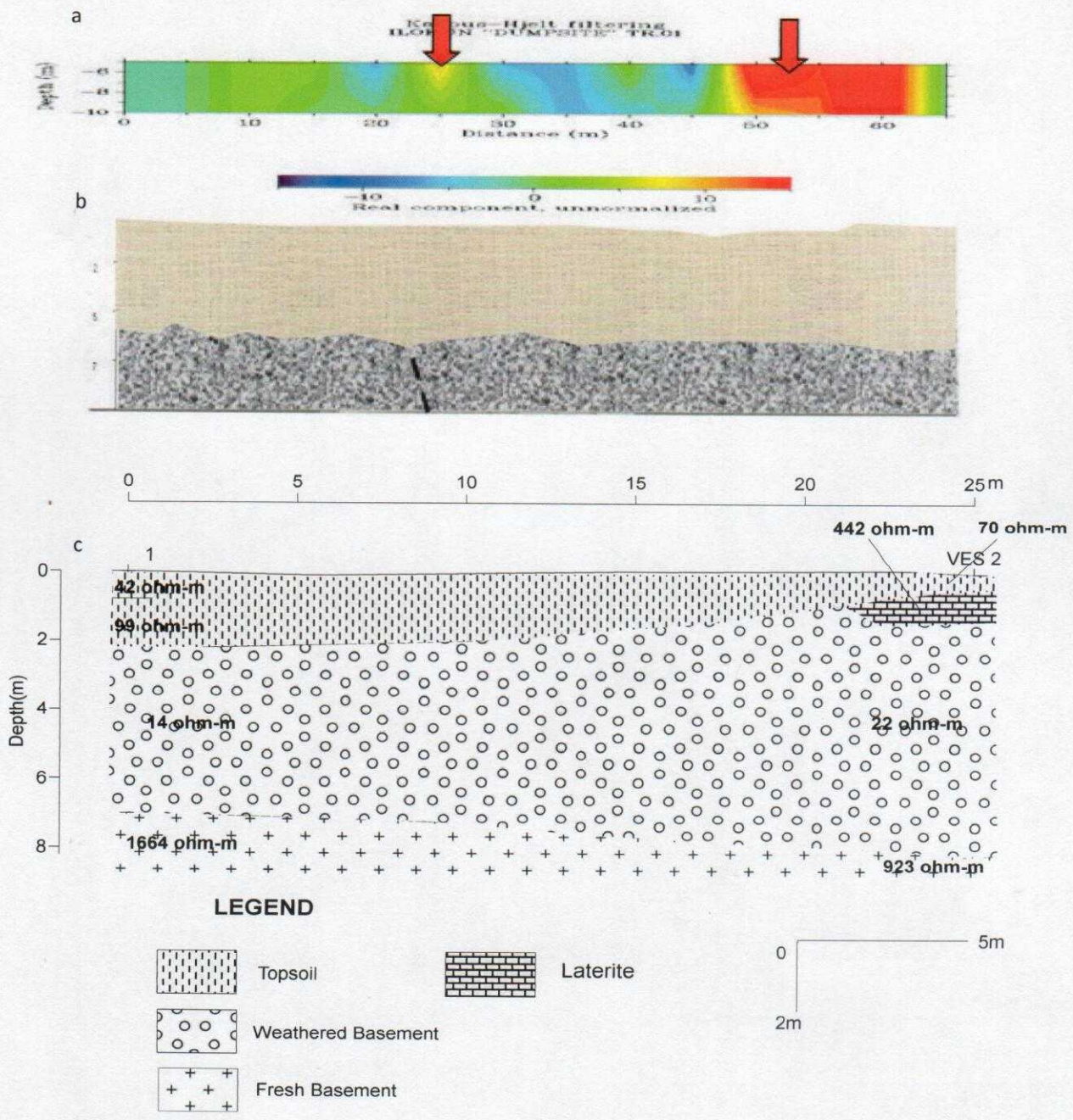


Figure 4.27a-c: 2-D Resistivity Structure, KH Model and Geoelectric and Geomagnetic section of Traverse 1

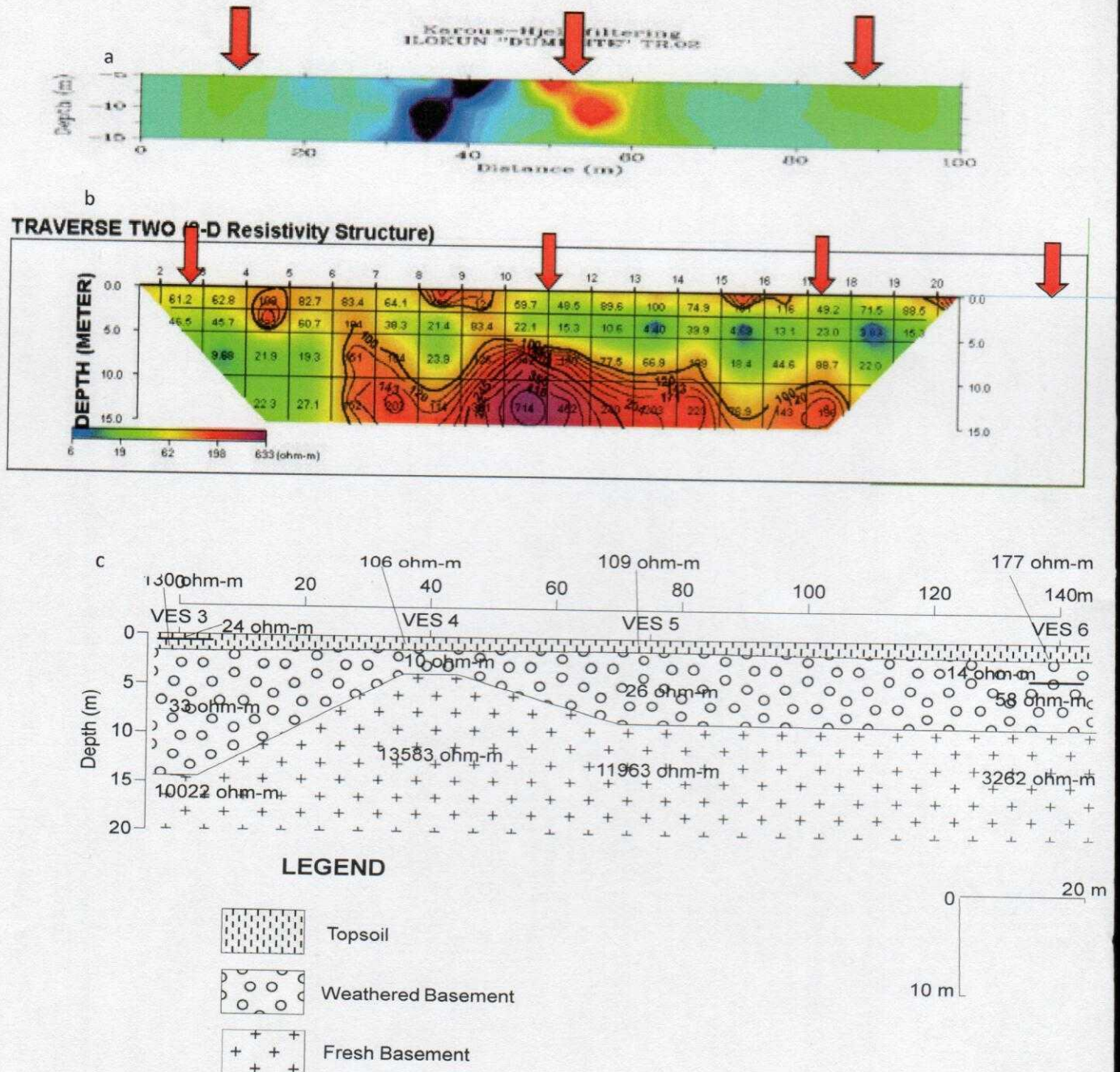


Figure 4.28a-c: 2-D Resistivity Structure, KH Model and Goelectric section of Traverse 2

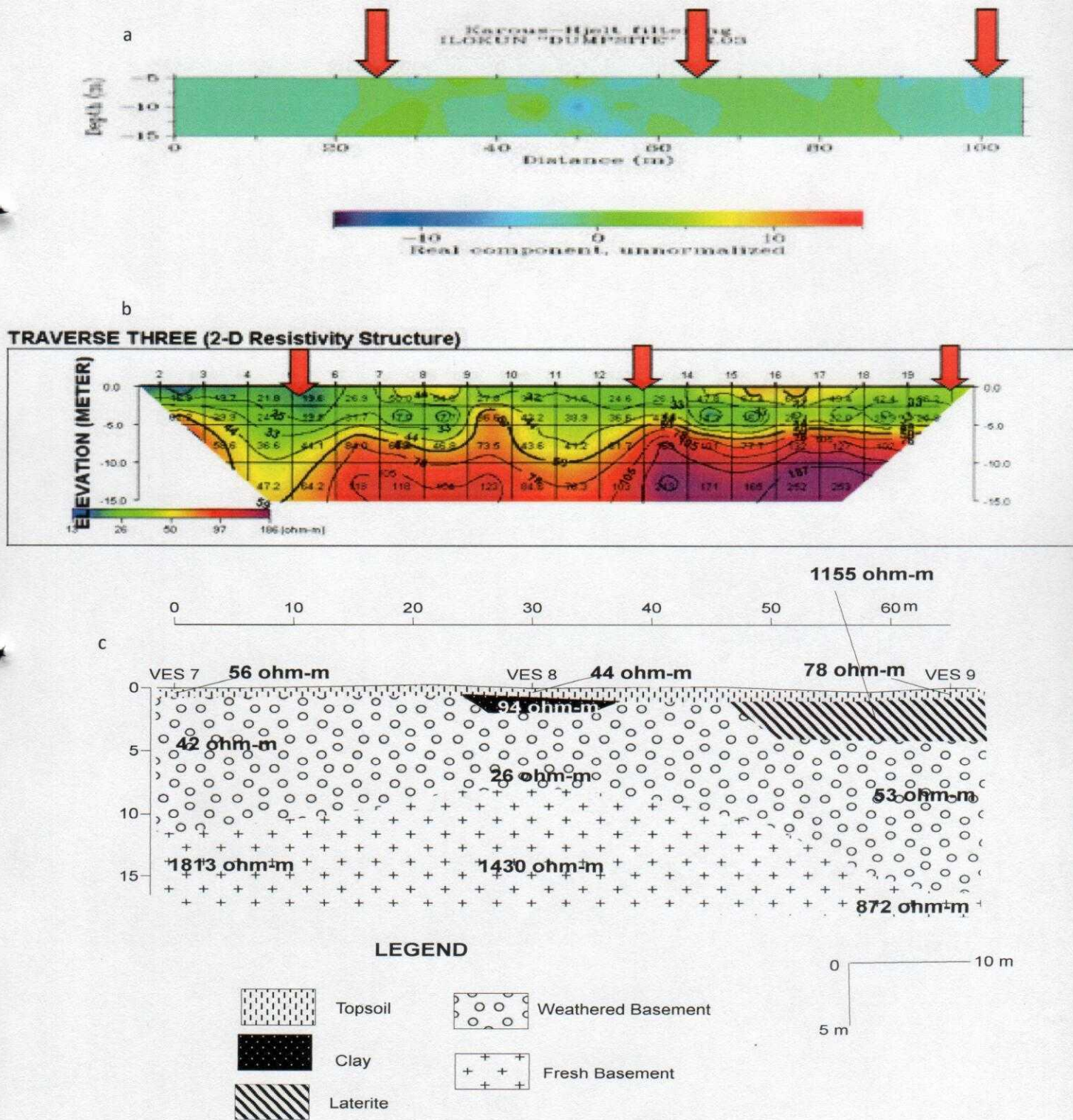


Figure 4.29a-c: 2-D Resistivity Structure, KH Model and Geoelectric section of Traverse 3

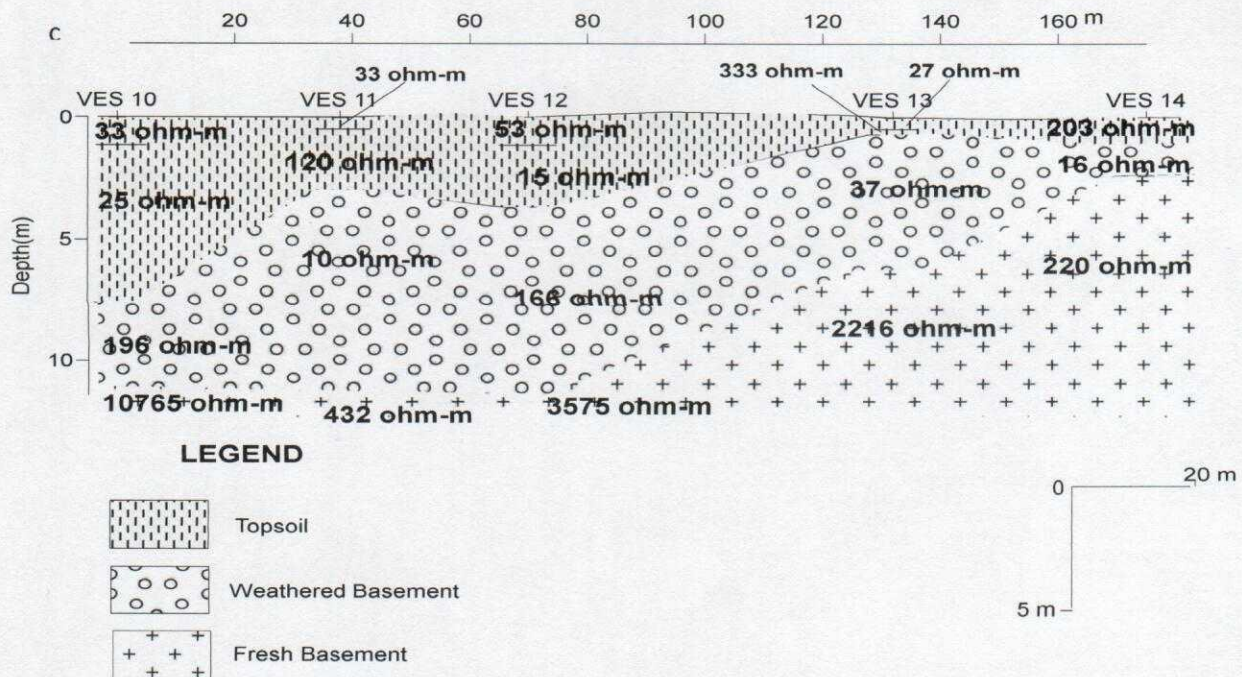
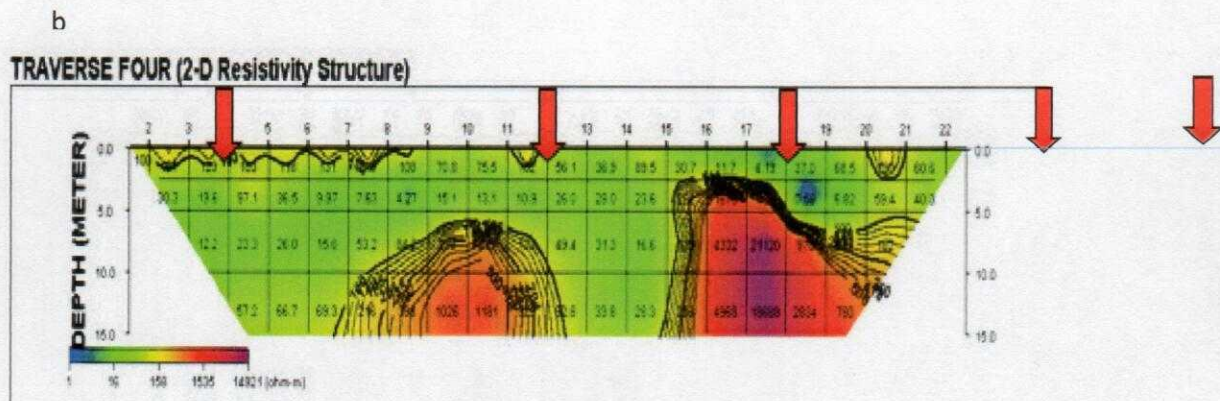
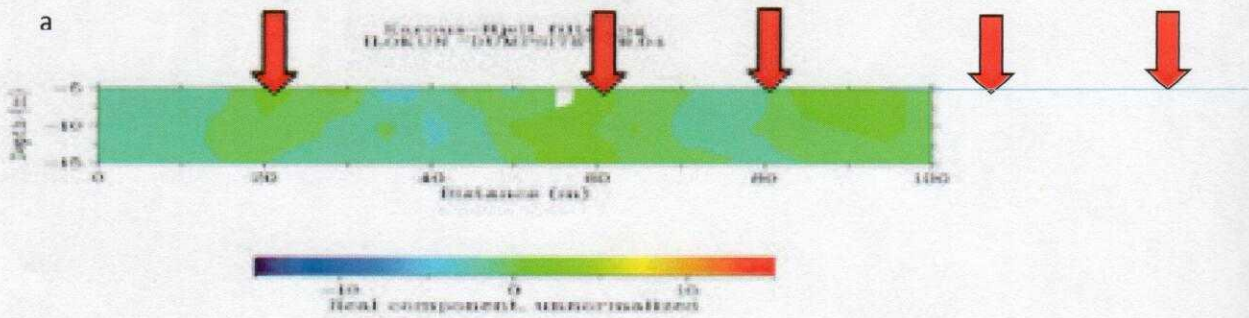
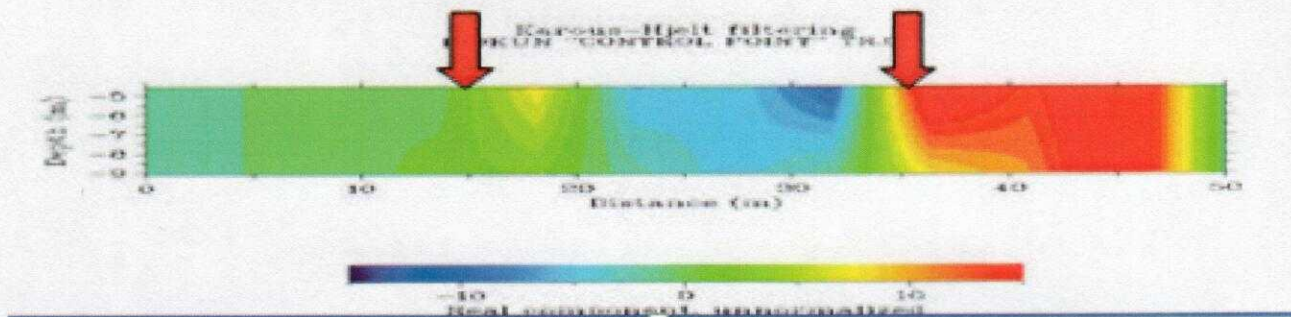


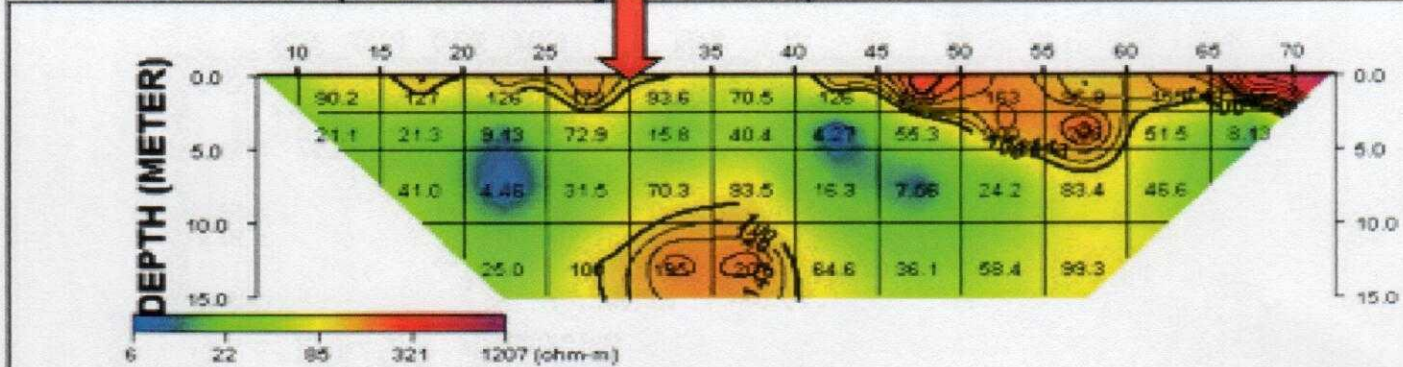
Figure 4.30a-c: 2-D Resistivity Structure, KH Model and Geoelectric section of Traverse 4

a



b

TRAVERSE FIVE (2-D Resistivity Structure)



c

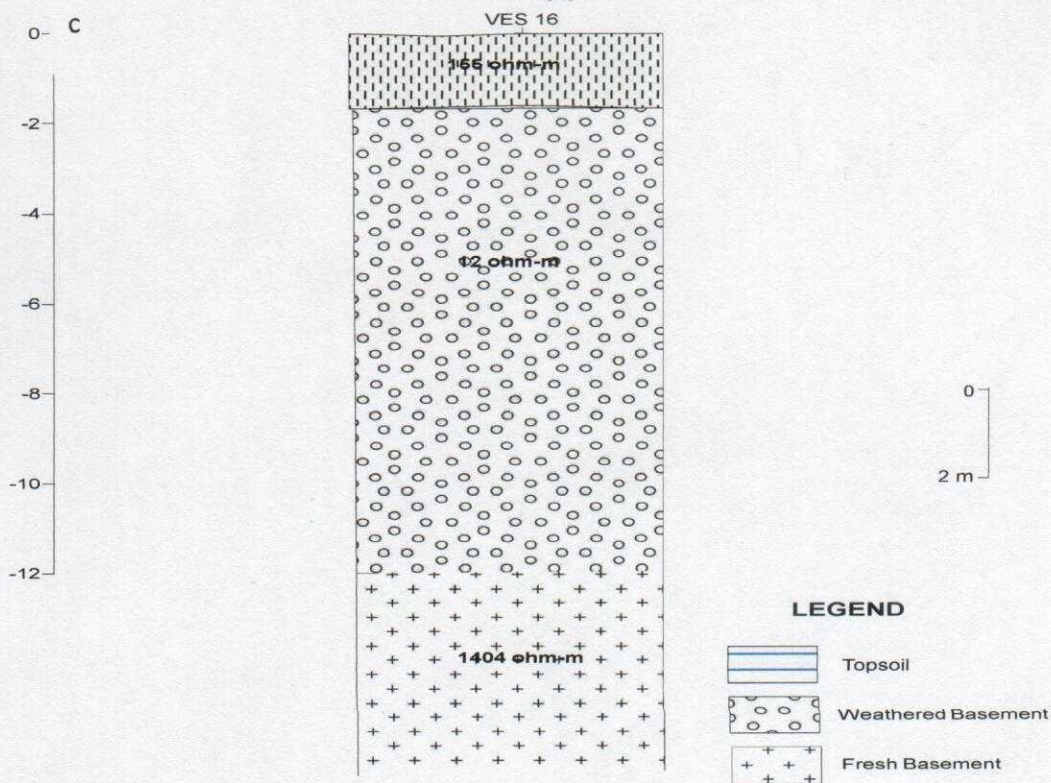


Figure 4.31a-c: KH Model, 2-D Resistivity structure and Geoelectric section of Travers 6

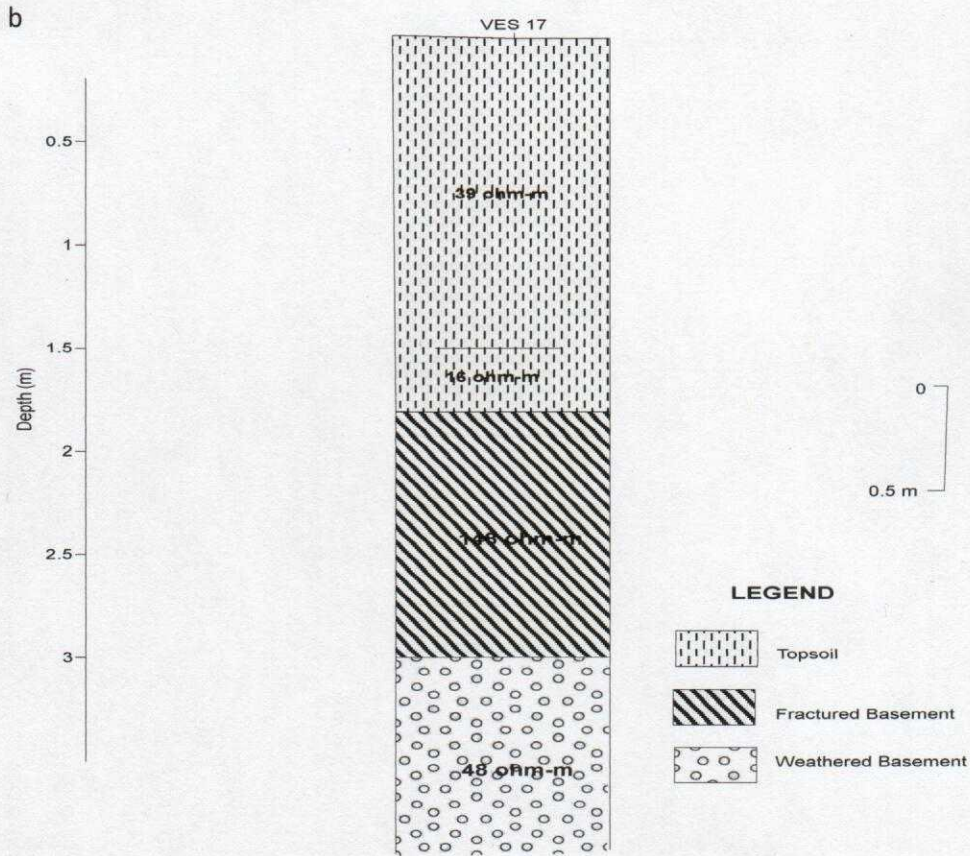
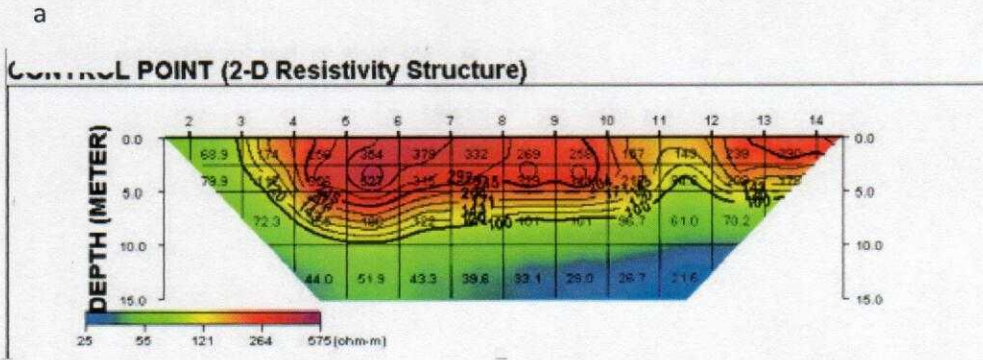


Figure 4.32a-b: 2-D Resistivity Structure and Geo section of Control point

4.2.6 GEOELECTRIC MAPS

Isoresistivity map of topsoil

The topsoil resistivity varies from 30 to 210 ohm-m. The map shows that the topsoil resistivity is less than 50 ohm-m to the north and the northwest typifying a clayey unit and/or leachate polluted zones (Figure 4.33). The moderate resistivity zones found in the west, northwestern and the southwestern part of the study area indicates the presence of sandy clay and clayey sand within these areas while the high resistivity zone found in the eastern and southwestern part around VES is typical of a sandy topsoil which have not being polluted by the leachates. The traverse 3 and some part of traverse 4 are the traverse lines that have low resistivity value which could be due to leachate impact.

Isopach map of topsoil

The isopach (thickness) map varies from 0.5 to 1.6. The map (Figure 4.34) shows that VES 4, 5, 6 and 14 have high thicknesses. VES 1, 2, 3, 8, 9, 10, 11 and 13 have low thicknesses (i.e.; they have thin layers). Due to the porous and permeable nature of areas with thick topsoil, the subsurface is still vulnerable to infiltration of leachates.

Isoresistivity map of weathered layer

Figure 4.35 shows the isoresistivity map of the weathered layer. This layer have resistivity value ranging from 6 to 52 ohm-m. The map shows that the weathered layer of VES 1, 4, 10, 11 and 12 have a very low resistivity value of less than 20 ohm-m. The areas with resistive weathered layer are around VES 7, 8 and 9.

Isopach map of weathered layer

The weathered layer has thickness varying from 1.5 to 16.5 ohm-m. The map (Figure 4.29) shows the weathered layer has thickness less than 4.5m at the western and the northwestern; areas with moderate thickness are found in some areas around the western, southwestern and

the northwestern part of the study area. Areas with low thickness are found in the eastern and the northeastern part of the study area.

Isoresistivity of the basement

The basement resistivity ranges from -1500 to 13500 ohm-m. The map shows that areas at the north, western and the northwestern part of the study area have a very low resistivity value of even as low as -1500 ohm-m (Figure 4.30). The low resistivity values of the basement is indicative of the presence of leachate weathering and polluting the basement formation.

Elevation map

The elevation of the study varies from 388 to 407m. The map clearly shows the direction flow of the leachate in the dumpsite (Figure 4.31). Due to the high elevation of the control point and the hand dug well at the village, leachate from the dumpsite will be unable to flow upward towards to pollute the wells, rather, the leachate will flow downward. Areas around the eastern and the northeastern part of the study area are more polluted than areas at the western part of the dumpsite.

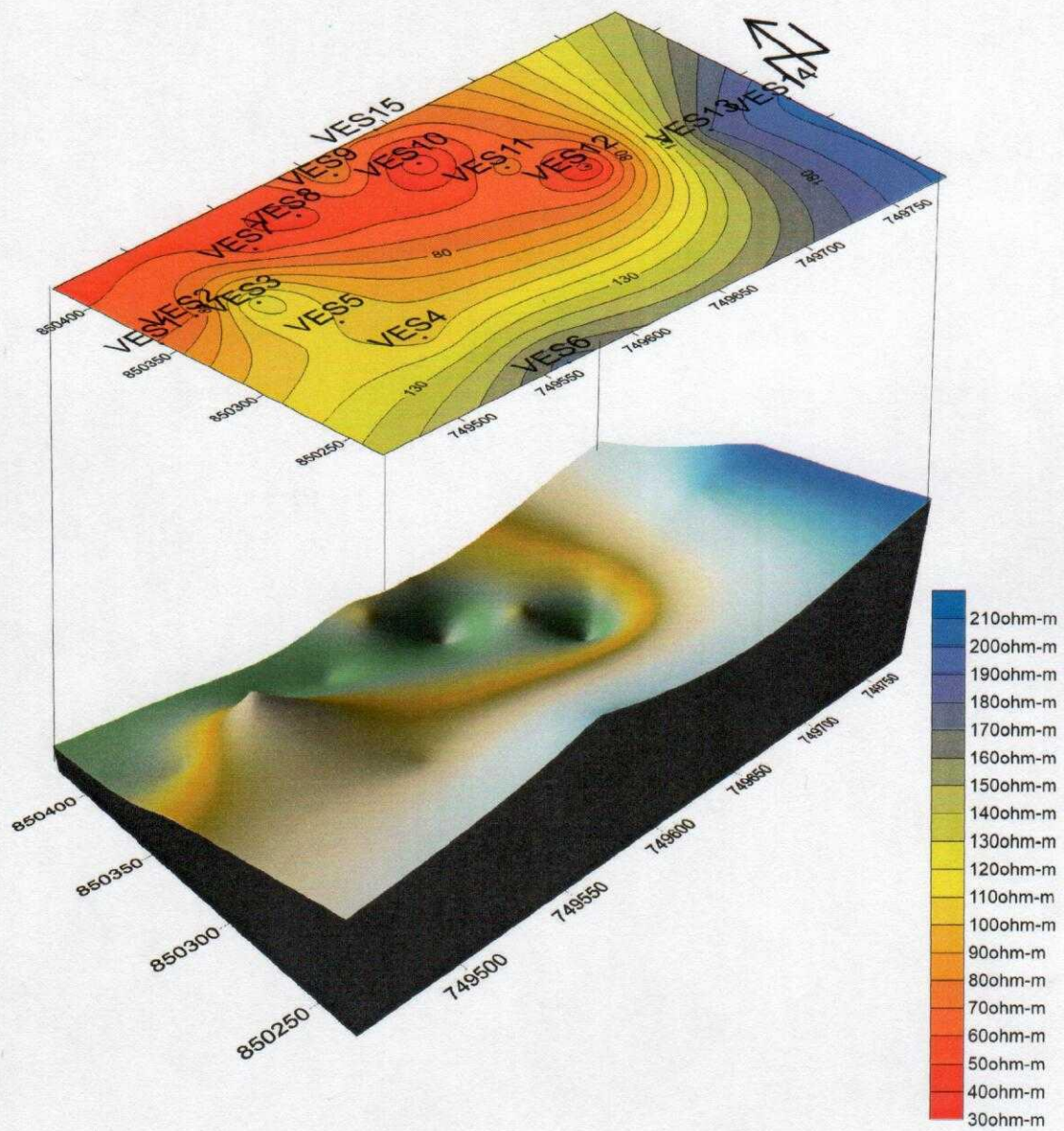


Figure 4.33: Isoresistivity map of Topsoil

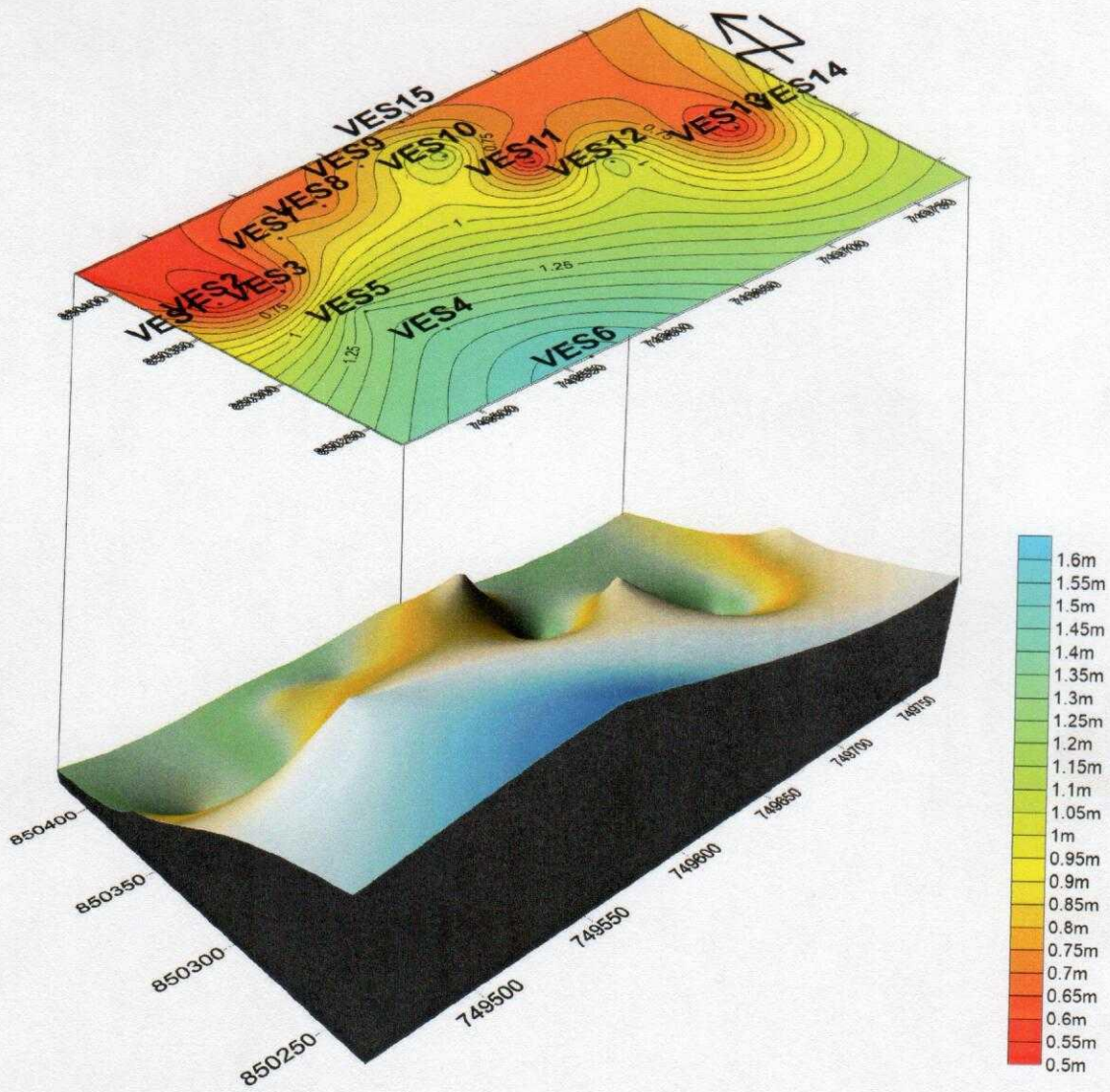


Figure 4.34: Isopach map of Topsoil

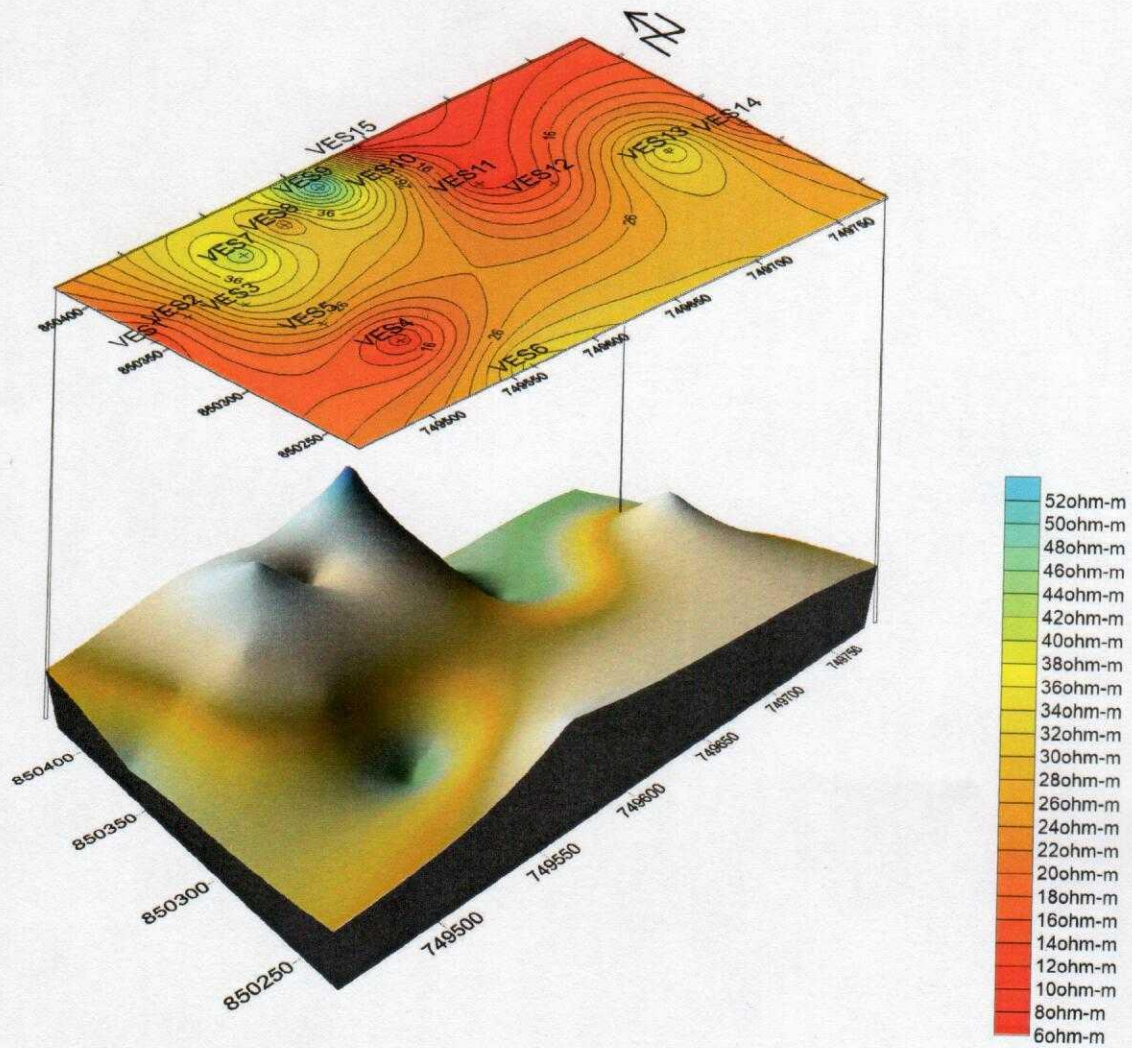


Figure 4.35: Isoresistivity map of Weathered Layer

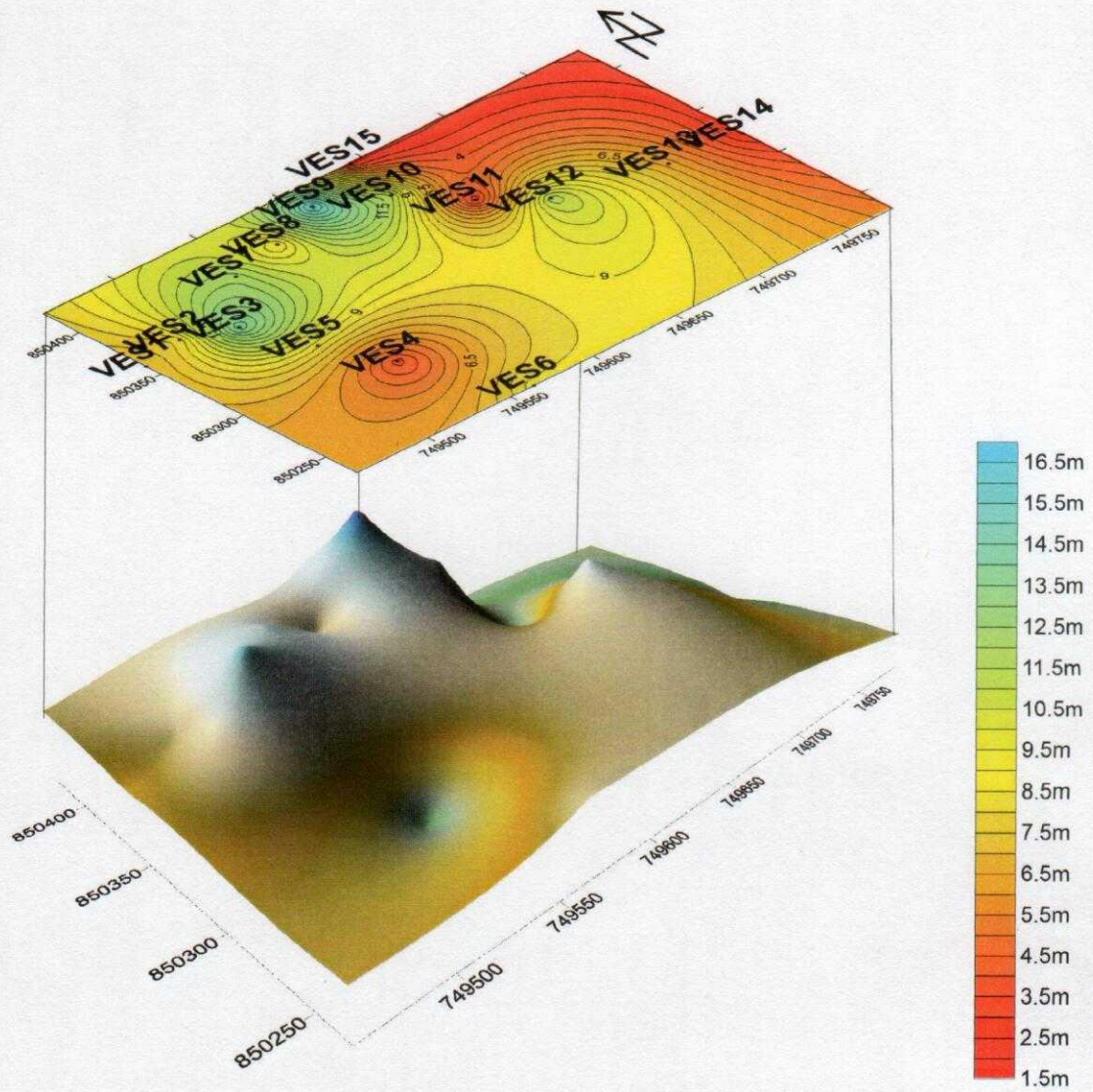


Figure 4.36: Isopach map of Weathered Layer

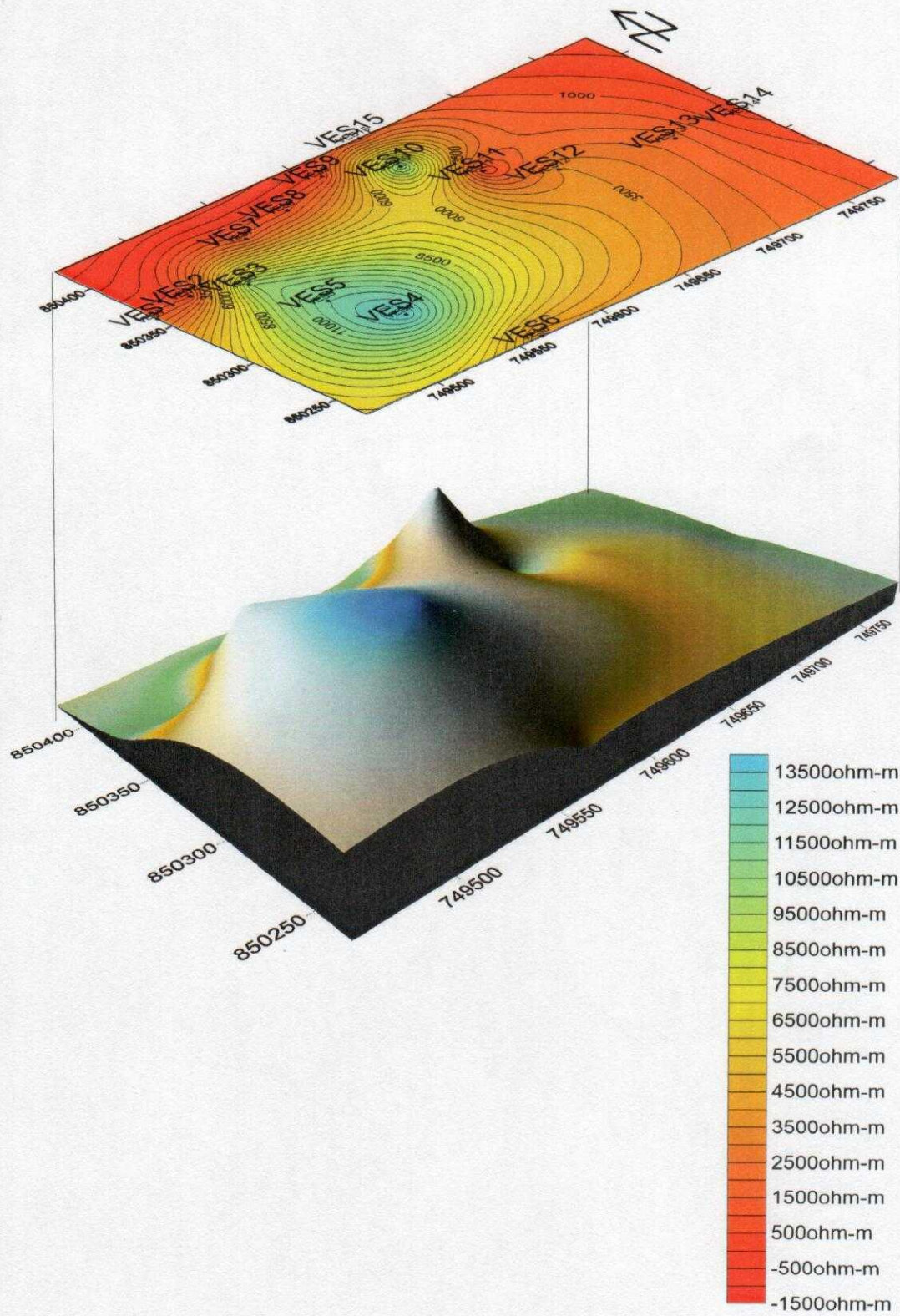


Figure 4.37: Isoresistivity map of Fresh basement

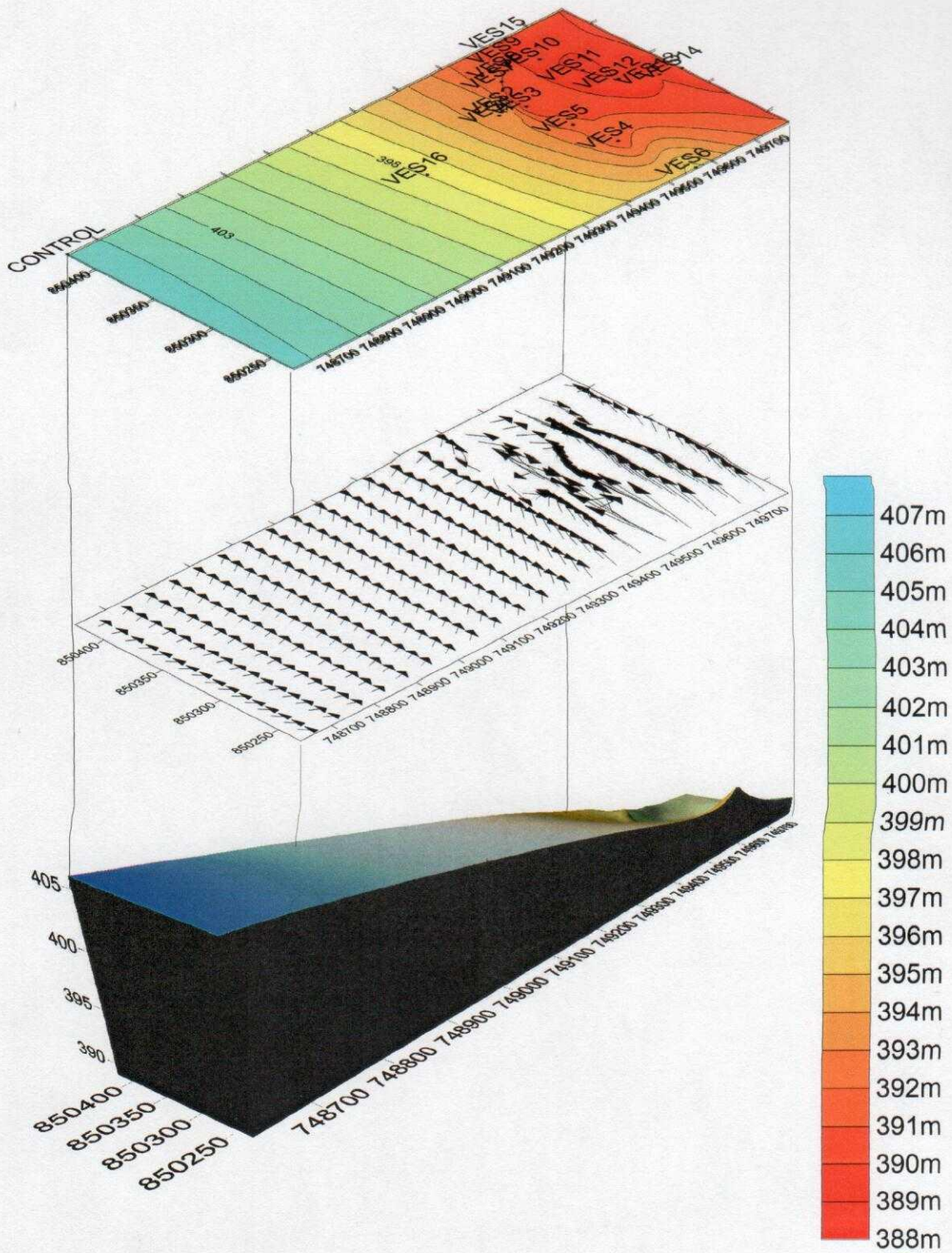


Figure 4.38: Elevation map of the study area

4.7 PHYSICO-CHEMICAL ANALYSIS

The results of the Physico-chemical analysis of the water samples collected from the village and the control points are shown in Tables 4.2 and Table 4.3.

Table 4.2: Physico-chemical analysis of the water sample collected at the Control point

PARAMETERS		CONTROL POINT	FEP A (1988)	WHO (1991)
PHYSICAL	Temperature (°C)	28.6		
	Turbidity (NTU)	0.001	Nil	
	Conductivity (Uhoms/cm)	142.5		Nil
CHEMICAL (mg/L)	pH	6.235	6.0-8.5	7-8.5
	Total dissolved solid (TDS)	76.535	<200	Nil
	Total solid (TS)	90.05		
	Total suspended solid(TSS)	13.515		500-1500
	Total Alkalinity	54.5	30-500	
	Total hardness	50.3		
	Chloride	71.005	<2.5	200-600
	Nitrate	4.21	Virtually absent	50-100
	Sulphate	5.2	<50	200-400
	Phosphate	3.15		
	DO	4.2	Air saturation	
	BOD	1.3		Nil
	COD	2.25		Nil
MINERALS (mg/L)	Na	11.35		Nil
	K	9.15		
	Ca	14.215		
	Mg	12.615		
	Zn	1.15	Virtually absent	
	Mn	nd	Absent	
	Cu	nd	Virtually absent	1-1500
	Fe	0.015	Virtually absent	0.03-1.0
	Pb	nd	Absent	0.01
	Cr	nd	Absent	0.5

Tables 4.3: Physico-chemical analysis of water sample collected from the village

PARAMETERS		HAND DUG WELL IN THE VILLAGE	FEPA (1988)	WHO (1991)
PHYSICAL	Temperature (°C)	28.4		
	Turbidity (NTU)	0.001	Nil	
	Conductivity (Uhoms/cm)	140.5		Nil
CHEMICAL (mg/L)	pH	6.26	6.0-8.5	7-8.5
	Total dissolved solid	79.815	<200	Nil
	Total solid	94.425		
	Total suspended solid	14.61		500-1500
	Total Alkalinity	60	30-500	
	Total hardness	52.515		
	Chloride	128.69	<2.5	200-600
	Nitrate	5.725	Virtually absent	50-100
	Sulphate	5.35	<50	200-400
	Phosphate	3.5		
	DO	3.25	Air saturation	
	BOD	1.11		Nil
	COD	2.35		Nil
	MINERALS (mg/L)	Na	12.3	
K		11.4		
Ca		14.735		
Mg		13.23		
Zn		1.225	Virtually absent	
Mn		nd	Absent	
Cu		nd	Virtually absent	1-1500
Fe		0.04	Virtually absent	0.03-1.0
Pb		nd	Absent	0.01
Cr		nd	Absent	0.5

DO= Dissolved Oxygen nd= not detected

BOD=Biological Oxygen Demand

COD= Chemical Oxygen Demand

CHAPTER FIVE

CONCLUSION AND RECOMMENDTION

5.1 CONCLUSION

The results revealed the presence of conductive zones on the VLF-EM 2-D models obtained on seven traverses within the study area. The conductive zones correspond to the thick overburden above the basement and basement fractures revealed by the geo-electric section sections. They also appeared as basement depression, fractures, fault, and/or fracturing of the basement attributed to the rock type present within the study area, which is Migmatite.

Low resistivity zones (topsoil and weathered layer) were observed on the geo-electric sections. The low resistivity zones were also revealed by the 2-D dipole-dipole subsurface resistivity image beneath the five traverses established for the dipole-dipole technique. The low resistivity zone was mapped as leach (leachate) increases continuously with depth as revealed by the subsurface images beneath traverses 2, 3 and 4 from the northwestern to the southwestern portion of the study area. The geomagnetic maps generated for each traverses also showed the fractures/fault through which the leachate seeped through.

The topsoil isoresistivity map showed that large parts of the dumpsite has being affected by leachate. Our result was even justified by the elevation map which clearly revealed the westward flow of the leachate. The isoresistivity map of the weathered layer revealed that the weathered layer's resistivity is low around the west, southwestern and northeastern part of the study area which corroborated with the topsoil isoresistivity map of the study area.

The results of the physico-chemical analysis of the water samples taken from wells in the village and at a distant control point revealed that the electrical conductivity, turbidity, Total Dissolved solid (TDS), Total solid (TS), Total suspended solid (TSS), Total Alkalinity and Chloride were

within the recommended drinking standard range postulated by the World Health Organization. Moreover, other physicochemical parameters analyzed such as Chemical Oxygen Demand, Dissolved Oxygen, Biological Oxygen Demand, Na, K, Ca, Mg, Zn and Fe were also within the WHO and FEPA recommended standard for drinking water. The analysis also showed that no element of Mn, Cu, Pb and Cr were contained in the water samples. It can then be said that the water in the village and at the control point are not polluted.

Based on the results obtained from this research work, it could then be concluded that the leachate from the dumpsite is gradually migrating to the eastern, northeastern and southeastern part of the study area polluting the near surface and underground water within the area.

Also, integrated geophysical methods (such as Electromagnetics, Magnetics and Electrical Resistivity methods used in this study) are efficient geophysical methods in evaluating the impact of waste dump sites on groundwater.

5.2 RECOMMENDATION

It could therefore be recommended that;

- Geophysical investigations should be carried out in mapping suitable areas for siting waste dump.
- The geology of an area should be understood or known before earmarking the area for waste dump siting.
- Additional geophysical methods such as Self-Potential method (SP) could be employed for further investigation.
- More detailed water sample analysis (hydrochemical) should be carried out within the dumpsite.

REFERENCES

- Ajibade, A.C and Fitches W.R. (1988): The Nigeria Precambrian and the Pan-African Orogeny, Precambrian Geology of Nigeria, pp.45-53.
- Akindele.O, Oyinloye (2011): Geology and Geotectonic Setting of the Basement Complex Rocks in Southwestern Nigeria: Implication on Provenance and Evolution, Earth and Environmental Science, Dr. Imran Ahmad Dar (Ed.) ISBN: 978-953-307-468-9. Intech. (2011)
- Bagchi, A., 1987: Natural attenuation mechanisms of landfill leachate and effects of various factors on the mechanisms. Waste Manage. Res. 5, 453–464.
- Bahout, E., Hadjinicolaou, J., Yong, R.N., 1995: Characterization and marketability of bottom ash from municipal incinerators. In: Sarsby, R.W. Ed., Waste disposal by landfill GREEN'93. A.A. Balkema, Rotterdam, pp. 233–237.
- Barker, R.D., 1990: Improving the quality of resistivity sounding data in landfill studies. In: Ward, S.H. Ed. Geotech. Environ. Geophys. vol. 1 Society of Exploration Geophysicists, pp. 245–251.
- Bennett, P.C., Siegel, D.I., 1987: Increased solubility of quartz in water due to complexing by organic compounds. Nature 326, 684–686.
- Birks, J., Eyles, C.A., 1997: Leachate from landfills along the Niagara Escarpment. In: Eyles, N. Ed., Environmental Geology of Urban Areas. Geological Assoc. Canada, Canada, pp. 347–363, Chap. 24
- Boesse, T.N and Ocan O.O (1988): Geology and evolution of the Ife-Ilesha Schist-belt southwestern Nigeria. Symposium on Benin- Nigeria geo-traverse of Proterozoic Calkin,

- S., 1989. A shallow seismic refraction survey of the Mallard North Landfill — Hanover Park, IL. MS thesis, Northern Illinois Univ
- Dearlove, J.P.L., 1995: Geochemical interaction processes between landfill clay liner materials and organo-metallic landfill leachate. In: Sarsby, R.W. Ed., Waste Disposal by Landfill GREEN'93. A.A. Balkema, Rotterdam, pp. 409–414.
- De Rooy, C., 1986: Use of the electromagnetic method for groundwater prospecting in Nigeria. Proceedings of the First Annual Symposium, Nigeria Water and Sanitation Association, July 1986. Lagos, pp. 45-67.
- Dobin, M.B. (1976): Introduction to Geophysical prospecting (2nd edition) Mc Graw-Hill book, London.
- Dobrin, M.B. & Savit, C.H. (1988) Introduction to Geophysical Prospecting (4th edn). McGraw Hill, New York
- Ebisemiju F.S (1979): 'Analysis of Drainage Basin and Similar Parameter in relation to soil and Vegetation Characteristics', Nig. Geog. Journal 2:37-44 (1989)
- Egbuniwe I.G (1982): Geotectonic evolution of Maru Belt, northwestern Nigeria, unpublished ph.D thesis of the University of Wales, UK.
- Fang, H.Y., 1995a: Engineering behavior of urban refuse, compaction control and slope stability analysis of landfill. In: Sarsby, R.W. Ed., Waste Disposal by Landfill— GREEN'93. A.A. Balkema, Rotterdam, pp. 47–72.
- Fang, H.Y., 1995b: Bacteria and tree root attack on landfill liners. In: Sarsby, R.W. Ed., Waste Disposal by Landfill — GREEN'93. A.A. Balkema, Rotterdam, pp.419–426.
- Farquhar, G.J., 1989: Leachate: production and characterization. Can. J. Civ. Eng. 16, 317–325.

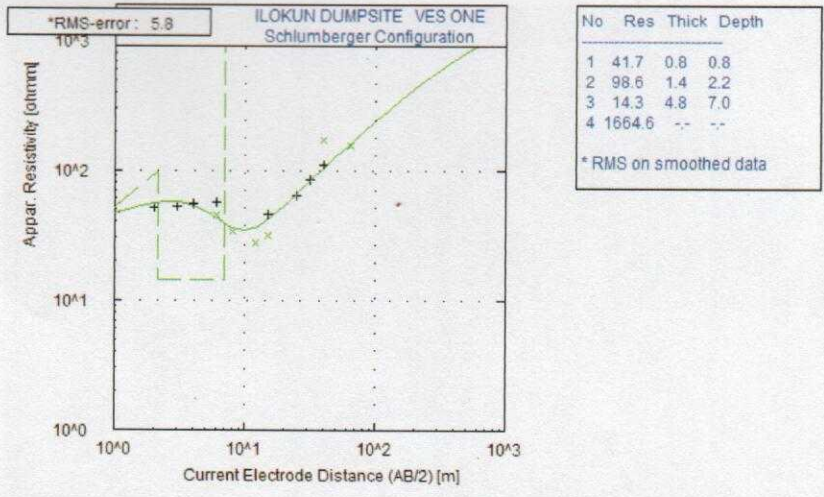
- FEPA, 1988. Present water quality status in Nigeria. Federal Environmental Protection Agency, Lagos. pp: 35-41.
- Folami S.L. (1980): Paleomagnetism and rock magnetism of Ice land drill core samples unpublished MSc. Thesis, University of Washington, pg. 45.
- Hussain, T., Hoda, A., and Khan (1989): Impact of sanitary Landfill on Groundwater Quality. *Water, Air and Soil pollution* 45:191-206
- Karous M, Hjelt SE (1983). Linear Filter of VLF Dip-Angle Measurements. *Geophys. Prospect.* 31: 782-794.
- Kjeldsen, P., 1993: Groundwater pollution source characterization of an old landfill. *J. Hydrology* 142, 349-371.
- Kovacic, D., Mayer, D., Muhovec, I., 1995: Geotechnical characteristics of Zagreb waste disposal site and possibilities of its reclamation. In: Sarsby, R.W. Ed., *Waste Disposal by Landfill — GREEN'93*. A.A. Balkema, Rotterdam, pp. 543–547.
- Lewin, K., Young, C., Blakey, N., 1997: Management of the environmental impacts of landfilling on the Sherwood Sandstone. In: Chilton, J. Ed., *Groundwater in the Urban Environment*. A.A. Balkema, Rotterdam, pp.611–615.
- Lorenzo De Carlo, Maria Teresa Perri and Rita Deiana (2013): Characterization of a dismissed landfill via electrical resistivity topography and mise-a-la masse method. *Journal of Applied Geophysics* 98 (2013) 1-10.
- MacFarlane, D.S., Cherry, J.A., Gillham, R.W., Sudicky, A. et al., 1983: Migration of contaminants in groundwater at a landfill: a case study. *J. Hydrol.* 63, 1–29.

- Meju, M.A. 2000: Geoelectrical investigation of old/abandoned, covered landfill sites in urban areas: model development with a genetic diagnosis approach. *Journal of Applied Geophysics*, 44, pp 115-150
- Olorunfemi, M.O and Olorumiwo, M.A 1987: Geophysical Investigation for Groundwater in Precambrian Terrain; a case study of Ikau, Southwestern Nigeria. *Journal of African Earth Sciences*, vol 6.No 6. Pp. 787-796.
- Opeyemi A. 2013: Integrated Geophysical Characterization of Subsurface conditions around Ilesha Dumpsite: Case of Southwestern Nigeria. *Asian Journal of Applied Science and Engineering*, Volume 2, No 2 (2013).
- Owoeye, A.O (2000): an aeromagnetic interpretation of Orisumbare area in Ondo state. Unpublished B. Tech thesis Department of Geophysics FUTA.
- Oyinloye, A.O (1992): Genesis of the Iperindo gold deposit, Ilesha schist belt, Southwestern Nigeria. Unpublished thesis of the University of Wales, Cardiff, UK. Pp 1.267.
- Palacky, G.J., 1987: Resistivity characteristics of geological targets. In: Nabighian, M.N. Ed., *Electromagnetic Methods in Applied Geophysics — Theory* vol. 1 Soc. Expl. Geophys, pp. 53–129, *Investigations in Geophysics Series*, vol. 3.
- Radnoff, D., Hollingshead, S., Anderson, G., 1992: What legacy are we leaving with future landfill leachates? *Environ. Sci. Eng.* 26, 58–60.
- Raghynath H.M.202: *Hydrogeology an aerial photography. A textbook on Groundwater* (2nd edition). New Age International publisher, New Delhi; India. Pp 58-63.
- Raghynath, H.M, 2002: *Hydrogeology and aerial photography. A textbook on Groundwater* (2nd edition). New Age International publisher, New Delhi, India pp.58-63.

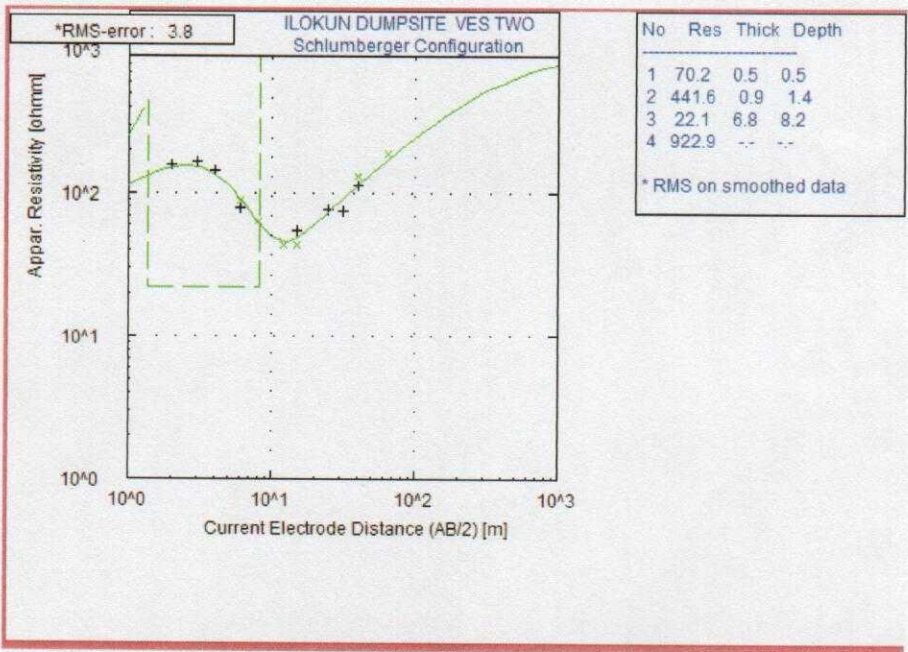
- Rahaman, M.A (1988): Recent advances in the study of the basement complex of Nigeria. Symposium on the Geology of Nigeria, Obafemi Awolowo University, Nigeria.
- Rahaman, M.A and Ocan, O.O. (1978): On relationship in the Precambrian magmatic gneisses of Nigeria *J.Min and Geol.vol.15, No 1 (abs).*
- Robinson, H.D., 1989: Development of methanogenic conditions within landfills, Proc. of the Second International Landfill Symposium, Porto Conte Sardinia, paper XXIX.
- Shemang E. M.1990: Electrical depth sounding at selected well sites within the Kubari river basin, Zaria, Nigeria. Unpublished M.Sc. Thesis A.B.U. Zaria, pp. 108
- Stoller, R.L., Roux, P., 1973: Earth resistivity survey: a method for defining groundwater contamination. *Ground Water* 13, 145–150
- Ugwu, SA and Nwosu, JI (2009): Effect of Waste Dumps on Groundwater in Choba using Geophysical Method. *Journal of Applied Sciences and Environmental Management* 13(1): 85-89
- Whiteley, R.J., Jewell, C., 1992: Geophysical techniques in contaminated lands assessment:-do they deliver? *Explor. Geophys.* 23, 557–565.
- Woakes, M. Ajibade C.A., Rahaman, M.A., (1987): Some metallogenic features of the Zartman, R.E. Dou, B.R. (1981): *Plumbotectonixs Techonophysics*, 75, 135-162.
- World Health Organization Standard (WHO) Guidelines for Drinking Water, FEPA (1991).
- Yemisi C. Ajisafe (2015): Geophysical Investigation around an Active Landfill Site in Ilokun, Ado-Ekiti; Southwestern Nigeria, *IJIRD*. No14 Issue 5. ISSN 2278-0211 (online).

APPENDIX

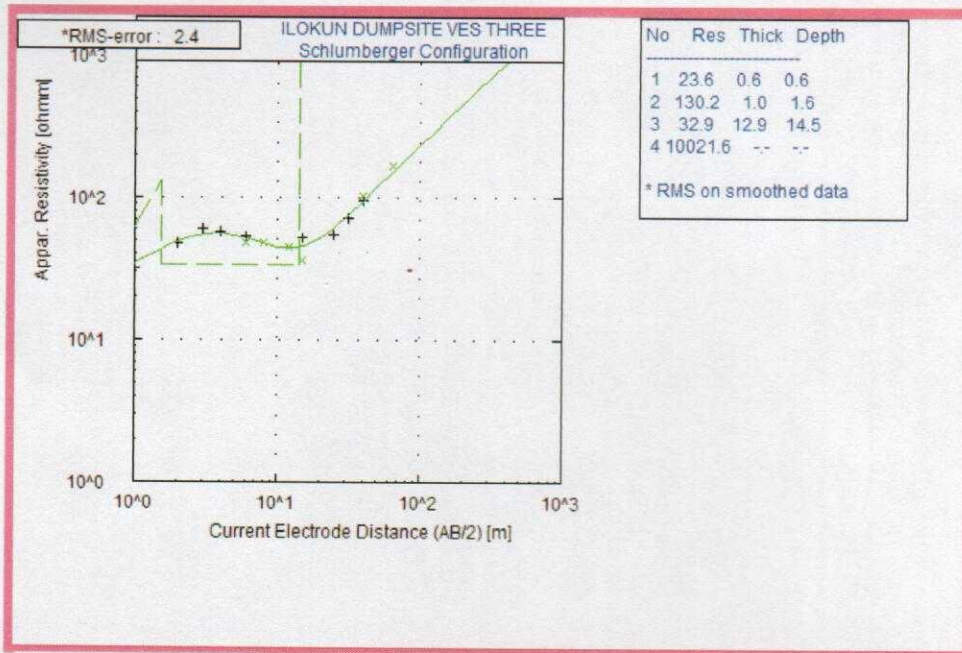
Vertical Electrical Sounding Curves



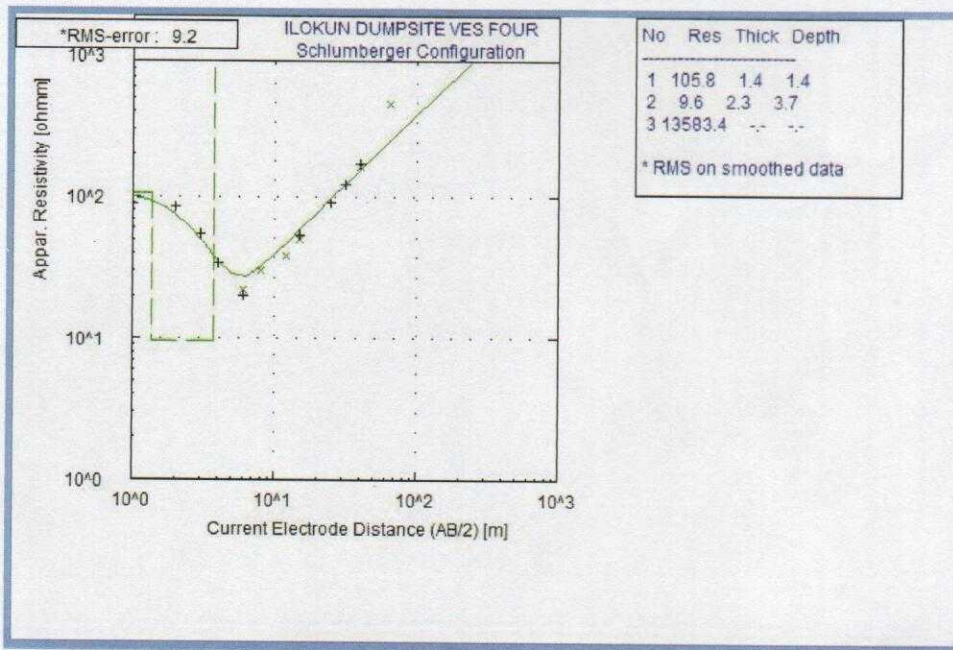
Curve type: KH



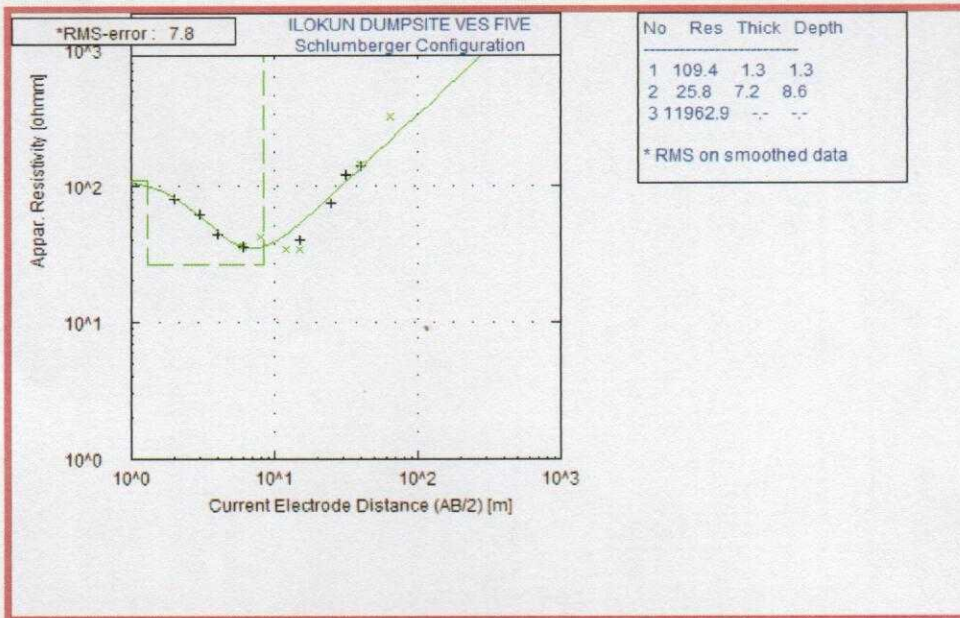
Curve type: KH



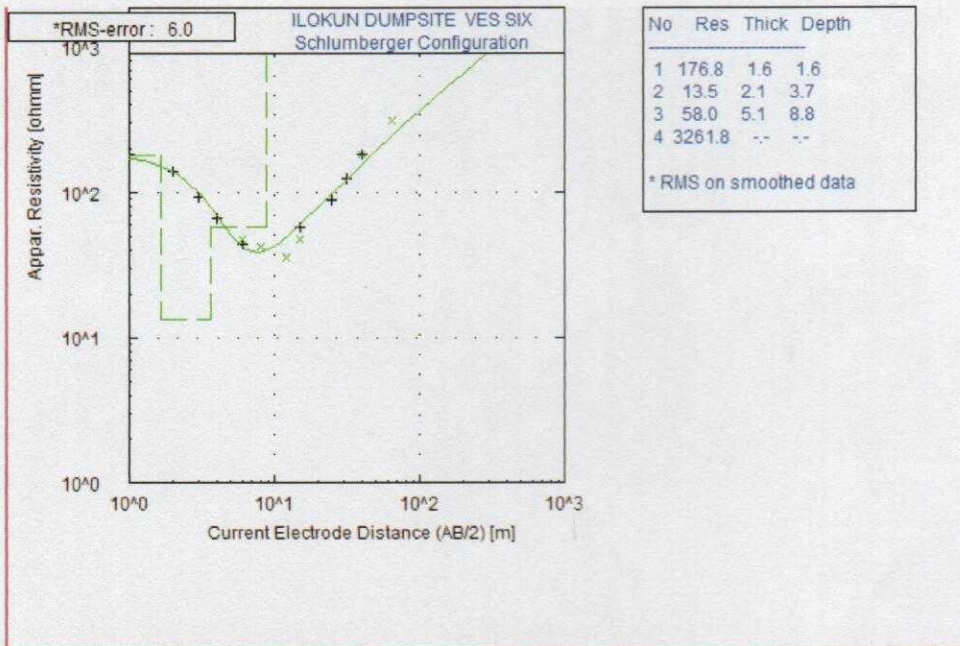
Curve type: KH



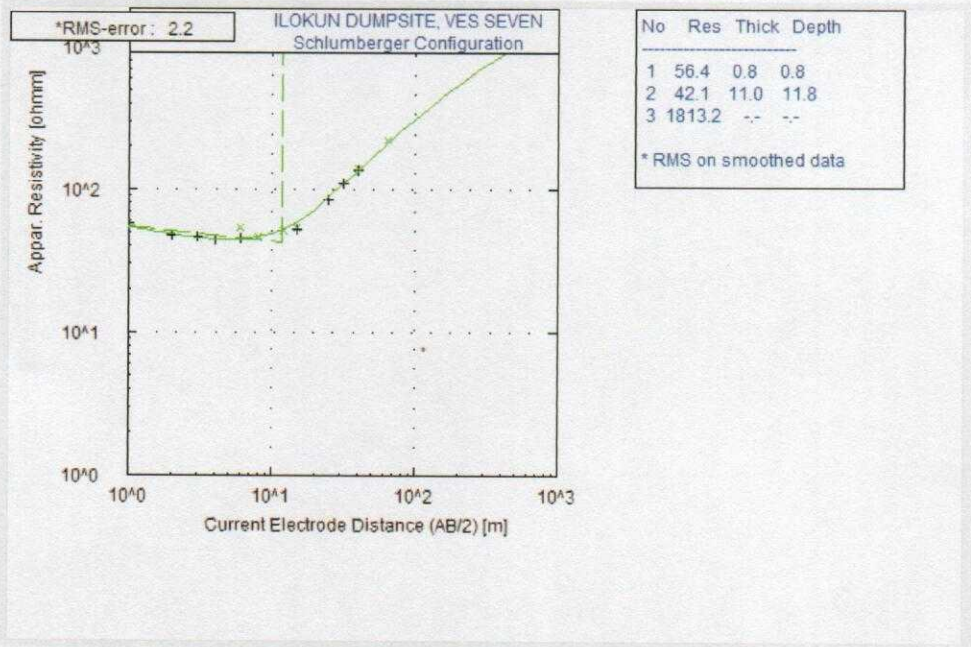
Curve type: H



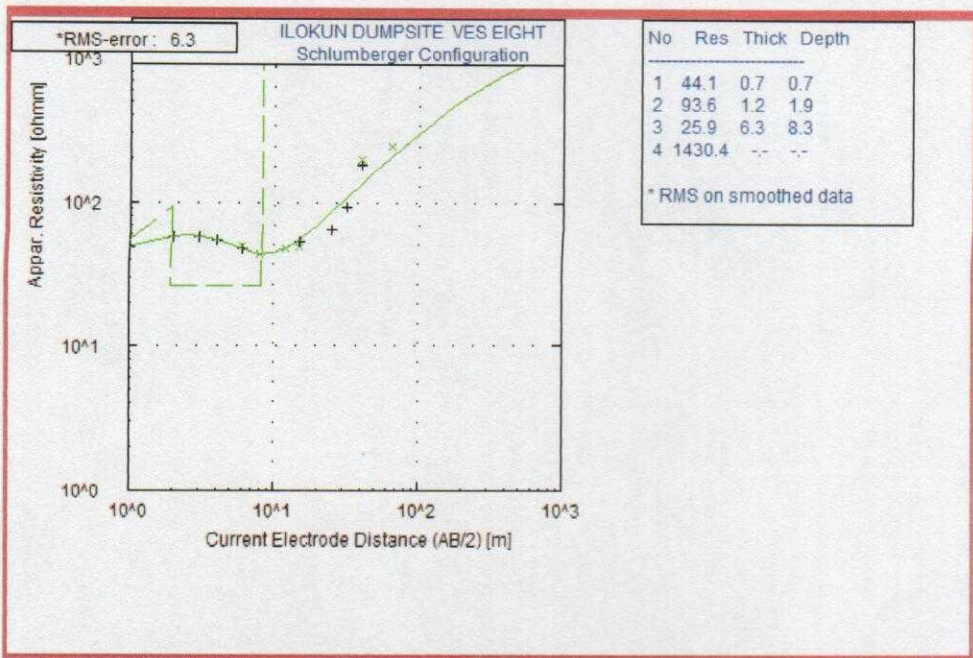
Curve type: H



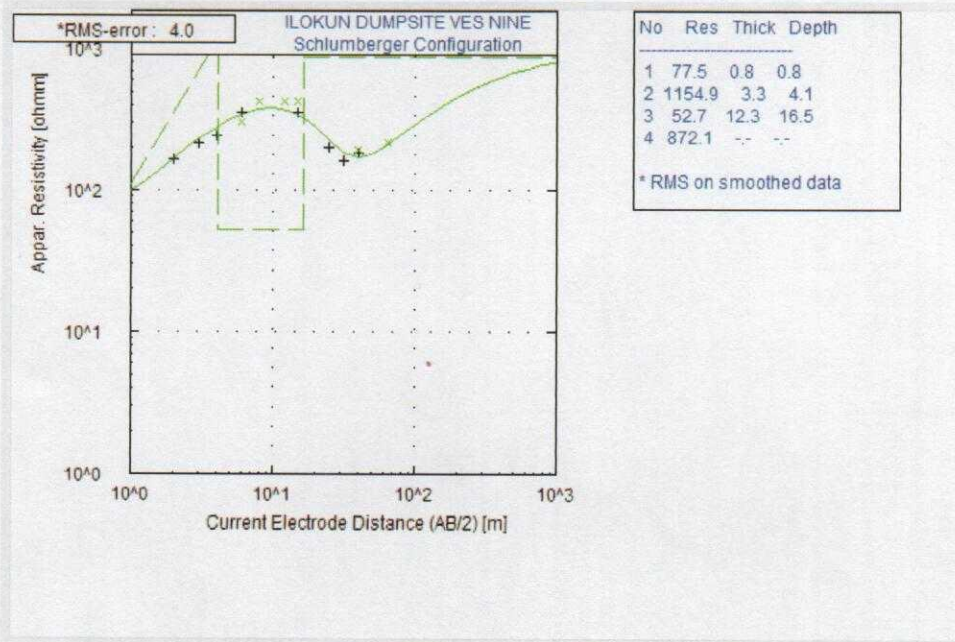
Curve type: HA



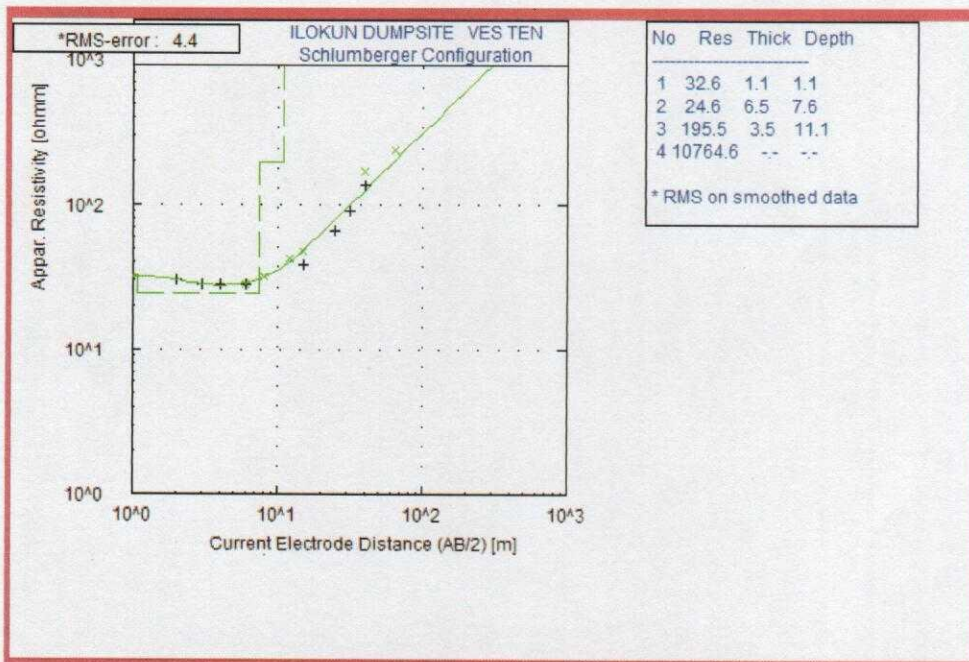
Curve type: H



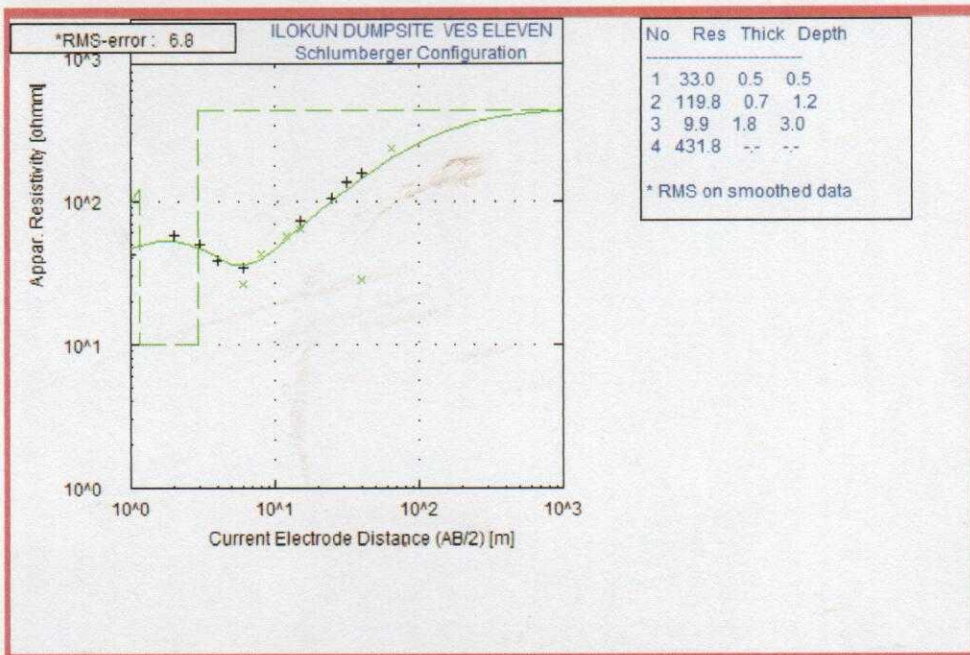
Curve type: KH



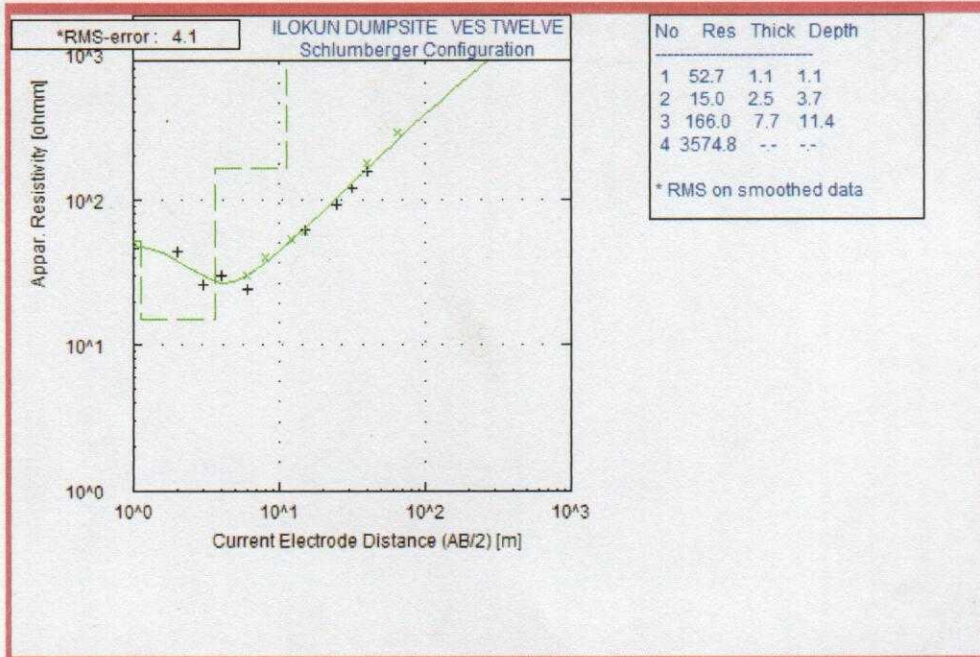
Curve type: KH



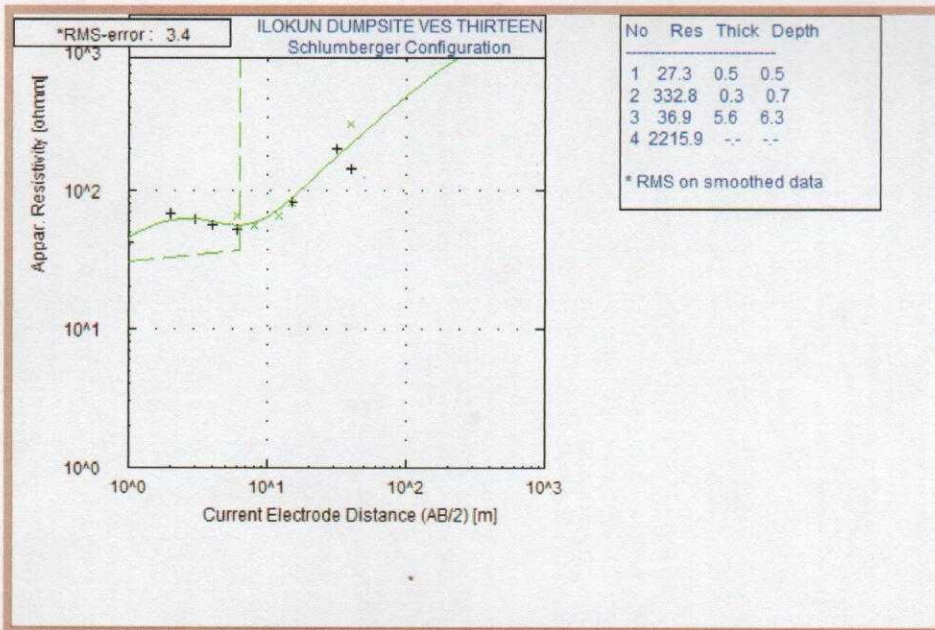
Curve type: HA



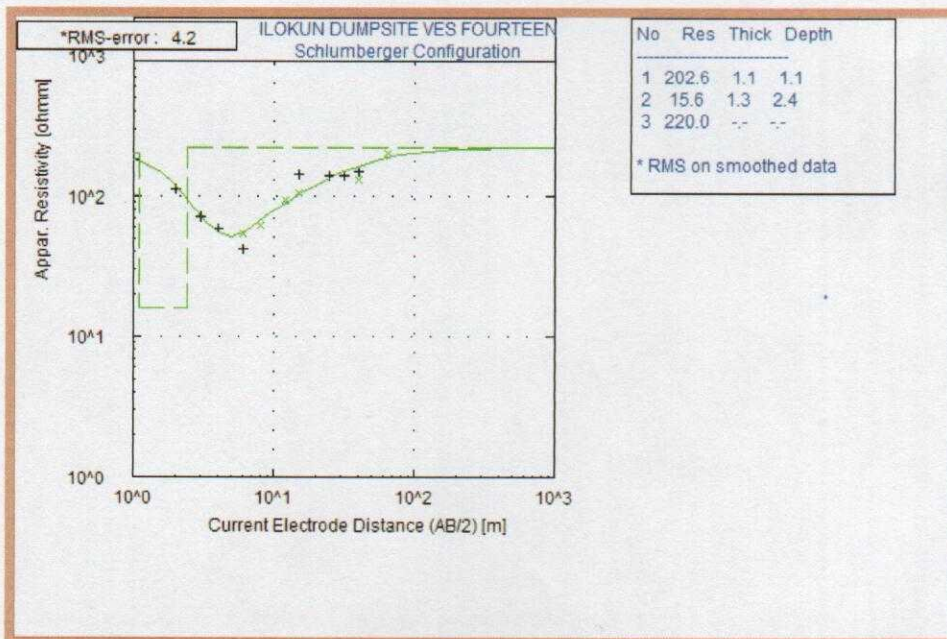
Curve type: KH



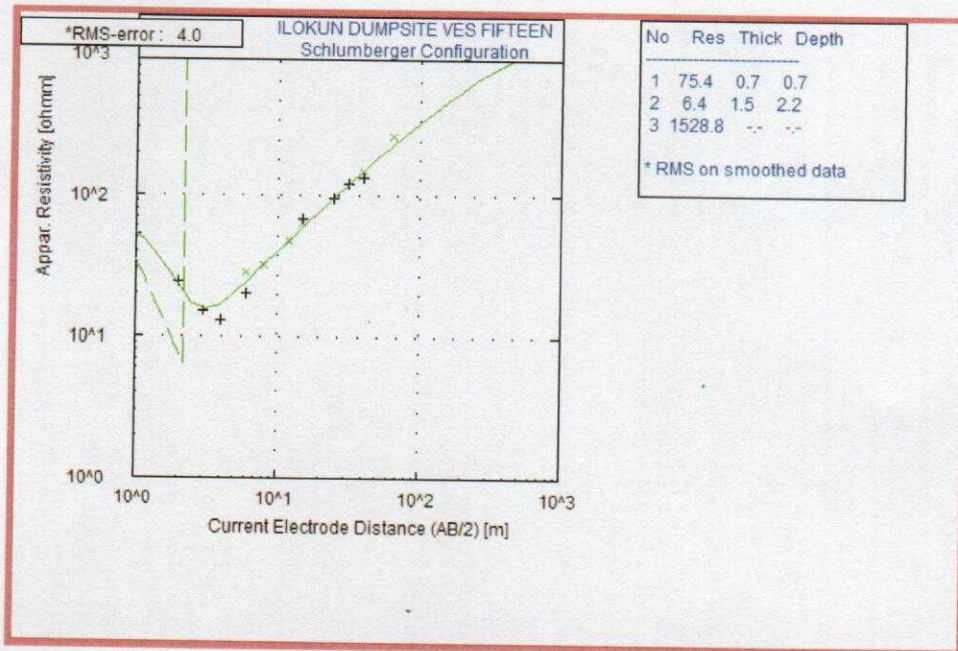
Curve type: HA



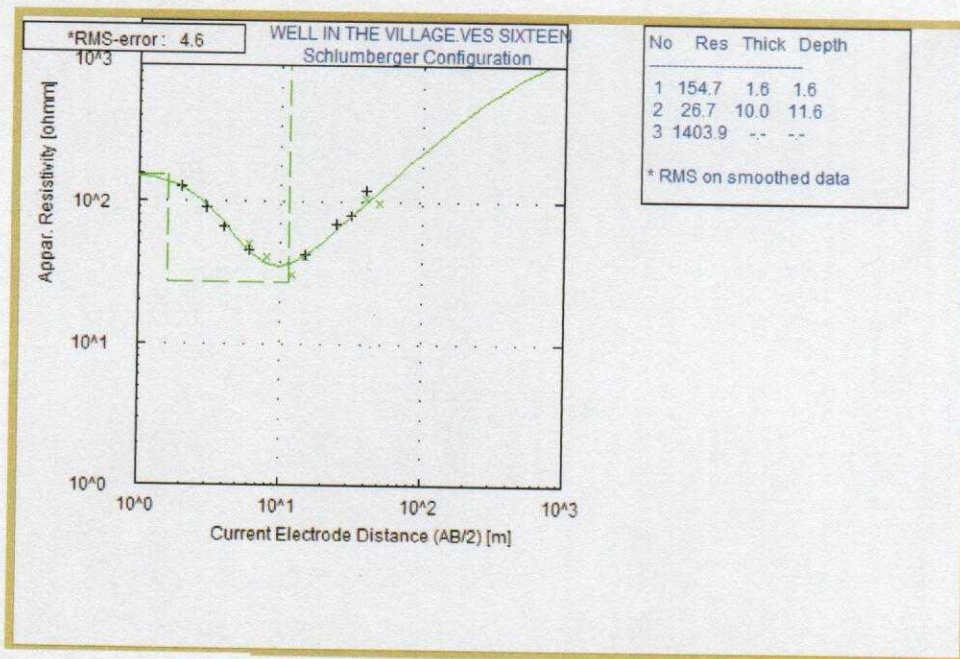
Curve type: KH



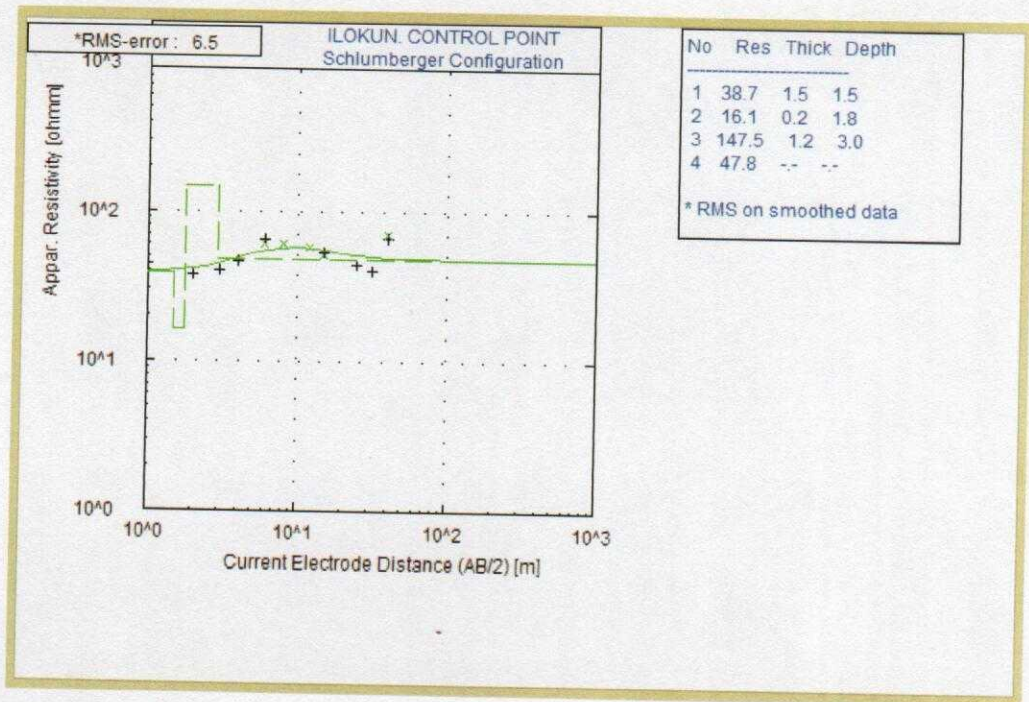
Curve type: KH



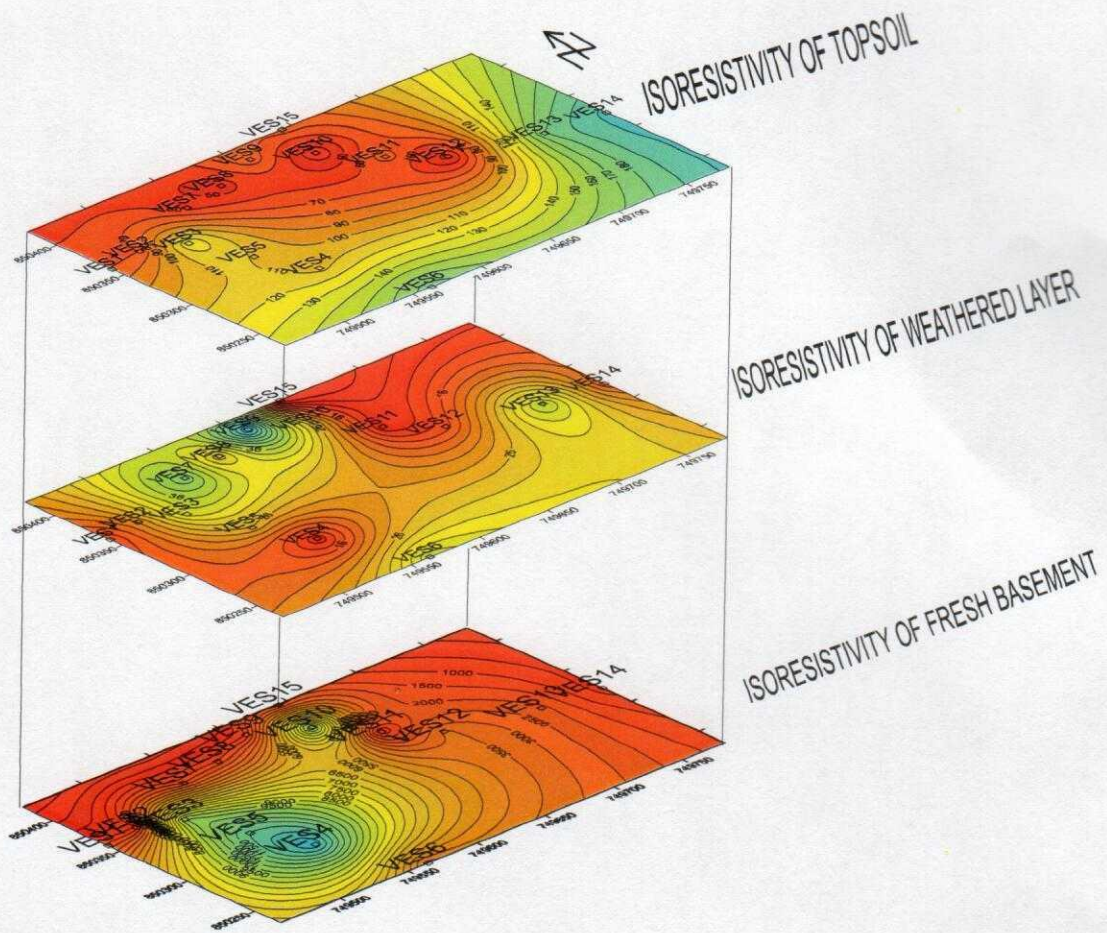
Curve type: H



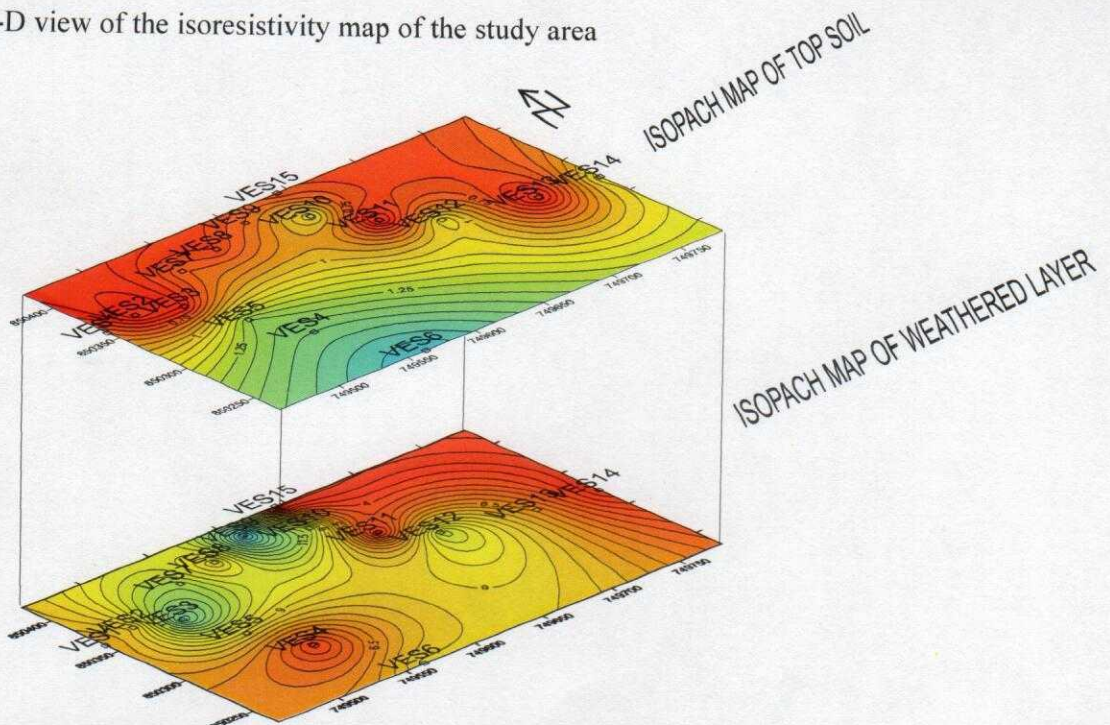
Curve type: H



Curve type: HK



3-D view of the iso-resistivity map of the study area



3-D view of the isopach map of the study area

ELECTROMAGNETICS (VLF-EM) FIELD RECORD				
Date: 31-05-2015			Station separation: 5 m	
Instrument: ABEM WADI			Traverse Azimuth: E-W	
Observer: Fashina Timilehin Gbenga			Co-ordinate: 0001/0000	
Traverse No: 1			Frequency: 25.5 KHz	
Site description: Ilokun dumpsite, Ado-Ekiti			Signal strength: 3	
Station No	Raw Real (%)	Raw Imaginary (%)	Filtered Real (%)	Filtered Imaginary (%)
0	0	80.1	5.4	6
1	5.5	57.9	4.2	2.6
2	0.8	73.6	-2	-0.8
3	-3.1	66	-0.3	2.3
4	3.6	62.9	0.2	-0.6
5	-7.6	77.6	8.8	9.2
6	19.2	30.2	3.9	3.8
7	-14.1	57.5	-8.2	-14.4
8	8.4	82.1	-5.6	-9.6
9	-15.1	85.1	-8.7	-9
10	-0.1	99.9	20.6	-6.3
11	18.9		17.9	-1.3
12	4.2		2.9	-0.8
13	1.8		1.8	0

ELECTROMAGNETICS (VLF-EM) FIELD RECORD				
Date: 31-05-2015			Station separation: 5 m	
Instrument: ABEM WADI			Traverse Azimuth: N-S	
Observer: Fashina Timilehin Gbenga			Co-ordinate: 0002/0000	
Traverse No: 2			Frequency: 25.5 KHz	
Site description: Ilokun dumpsite, Ado-Ekiti			Signal strength: 3	
Station No	Raw Real (%)	Raw Imaginary (%)	Filtered Real (%)	Filtered Imaginary (%)
0	0	62.9	0	-6.5
1	0.6	85.9	0	-10
2	-2.6	99.9	6.5	-4.5
3	8.5	99.9	8.5	3.5
4	1.6	82.5	1.6	3
5	1.4	84.9	1.4	-4.4
6	0	99.9	0	-4.2
7	0.1	99.9	-9.4	5.4
8	0	99.9	-42.5	29.4
9	-41.8	8.4	-44.1	31.9
10	-12.6	0.5	-9.1	8
11	-3.4	2.8	-4.7	2.9
12	-1.4	8.9	-0.2	0.5
13	2	2.4	-0.4	1.7
14	-2.9	0.2	-0.9	-0.4
15	2.1	7.4	-0.7	2.5
16	-2.6	-8.2	-2.5	1.8
17	-0.7	0.5	1.9	-2
18	1.9	0.8	2.1	1.1
19	0.8	-1.8	0	1.5
20	-0.4	-5.3	-0.4	1.3

ELECTROMAGNETICS (VLF-EM) FIELD RECORD				
Date: 31-05-2015			Station separation: 5 m	
Instrument: ABEM WADI			Traverse Azimuth: W-E	
Observer: Fashina Timilehin Gbenga			Co-ordinate: 0003/0000	
Traverse No: 3			Frequency: 25.5 KHz	
Site description: Ilokun dumpsite, Ado-Ekiti			Signal strength: 3	
Station No	Raw Real (%)	Raw Imaginary (%)	Filtered Real (%)	Filtered Imaginary (%)
0	0	-4.1	1	-0.4
1	0.3	-3.7	3.6	-1.3
2	3.2	-0.9	3.6	-1.6
3	1.1	1.9	0.6	0
4	0.2	-2.2	-0.3	0.3
5	-0.9	-0.2	-0.5	-0.7
6	1.2	-0.8	-1.9	-1.2
7	-4.7	4	2.1	-1.3
8	6	2.2	2.7	-0.2
9	-3	4.6	-2.9	0.3
10	-0.2	-0.8	1.2	-0.2
11	1.7	5.7	-3.2	-0.4
12	-4.3	1.6	-5	1.5
13	-1.3	0	-2.1	0.2
14	-1.8	0.8	-2	0.5
15	0	0.3	-2.7	1.9
16	-2.6	-4.2	-3.3	2.8
17	-1.4	-8.9	-1.7	1.1
18	0	-7.5	-2.9	-1.9
19	-4.3	-3.1	1.7	-3.6
20	5.1	4.1	4.8	-2.6
21	0.3	3.5	0.3	-0.6

ELECTROMAGNETICS (VLF-EM) FIELD RECORD				
Date: 31-05-2015			Station separation: 5 m	
Instrument: ABEM WADI			Traverse Azimuth: W-E	
Observer: Fashina Timilehin Gbenga			Co-ordinate: 0003/0000	
Traverse No: 3			Frequency: 25.5 KHz	
Site description: Ilokun dumpsite, Ado-Ekiti			Signal strength: 3	
Station No	Raw Real (%)	Raw Imaginary (%)	Filtered Real (%)	Filtered Imaginary (%)
0	0	-1.1	1.1	1
1	1.3	-5.9	-0.8	-0.5
2	-0.6	0.4	-6.1	-1.2
3	-5.3	-0.6	-6.3	1.3
4	-2.2	-3.2	-2.1	1.4
5	-1.3	-9.3	0.7	-1.9
6	1.4	6.6	1.9	1
7	1.7	-7.8	-2.6	7.8
8	-3.9	-20.7	-3.8	3.5
9	-0.4	-19.1	-2	-0.5
10	-2	-14.7	-3	-2.1
11	-1.2	-11.9	-0.7	-2.5
12	-0.8	-8.6	2.1	-1.8
13	2.4	-7.7	2.9	-0.9
14	0.6	-7.8	1.9	-1.1
15	2.2	-5	0.4	-0.4
16	-2	-6.4	1	0.9
17	2.3	-8.5	4	0.7
18	2.2	-8.5	0.9	0.7
19	-0.6	-9.8	-0.1	1.2
20	0.4	-11.9	0.4	0.7

ELECTROMAGNETICS (VLF-EM) FIELD RECORD				
Date: 31-05-2015			Station separation: 5 m	
Instrument: ABEM WADI			Traverse Azimuth: W-E	
Observer: Fashina Timilehin Gbenga			Co-ordinate: 0005/0000	
Traverse No: 5			Frequency: 25.2 KHz	
Site description: Ilokun dumpsite, Ado-Ekiti			Signal strength: 8	
Station No	Raw Real (%)	Raw Imaginary (%)	Filtered Real (%)	Filtered Imaginary
0	0	-3.4	-0.7	-1.1
1	-1.3	-2.1	0.9	-2.6
2	2.4	6	0.6	-0.7
3	-1.9	-0.8	-4.3	0.9
4	-3.1	0.9	-0.5	-0.8
5	1.6	1.2	-1.3	-1.3
6	0	3.9	-14.1	-3.2
7	-5.4	11.4	-18	-2.4
8	-9.1	8.3	-6	-3.1
9	-1	18.1	1.8	-4.1
10	2.4	20.4	2.4	-1.1

ELECTROMAGNETICS (VLF-EM) FIELD RECORD				
Date: 31-05-2015			Station separation: 5 m	
Instrument: ABEM WADI			Traverse Azimuth: N-S	
Observer: Fashina Timilehin Gbenga			Co-ordinate: 0006/0000	
Traverse No: 6			Frequency: 25.2 KHz	
Site description: Ilokun dumpsite, Ado-Ekiti			Signal strength: 8	
Station No	Raw Real (%)	Raw Imaginary (%)	Filtered Real (%)	Filtered Imaginary
0	0	-0.3	-2.3	-2.1
1	-3.3	8.8	-1.3	1.6
2	3.8	-2.9	-4.4	5.1
3	-1.3	-14.3	3.5	-3.4
4	13.9	8.2	9.7	-6.2
5	-2.9	10.5	-6.4	-6.8
6	3.1	4.5	-13	-23.4
7	-23.5	99.9	7.4	-0.1
8	26	5.6	26	23.2
9	2.7	5.4	5.2	-1
10	7.3	14.6	7.3	1.8

ELECTROMAGNETICS (VLF-EM) FIELD RECORD				
Date: 31-05-2015			Station separation: 5 m	
Instrument: ABEM WADI			Traverse Azimuth: W-E	
Observer: Fashina Timilehin Gbenga			Co-ordinate: 0007/0000	
Traverse No: 7			Frequency: 25.2 KHz	
Site description: Ilokun dumpsite, Ado-Ekiti			Signal strength: 8	
Station No	Raw Real (%)	Raw Imaginary (%)	Filtered Real (%)	Filtered Imaginary (%)
0	0	16.9	-1.3	0.9
1	-2.2	15	1.6	1.7
2	3.1	10.6	3.2	1.1
3	0.9	14.3	-2.9	2
4	-1.2	3.8	-10.8	0.9
5	-9.3	11.8	-10.3	-1.6
6	-5.2	9.9	4	0.1
7	6.5	11.7	8.2	-0.7
8	4	9.3	-0.1	-1.4
9	-1.8	17	-3.5	-0.9
10	-2.1	12.1	-2.1	1.1

MAGNETICS DATA SHEETS

TRAVERSE 1

STATION	MAG1(nT)	MAG2(nT)	AVERAGE(nT)	Time(hr)	Time(min)	Time(sec)
0	33216.51	33216.61	33216.56	2	57	27
5	33203.01	33200.35	33201.68	2	58	8
10	33111.27	33111.07	33111.17	2	58	38
15	32548.57	32548.78	32548.675	2	59	10
20	34067.34	34691.53	34379.435	2	59	53
25	33451.03	33448.3	33449.665	3	0	33
30	33303.05	33301.53	33302.29	3	1	3
35	33313.21	33312.61	33312.91	3	1	33
40	33324.15	33321.77	33322.96	3	2	7
45	33333.66	33331.81	33332.735	3	2	34
50	33347.95	33346.87	33347.41	3	3	0
55	33349.37	33351.79	33350.58	3	3	31
60	33355.53	33352.24	33353.885	3	4	2
65	33293.3	33294.91	33294.105	3	4	54

TRAVERSE 2

STATION	MAG1(nT)	MAG2(nT)	AVERAGE(nT)	Time(hr)	Time(min)	Time(sec)
0	33302.74	33313.86	33308.3	3	6	50
5	33471.51	33472.54	33472.025	3	7	18
10	33408.72	33410.65	33409.685	3	7	43
15	33367.92	33370.97	33369.445	3	8	7
20	33346.8	33351.42	33349.11	3	8	30
25	33300.78	33303.47	33302.125	3	8	52
30	33308.32	33315.44	33311.88	3	9	14
35	33305.62	33305.81	33305.715	3	9	39
40	33317.4	33319.29	33318.345	3	10	0
45	33285.58	33288.16	33286.87	3	10	25
50	33324.24	33327.48	33325.86	3	10	46
55	33374.69	33379.21	33376.95	3	12	13
60	33341.93	33346.59	33344.26	3	12	37
65	33314.96	33316.33	33315.645	3	12	55
70	33302.51	33304.15	33303.33	3	13	20
75	33364.11	33364.22	33364.165	3	13	43
80	33351.6	33354.38	33352.99	3	14	20
85	33380.07	33381.21	33380.64	3	14	40
90	33387.6	33386.78	33387.19	3	15	9
95	33377.06	33376.01	33376.535	3	15	31
100	33405.05	33409.63	33407.34	3	15	53

TRAVERSE 3

STATION	MAG1(nT)	MAG2(nT)	AVERAGE(nT)	Time(hr)	Time(min)	Time(sec)
0	33574.39	33575.16	33574.775	3	18	40
5	33585.96	33586.88	33586.42	3	19	7
10	33561.38	33561.68	33561.53	3	19	40
15	33593.83	33595.9	33594.865	3	20	2
20	33605.91	33606.06	33605.985	3	20	19
25	33616.58	33618.41	33617.495	3	20	39
30	33660.9	33657.53	33659.215	3	21	1
35	33620.14	33619.9	33620.02	3	21	20
40	33567.23	33565.45	33566.34	3	21	40
45	33564.87	33568.49	33566.68	3	22	0
50	33545.59	33547.21	33546.4	3	22	18
55	33555.89	33557.31	33556.6	3	22	42
60	33563.31	33564.16	33563.735	3	23	4
65	33560.15	33558.84	33559.495	3	23	24
70	33566.32	33564.42	33565.37	3	23	44
75	33534.41	33532.86	33533.635	3	24	5
80	33556.56	33559.45	33558.005	3	24	34
85	33584.12	33584.29	33584.205	3	25	35
90	33609.46	33609.9	33609.68	3	26	3
95	33642.05	33624.23	33633.14	3	26	24
100	33646.23	33642.42	33644.325	3	26	47
105	33666.49	33664.73	33665.61	3	27	18

TRAVERSE 4

STATION	MAG1(nT)	MAG2(nT)	AVERAGE(nT)	Time(hr)	Time(min)	Time(sec)
0	33618	3361.89	18489.945	3	28	5
5	33609.04	33603.95	33606.495	3	28	48
10	33361.86	33561.15	33461.505	3	29	13
15	33645.09	33653.14	33649.115	3	29	37
20	33571.39	33573.4	33572.395	3	30	3
25	33561.68	33564.64	33563.16	3	30	30
30	33562.64	33567.95	33565.295	3	31	20
35	33530.39	33532.7	33531.545	3	31	48
40	33497.38	33494.76	33496.07	3	32	15
45	33449.38	33450.18	33449.78	3	32	45
50	33387.11	33391.06	33389.085	3	33	9
55	33430.43	33426.33	33428.38	3	33	37
60	33432.11	33431.05	33431.58	3	34	2
65	33421.93	33419.02	33420.475	3	34	25
70	33419.81	33424.61	33422.21	3	34	55
75	33381.14	33384.46	33382.8	3	35	17
80	33379.69	33381.55	33380.62	3	35	37
85	33338.56	33342.65	33340.605	3	36	0
90	33310.57	33313.97	33312.27	3	36	25
95	33302.32	33302.42	33302.37	3	36	53

TRAVERSE 5

STATION	MAG1(nT)	MAG2(nT)	AVERAGE(nT)	Time(hr)	Time(min)	Time(sec)
0	33647.21	33647.47	33647.34	3	42	43
5	33649.58	33649.58	33649.58	3	43	27
10	33659.66	33660.15	33659.905	3	43	48
15	33658.07	33657.81	33657.94	3	44	8
20	33638.06	33642.24	33640.15	3	44	28
25	33636.83	33638.36	33637.595	3	44	46
30	33633.73	33633.64	33633.685	3	45	5
35	33683.94	33684.29	33684.115	3	45	20
40	33709.24	33717.26	33713.25	3	45	45
45	33747.69	33743.53	33745.61	3	46	0
50	33843.85	33840.97	33842.41	3	46	25

TRAVERSE 6

STATION	MAG1(nT)	MAG2(nT)	AVERAGE(nT)	Time(hr)	Time(min)	Time(sec)
0	33645.22	33639.2	33642.21	3	57	29
5	33654.54	33658.45	33656.495	3	58	7
10	33625.59	33625.44	33625.515	3	58	25
15	33534.92	33534.95	33534.935	3	58	46
20	33241.21	33250.09	33245.65	3	59	5
25	33686.62	33690.02	33688.32	3	59	25
30	33525.94	33522.89	33524.415	3	59	47
35	33617.32	33621.93	33619.625	4	3	35
40	33645.72	33643.74	33644.73	4	3	59
45	33353.47	33360.68	33357.075	4	4	21
50	33721.16	33713.7	33717.43	4	4	45

TRAVERSE 7

STATION	MAG1(nT)	MAG2(nT)	AVERAGE(nT)	Time(hr)	Time(min)	Time(sec)
0	33726.17	34730.6	34228.385	4	11	44
5	34180.85	34261.41	34221.13	4	12	9
10	34268.03	34261.26	34264.645	4	12	33
15	34429.29	34434.4	34431.845	4	12	54
20	34199.22	34191.02	34195.12	4	13	15
25	34651.93	33651.45	34151.69	4	13	45
30	33590.47	33588.93	33589.7	4	14	12
35	33698.25	33697.55	33697.9	4	14	35
40	33755.51	33749.08	33752.295	4	14	59
45	33673.53	33675.43	33674.48	4	15	30
50	33610.65	33607.89	33609.27	4	16	5

VERTICAL ELECTRICAL SOUNDING DATA SHEETS

VES 1

AB/2 (m)	MN	G	ρ (Ω)	ρa (Ωm)
1	0.5	6.28	7.466	46.9
2	0.5	25.13	2.059	51.7
3	0.5	56.55	0.9282	52.5
4	0.5	100.53	0.5518	55.5
6	0.5	226.19	0.2515	56.9
6	1	113.1	0.3915	44.3
8	1	201.06	0.1653	33.2
12	1	452.39	0.06066	27.4
15	1	706.86	0.04402	31.1
15	2	353.43	0.1278	45.2
25	2	981.75	0.06482	63.6
32	2	1608.5	0.05255	84.5
40	2	2513.27	0.04331	108.8
40	5	1005.31	0.1673	168.2
65	5	2654.65	0.05863	155.6

VES 2

AB/2 (m)	MN	G	ρ (Ω)	ρa (Ωm)
1	0.5	6.28	16.02	100.6
2	0.5	25.13	6.279	157.8
3	0.5	56.55	2.921	165.2
4	0.5	100.53	1.41	141.7
6	0.5	226.19	0.3459	78.8
6	1	113.1	0.7842	88.7
8	1	201.06	0.3185	64
12	1	452.39	0.09627	43.6
15	1	706.86	0.06158	43.5
15	2	353.43	0.1562	55.2
25	2	981.75	0.07913	77.7
32	2	1608.5	0.04686	75.4
40	2	2513.27	0.04514	113.4
40	5	1005.31	0.1288	129.5
65	5	2654.65	0.0705	187.2

VES 3

AB/2 (m)	MN	G	ρ (Ω)	ρa (Ωm)
1	0.5	6.28	2.546	32
2	0.5	25.13	0.9688	48
3	0.5	56.55	0.5285	60
4	0.5	100.53	0.2911	58
6	0.5	226.19	0.1186	54
6	1	113.1	0.216	48
8	1	201.06	0.05671	47
12	1	452.39	0.04889	44
15	1	706.86	0.02505	36
15	2	353.43	0.07233	52
25	2	981.75	0.01643	55
32	2	1608.5	0.02262	72
40	2	2513.27	0.01897	96
40	5	1005.31	0.05052	102
65	5	2654.65	0.03084	164

VES 4

AB/2 (m)	MN	G	ρ (Ω)	ρa (Ωm)
1	0.5	6.28	7.040	88
2	0.5	25.13	1.663	84
3	0.5	56.55	0.2759	55
4	0.5	100.53	0.1714	34
6	0.5	226.19	0.04392	20
6	1	113.1	0.1014	22
8	1	201.06	0.09820	30
12	1	452.39	0.03357	38
15	1	706.86	0.03601	50
15	2	353.43	0.07649	54
25	2	981.75	0.04849	90
32	2	1608.5	0.2140	120
40	2	2513.27	0.03378	170
40	5	1005.31	0.07994	160
65	5	2654.65	0.08602	456

VES 5

AB/2 (m)	MN	G	ρ (Ω)	ρa (Ωm)
1	0.5	6.28	8.450	106
2	0.5	25.13	1.602	80
3	0.5	56.55	0.5447	62
4	0.5	100.53	0.2201	44
6	0.5	226.19	0.07750	36
6	1	113.1	0.1572	36
8	1	201.06	0.1024	42
12	1	452.39	0.03662	34
15	1	706.86	0.01044	34
15	2	353.43	0.02607	40
25	2	981.75	0.1420	75
32	2	1608.5	0.04484	120
40	2	2513.27	0.02800	140
40	5	1005.31	0.07162	144
65	5	2654.65	0.06087	324

VES 6

AB/2 (m)	MN	G	ρ (Ω)	ρa (Ωm)
1	0.5	6.28	14.3	180
2	0.5	25.13	2.769	140
3	0.5	56.55	0.8339	94
4	0.5	100.53	0.3317	66
6	0.5	226.19	0.09546	44
6	1	113.1	0.213	48
8	1	201.06	0.1044	42
12	1	452.39	0.04007	36
15	1	706.86	0.03429	48
15	2	353.43	0.08217	58
25	2	981.75	0.04484	88
32	2	1608.5	0.03844	124
40	2	2513.27	0.03581	180
40	5	1005.31	0.09171	182
65	5	2654.65	0.05762	306

VES 7

AB/2 (m)	MN	G	ρ (Ω)	ρa (Ωm)
1	0.5	6.28	9.049	57
2	0.5	25.13	1.886	47
3	0.5	56.55	0.8531	46
4	0.5	100.53	0.4329	44
6	0.5	226.19	0.2008	45
6	1	113.1	0.4686	53
8	1	201.06	0.2302	46
12	1	452.39	0.1136	51
15	1	706.86	0.07466	53
15	2	353.43	0.1481	52
25	2	981.75	0.21	85
32	2	1608.5	0.2891	110
40	2	2513.27	0.05356	135
40	5	1005.31	0.14	141
65	5	2654.65	0.08308	221

VES 8

AB/2 (m)	MN	G	ρ (Ω)	ρa (Ωm)
1	0.5	6.28	7.771	49
2	0.5	25.13	2.313	58
3	0.5	56.55	1.014	57
4	0.5	100.53	0.5498	55
6	0.5	226.19	0.2059	47
6	1	113.1	0.4382	50
8	1	201.06	0.216	43
12	1	452.39	0.1044	47
15	1	706.86	0.06878	49
15	2	353.43	0.1531	54
25	2	981.75	0.06634	65
32	2	1608.5	0.05813	94
40	2	2513.27	0.07152	180
40	5	1005.31	0.1947	196
65	5	2654.65	0.09171	243

VES 9

AB/2 (m)	MN	G	ρ (Ω)	ρa (Ωm)
1	0.5	6.28	9.536	100
2	0.5	25.13	6.664	167
3	0.5	56.55	3.804	215
4	0.5	100.53	2.434	245
6	0.5	226.19	1.562	360
6	1	113.1	1.917	300
8	1	201.06	2.353	420
12	1	452.39	1.836	420
15	1	706.86	2.434	420
15	2	353.43	3.201	360
25	2	981.75	1.701	200
32	2	1608.5	0.06229	160
40	2	2513.27	0.06371	180
40	5	1005.31	0.145	190
65	5	2654.65	0.08217	218

VES 10

AB/2 (m)	MN	G	ρ (Ω)	ρa (Ωm)
1	0.5	6.28	2.526	32
2	0.5	25.13	0.5894	30
3	0.5	56.55	0.2536	28
4	0.5	100.53	0.141	28
6	0.5	226.19	0.06218	28
6	1	113.1	0.1197	28
8	1	201.06	0.07963	32
12	1	452.39	0.04615	42
15	1	706.86	0.03418	48
15	2	353.43	0.05508	38
25	2	981.75	0.03327	66
32	2	1608.5	0.028	90
40	2	2513.27	0.02688	136
40	5	1005.31	0.08379	168
65	5	2654.65	0.04433	236

VES 11

AB/2 (m)	MN	G	ρ (Ω)	ρa (Ωm)
1	0.5	6.28	3.307	42
2	0.5	25.13	1.156	58
3	0.5	56.55	0.4484	50
4	0.5	100.53	0.1917	38
6	0.5	226.19	0.07669	34
6	1	113.1	0.1126	26
8	1	201.06	0.1024	42
12	1	452.39	0.06087	56
15	1	706.86	0.04463	64
15	2	353.43	0.1044	74
25	2	981.75	0.05407	106
32	2	1608.5	0.0425	136
40	2	2513.27	0.03144	158
40	5	1005.31	0.0142	28
65	5	2654.65	0.04402	234

VES 12

AB/2 (m)	MN	G	ρ (Ω)	ρa (Ωm)
1	0.5	6.28	3.733	46
2	0.5	25.13	0.8856	44
3	0.5	56.55	0.2272	26
4	0.5	100.53	0.144	30
6	0.5	226.19	0.5194	24
6	1	113.1	0.1328	30
8	1	201.06	0.1014	40
12	1	452.39	0.05884	54
15	1	706.86	0.04301	60
15	2	353.43	0.09171	62
25	2	981.75	0.04778	94
32	2	1608.5	0.03733	120
40	2	2513.27	0.03084	156
40	5	1005.31	0.08744	176
65	5	2654.65	0.05376	286

VES 13

AB/2 (m)	MN	G	ρ (Ω)	ρa (Ωm)
1	0.5	6.28	3.368	42
2	0.5	25.13	1.359	68
3	0.5	56.55	0.5468	62
4	0.5	100.53	0.2779	56
6	0.5	226.19	0.1136	52
6	1	113.1	0.3337	65
8	1	201.06	0.2059	55
12	1	452.39	0.06046	65
15	1	706.86	0.05721	80
15	2	353.43	0.1166	82
25	2	981.75	0.06391	126
32	2	1608.5	0.1105	356
40	2	2513.27	0.0284	142
40	5	1005.31	0.1531	308

VES 14

AB/2 (m)	MN	G	ρ (Ω)	ρa (Ωm)
1	0.5	6.28	14.6	184
2	0.5	25.13	2.252	114
3	0.5	56.55	0.636	72
4	0.5	100.53	0.2262	59
6	0.5	226.19	0.0913	42
6	1	113.1	0.2373	54
8	1	201.06	0.1521	62
12	1	452.39	0.1014	92
15	1	706.86	0.07507	106
15	2	353.43	0.2049	144
25	2	981.75	0.0143	140
32	2	1608.5	0.04301	140
40	2	2513.27	0.02972	150
40	5	1005.31	0.0422	130
65	5	2654.65	0.2333	200

VES 15

AB/2 (m)	MN	G	ρ (Ω)	ρa (Ωm)
1	0.5	6.28	4.078	52
2	0.5	25.13	0.4859	24
3	0.5	56.55	0.1318	15
4	0.5	100.53	0.03439	13
6	0.5	226.19	0.04494	20
6	1	113.1	0.1247	28
8	1	201.06	0.08116	32
12	1	452.39	0.05255	48
15	1	706.86	0.04534	64
15	2	353.43	0.09688	68
25	2	981.75	0.0354	95
32	2	1608.5	0.02921	120
40	2	2513.27	0.02627	132
40	5	1005.31	0.07223	146
65	5	2654.65	0.04889	260

VES 16

AB/2 (m)	MN	G	ρ (Ω)	ρa (Ωm)
1	0.5	6.28	24.95	157
2	0.5	25.13	5.062	127
3	0.5	56.55	1.613	91
4	0.5	100.53	0.665	67
6	0.5	226.19	0.2424	45
6	1	113.1	0.4666	50
8	1	201.06	0.1978	40
12	1	452.39	0.06685	30
15	1	706.86	0.0565	40
15	2	353.43	0.1176	42
25	2	981.75	0.01917	70
32	2	1608.5	0.01298	80
40	2	2513.27	0.05255	120
40	5	1005.31	0.6573	105
50	5	2654.65	0.03702	98

CONTROL POINT

AB/2 (m)	MN	G	ρ (Ω)	ρa (Ωm)
1	0.5	6.28	6.949	44
2	0.5	25.13	1.46	37
3	0.5	56.55	0.704	40
4	0.5	100.53	0.4108	46
6	0.5	226.19	0.1744	39
6	1	113.1	0.5792	60
8	1	201.06	0.3023	61
12	1	452.39	0.1288	58
15	1	706.86	0.07142	51
15	2	353.43	0.1511	53
25	2	981.75	0.04829	44
32	2	1608.5	0.01795	40
40	2	2513.27	0.02657	67
40	5	1005.31	0.1227	70

TRAVERSE THREE

C1	C2	P1	P2	K	R(Ω)	pa (Ω m)
0	1	2	3	94.2478	0.2749	25.9
		3	4	376.9911	0.286	107.8
		4	5	942.4778	0.05143	48.5
		5	6	1884.956	0.02008	37.8
		6	7	3298.672	0.01531	50.5
1	2	3	4	94.2478	0.2627	24.8
		4	5	376.9911	0.0701	26.4
		5	6	942.4778	0.02891	27.2
		6	7	1884.956	0.01968	37.1
		7	8	3298.672	0.02576	84.9
2	3	4	5	94.2478	0.2789	26.3
		5	6	376.9911	0.07568	28.5
		6	7	942.4778	0.03976	37.5
		7	8	1884.956	0.021	39.6
		8	9	3298.672	0.01369	45.2
3	4	5	6	94.2478	0.2104	19.8
		6	7	376.9911	0.07	26.4
		7	8	942.4778	0.04	37.7
		8	9	1884.956	0.021	39.6
		9	10	3298.672	0.01247	41.1
4	5	6	7	94.2478	0.2496	23.5
		7	8	376.9911	0.08	30.2
		8	9	942.4778	0.0401	37.8
		9	10	1884.956	0.02315	43.6
		10	11	3298.672	0.01572	51.9
5	6	7	8	94.2478	0.3063	28.9
		8	9	376.9911	0.07781	29.3
		9	10	942.4778	0.033423	31.5
		10	11	1884.956	0.02016	38
		11	12	3298.672	0.011459	37.8
6	7	8	9	94.2478	0.309822	29.2
		9	10	376.9911	0.074538	28.1
		10	11	942.4778	0.041274	38.9
		11	12	1884.956	0.023077	43.5
		12	13	3298.672	0.017856	58.9
7	8	9	10	94.2478	0.301333	28.4
		10	11	376.9911	0.09788	36.9
		11	12	942.4778	0.042972	40.5
		12	13	1884.956	0.025783	48.6
		13	14	3298.672	0.018007	59.4

8	9	10	11	94.2478	0.649352	61.2
		11	12	376.9911	0.493115	185.9
		12	13	942.4778	0.045094	42.5
		13	14	1884.956	0.023714	44.7
		14	15	3298.672	0.041077	135.5
9	10	11	12	94.2478	0.358629	33.8
		12	13	376.9911	0.085413	32.2
		13	14	942.4778	0.039789	37.5
		14	15	1884.956	0.026791	50.5
		15	16	3298.672	0.019159	63.2
10	11	12	13	94.2478	0.315127	29.7
		13	14	376.9911	0.122815	46.3
		14	15	942.4778	0.049762	46.9
		15	16	1884.956	0.024987	47.1
		16	17	3298.672	0.019826	65.4
11	12	13	14	94.2478	0.324676	30.6
		14	15	376.9911	0.124406	46.9
		15	16	942.4778	0.050081	47.2
		16	17	1884.956	0.037985	71.6
		17	18	3298.672	0.019493	64.3
12	13	14	15	94.2478	0.333164	31.4
		15	16	376.9911	0.089127	33.6
		16	17	942.4778	0.054962	51.8
		17	18	1884.956	0.034112	64.3
		18	19	3298.672	0.017067	56.3
13	14	15	16	94.2478	0.306638	28.9
		16	17	376.9911	0.098411	37.1
		17	18	942.4778	0.058039	54.7
		18	19	1884.956	0.034484	65
		19	20	3298.672	0.020432	67.4
14	15	16	17	94.2478	0.437145	41.2
		17	18	376.9911	0.0817	30.8
		18	19	942.4778	0.042972	40.5
		19	20	1884.956	0.025836	48.7
		20	21	3298.672	0.01825	60.2
15	16	17	18	94.2478	0.446695	42.1
		18	19	376.9911	0.101329	38.2
		19	20	942.4778	0.060903	57.4
		20	21	1884.956	0.035226	66.4
		21	22	3298.672	0.023737	78.3
16	17	18	19	94.2478	0.501868	47.3
		19	20	376.9911	0.103185	38.9

		20	21	942.4778	0.056871	53.6
		21	22	1884.956	0.057508	108.4
		22	23	3298.672		
17	18	19	20	94.2478	0.354385	33.4
		20	21	376.9911	0.111408	42
		21	22	942.4778	0.049762	46.9
		22	23	1884.956		
		23	24	3298.672		
18	19	20	21	94.2478	0.386216	36.4
		21	22	376.9911	0.096554	36.4
		22	23	942.4778		
		23	24	1884.956		
		24	25	3298.672		
19	20	21	22	94.2478	0.337408	31.8
		22	23	376.9911		
		23	24	942.4778		
		24	25	1884.956		
		25	26	3298.672		

TRAVERSE FOUR

C1	C2	P1	P2	K	R(Ω)	pa (Ω m)
0	1	2	3	94.2478	0.684366	64.5
		3	4	376.9911	0.084087	31.7
		4	5	942.4778	0.029072	27.4
		5	6	1884.956	0.02	37.7
		6	7	3298.672	0.011156	36.8
1	2					
		3	4	94.2478	0.63662	60
		4	5	376.9911	0.105573	39.8
		5	6	942.4778	0.047004	44.3
		6	7	1884.956	0.010451	19.7
		7	8	3298.672	0.010762	35.5
2	3	4	5	94.2478	0.714075	67.3
		5	6	376.9911	0.100798	38
		6	7	942.4778	0.037773	35.6
		7	8	1884.956	0.013104	24.7
		8	9	3298.672	0.024858	82
3	4	5	6	94.2478	1.007981	95
		6	7	376.9911	0.191782	72.3
		7	8	942.4778	0.022176	20.9
		8	9	1884.956	0.010239	19.3

		9	10	3298.672	0.011853	39.1
4	5	6	7	94.2478	0.569775	53.7
		7	8	376.9911	0.105573	39.8
		8	9	942.4778	0.080639	76
		9	10	1884.956	0.020425	38.5
		10	11	3298.672	0.015491	51.1
5	6	7	8	94.2478	0.772432	72.8
		8	9	376.9911	0.046155	17.4
		9	10	942.4778	0.022388	21.1
		10	11	1884.956	0.056765	107
		11	12	3298.672	0.095796	316
6	7	8	9	94.2478	0.425474	40.1
		9	10	376.9911	0.037932	14.3
		10	11	942.4778	0.041911	39.5
		11	12	1884.956	0.075864	143
		12	13	3298.672	0.081548	269
7	8	9	10	94.2478	0.517784	48.8
		10	11	376.9911	0.099737	37.6
		11	12	942.4778	0.047322	44.6
		12	13	1884.956	0.024138	45.5
		13	14	3298.672	0.012581	41.5
8	9	10	11	94.2478	0.427596	40.3
		11	12	376.9911	0.080108	30.2
		12	13	942.4778	0.033423	31.5
		13	14	1884.956	0.02	37.7
		14	15	3298.672	0.019068	62.9
9	10	11	12	94.2478	0.531577	50.1
		12	13	376.9911	0.156237	58.9
		13	14	942.4778	0.077243	72.8
		14	15	1884.956	0.192047	362
		15	16	3298.672	0.056386	186
10	11	12	13	94.2478	0.444573	41.9
		13	14	376.9911	0.041646	15.7
		14	15	942.4778	0.06398	60.3
		15	16	1884.956	0.026844	50.6
		16	17	3298.672	0.018401	60.7

11	12	13	14	94.2478	0.610094	57.5
		14	15	376.9911	0.442981	167
		15	16	942.4778	0.056765	53.5
		16	17	1884.956	0.02329	43.9
		17	18	3298.672	0.011156	36.8
12	13	14	15	94.2478	0.481709	45.4
		15	16	376.9911	0.097085	36.6
		16	17	942.4778	0.020054	18.9
		17	18	1884.956	0.012096	22.8
		18	19	3298.672	0.012065	39.8
13	14	15	16	94.2478	0.200535	18.9
		16	17	376.9911	0.066049	24.9
		17	18	942.4778	0.240854	227
		18	19	1884.956	0.015544	29.3
		19	20	3298.672	0.029406	97
14	15	16	17	94.2478	0.515662	48.6
		17	18	376.9911	0.100533	37.9
		18	19	942.4778	0.251465	237
		19	20	1884.956	0.131038	247
		20	21	3298.672	0.049717	164
15	16	17	18	94.2478	0.397887	37.5
		18	19	376.9911	0.148279	55.9
		19	20	942.4778	0.204779	193
		20	21	1884.956	0.166052	313
		21	22	3298.672	0.130659	431
16	17	18	19	94.2478	0.767127	72.3
		19	20	376.9911	0.145892	55
		20	21	942.4778	0.124141	117
		21	22	1884.956	0.044245	83.4
		22	23	3298.672	0.241309	796
17	18	19	20	94.2478	0.018992	1.79
		20	21	376.9911	0.032362	12.2
		21	22	942.4778	0.016022	15.1
		22	23	1884.956	0.044723	84.3
		23	24	3298.672	0.036378	120
18	19	20	21	94.2478	0.528394	49.8
		21	22	376.9911	0.020584	7.76

		22	23	942.4778	0.01061	10
		23	24	1884.956	0.00817	15.4
		24	25	3298.672		
19	20	21	22	94.2478	0.581446	54.8
		22	23	376.9911	0.098411	37.1
		23	24	942.4778	0.044245	41.7
		24	25	1884.956		
		25	26	3298.672		
20	21	22	23	94.2478	0.790469	74.5
		23	24	376.9911	0.254648	96
		24	25	942.4778		
		25	26	1884.956		
		26	27	3298.672		
21	22	23	24	94.2478	0.51354	48.4
		24	25	376.9911		
		25	26	942.4778		
		26	27	1884.956		
		27	28	3298.672		

TRAVERSE TWO

C1	C2	P1	P2	K	R(Ω)	ρ_a (Ω m)
0	1	2	3	94.2478	0.511418	48.2
		3	4	376.9911	0.096023	36.2
		4	5	942.4778	0.042866	40.4
		5	6	1884.956	0.018038	34
		6	7	3298.672	0.01734	57.2
1	2					
		3	4	94.2478	0.5963	56.2
		4	5	376.9911	0.127854	48.2
		5	6	942.4778	0.037985	35.8
		6	7	1884.956	0.012467	23.5
		7	8	3298.672	0.009216	30.4
2	3	4	5	94.2478	0.694976	65.5
		5	6	376.9911	0.104512	39.4
		6	7	942.4778	0.041805	39.4
		7	8	1884.956	0.009072	17.1
		8	9	3298.672	0.018553	61.2
3	4	5	6	94.2478	0.75015	70.7
		6	7	376.9911	0.149871	56.5

		7	8	942.4778	0.035226	33.2
		8	9	1884.956	0.015809	29.8
		9	10	3298.672	0.012793	42.2
4	5	6	7	94.2478	0.849887	80.1
		7	8	376.9911	0.2008	75.7
		8	9	942.4778	0.079047	74.5
		9	10	1884.956	0.048012	90.5
		10	11	3298.672	0.020099	66.3
5	6	7	8	94.2478	0.588873	55.5
		8	9	376.9911	0.280378	105.7
		9	10	942.4778	0.065041	61.3
		10	11	1884.956	0.040107	75.6
		11	12	3298.672	0.025131	82.9
6	7	8	9	94.2478	0.850948	80.2
		9	10	376.9911	0.344836	130
		10	11	942.4778	0.075121	70.8
		11	12	1884.956	0.056235	106
		12	13	3298.672	0.033953	112
7	8	9	10	94.2478	0.728929	68.7
		10	11	376.9911	0.068967	26
		11	12	942.4778	0.034696	32.7
		12	13	1884.956	0.018356	34.6
		13	14	3298.672	0.020584	67.9
8	9	10	11	94.2478	1.061033	100
		11	12	376.9911	0.875352	330
		12	13	942.4778	0.497624	469
		13	14	1884.956	0.026685	50.3
		14	15	3298.672	0.039561	130.5
9	10	11	12	94.2478	0.465793	43.9
		12	13	376.9911	0.170296	64.2
		13	14	942.4778	0.08796	82.9
		14	15	1884.956	0.088066	166
		15	16	3298.672	0.090036	297
10	11	12	13	94.2478	0.446695	42.1
		13	14	376.9911	0.064988	24.5
		14	15	942.4778	0.109499	103.2
		15	16	1884.956	0.02382	44.9

		16	17	3298.672	0.015825	52.2
11	12	13	14	94.2478	0.412742	38.9
		14	15	376.9911	0.056235	21.2
		15	16	942.4778	0.030982	29.2
		16	17	1884.956	0.011141	21
		17	18	3298.672	0.010641	35.1
					#DIV/0!	
12	13	14	15	94.2478	0.342714	32.3
		15	16	376.9911	0.068967	26
		16	17	942.4778	0.0226	21.3
		17	18	1884.956	0.022706	42.8
		18	19	3298.672	0.009367	30.9
13	14	15	16	94.2478	0.787286	74.2
		16	17	376.9911	0.06711	25.3
		17	18	942.4778	0.02886	27.2
		18	19	1884.956	0.013157	24.8
		19	20	3298.672	0.005426	17.9
14	15	16	17	94.2478	0.387277	36.5
		17	18	376.9911	0.057296	21.6
		18	19	942.4778	0.021963	20.7
		19	20	1884.956	0.014006	26.4
		20	21	3298.672	0.020402	67.3
15	16	17	18	94.2478	0.449878	42.4
		18	19	376.9911	0.064988	24.5
		19	20	942.4778	0.047959	45.2
		20	21	1884.956	0.018674	35.2
		21	22	3298.672	0.009337	30.8
16	17	18	19	94.2478	0.626009	59
		19	20	376.9911	0.063662	24
		20	21	942.4778	0.038091	35.9
		21	22	1884.956	0.03703	69.8
		22	23	3298.672		
17	18	19	20	94.2478	0.24616	23.2
		20	21	376.9911	0.066315	25
		21	22	942.4778	0.016658	15.7
		22	23	1884.956		
		23	24	3298.672		

18	19	20	21	94.2478	0.742723	70
		21	22	376.9911	0.032362	12.2
		22	23	942.4778		
		23	24	1884.956		
		24	25	3298.672		
19	20	21	22	94.2478	0.290723	27.4
		22	23	376.9911		
		23	24	942.4778		
		24	25	1884.956		
		25	26	3298.672		

TRAVERSE SIX

C1	C2	P1	P2	K	R(Ω)	ρ_a (Ωm)
0	1	2	3	94.2478	0.601606	56.7
		3	4	376.9911	0.101329	38.2
		4	5	942.4778	0.035969	33.9
		5	6	1884.956	0.015226	28.7
		6	7	3298.672	0.011247	37.1
1	2					
		3	4	94.2478	0.380911	35.9
		4	5	376.9911	0.049073	18.5
		5	6	942.4778	0.022176	20.9
		6	7	1884.956	0.014218	26.8
		7	8	3298.672	0.008579	28.3
2	3	4	5	94.2478	0.494441	46.6
		5	6	376.9911	0.082495	31.1
		6	7	942.4778	0.026208	24.7
		7	8	1884.956	0.022229	41.9
		8	9	3298.672	0.011459	37.8
3	4	5	6	94.2478	0.707709	66.7
		6	7	376.9911	0.065784	24.8
		7	8	942.4778	0.033529	31.6
		8	9	1884.956	0.010345	19.5
		9	10	3298.672	0.014188	46.8
4	5	6	7	94.2478	0.676939	63.8
		7	8	376.9911	0.077986	29.4
		8	9	942.4778	0.030558	28.8
		9	10	1884.956	0.011459	21.6

		10	11	3298.672	0.008458	27.9
5	6	7	8	94.2478	0.644047	60.7
		8	9	376.9911	0.176397	66.5
		9	10	942.4778	0.33518	315.9
		10	11	1884.956	0.087164	164.3
		11	12	3298.672	0.158245	522
6	7	8	9	94.2478	0.692854	65.3
		9	10	376.9911	0.079047	29.8
		10	11	942.4778	0.02642	24.9
		11	12	1884.956	0.017666	33.3
		12	13	3298.672	0.038743	127.8
7	8	9	10	94.2478	0.487014	45.9
		10	11	376.9911	0.068702	25.9
		11	12	942.4778	0.042017	39.6
		12	13	1884.956	0.026048	49.1
		13	14	3298.672	0.034135	112.6
8	9	10	11	94.2478	0.762883	71.9
		11	12	376.9911	0.136873	51.6
		12	13	942.4778	0.028223	26.6
		13	14	1884.956	0.006525	12.3
		14	15	3298.672	0.012278	40.5
9	10	11	12	94.2478	1.277483	120.4
		12	13	376.9911	0.920181	346.9
		13	14	942.4778	4.626104	4360
		14	15	1884.956	1.044003	1967.9
		15	16	3298.672	1.014014	3344.9
10	11	12	13	94.2478	13.18015	1242.2
		13	14	376.9911	18.15003	6842.4
		14	15	942.4778	17.80997	16785.5
		15	16	1884.956	15.72	29631.5
		16	17	3298.672		
11	12	13	14	94.2478	10.63049	1001.9
		14	15	376.9911	17.10995	6450.3
		15	16	942.4778	16.13004	15202.2
		16	17	1884.956		
		17	18	3298.672		

12	13	14	15	94.2478	1.196845	112.8
		15	16	376.9911	0.038462	14.5
		16	17	942.4778		
		17	18	1884.956		
		18	19	3298.672		
13	14	15	16	94.2478	1.379343	130
		16	17	376.9911		
		17	18	942.4778		
		18	19	1884.956		
		19	20	3298.672		

CONTROL POINT

C1	C2	P1	P2	K	R(Ω)	ρ_a (Ωm)
0	1	2	3	94.2478	0.810629	76.4
		3	4	376.9911	0.256505	96.7
		4	5	942.4778	0.106528	100.4
		5	6	1884.956	0.052521	99
		6	7	3298.672	0.018856	62.2
1	2					
		3	4	94.2478	0.86262	81.3
		4	5	376.9911	0.219103	82.6
		5	6	942.4778	0.099207	93.5
		6	7	1884.956	0.041699	78.6
		7	8	3298.672	0.015006	49.5
2	3	4	5	94.2478	0.984638	92.8
		5	6	376.9911	0.280908	105.9
		6	7	942.4778	0.135812	128
		7	8	1884.956	0.027693	52.2
		8	9	3298.672	0.012884	42.5
3	4	5	6	94.2478	2.970892	280
		6	7	376.9911	0.639272	241
		7	8	942.4778	0.162338	153
		8	9	1884.956	0.051036	96.2
		9	10	3298.672	0.022706	74.9
4	5	6	7	94.2478	3.533239	333
		7	8	376.9911	0.697629	263
		8	9	942.4778	0.190986	180
		9	10	1884.956	0.068967	130
		10	11	3298.672	0.023828	78.6
5	6	7	8	94.2478	3.130047	295
		8	9	376.9911	0.652535	246
		9	10	942.4778	0.199474	188

		10	11	1884.956	0.064192	121
		11	12	3298.672	0.019887	65.6
6	7	8	9	94.2478	2.970892	280
		9	10	376.9911	0.602136	227
		10	11	942.4778	0.156184	147.2
		11	12	1884.956	0.04329	81.6
		12	13	3298.672	0.024646	81.3
7	8	9	10	94.2478	3.469577	327
		10	11	376.9911	0.530517	200
		11	12	942.4778	0.119897	113
		12	13	1884.956	0.055174	104
		13	14	3298.672	0.022312	73.6
8	9	10	11	94.2478	2.355493	222
		11	12	376.9911	0.368709	139
		12	13	942.4778	0.149606	141
		13	14	1884.956	0.047481	89.5
		14	15	3298.672	0.016219	53.5
9	10	11	12	94.2478	1.782535	168
		12	13	376.9911	0.588873	222
		13	14	942.4778	0.161277	152
		14	15	1884.956	0.049497	93.3
		15	16	3298.672	0.019887	65.6
10	11	12	13	94.2478	1.315681	124
		13	14	376.9911	0.275869	104
		14	15	942.4778	0.069179	65.2
		15	16	1884.956	0.039046	73.6
		16	17	3298.672		
11	12	13	14	94.2478	1.962911	185
		14	15	376.9911	0.281174	106
		15	16	942.4778	0.081381	76.7
		16	17	1884.956		
		17	18	3298.672		
12	13	14	15	94.2478	2.217558	209
		15	16	376.9911	0.384624	145
		16	17	942.4778		
		17	18	1884.956		
		18	19	3298.672		
13	14	15	16	94.2478	2.673802	252
		16	17	376.9911		
		17	18	942.4778		
		18	19	1884.956		
		19	20	3298.672		